AN ELASTIC PLASTIC APPROACH: MODELING DEFORMATION OF DENSE SAND

by

GERALD W. FERRIS

A thesis
Submitted to the Faculty of Graduate Studies
in partial fulfillment of the requirements for the degree of

MASTER OF SCIENCE

Department of Civil and Geological Engineering
University of Manitoba
Winnipeg, Manitoba

February, 2000

THE UNIVERSITY OF MANITOBA

FACULTY OF GRADUATE STUDIES
*****
COPYRIGHT PERMISSION PAGE

An Elastic Plastic Approach: Modeling Deformation of Dense Sand

BY

Gerald W. Ferris

A Thesis/Practicum submitted to the Faculty of Graduate Studies of The University of Manitoba in partial fulfillment of the requirements of the degree of Master of Science

Abstract

This thesis examines the mechanical behaviour of dense (dilative) sand. The dense sand was tested under high pressure conditions (80 MPa in one dimensional compression and a confining pressure of 7.2 MPa in triaxial testing) and high temperatures (up to 100°C). The behaviour of the dilative sand could be successfully described by using elastic plastic concepts.

The triaxial testing program used modified equipment from the University of Manitoba's Soil Mechanics Laboratory (larger specimen sizes). The testing methodology followed typical drained triaxial testing methods, but the temperatures and pressures at which the tests were performed where much higher than typical. The 1-D compression testing was performed in a newly designed and constructed test apparatus.

The elastic-plastic model Cam Clay was able to capture many of the aspects of the dilative sands behaviour, modifications to the base model were necessary to account for particle breakage at high stress levels and variations in shear stiffness with shear strain.

The normal compression line of sand is considered to be defined in the grain crushing region. The isotropic compression testing performed did not reach stress levels high enough to induce grain crushing. A new equation was developed to describe the isotropic compression behaviour of sand prior to reaching the normal compression line.

Triaxial testing was performed at three different temperatures to determine the effect of temperature. No consistent effect of temperature was encountered in either isotropic compression or triaxial shear.

Acknowledgments

Funding for the research program undertaken in this thesis was provided by Atomic Energy of Canada. The research program was supervised by Professor J. Graham. I am truly grateful for his support and wisdom in guiding not only my research program but the beginning of my career.

I would like to extend thanks to my fellow graduate students, T. Crilly, N. Tanaka, T. Kirkham, G. Tang, B. Wiebe, J. Tukaluk and J. Blatz. The camaraderie and willingness to help each other in our various research projects was a highlight of my time at the University of Manitoba and since. I would like to acknowledge N. Piamsalee for providing helpful technical assistance.

Finally I would like to express my sincere thanks and love to Alex Birkholz for her encouragement and support throughout my study.

Table of Contents

List of Tables

List of Figures

Definition of Symbols

This list contains the definitions of symbols and the page that the symbols first appears.

ε_1	major principal strain	4
ε_2	intermediate principal strain	4
ε_3	minor principal strain	4
ε_a	axial strain	4
ε_s	shear strain	5
ε_s^e	elastic shear stain	5
ε_s^p	plastic shear strain	5
ε_v	volume strain	5
ε_v^e	elastic volume strain	5
ε_v^p	plastic volume strain	5
ϕ	Mohr-Coulomb friction angle	20
Γ	intercept of the critical state line in compression plane	8
κ	slope of unload reload line	8
λ	slope of normal compression line	8
λ_c	slope of the critical state line	8
η	Stress ratio, q/p	8
η_0	Stress ratio for isotropic compression	21
σ_1	major principal stress	4
σ_2	intermediate principal stress	4
σ_3	minor principal stress	4

σ_a	axial stress	4
σ_r	radial stress	4
σ_n	normal stress	12
ρ	density	42
ρ_{max}	maximum density	42
ψ	state parameter	10
τ	shear strength	12
B_p	breakage potential	25
B_t	total breakage	26
B_r	relative breakage	26
C_r	unload reload compression index	49
C_c	compression index	50
D	plastic potential	8
D	grain size diameter	25
D_i	initial confined modulus	55
D_c	crushing confined modulus	55
D_r	unload reload confined modulus	55
D_r	relative density, ρ / ρ_{max}	17
e	voids ratio	20
e_{max}	maximum voids ratio	20
e_{min}	minimum voids ratio	20
e_c	voids ratio at critical state	20

G	shear modulus	8
G_{max}	maximum shear modulus	98
I_D	density index	52
K	constant from Rowe's stress dilatancy equation	19
K_0	stress ratio for isotropic compress	21
M	shape factor for Cam Clay ellipse/ slope of critical state line, q_c / p_c	8
N	constant from Chu's stress dilatancy equation	19
p	mean stress	5
p_o	mean stress used to scale the Cam Clay ellipse	8
p_c	mean stress at critical state	8
p_c	crushing mean stress	100
q	shear stress	5
q_c	shear stress at critical state	8
R	overconsolidation ratio	10
V	specific volume	8
V_{max}	maximum specific volume	100
V_{min}	minimum specific volume	100
V_{crush}	crushing specific volume	100
V_κ	intercept of unload reload line in compression plane	8
V_λ	intercept of normal compression line in compression plane	8
u	porewater pressure	13

Chapter 1 Introduction

The Canadian concept for disposal of radioactive nuclear fuel waste involves burial of the waste in the plutonic rock of the Canadian Shield at a depth of 500 m to 1,000 m. The radioactive waste will be contained in long-lasting metal containers, packed with granular particulate and surrounded by a low-permeability barrier. Figure 1.1 shows a possible container design developed by Atomic Energy of Canada Limited (AECL). The low-permeability barrier will be a sand-bentonite mixture known as buffer. Considerable work has been performed at the University of Manitoba and other laboratories to characterize buffer behaviour. The behaviour of the particulate inside the container has received much less attention.

Expected conditions in the proposed disposal area include: temperatures up to 100°C caused by radioactive decay of waste material, and pressures up to 13 MPa consisting of 3 MPa swelling pressure from the buffer and up to 10 MPa due to hydrostatic pressure from groundwater. The pressure from the groundwater and buffer will act on the metal container walls and will be transferred, in part, to the packed particulate inside. Consequently tests were conducted on candidate sand at both high temperatures and pressures.

To predict the performance of the disposal scheme, AECL requires models which can predict behaviour of all components of the scheme (rock, buffer, metal canister and

packed particulate) under the temperatures and pressures expected in a repository. AECL has developed criteria to describe the required performance of the particulate in a packed-particulate container system, (Teper 1980). This thesis report focuses on developing a framework to model the particulates which AECL has identified as acceptable according to these criteria (Teper 1980).

To model the reaction of the packed particulate container in different expected scenarios, a constitutive model is required which can predict the strain response to varying pressures. Elastic-plastic models are powerful descriptors of soil behaviour and sand, in part, can be treated as an elastic-plastic material (Wood 1990). To describe sand for modeling purposes, it is necessary to define the material properties required by a suitable elastic-plastic model. This can be accomplished through careful testing which was the principal purpose of the research project.

This thesis report demonstrates that dense sand tested under high stress and high temperature can be effectively modeled using an elastic-plastic soil model. The elastic-plastic model, Cam Clay was used to model the test results, though some modifications to the basic model were introduced to more effectively predict dense sand behaviour.

A testing program was undertaken at the University of Manitoba to characterize the mechanical behaviour of three sands identified by AECL as a likely candidate particulate. The three sands consisted of two different gradations of a silica sand and 1 mm diameter glass beads. The materials were supplied to the author by AECL. All specimens tested

were air dry. One-dimensional (1-D) compression tests were completed to determine some aspects of the elastic-plastic behaviour at stresses (80 MPa) higher than could be achieved in the existing triaxial cells. Triaxial compression tests were completed to determine strength and deformation properties of the sand at confining pressures up to 7 MPa. Triaxial and 1-D testing were performed at temperatures of 27°C, 65°C and 100°C.

Existing equipment at the University of Manitoba laboratories was used where possible, though a significant amount of new equipment was designed by the author and manufactured for the testing program. The new equipment included: a new mold for making butyl rubber membranes, a membrane stretcher, a new pedestal and top cap for the triaxial cell, new instrumentation for measurement of deformation of specimens in the triaxial cell and a new one dimensional compression cell. Existing loading frames were used for compression of the specimens in one dimensional testing and triaxial testing.

This thesis report examines existing literature on the behaviour and elastic-plastic modeling of sand, outlines the experimental equipment and procedures used, reports test results, and reports conclusions based on the testing program.

Chapter 2 Literature Review

2.1 Introduction

As soils can carry much more compressive strain than tensile strain, compressive stresses and strains are normally considered as positive in geotechnical engineering. Engineering stress and strain are used throughout this thesis report. The major, intermediate and minor principal stresses are noted by σ_1, σ_2 and σ_3, respectively. The strains corresponding to these principal stresses are ε_1, ε_2 and ε_3. The testing program was conducted on air dry sand. Therefore, all stresses are effective stresses and the normal symbol for effective stress (′) has been omitted for simplicity and clarity.

Two types of tests were performed as part of the thesis project: one-dimensional compression and drained triaxial compression. These tests each imposed different stress and strain conditions on the soil.

The one-dimensional compression test restricts the ε_2 and ε_3 strains to zero. Axial stress, σ_a (σ_1) is applied to the top of the specimen which results in axial deformation ε_a (ε_1). The addition of axial stress, causes lateral stress to develop in the specimen since the lateral strain is restricted to zero. Radial stresses, σ_r ($\sigma_r = \sigma_2 = \sigma_3$) are generally not measured in 1-D tests.

The triaxial compression test allows independent application of axial stress, $\sigma_a = \sigma_1$, the major principal stress and radial stress or cell pressure, σ_r ($\sigma_2=\sigma_3=\sigma_r$). These two independently controlled stresses can be combined into a mean stress tending to cause volume strain, $p = (\sigma_a + 2\sigma_r)/3$; and a deviator stress tending to cause shear strain, $q = \sigma_a - \sigma_r$. Axial strain, radial strain and volume strain of the specimen can be measured separately. Strains corresponding to the p stress component and the q stress component are, respectively: volume strain $\varepsilon_v = \varepsilon_a + 2\varepsilon_r$ and shear strain $\varepsilon_s = 2/3(\varepsilon_a - \varepsilon_r)$. The p-ε_v and q-ε_s stress-strain spaces are the standard choice used in elastic plastic soil mechanics formulations (Wood 1990).

2.2 Introduction to Elastic-Plastic Soil Mechanics (EPSM)

The fundamental assumption of EPSM is that strains can be separated into two components, a recoverable elastic strain component and an irrecoverable plastic strain component. In notation form this is written as $\varepsilon_v = \varepsilon_v^e + \varepsilon_v^p$ for volume strain and, similarly, for shear strain as $\varepsilon_s = \varepsilon_s^e + \varepsilon_s^p$.

An EPSM model consists of five main components: elastic parameters, a yield surface, a flow rule, a strength law and a hardening law. The yield surface separates regions of elastic behaviour described by elastic parameters from regions of plastic behaviour described by the flow rule and hardening law.

An EPSM model predicts only elastic strains when applied stresses are less than stresses on the yield surface. If an applied stress is greater than the current yield surface, predicted strains will have both elastic and plastic components. Depending on the stress vector, plastic strain components are generally larger than corresponding elastic components. Development of plastic straining (plastic strains have both a volumetric and shear strain component) in response to stresses in excess of the current yield surface is controlled by the flow rule. The plastic hardening law describes how the yield surface changes in response to plastic strains. Combinations of mean and shear stress acting on the soil can not be greater than the current yield surface. When a combination of stresses greater than the yield surface is applied, plastic strains develop in response to this stress and enlarge the yield surface to include the current stress state. Such models are commonly called "volumetric hardening elastic plastic models." The strength law describes stress states at which the material fails in shear.

The original elastic plastic soil model for soil was Cam Clay, which was developed at Cambridge University in the United Kingdom. One of the major features of Cam Clay is the existence of a condition called critical state which defines the strength law. Critical state is a unique condition at high strains where porewater pressure, volume strain, mean stress and deviator stress do not change with continued changes in shear strain. The concept of critical state and an elastic plastic formulation were used as the basis of the Cam Clay model (Roscoe, Schofield and Wroth 1958, Schofield and Wroth 1968 and Roscoe and Burland 1968).

Modifications to the original formulations of Cam Clay have been made in order to better model the observed behaviour soils. The modifications have created a family of critical state soil mechanics (CSSM) models, with the Cam Clay formulation being the basis of most these models.

One of the conditions required in the CSSM family of models is the existence of a unique relationship between applied mean stress and specific volume in isotropic compression, a so called normal compression line. While this has been observed for clays, such a relationship was not found for sands in the typical geotechnical stress range (Been, Jefferies and Hachey 1991, Konrad and Pouliot 1997). Such a relationship has been observed for weak grained sand (Coop 1990) and for all sands at high stress levels.

The critical state does exist in sands (Chu 1995) and was used as the basis for NOR Sand (Jefferies 1993, Jefferies and Been 1992) which describes shearing behaviour of sand based on the relationship of the current state to the critical state line. More details of these models are given in following sections.

2.3 Cam Clay

The CSSM model normally used as the baseline model for definition of parameters and concepts is modified Cam Clay (Roscoe and Burland 1968, Wood 1990). Figure 2.1

illustrates the features of the Cam Clay model. A complete description of the equations relating stresses and strains in the Cam Clay model can be found in Wood (1990). This model includes the following assumptions/features as seen in Figure 2.1.

1. Elasticity is isotropic and defined by straight lines of slope κ in V- *ln* p space, $V = V_\lambda + \kappa ln p$;
2. Yield loci are elliptical, $p/p_o = M^2/(M^2+\eta^2)$;
3. Volumetric hardening is defined by straight lines of slope λ in V versus *ln* p graphs, $V = V_\lambda + \lambda ln p$;
4. Large strain failure (critical state) is controlled by a Coulomb-Mohr failure criterion with slope $M = q_c / p_c$ in q versus p plots and by a straight line in V versus *ln* p plots; $V_c = \Gamma + \lambda_c ln p$, and;
5. The flow rule is associated, the plastic potential is coincident with yield loci and given by $D = M^2-\eta^2 / 2\eta$.

The Cam Clay equation which relates the change in elastic volume stress to the change in mean stress is $\delta\varepsilon_v^e = \kappa / Vp\ \delta p$. Similarly the equation $\delta\varepsilon_s^e = \delta q / 3G$ relates elastic changes in shear strain to the change in shear stress, the model assumes constant values of the shear modulus G. These equations describe isotropic elasticity, that is, changes in mean stress does not contribute to shear strain, and shear stress changes do not contribute to volume strain.

The equation in Cam Clay which relates the change in plastic volume strain to changes in mean stress and shear stress is:

$$\delta\varepsilon_v^p = (\lambda - \kappa)\,(M^2-\eta^2) / (M^2+\eta^2)\,Vp\,\delta p + 2\eta\,(\lambda - \kappa) / Vp(M^2+\eta^2)\,\delta q.$$

Similarly the equation:

$$\delta\varepsilon_s^p = 2\eta\,(\lambda - \kappa) / Vp(M^2+\eta^2)\,\delta p + 4\eta^2(\lambda - \kappa) / Vp\,(M^2+\eta^2)\,(M^2-\eta^2)\,\delta q$$

relates plastic change in shear strain to the change in mean stress and shear stress. These equations (from Wood 1990) only operate when plastic strains are occurring.

The Cam Clay model was the first soil model to successfully link strength and volume change. It is broadly acceptable for clays and less so for sands. The reasons for this are expanded in later sections of this report. The CSSM family remains one of the few widely accessible soil models which link elastic and plastic behaviour.

Modifications to the original Cam Clay model are discussed in later sections. The modifications have been made to match more closely the observed behaviour of sand.

2.4 Nor Sand

Critical state model formulations have not been widely used or accepted to describe the behaviour of sand. This is despite its linking of elastic and plastic behaviour and the linking of strength and deformation properties. Sand has been considered "easy" to design for, since under most working loads sand can be considered elastic, or in other situations completely plastic. Simple models which only take into account the parameter considered most critical, have been successful for the most part. This, combined with CSSM's failure to reproduce strain softening after peak strength and dilation of dense sands (most natural sands are dense) means that models of the Cam Clay type have not been used for sands to any great extent.

The Nor-Sand model (Jefferies and Been 1992, Jefferies 1993) is part of the general CSSM family, whose main characteristics are the critical state line and the linking of strength and volume change. It differs in two main ways from Cam Clay: it uses a rate-based state parameter, ψ instead of void ratio to size the current yield surface and it allows an infinite number of normal compression lines. A complete description of the equations relating stresses and strains in the Nor-Sand model can be found in Jefferies and Been (1992).

The basis of the Nor-Sand model is the so called 'state parameter'. State parameter can be successfully correlated to many other parameters and used to describe sand behaviour

tested in a variety of different loading scenarios (Been and Jefferies1985). The state parameter, ψ as shown in Figure 2.2 relates the distance of the current specific volume of sand to the equivalent specific volume at the same mean stress on the critical state line. Also shown in Figure 2.2 is the overconsolidation ratio, R which is the ratio of past highest stress to current stress.

Nor-Sand has been shown to effectively model the behaviour of sand stressed in a variety of loading conditions once the soil parameters are established (Jefferies and Been, 1992 and Been, Jefferies and Hachey, 1992). The critical state line was established using drained and undrained tests on dense sand. The model parameters could then be established from one further undrained test on a loose sand specimen. The model was used to predict both liquefaction of a very loose sand in an undrained test and reversal of curvature in the stress path for a dense sand in an undrained test.

2.5 Review of Sand Behaviour

Sand, when subjected to shear stress, can be classified as having one of two broad types of behaviour: loose (compressive) or dense (dilative). The typical shearing behaviour of dense sand (1) and loose sand (3) is shown in Figure 2.3. A dense sand reaches a distinct peak strength with increases in strain. After peak resistance the amount of deviator (shear) stress which can be supported decreases with increasing strain. With the exception of a small amount of initial compression, throughout shear straining of dense

sand, the total volume increases. This is known as dilatancy. A loose sand generally does not have a distinct peak strength and deformations are larger compared with the same stress applied to a dense sand. A loose sand will contract or maintain the same volume when sheared. Most natural sands are dense in the normal range of working stresses (Sladen 1992). When applied stresses are below the peak strength, small deformations result.

When sands are sheared with large values of confining stress applied to the specimen the behaviour changes (Lee and Seed, 1967, Vesic and Clough, 1968, Lo and Roy, 1973). Loose specimens at high stress have the same generally compressive behaviour as at lower stresses but the ratio of peak strength over confining stress (τ/σ_n) is reduced. Also the specimens are more contractive than at lower values of confining stress. Dense specimens experience greater changes. At high pressures the sand which would behave as a "dense" (expansive) sand now behaves as "loose" (contractive). There is no distinct peak, and volume change is contractive. This is shown in Figure 2.4, where the initial densities of the specimens were the same, the only difference being the cell pressure at which shearing took place (the ratio τ/σ_n is here represented by σ_1/σ_3). In this way, the behaviour of sand depends on both the density and the level of stress applied to the sand. The strength of the CSSM approach is that it couples volume change with strength. Thus, it would appear necessary that a successful CSSM approach should be able to bring together the current stress level and density to predict shearing behaviour.

In the high pressure testing performed in this project, it was noted that sand particles experienced grain crushing as in high pressure testing performed by other researchers (Vesic and Clough 1968). The amount of grain crushing depended on the type of test and sand grain characteristics. Literature on grain crushing is summarized in Section 2.8.

2.6 Sand Behaviour: A Critical State Approach

This section summarizes sand behaviour as measured in the laboratory and shows how this behaviour fits into a critical state framework. Because of its relationship to the needs of AECL, the testing program performed in the laboratory phase of this thesis concerned itself with dry sand near maximum density. Tests were performed in either 1-D compression or in drained triaxial compression. The two models described earlier and the behaviour summarized in this section all discuss drained and undrained behaviour of loose and dense sand.

2.6.1 Critical State

Critical state soil mechanics depends on the existence of a unique critical state line, CSL, in p-q space. Critical state is defined as a condition where: $\delta p / \delta \varepsilon_s = \delta q / \delta \varepsilon_s = \delta \varepsilon_v / \delta \varepsilon_s = \delta u / \delta \varepsilon_s = 0$. Although the original seed for the critical state concept came from shear testing of sand (Casagrande 1936), the existence of a unique critical state line for sands has been strongly contested.

Research on critical states in sand has followed two paths: drained testing and undrained testing. Undrained testing of loose sands during liquefaction led to the term 'steady state' (Poulos 1981) and to the state parameter described in Figure 2.2. Testing showed that a unique relationship, termed steady state line (SSL) existed between voids ratio and mean stress existed at large strain failure in the order of 10%. Researchers testing drained sand used the term 'critical state'. Testing dense sand at pressures in the range of 10 kPa to about 500 kPa found a unique line (CSL) relating voids ratio and mean stress at large strain failure. Drained testing of dense sand is not a very successful procedure for defining the CSL (Chu 1995), because of one or more shear bands may develop when shearing. The exception is when high stress levels inhibit dilatancy. It appeared that the drained and undrained testing did not lead to a unique relationship between voids ratio and mean stress, but to two (Casagrande 1975). The two lines were termed the S-line for drained testing and the F-line for undrained testing.

Through careful testing, the SSL and the CSL have since been shown to be the same condition, and are independent of the stress path followed to reach this state (Been et al. 1991, Chu 1995, Konrad 1997). Researchers have performed tests through large stress ranges on both dense and loose sand in drained and undrained tests. All the tests come to a single unique line at critical state, but the unique line is bilinear, as shown in Figure 2.5. The bilinear nature of the CSL is due to grain crushing at high stress (Been et al 1991, Konrad 1996). In general, for clean quartz sand, the slope of the CSL changes in voids

ratio-log mean stress space in the range of 0.5 MPa to 1 MPa (Ishihara 1993). Testing on weaker carbonate sands has shown the change to occur at about 180 kPa (Coop 1990).

Jefferies and Been assumed the existence of a unique CSL, and used Nor-sand to predict end-of-test results for 20% axial strain (the usual limit in a triaxial test). This resulted in two distinct lines shown in Figure 2.6: the S-line from drained tests and the F-line from undrained tests.

Recently, the uniqueness and bilinear nature of the CSL have become accepted by the majority of researchers (Ishihara 1993 and Robertson and Fear 1995). Neither Nor-sand or Cam Clay currently allow a bilinear CSL of the type shown in Figure 2.5 even though the experimental evidence is strong.

2.6.2 Isotropic Compression

The isotropic compression test is used to determine three of the five Cam Clay parameters: λ, κ and p_o. If the normal compression line, NCL, does not exist for sands, the Cam Clay model is of doubtful value for sands. From previous paragraphs it will be remembered that the non-uniqueness of normal compression lines for sand has led to the establishment of Nor-sand, which allows for an infinite number of normal compression lines.

Isotropic compression testing to pressures of up to about 1 MPa, as shown in Figure 2.7, have shown the non-uniqueness of the NCL (Sladen and Oswell 1985 and Konrad and Pouliot 1997). Isotropic compression tests show that NCL's are unique for different initial voids ratios, and that their slope varies with initial voids ratio.

Figure 2.8 shows the results of testing sand in isotropic compression in tests up to a stress of 10 MPa (Lee and Seed 1967). For stresses below 1 MPa, the results for different densities are distinct and depend on the initial voids ratio. At higher stresses, all isotropic compression test results converge so that at the highest stress applied, the voids ratio varies only slightly, regardless of initial voids ratio. It was noted that time dependent volume changes occurred when the cell pressure was applied.

Isotropic compression testing of carbonate sand to cell pressures of up to 8 MPa, shown in Figure 2.9a, produced a unique NCL (Coop 1990, Coop and Lee 1993). The NCL was considered to be a manifestation of grain crushing. A stress level of about 1 MPa to 2 MPa was required to bring the isotropically compressed specimens to this unique NCL. Loose specimens reached the NCL at lower stresses than dense specimens. It was also concluded that the slope of the unload reload line, κ, was about the same as the slope of the initial loading. Prior to reaching a mean stress of about 1 MPa, the isotropic compression lines were distinct and they varied with initial voids ratio, as shown in Figure 2.7.

One dimensional compression testing results on carbonate sand (Coop 1990), shown in Figure 2.9 b, have been plotted alongside the interpreted NCL from isotropic compression testing. The slope of the two compression lines are similar after the initiation of particle breakage, which occurred at a lower value of mean stress. Prior to the initiation of particle breakage, the 1-D results were distinct and varied with initial voids ratio.

2.6.3 Pre-Failure Stress-Strain Relationships

The pre-failure, or small strain behaviour has received increasing attention as deformation predictions become a critical element in design (Simpson et al. 1979, Burland 1989, Simpson 1992). The recognition that traditional elastic solutions could not predict measured movements (Simpson et al 1979) led researchers to focus on soil behaviour at small strains. Measurements of field data (Jardine et al 1986) and laboratory data (Burland 1989) showed that shear stiffness was a function of shear strain.

The shear stiffness, G, of sand depends on four factors: shear strain, confining pressure (Iwasaki et al. 1978), initial voids ratio (Iwasaki et al. 1978, Porovic and Jardine 1993) and stress history (Coop and Lee 1993). The stiffness of sand reduces with increasing shear strain (Iwasaki et al. 1978), as shown in Figure 2.10. Increasing initial voids ratio from loose (Dr=18%) to dense (Dr=70%) increased the value of initial G by 30% (Porovic and Jardine 1994), shown in Figure 2.11. Increasing the applied cell pressure with the initial voids ratio being constant increased the initial value of G, as shown in

Figure 2.12. When specimens were isotopically or one-dimensionally compressed and then unloaded, the measured initial G at the beginning of reloading was greater than if the specimen had not been unloaded, see Section 2.6.6 and Figure 2.19.

In addition to this variable shear modulus, careful testing of sands showed that shearing behaviour was not completely elastic (Duncan and Chang 1970, shown in Figure 2.13). The unload-reload cycle does not follow the original loading path. Applied shear stresses of only a few kPa have been shown to produce incompletely recoverable behaviour (Atkinson 1993).

Two main approaches have been used to model the pre-failure deformation of soils: non-linear elasticity (Duncan and Chang 1970, Jardine et al 1986) and multi-cap elastic plastic models (Al Tabba and Wood 1989, Stallebrass et al. 1994).

The non-linear elastic approach uses a variable shear stiffness throughout the range of stresses to be applied. One approach is to fit the stress strain curve with a power law (Duncan and Chang 1970), which defines the elasticity up to peak stress. Another approach is to fit the shear modulus *versus* shear strain curve with a multi-parameter equation (Jardine et al. 1986) which defines the elasticity from zero shear to peak stress.

The multi-cap elastic plastic approach fits an inner "true" elastic boundary surface within the existing boundary surface of Cam Clay. The size of the inner cap is related to the stress conditions and the size of the Cam Clay yield surface. The inner cap contains all

perfectly linear elastic behaviour. Once this boundary is reached, the behaviour transitions to plastic behaviour on the Cam Clay yield surface. Rather than varying the elasticity, another approach is to allow some plastic strains to occur within the Cam Clay 'elastic' zone (Dafalias and Herrmann 1980). The amount of plastic strain which occurs within the Cam Clay yield surface depends on the closeness of the stress path to the yield surface.

2.6.4 Peak Strength and Dilatancy

The peak strength of sand includes three components (Lee and Seed 1967, as shown in Figure 2.14): mineral friction, grain crushing and dilatancy. The peak shear strength of loose sands at low mean pressures is slightly higher than the mineral friction. Peak failure strength is in this case equal to the critical state strength. In contrast, dense sand tested at low mean pressures has a peak strength greater than the critical state strength. This is caused by dilatancy. As described in Section 2.5, dense sand becomes contractive and acts as loose sand at high values of mean stress. Put another way, at some value of mean stress, dilatancy is negated. Grain crushing is described in Section 2.8. It becomes a larger component of the peak strength as the mean pressure increases.

Methods to calculate the effect of dilatancy, or volume increase upon shearing, are based on measured volume changes with shear. The dilatancy equation from the Cam Clay work hypothesis (Roscoe and Burland 1958) is $(q/p) = M - (d\varepsilon_v/d\varepsilon_s)$. An equation

relating dilatancy measured in a drained triaxial compression test was developed by Rowe (1962), it takes the form $(\sigma_a/\sigma_r) = K\ (1-(d\varepsilon_v/d\varepsilon_a)$. For tests with constant stress ratio q/p, or constant strain ratio $d\varepsilon_v/d\varepsilon_a$ tests, the dilatancy equation takes the form, $(q/p) = N\ (\ 1\ -\ 1/3\ (d\varepsilon_v/d\varepsilon_a))$ (Chu 1993). The equation is valid for the dilatancy range $-0.54<(d\varepsilon_v/d\varepsilon_a)<1$. The parameter N is a material property. Comparison of these three dilatancy rules is shown in Figure 2.15, where each equation predicts a different stress ratio σ_1/σ_3 for the same dilatancy level. Two of these equations, (1) and (3), in Figure 2.15 were developed for specific test conditions and are not valid for the other test condition.

The state parameter can be used to predict both the peak stress ratio and dilatancy at failure (Been and Jefferies 1985, Wood 1990). Comparisons of the state parameter measured prior to the start-of-shearing with dilation rates at failure, are shown in Figure 2.16 Comparisons of the state parameter measured prior to start of shear to peak shearing angle, ϕ, are shown in Figure 2.17. Normalization of the state parameter to the achievable voids ratio of sand has been suggested (Wood 1990, Konrad 1996) to allow comparison between different sands. The normalized state parameter takes the form $(e - e_c\ /\ e_{max} - e_{min})$

One consequence of the critical state condition being at zero dilation, is that the phase transformation in dense sand, which instantaneously has zero dilation, has the same stress ratio q / p as critical state (Coop 1990, Atkinson 1993).

2.6.5 Plastic Deformations, Yield Surface

In the Cam Clay model, the yield surface and the plastic potential are coincident, and the plastic flow is said to be associated. The shape of the yield surface and associated flow is difficult to confirm for sand (Wood 1990). Yielding in isotropic compression for sand is difficult to interpret, due to the non-unique nature of a isotopic compression lines which depend on initial voids ratio. Yield surfaces in shear, shown in Figure 2.18, indicate the yield surface is approximately shaped like a Cam Clay ellipse, although evidence is limited. Equations and formulations of sand with a non-associated plastic flow have also been presented. One formulation has the yield surface as a rotated distorted ellipse centered on the K_0 line, (converted to η_0 in p - q space) and the plastic potential as another rotated distorted ellipse centered on the $\eta_0 / 2$ line (Davies and Newson 1993).

2.6.6 Overconsolidation of Sands

The initial definition of state parameter was measured as the difference between the current voids ratio along the isotropic consolidation line and the voids ratio of the CSL at 1 kPa (Been and Jefferies 1985). Due to the non-linearity of the CSL through a large stress range, and an apparently infinite number of NCL's with differing slopes, the state parameter's definition has since been changed. Currently the state parameter is defined as the difference between the current voids ratio and the voids ratio on the CSL at the

current pressure. The original definition of state parameter included the term, R, which was defined based on current pressure compared to the past highest pressure on the NCL. The parameter R, was intended to handle the effects of overconsolidation, shown in Figure 2.2.

Testing of sand to determine the small strain stiffness has shown that specimens that are isotropically compressed and unloaded have a higher initial shear modulus than those not unloaded (Porovic and Jardine 1994). Two separate undrained triaxial compression tests were performed on carbonate sand at the same voids ratio, one was compacted, the other, was consolidated (Coop and Lee 1993). The consolidated specimen was stiffer than the compacted specimen, as shown in Figure 2.19.

2.7 One-Dimensional Compression

Sand exhibits three stages of behaviour when subjected to confined compression through a large stress range (Hagerty et al 1993). Stage one is low stress behaviour, before particle crushing begins. Stage two behaviour is dominated by grain crushing. Stage three behaviour is at extremely high stress levels where almost all the grain crushing is complete. The three stages of confined compression are shown in Figure 2.20.

Stage one behaviour is generally characterized by increasing stiffness with increasing stress. The stress strain curves are concave upwards (in the stress direction) for stresses

less than about 15 MPa. The increasing stiffness is due to looser areas within the sand matrix compressing to form a denser, stiffer sand (Lambe and Witman 1979). The model proposed by Hagerty et al. describes stage one behaviour using a constant value of secant confined modulus, defined from zero stress to the stress at the onset of grain crushing.

The second stage of confined compression is separated from the first stage by a yield point. Yielding is a result of the onset of particle crushing, as shown in Figure 2.20. The second stage of behaviour is a combination of the crushing of soil particles and reorganization/crushing of the resulting matrix. Throughout the second stage of loading, the value of confined modulus is lower than the initial confined modulus (Lambe and Witman 1979, Hagerty et al 1993).

The third stage of behaviour occurs when sand particles are crushed to a size where the stress on individual particles is below the stress required to fracture the particle. The third stage is labeled "apparent pseudoelastic behaviour", shown in Figure 2.20. The third stage of behaviour begins in the figure at an applied stress of 150-200 MPa, and is modeled using a constant confined modulus. The final value of confined modulus is significantly higher than the initial confined modulus value.

The stress at which crushing begins (yield stress) depends on (Hagerty et al 1993, Lee and Farhoomand 1963):

a) density - dense sand yields at higher stresses than loose sand

b) particle characteristics - rounded particles require higher stress to induce particle crushing than angular particles of the same size. A larger grain size requires less stress than a smaller particle to induce yielding. A well graded sand will yield at a higher stress level than a poorly graded sand

c) mineralogy - when individual grains are weaker, yield stress is smaller

When sand is subjected to unload reload cycles at stress levels below the yield stress, most of the strain is recoverable. However, some non-recoverable strains do occur, as shown in Figure 2.21. The plastic strains are due to rearrangement of particles and breakage of weak particles (Lambe and Whitman 1979). As seen in Figure 2.21, the slope of the unload reload curve is about equal to the initial slope, when stresses are less than the yield stress. The slope of the unload reload line is about the same as the slope of first time loading even when first time loading stress exceeds the yield stress. The slope of the initial loading line varies when stresses exceeded the yield stress, due to plastic strains.

The slope calculated from a one-dimensional compression test plotted in *ln*p-V (V=e+1) space is about the same as the slope calculated from a isotropic compression test on the same material (Atkinson and Bransby 1978, Coop 1990). Isotropic and one dimensional compression tests were performed on carbonate sands, as shown in Figure 2.9. The carbonate sand particles are weak, and the stress level of both tests were high enough so that particle crushing was occurring. The slopes of the test results appear identical. The NCL is a result of grain crushing of sand particles (Coop 1990).

Compared with a dense sand, more volume strain occurs when a loose sand is compressed (Hagerty et al 1993). The volume strain in a loose sand prior to crushing is due to particle rearrangement in the sand matrix. This makes identification of the yield stress more difficult in a loose sand than in a dense sand. Due to rearrangement of the sand matrix, a loose sand will not have the same slope in first time loading as in an unload reload cycle.

2.8 Grain Crushing

During compression to high stress levels, sand grains undergo changes in grain size, gradation and shape. The factors which control how much sand grains will crush are mineralogy, particle size, particle shape and stress levels. There are two different phases of particle breakage (Yudhbir and Wood 1989):

(1) Low stress levels - grain modifications are due to protrusions on the individual grains being knocked off. This reduces the grain angularity and produces some small changes in gradation

(2) Very high stresses - the grains are split or crushed. This produces angular grains and changes the gradation

The potential of sand grains to be crushed is quantified using breakage potential, B_p, the area on a gradation curve between the initial grading curve and a vertical line at

D=0.074 mm (Hardin 1985). The amount of particle breakage is quantified after compression using, total breakage B_t, calculated as the area between the initial and final grading curves above D=0.074 mm. These definitions are shown in Figure 2.22. Particles smaller than D=0.074 mm did not contribute significantly to crushing (Hardin 1985), comparing different sands showed that the, relative breakage $B_r = B_t / B_p$ best expressed how the crushing behaviour changed with size and mineralogy.

A correlation between B_r and the applied stress at critical state was shown to exist for carbonate sand (Coop and Lee 1993), as shown in Figure 2.23. This relationship supports the idea that the normal compression line and ultimate state line at high stress are due to crushing (Coop and Lee 1993). It also reflects a relationship between applied stress and specific volume.

2.9 Temperature Effects

Thermal testing of oil sands (Agar et al 1986) found that a small decrease of volume took place upon initial heating. This was attributed by the authors to a collapse of the original grain structure. Following the initial volume decease, the specimen increased in volume at the same rate as predicted by theoretical thermal expansion of the mineral. Cooling of the specimen resulted in volume decrease at the same rate as heating. The initial volume loss upon initial heating was not recovered.

Vesic and Clough (1968) showed that temperatures of up to 600 °C had no effect on the shearing behaviour of sand. No other studies of temperature effects became known to the author.

Chapter 3 Materials, Equipment and Procedures

3.1 Introduction

Thirty-three separate tests were performed for this thesis project: ten one-dimensional compression tests and 23 triaxial compression tests. The pressure imposed on the sands was up to 9 MPa confining pressure in the triaxial cell and 80 MPa axial stress in the one-dimensional compression cell. The testing was performed at room temperature, 65°C or 100°C.

The one-dimensional compression cell was designed by the author for use in this testing program. The one-dimensional compression cell (Figure 3.1) consists of a thick-walled cylinder (or confining ring) having a separate base and a movable top cap. Loading is applied through the top cap and the cylinder restrains the specimen from deforming radially. Axial deformation is measured from movement of the top cap.

The high temperature high pressure (HITEP) triaxial cells at the University of Manitoba were designed and built by Lingnau (1993) as part of his doctoral program. Modifications to the HITEP cells were subsequently made by Tanaka (1995) and Crilly (1996) for their postgraduate programs. The HITEP cells have a capacity of 10 MPa and 100°C. A triaxial cell is a pressure vessel, which allows application of an all-round

pressure through a fluid and separate axial stress. Additional axial stress is applied to the specimen by a loading ram which passes through the top of the container, as shown in Figure 3.2. Instrumentation for measuring the applied stresses and resulting strains is mounted both inside and outside the cell. More details of the test equipment are given in later sections.

Three sands were tested during the program: 1 mm diameter Ballotini and two gradations of 'Frac' (fractionated) sand. The 'Frac' sand is a semi-rounded quartz sand). The following sections provide more details of the test materials, equipment used for testing and the procedures followed during testing.

3.2 Test Materials

The sand materials tested in this program were: 20-40 frac sand, 16-25 frac sand and Ballotini ("20-40" means a material whose particles pass through a sieve with 20 meshes per inch but is retained on 40 meshes per inch). The materials were provided by AECL. Frac sand is the sand component of the sand-bentonite mixture known as "buffer". Specifications of the sand were reported by Gray, Cheung and Dixon (1984). The Ballotini, consisting of glass beads nominally 1 mm diameter, is commercially available from CATAPHOTE, Jackson, Mississippi. Grain size distributions of these sands based on sieve analysis are shown in Figure 3.3.

Properties of the three sands are summarized in Table 3.1. Properties include: minimum density (ASTM D4254 -91) and maximum density (ASTM D4253-93), specific gravity (ASTM D854-92) and breakage potential (Hardin 1989). All tests were performed on air dry specimens.

3.3 Experimental Equipment

3.3.1 One Dimensional (1-D) Compression Cell

A schematic diagram of the one-dimensional (1-D) compression cell, manufactured of stainless steel is shown in Figure 3.1. The cell has three main components: a confining ring, base, and top cap. The confining ring has an outside diameter of 90 mm and an inner diameter of 64 mm. Load was transferred from a loading frame to the specimen through a 64 mm diameter, 50 mm high stainless steel top cap.

Vertical loads were applied to the specimens using a United Testing System (R - 25799) loading frame with a capacity of 300 kN (60,000 lbs). A dial gauge was used to measure movement of the loading head and recorded manually.

To account for apparatus compliance, a load test was performed to the maximum pressure using only the top cap and base of the 1-D cell. Measurements of the resulting deflections were recorded and used to correct the results of subsequent tests on sand specimens.

During testing, the materials scored the inside of the cylinder, and formed indentations on the top cap and base of the 1-D cell. This was not believed to adversely affect the quality of the results but it does indicate the high pressures achieved in the program. Further information on these observations can be found in Ferris and Graham 1996 a, b, c, d.

3.3.2 Triaxial Cell

A schematic diagram of the HITEP triaxial cell, with the cell components and associated measuring instrumentation is shown in Figure 3.2. Excluding the pedestal base and piston which were both stainless steel and the top cap made of titanium, the HITEP triaxial cell was manufactured from nickel plated mild steel. Details of the design and fabrication of the HITEP cell were presented by Lingnau (1993). Descriptions of the major components and further modifications to the HITEP cells can be found in Crilly (1996).

One modification made by the author to the HITEP system was to increase the diameter of the top cap and pedestal from 50 mm to 63.5 mm. This was done to almost double the

specimen volume while maintaining a 2:1 height to diameter ratio. The new pedestal design was based on the improved second-generation pedestal design discussed by Crilly (1996). The pedestal extends through a 50 mm diameter hole in the cell base and is sealed using a large diameter O-ring. This pedestal was designed by Crilly (1996) and Tanaka (1995) to stop potential leakage into the specimen. A new titanium top cap was manufactured to fit the larger 63.5 mm diameter specimen.

Internal instrumentation to measure specimen deformation was added as part of this testing program. All tests were performed on air dry specimens, making the volume change device used by previous researchers on saturated clays unusable in this program. Measurement of changes in specimen dimensions in this program was achieved by using internally mounted linear variable differential transformer's (LVDT).

A schematic diagram of the instrumentation used to measure deformations in isotropic compression testing is shown in Figure 3.4. The horizontally mounted LVDTs measured the diameter change. The larger LVDT was mounted directly on the side of the specimen and recorded height changes over a gauged length. This instrumentation was only used for isotropic compression testing. Large changes in specimen height during shear would bend the pistons on the horizontally mounted LVDTs.

A schematic diagram of specially designed and constructed instrumentation used to record diameter changes during triaxial compression testing is shown in Figure 3.5. This

device, which will be described later, measured diameter change during the isotropic compression phase of each test, as well as during the constant cell pressure shear phase.

No instrumentation was used to measure axial strain during the isotropic compression of the specimens to be sheared. Therefore, relationships between the axial and radial strain were developed in six isotropic compression tests. These relationships were used to calculate the axial strain during the isotropic compression prior to shearing in the 23 triaxial compression tests.

3.3.3 Specimen-Forming Split Mold

A new specimen-forming split mold was manufactured to form specimens with a diameter of 63.5 mm. A schematic diagram of the specimen forming split mold is shown in Figure 3.6. The main features of this design are: a clamping ring, side holes and the lower grove. The clamping ring is used to hold together the split mold. Side holes allow a vacuum to be used to pull the membrane against the inside of the specimen-forming mold during specimen preparation. The lower grove allows an O-ring to be applied to hold the membrane to the pedestal prior to application of vacuum pressure and removal of the mold. In addition, a special mold was manufactured to cast the butyl rubber membranes used to encase the 63.5 mm specimens.

3.4 HITEP Triaxial Cell: Peripherals

This section discusses only the new instrumentation that was introduced for this program. Lingnau (1993) provides further information on the instrumentation used in the HITEP triaxial cells. Information about the choice of butyl rubber membranes used for high temperature testing is given by Tanaka (1995).

3.4.1 Axial Load

Axial loading was provided by a strain controlled 100 kN ELE load frame, with the axial load being measured by an internal load cell. For this testing program, a new Interface model 1211 - 44 kN (10 000 lb.) replaced an Interface 1211 - 22kN load cell used by earlier researchers. The 1211-44 kN load cell was pressure vented and temperature compensated similar to the previous load cell. The new load cell was of the same dimensions as the previous load cell, and was able to be submerged in the silicone oil used as cell fluid. The load cell was calibrated using a load frame in the structures laboratory at the University of Manitoba.

3.4.2 Internal Radial Displacement

Two different sets of (LVDT's) were used internally to directly measure the radial deformations of the specimens. These were shown schematically in Figure 3.4 and Figure 3.5.

For tests under isotropic compression only, two Trans Tek 0241 LVDTs were used. The LVDTs have a working range of approximately 5 mm and resolution of 0.5% at full scale. The outer casing was held stationary and the center rod moved as the specimen changed diameter. This instrumentation configuration is indicated in Figure 3.4.

Two model 0242 Trans Tek LVDT's were used to measure diameter changes in the 23 standard drained triaxial compression tests. The LVDT's were mounted on the device shown in Figure 3.5, which was in turn mounted to one of the internal tie rods of the cell. Movement of the two sliding arms along the stationary arms was measured by two LVDT's mounted along either stationary arm. Measurements from the two LVDT's was average to calculate the diameter change of the specimen. The two sliding arms were held in contact to the specimen by springs. The two model 0242 LVDT's have a working range of 12.7 mm and resolution of 0.5% at full scale.

The LVDT's were calibrated using a micrometer. The calibration was checked regularly throughout the experimental program, ensuring that the calibration factor was constant.

3.4.3 Internal Axial Displacement

A Trans Tek 0242 LVDTs was used to measure axial displacement during the six isotropic compression tests. The LVDT was mounted directly on to the cylindrical surface of the specimen. As shown in Figure 3.4, the LVDT measured length changes over the center portion of specimen. This was to minimize end effects. The distance over which the LVDT recorded height change was termed the gauge length. It was recorded before and after each test.

3.4.4 External Axial Displacement

Axial displacement during shearing was measured externally using a model 0244 Tran Tek LVDT. The 0244 Trans Tek LVDT has a working range of 25 mm with a resolution of 5% full scale. The LVDT was fixed to the top of the triaxial cell. It measured movement of the piston that was attached to the load cell, and hence the top of the specimen.

3.4.5 Data Acquisition and Storage

Axial stress and axial deformation were manually recorded throughout the 1-D compression testing. The manually recorded data were later transferred to a spreadsheet.

Results from isotropic compression tests and triaxial compression tests were recorded and stored using a computer and a data acquisition system (DAS). The DAS used for the majority of the tests was the existing system developed at the University of Manitoba and previously described by Lingnau (1993). The DAS was capable of carring 16 channels of information and could be used simultaneously on two different triaxial cells. The DAS and collection system were updated for the final few tests in the program. Labtek notebook and a new DAS were installed to allow greater flexibility in type and amount of data collected. The system consisted of two cards which received voltages from the various instruments. Voltages were sent to the computer where they were converted to data reading through calibration factors. The data were then displayed in real time and recorded to a file. The file of raw data was transferred to a spreadsheet for further manipulation.

3.5 Testing Procedures

As mentioned earlier, the test program consisted of ten 1-D compression tests, six non-standard isotropic compression tests and 23 high pressure drained triaxial compression

tests. The 1-D compression tests were performed in about one-half day each. The isotropic compression tests required one day each at room temperature, or two days if heated to 65°C or 100°C. Each triaxial compression test took two days to perform at room temperature, or three days if heated to 65°C or 100°C. While the number of tests is not exceptionally large, it should be emphasized that the tests were non-standard. The densities, stress levels and elevated temperatures in the program meant that considerable care had to be given to preparing specimens, ensuring good performance of membranes, test equipment and instrumentation. Much more attention was given to specimen deformations than is normal in such work.

3.5.1 Specimen Preparation

All specimens for the three test types were formed through dry pluviation, with additional tamping and vibration following the method described by Bishop and Henkel (1962). This procedure has been further detailed by Ferris and Graham (1996 e-j). The method worked very well for Ballotini and allowed specimens to be formed at or very near maximum density. This was important because AECL wanted material inside their containers to be as dense as possible. The minimum and maximum density, as well as voids ratio range for the materials are listed in Table 3.1. The method of specimen formation produced similar results for 'frac' sand, although the relative densities were not as high as those achieved for Ballotini. Details of the achieved densities for all tests will be given in Chapters 4 and 5.

3.5.2 One-Dimensional Compression

Specimens were prepared in the 1-D cell, close to the loading frame. A known mass of sand was placed into the cell and the height of the specimen was measured after the loading cap was placed on top of the specimen and rotated to produce a smooth top surface. Loading was performed in a strain controlled manner, with stresses being measured at fixed increments of strain. Prior to testing, a small seating load was applied and the deflectometer was zeroed. Cycling of the load (load-unload-reload) was performed in some tests.

3.5.3 Isotropic Compression

With one exception, the isotropic compression tests followed standard methods (Head 1991). After the specimen had been placed in the forming mold and the membrane attached to the top cap, approximately 0.1 MPa of suction was applied to the specimen. This allowed it to stand while the forming mold was removed. This is a significantly larger suction than is normally used. The minimum cell pressure used in the test program was 1.5 MPa so the 0.1 MPa applied suction was small relative to the cell pressure used in the tests. The instrumentation was installed and zeroed with the suction applied. Instruments recorded any changes to the specimen's dimensions. Once the cell sleeve had been installed and the initial cell pressure was applied, the suction was removed.

Isotropic compression tests that were not part of a triaxial compression test were subjected to a number of unload-reload cycles.

3.5.4 Triaxial Compression

The shear tests were standard consolidated drained triaxial compression tests (Head 1991), except that the cell pressures, and in many cases the temperatures, were much higher than usual. Throughout shearing, the cell pressure was held constant. Shearing was caused, as normal, by a strain-controlled increase in axial stress. In some of the tests, load cycling was performed. Shearing was stopped at around 10-12% axial strain.

3.6 Post test procedure

When the test was completed, a 0.1 MPa suction was reapplied to the specimen and the cell pressure reduced to zero. Final dimensions of the specimens were measured, and their final shape noted.

Sieve analysis was performed after completion of the test on most specimens. This was done to measure particle degradation caused by the stresses applied in the test. Tested material was not reused in subsequent tests.

Chapter 4 One-Dimensional Compression

4.1 Experimental Program

This chapter presents details of the one-dimensional (1-D) compression testing. The 1-D testing was performed to examine compression behaviour of dense sand at very high stress. The HITEP triaxial cell at the U of M's soil mechanics laboratory was limited to a maximum cell pressure of 10 MPa. In contrast, the newly manufactured 1-D compression cell was used to a maximum of 81 MPa applied axial stress. The 1-D compression test was also used to give a qualitative indication of expected behaviour in triaxial compression tests.

The 1-D compression test has an inherent indeterminacy in the stress conditions. The test apparatus imposes a condition of zero lateral strain. Application of vertical stress, in combination with zero lateral strain, is known as K_0-stressing. The K_0 (ratio of vertical to horizontal stress) conditions are unknown under the initial conditions, and vary with increasing applied vertical stress. As is customary, the cell was unable to read lateral stresses.

Ten tests were performed: five tests on Ballotini, two on 16-25 frac sand, and three on 20-40 frac sand. The tests followed the procedures outlined in Section 3.6. Table 4.1 summarizes the key sand properties and stress condition used in the testing program. The

table lists: test designation, material tested, initial voids ratio, density index, breakage potential and maximum axial applied stress.

The initial density index for the tests on Ballotini were in the range of 0.95-0.99, except in T1807, which had an initial density index of 0.85. The initial density index for the tests on 'Frac' sand ranged from 0.85 to 0.68. The minimum density index of 0.68 translates to a relative density (ρ/ρ_{max}) of 94%, indicating that even the lowest density in the test series corresponded to very dense material.

4.2 Experimental Results

4.2.1 Ballotini

Tests T1804 through T1808 were performed on Ballotini. The breakage potential of 92.8 was calculated from sieve analysis results, like those shown in Figure 3.3. Based on measured mass and dimensions, the initial density of the specimen was calculated. The initial density was used to calculate the initial voids ratio and density index, shown in Table 4.1. The calculation of density index used the previously calculated values of minimum and maximum voids ratio listed in Table 3.1. The initial voids ratio for these five tests varied from 0.5382 to 0.5567. These values translate to high density indices ranging from 0.998 to 0.848. The maximum axial stress applied for each test, listed in Table 4.1, varied from about 40 MPa for T1804 through T1806 to about 50 MPa for T1807 and T1808.

Results from the five 1-D compression tests on Ballotini are plotted in two ways in Figure 4.1. Figure 4.1a plots the results in terms of applied axial stress *versus* axial strain. Figure 4.1b plots the results in terms of the *log* of applied axial stress *versus* voids ratio. Separate plots for individual tests can be found in Ferris and Graham (1996a, 1996b).

Stress-strain curves for the five tests are concave towards the stress axis. Similar magnitudes of strain for applied stress were developed in all tests. Strains at 40 MPa applied stress ranged from 1.9% to 2.6%, shown in Figure 4.1a.

The confined compression lines shown in Figure 4.1b, indicate that the compression lines are similar when the initial voids ratios are similar. Tests T1805 and T1808 had initial voids ratios of 0.5440 and 0.5416 respectively. Results of 1-D compression of these two tests are almost identical. Similarly, initial voids ratios for T1804 and T1806 led to similar 1-D compression results. Tests with higher initial voids ratios (looser) were more compressible. The general shape of the curves in Figure 4.1b can be idealized as initially broadly linear, with development of curvature occuring as the stress level approaches 30 MPa.

Figure 4.2 plots results from test T1806, including the unloading and reloading cycles that were performed. Similar to Figure 4.1, results are plotted in both applied stress *versus*

axial strain space, shown in Figure 4.2a, and log applied stress *versus* voids ratio space, shown in Figure 4.2b.

Figure 4.2 indicates that some plastic strains are developed in the test. At an axial stress of 1.5 MPa, the voids ratio was about 0.533 for first time loading, and about 0.523 in the final unload cycle. The slope of the compression line for initial loading is steeper than the unload line, but only slightly steeper than the reload line, as shown in Figure 4.2b.

Some particle breakage can be seen from the before and after grain size distributions shown in Figure 4.3. Table 4.2 summarizes the important particle breakage parameters which are: total breakage, relative breakage and the stress level where cracking sounds were heard. Total breakage is a measure of the change grain size of the distribution for particles which will break. Relative breakage is a ratio of the amount of particle breakage which occurred to the amount which could occur. The definitions of total and relative breakage are given in Section 2.8.

The total breakage provides a way of measuring particle breakage, and in this case confirms that particles were being crushed during the tests. The stress level at which sounds of particle breakage could be heard aurally, was at about 36 MPa; about the same stress level where the curvature of the compression lines began, see Figure 4.1b.

4.2.2 'Frac' Sand

Tests T1809 through T1813 were performed on 'Frac' sand. Tests T1809 and T1810 were on the 16 - 25 sieve fraction and the other three tests were on the 20 - 40 sieve fraction. Breakage potentials of 70.1 and 48.2 were calculated respectively for the 16 - 25 and 20 - 40 sieve fractions from the sieve analysis results shown in Figure 3.3. Based on measured mass and dimensions, the initial density of each specimen was also calculated. The initial density was used to calculate that initial voids ratio and density index, is shown in Table 4.1. Calculation of density index the used previously calculated minimum and maximum voids ratios, listed in Table 3.1. The initial voids ratios for the two tests on the 16-25 sieve fraction varied from 0.4685 to 0.4711. This translates to density indices ranging from 0.811 to 0.820. The initial voids ratios for the three tests on the 20-40 sieve fraction varied from 0.4730 to 0.5221, which translates to density indices ranging from 0.854 to 0.678. The maximum axial stress applied for each test, listed in Table 4.1, was 80.5 MPa for tests T1809 through T1813.

To show how initial voids ratio would affect the response of the sand to loading, the three tests on the 20-40 sieve fraction were performed at progressively higher values of initial voids ratio.

Results from the five 1-D compression tests on 'Frac' sand are plotted in the two ways shown in Figure 4.4. Figure 4.4a plots the results in terms of applied axial stress *versus*

axial strain. Figure 4.4b plots the results in terms of the *log* of applied axial stress *versus* voids ratio. Plots for individual tests can be found in Ferris and Graham (1996c, 1996d).

Stress strain curves can be broken into two parts as shown in Figure 4.4a. The initial portion of the curve is concave towards the stress axis until approximately 50 MPa. Beyond this stress, a change in slope of the plotted results occurs, resulting in a second region of behaviour where a linear relationship exists between axial stress and strain.

The confined compression lines shown in Figure 4.4b, indicate the similarities and differences between the behaviour of the 16 -25 sieve fraction and the 20 - 40 sieve fraction of the same sand. Both sieve fractions become compressible, that is, they yield, at high stresses of about 35 MPa for the 16-25 sand and 43 MPa for the 20-40 sand, respectively. The effects of initial voids ratio can be seen in both gradations of the sand. Once the stress level is higher than the yield stress the behaviour for each test is almost identical. The slopes of the more compressible, post yield behaviour for the two different gradations are different.

The general shape of the curves in Figure 4.4b can be idealized as initially broadly bilinear. The first line describes the initial behaviour and the second describes the more compressible behaviour, with a yield point defining the change between the two linear portions. The similarity with the behaviour shown in Figure 2.9 is apparent.

Figure 4.5 plots results from test T1810 (on 16 – 25 frac sand), including unloading and reloading cycles. Similar to Figure 4.4, results are plotted in both applied stress *versus* axial strain space, shown in Figure 4.5a; and log applied stress *versus* voids ratio space, shown in Figure 4.5b.

Unlike the testing performed on Ballotini, 'Frac' sand showed considerably different behaviour in unload reload cycles from initial loading. It should be noted that the 'Frac' specimens were compressed to a maximum axial stress of 81 MPa, between 30 MPa and 40 MPa higher than the stress used on the Ballotini. Figure 4.5 plots the results for test T1810, in both axial stress *versus* axial strain space (Figure 4.5a) and *log* axial stress *versus* voids ratio space (Figure 4.5b).

The slopes of the unload-reload compression lines, shown in Figure 4.5b, are basically identical, regardless of the location in the initial loading curve. The first unload-reload cycle was performed near the transition to more compressible behaviour (grain crushing), and the second cycle was performed when the compressible behaviour was dominant. The figure indicates that plastic strains were developed in the test. At an axial stress of 1.5 MPa, the voids ratio was about 0.463 for first time loading, and about 0.382 in the final unload cycle. The slope of the compression line for initial loading is steeper than the unload-reload line, as shown in Figure 4.2b.

Some particle breakage occurred in the tests on 'Frac' sand, as seen from the 'before' and 'after' grain size distributions shown in Figure 4.6. Figure 4.6a plots before and after testing sieve analysis results for 16-25 'Frac' sand. Figure 4.6b plots before and after testing sieve analysis results for 20-40 'Frac' sand. Table 4.2 summarizes the important particle breakage parameters: total breakage, relative breakage and the stress level where cracking sounds were heard. The definitions of total and relative breakage were given in Section 2.8.

The total breakage numbers of 13 to 16 show that a consistent amount of particle breakage was occurring, and that more breakage occurred in these tests than those on Ballotini. The stress level at which sounds of particle breakage started to occur was about the same stress level where the curvature of the compression lines began to curve and the behaviour changed, see Figure 4.4b. The stress where noise first was heard for the 20 - 40 sand was higher for lower values of voids ratio (denser sand).

4.3 Interpretation of 1-D Compression Results

There are three stages of sand response to high stress loading (Hagerty et al 1993): prior to grain crushing, while grain crushing is occurring and after all grain crushing has taken place (Figure 2.20). The first and second stages of response were measured during this test program. In 1-D testing, Hagerty suggested that the third stage of behaviour began at

an applied stress level of 250 Mpa. Maximum axial stress in this program was 81 MPa, much lower than required to completely crush all the sand grains.

There are two main ways to interpret results from a one-dimensional compression tests: using stress-strain graphs and calculating a confined modulus (stiffness), or using the *log* stress voids ratio graphs and calculating a compression index.

4.3.1 Compression indices

The classic method of interpreting one-dimensional compression test results can be performed using the information plotted in Figure 4.1b and Figure 4.3b. This method is generally used for clays to determine not only deformations, but also the time dependent nature of the deformation. This way of interpreting data is also valid for sands. The term 'preconsolidation pressure', used in the classic interpretation of one-dimensional compression data, represents the past highest pressure. It separates behaviour into distinct regions. Application of stresses lower than the preconsolidation pressure result in elastic or mostly recoverable behaviour, corresponding to stage 1 behaviour. Stresses greater than the preconsolidation pressure result in elastic-plastic behaviour, corresponding to stage 2. Stage 1 response is described by a single compression index, the unload-reload index, C_r. The index C_r relates the change in voids ratio per *log* unit of stress, in the range from initial stress to the preconsolidation pressure. At stresses higher than the preconsolidation pressure, the behaviour is described by the compression index,

C_c. Like C_r, C_c describes a linear relationship between changes of voids ratio and *log* applied stress.

Results of test T1806 (Ballotini) and T1810 (16-25 'Frac' sand) were plotted together in *log* axial stress *versus* voids ratio space, as shown in Figure 4.7. The different materials have about the same slope to the initial loading line. They also show that the slope of the line increases when the stress goes higher than about 30 MPa. Test T1806 was not stressed to the same level as T1810. The stress level imposed on the Ballotini was not high enough to begin stage 2 behaviour. Therefore, no yield stress or C_c index could be interpreted for the tests on Ballotini.

As shown in Figure 4.7, for test T1806, the unload-reload behaviour is not much different from first loading. In comparison, test T1810 showed significant differences between unload-reload behaviour compared to first time loading. This indicates that the elastic-plastic stage of response to high stress (in which grain crushing is dominant), has not been reached in test T1806, but has been reached in test T1810. The response of test T1806 is largely elastic and recoverable, whereas test T1810 clearly exhibits non-recoverable strains. Supporting evidence that grain crushing is not occurring to a large degree in T1806 is found in the sieve analysis results, shown in Figure 4.3. Similarly, as shown in Table 4.2, total breakage, B_t values, are relatively low for T1806 and the other tests on Ballotini. Conversely, as shown in Figure 4.6, significant change took place in the grain size distribution for the 'Frac' sand, and Table 4.2 lists relatively large values of B_t.

Stage 2 behaviour in a 1-D compression test can be considered analogous to normal compression behaviour in a triaxial compression test (Coop 1990). Normal compression in a sand is due to grain crushing (Coop and Lee 1993). The 'Frac' sand was interpreted as having both first stage behaviour (C_r) and second stage behaviour (C_c) based on grain crushing, and the observed change in stiffnes during stressing. The Ballotini was interpreted as only exhibiting first stage behaviour (C_r).

The yield stress for the 'Frac' sand was approximately 50 MPa, and the maximum value of stress in the tests on Ballotini was only 50 MPa. It is likely that at higher stress levels, Ballotini would also show yielding and stage two behaviour.

Table 4.3 lists the values of: unload-reload index (from initial loading and in an unload-reload cycle) C_r, compression index C_c and interpreted yield stress. Rather than the classic term 'preconsolidation pressure', 'yield stress' was used to describe the transition from stage one to stage two compression behaviour.

The index values listed in Table 4.3 were calculated as linear fits to the data plotted in Figures 4.1b and 4.4b. In addition to the data shown in the figures, most tests had some unload-reload cycles performed during testing. The complete results of all tests are given in detail in Ferris and Graham (1996a,b,c,d).

The C_r initial value for 'Frac' sand was calculated using data from the beginning of the test, to within 10 MPa of the yield stress. By using data within the range 0 MPa to 30 MPa, as well as the reloading portion of the unload reload cycles, the C_r initial value for Ballotini was calculated. The C_r unload-reload value was calculated from the unload reload cycle. The complete unloading portion of the curve was used, as well as the reloading data from the lowest stress, to within 10 MPa of the past highest stress.

The C_c index value was calculated by using data from 10 MPa higher than the yield stress, to the highest stress reached during the test.

The value of C_r for initial loading of 'Frac' sand was 0.022±0.006 and 0.0209±0.004 for 16-25 sieve fraction and 20-40 sieve fraction, respectively. The value of the C_r from unload-reload testing was 0.0103±0.005 and 0.005±0.003 for 16-25 sieve fraction and 20-40 sieve fraction, respectively. The differences in the two calculated values quantifies the change due to plastic strains occurring in the initial loading. Comparing the calculated index values indicates that the 20-40 sand is stiffer (less change to voids ratio per unit stress) than the 16-25 sand.

In tests T1811, T1812 and T1813, the values of I_D were 0.854, 0.713 and 0.678, respectively, and the yield stress were 50 MPa, 44.4 MPa and 44.4 MPa, respectively. The stresses corresponding to where noise began in the three tests were 50 MPa, 39 MPa and 25 MPa. A lower value of I_D indicates that a soil has a looser structure. This means

that there are fewer particle-to-particle contacts, and therefore a higher value of interparticle forces for the same amount of externally applied stress

The value of the initial C_r index varies inversely with the density index, I_D. Four of the five tests on Ballotini had a I_D of 0.97±0.03, while the fifth had I_D=0.85. The values C_r in the first four tests were 0.016±0.002, while the fifth had a C_r of 0.027. Therefore, the lower the density, the more compressible the sand. In the case of the Ballotini testing, a difference of 0.12 in I_D (approximately 10%) made the sand nearly twice as compressible. The steeper slope in test T1807 is shown in Figure 4.1b.

The tests on 'Frac' sand also show the inverse relationship between initial C_r and I_D. The values of I_D for tests T1811, T1812 and T1813 are 0.854, 0.713 and 0.678, respectively, with corresponding C_r initial values of 0.0193, 0.0184 and 0.0251. This reinforces the observation earlier that looser structures as measured by I_D are more compressible.

The value of C_c does not depend on initial compaction. For tests T1811, T1812 and T1813, the value of I_D are 0.854, 0.713 and 0.678, respectively, yet the C_c index was 0.2744±0.0007. The unload-reload C_r value is also independent of the initial density index.

The initial C_c values are about one order of magnitude larger than initial C_r values. The unload-reload C_r is about one to two orders of magnitude lower than C_c. Comparable

differences between the deformation properties for carbonate sand were reported by Coop (1990).

In tests performed on calcareous sand, Coop (1990) concluded that crushing was equivalent, in some ways, to the so-called 'normal consolidation' process in clays. In particular, grain crushing produces volumetric strain hardening and expansion of the region of elastic behaviour. Figure 4.5b plots the complete results, including two separate unload reload cycles for T1810. The first unload-reload cycle was performed at a stress value which was near the interpreted yield stress for that test. The unload-reload C_r calculated for the first cycle is equal to the C_r value from the second unload-reload cycle. The second unload reload cycle was started from a stress beyond the initial yield stress, the stress was reduced below the initial yield stress. Upon reloading, the sand did not yield until the stress level was near the past highest pressure. Stressing through the original yield stress had no effect on the behaviour.

4.3.2 Confined modulus

The traditional logarithmic method of plotting 1-D compression test results, described in Section 4.3.1 has two mathematical problems (Hagerty et al 1993): prediction of negative voids ratio at extremely high stresses, and infinite voids ratio at zero stress. To avoid these problems, some researchers (for example Hagerty et al 1993, and Hardin 1987) use a confined modulus approach. The modulus is derived from arithmetic plots of stress

versus strain. There are two different ways of calculating the confined modulus for a 1-D compression test: as a constant stiffness in a selected stress range starting from zero stress, or incremental stiffness.

The constant stiffness approach is discussed first. Similar to the compression index approach, four values were calculated for each test: initial confined modulus, yield stress, crushing confined modulus and unload-reload confined modulus. The entire first loading phase (prior to unload reload) was used to calculate the constant initial confined modulus, D_i, for Ballotini. No yield stresses were observed in tests on Ballotini, as discussed in section 4.3.1. Similarly, the initial confined modulus for 'Frac' sand was calculated as the slope of the stress-strain curve below the yield stress. The crushing confined modulus, D_c, describes second stage behaviour after crushing had begun. It was calculated from data at stresses higher than the yield stress. The unload-reload modulus, D_r, was calculated as the slope of an unload-reload portion of the tests after the crushing behaviour had been initiated.

The initial confined modulus, D_i, for Ballotini, 16-25 and 20-40 'Frac' sand are 2480±500 MPa, 2165±183 MPa and 1851±304 MPa, respectively. For 16-25 and 20-40 'Frac' sand the crushing confined modulus, D_c, was 715±64 MPa and 840±59 MPa, respectively. The D_c is less than one half of the D_i value. For 16-25 and 20-40 'Frac' sand the unload-reload modulus, D_r, was 10590±1650 MPa and 9925±775 MPa, respectively. This is about one order of magnitude higher than the initial modulus.

Calculated values of D_i, D_c and D_r in Table 4.4 appear to be related to initial density, as expressed by density index I_D in Table 4.1. The yield stress in 20-40 'Frac' sand increases with increased density index, see Tables 4.1 and 4.4. This behaviour was also found using the traditional logarthimic plotting technique. Comparing values of yield stress listed in Tables 4.3 and 4.4, the interpreted yield stress from the two different techniques are similar.

The confined modulus of stiffness can also be calculated incrementally. Figure 4.8a plots the incremental confined modulus *versus* axial strain for Ballotini. The confined modulus increases with increasing axial strain up to the maximum axial strain achieved in the tests, approximately 3%. Figure 4.8b plots the incremental confined modulus *versus* axial strain for the tests on 'Frac' sand. The confined modulus increased from about 1000 MPa, to about 2200 MPa with increasing strain until about 1-2% axial strain. Continued straining decreased the confined modulus to about 750 MPa at 3.5% axial strain. The confined modulus remained at about this value for the remainder of the tests, to an axial strain of about 6.5%.

The constant confined crushing modulus, D_c, of 715 MPa and 840 MPa for the two gradations of 'Frac' sand, is about the same as the constant value of stiffness calculated incrementally. However, the initial confined modulus calculated incrementally, is not similar to the constant initial confined modulus, D_i.

4.4 Conclusions

Sand tested in 1-D compression can have its behaviour separated into two phases of response to axial stress. Stage 1 behaviour is defined as having mostly elastic deformations with no grain crushing. Stage 2 behaviour is defined by grain crushing, with mostly plastic deformations. A yield stress separates the two phases of response to stressing. These two stages of response to stressing in a 1-D compression test are the first two stages of the three stage response proposed by Hagerty et al. (1993).

Stage 2 behaviour is analogous to normal compression in a triaxial compression test on clays. It increases the current yield stress as it occurs, and is independent of initial density. The two stage behaviour in a 1-D test allows an elastic-plastic description of the response to high-stress 1-D loading.

Initial loading in a 1-D test not only induces elastic strains, but plastic strains as well when the yield stress is exceeded. Unload-reload cycles reveal the elastic portion of strain resulting from loading.

Dense sands are stiffer than loose sands. Compared with loose sands, dense sands have a higher initial yield stress, and begin to crush at a higher applied stress.

Chapter 5 Triaxial Compression Testing

5.1 Experimental Program

This chapter presents results of isotropic compression and triaxial compression testing performed on Ballotini and 20-40 'Frac' sand in the HITEP triaxial cell. Testing was performed at three different temperatures: 27°C (room temperature), 65°C and 100°C. The tests were performed at different temperatures to quantify the effect of temperature, if any, on the behaviour of these two materials.

Six isotropic compression only tests were performed: one on Ballotini and five on 20-40 'Frac' sand. The test on Ballotini was performed at 27°C. Two of the five tests on 20-40 'Frac' sand were performed at 27°C, two more at 65°C and one test at 100°C. The initial specific volume for the test on Ballotini was 1.5408. For the tests on 20-40 'Frac' sand, the initial specific volume was 1.4818±0.006.

Twenty-three drained triaxial compression tests were performed: three on Ballotini and 20 on 20-40 'Frac' sand. The three tests on Ballotini were at room temperature. Seven of the 20 tests on 'Frac' sand were performed at room temperature, an additional seven at 65°C and six tests at 100°C. The cell pressure (radial stress) used for testing Ballotini ranged from 2.5 MPa to 7.5 MPa. The cell pressure used for the tests on 20 40 "Frac'

sand ranged from 1.5 MPa to 7.0 MPa. These stress ranges are much higher than normal in geotechnical engineering practice.

5.2 Critical State and Other Key Conditions in a Triaxial Test

Five key stages can be identified in drained triaxial compression tests. They are: initial conditions, end of consolidation/initial conditions for start of shear, transition, peak strength and critical state.

The specific volume, or density, at which the specimen is prepared, defines the initial condition of a triaxial compression test. Throughout the isotropic compression phase of a triaxial compression test, the specific volume decreases. Conditions at the end of isotropic compression are defined in terms of both specific volume and confining pressure. The start and end conditions for the isotropic compression portion of the test are shown schematically in Figure 5.1a. The combination of mean stress and specific volume, that is, the soil's "state" at the end of consolidation, define also the initial conditions for shearing. The soil's "state" at this stage has been compared to the critical state line, to define the state parameter, described in section 2.4 (Been and Jefferies 1985). The state parameter has been used by Been and Jefferies as an indicator of expected behaviour in the shear phase of triaxial compression tests.

For drained triaxial compression tests on a loose sand (a sand where the combination of density and confining pressure makes the sand compressive under shearing), the transition, peak and critical state are coincident. For triaxial compression tests on dense (expansive) sands, they are distinctly separate conditions as shown in Figures 5.1 and 5.2. All the sands tested in this program were dense.

During the early stages of shearing, dense sand compresses until, at some small value of shear strain, the sand starts to dilate and total volume increases. The stress-strain condition where the rate of change in volume is instantaneously zero, is termed 'transition'. The transition point is shown in Figure 5.2.

Further shearing of the soil continues until a peak shear stress is reached, shown in Figure 5.2a and 5.2b. Peak shear stress occurs at the maximum dilatancy rate (rate of volume expansion per axial compression), shown in Figure 5.2b. Further shearing continues to expand the soil, with the amount of shear stress which the sand can sustain decreasing until the critical state condition is reached, shown in Figure 5.2a and 5.2b. At critical state, shear strains do not cause further changes to either the shear stress or volume strain. These four key points in the shearing phase of a drained triaxial compression test are shown schematically in *log* mean stress *versus* specific volume space in Figure 5.1b.

5.3 Isotropic Compression Results

5.3.1 Introduction

Isotropic compression tests, like those described in Chapter 3 involve application of an equal all-round pressure to the specimen.

Two different series of isotropic compression tests were performed: (1) isotropic compression only, including unload-reload cycles; and (2) isotropic compression as the preliminary phase of triaxial shear tests. For tests with isotropic compression only, both axial and radial deformations were measured. In the tests where isotropic compression was part of a triaxial shear test, only radial deformations were measured.

Thermally induced volume changes when specimens were heated from room temperature to 65°C or 100°C, were not considered in calculations of the initial voids ratio at the beginning of consolidation. Heating was being examined, it was done prior to the start of isotropic compression with a constant mean stress applied to the soil and the drainage leads open. Agar et al. (1986) measured thermal expansion of an oil sand from room temperature to 65°C as 0% and 0.01% for confining stresses of 50 kPa and 6 MPa respectively. The measured thermal expansion of an oil sand to 100°C was 0.075% to 0.150% for confining stresses of 50 kPa and 6 MPa, respectively. Therefore, any errors due to not including the temperature effects in the present program are small.

5.3.2 Isotropic Compression with Unload - Reload Cycles

Test T1839 was performed on Ballotini and another five tests were performed on 20-40 'Frac' sand. Tests T1837 through T1839 were performed at room temperature, T1840 and T1841 at 65°C and T1842 at 100°C. Table 5.1 lists the following parameters for the isotropic compression tests: test designation, temperature, initial specific volume, initial density index, breakage potential and the maximum radial stress (cell pressure) applied. The breakage potential, defined earlier on the basis of grain size measurements, was 92.8 for Ballotini and 48.2 for the 20-40 'Frac' sand. The maximum applied radial stress was 8.8 MPa for test T1842, and approximately 10.4 MPa in the other five tests. These are exceptionally high stresses in relation to most soil testing. The average initial specific volume for tests on 20-40 'Frac' sand was 1.4818±0.0057; for an average initial density index of 0.822±0.02. The test performed on Ballotini had an initial specific volume of 1.5408 and density index of 0.977.

Results from the isotropic compression test T1839 on Ballotini are plotted in Figure 5.3, including unload reload cycles. The results are plotted in two different ways: mean stress, p, *versus* volume strain, ε_v, shown in Figure 5.3a; and *ln* mean stress, p, *versus* specific volume, V, shown in Figure 5.3b. Volume strains were calculated from axial and radial strains which were themselves calculated from direct measurements of deformations. The measurements also permitted calculation of any shear strains that developed. In an

isotropic compression test, the mean stress, p, is equal to the confining pressure, the radial and axial stress being equal. The specific volume at each value of mean stress was calculated from $V_i = V_0 (1 - \varepsilon_{vi})$.

The plot of stress-strain results for Ballotini, Figure 5.3a, is concave towards the stress axis. The plot, which includes unload - reload behaviour, shows that not all of the strain is recovered when the stress is removed, presumably from a combination of particle relocation and fracture. The maximum measured strain was $\varepsilon_v = 2.38\%$, at a radial stress of 10.2 MPa. The strains resulting from the isotropic stressing to about 10 MPa are summarized in Table 5.2. The specific volume of the specimen was changed from 1.5408 to 1.5042, as shown in Figure 5.3b. The shear strain in the test was calculated to be -0.202%. This indicates that the specimen was anisotropic as a result of the preparation method.

The test data from T1839 have also been plotted as *ln* mean stress, p, *versus* specific volume, V in Figure 5.3b. The figure shows that the behaviour is broadly linear though slightly curved. Obviously, the figure again shows that most of the volume strain is recoverable, following initial loading. Sieve analysis of the specimen following testing, shows no significant change to the particle size distribution (See section 5.5.2 for further discussion of particle size distribution).

Figure 5.4 is a plot of isotropic compression results, minus the unload-reload cycles, from the five isotropic compression tests on 'Frac' sand. The unload-reload plot was omitted

from this figure for clarity. Figure 5.4a plots the results as mean stress, p *versus* volume strain, ε_v. Figure 5.4b shows the same results plotted as *ln* p *versus* specific volume V.

The stress-strain curves are concave towards the stress axis, as shown in Figure 5.4a. Tests T1840 and T1841 at 65°C developed slightly more strain for the same applied stress level than similar tests T1837 and T1838 at 27°C. The values of volume strain are about 2.0% and 1.7%, respectively at the end of testing. Test T1842 (100°C) had a volume strain of 1.4% at 8.8 MPa, the same as for test T1838 at that stress level. There does not, at first sight, appear to be a consistent variation with temperature. However, it appears there was a loss of strain control in T1842 at about 0.5% strain. After this stage of the test strain changes were lower than at 27°C and 65°C. The specific volume at the maximum stress ranged from 1.4415 to 1.4595; the final calculated volume strain ranged from 1.67% to 2.34%. Similar to the test on Ballotini, shear strain was developed in these tests. Test results for maximum stress levels are given in Table 5.2.

The plots of the isotropic compression test data in mean stress *ln*p *versus* specific,V space, Figure 5.4b, indicate that the behaviour was broadly linear after about 1 MPa, and that the behaviour was similar, regardless of temperature. The effect of a lower initial specific volume in test T1840 appears to be greater than the effect of temperature. Similar to the test on Ballotini, although not shown here, the behaviour of the sand in unloading-reloading showed that following initial loading, volume changes due to loading/unloading cycles are mostly recoverable.

Sieve analysis of the specimens following testing shows no significant change to the particle size distribution. Details will be given in section 5.5.

These six tests were performed with independent local measurement of both axial and radial deformation. This allowed calculation of the radial and vertical strain throughout the course of stress application. A linear relationship between the ratio of axial strain to radial strain, $\varepsilon_a/\varepsilon_r$ and current mean stress, p was developed. The linear relationship for Ballotini was $\varepsilon_a/\varepsilon_r = 0.2628 + 0.04059$ p, and the relationship for 'Frac' sand was $\varepsilon_a/\varepsilon_r = 0.7577 + 0.02726$ p. The measured relationship between axial and radial strains was used later to calculate axial strain during the isotropic compression phase of triaxial compression testing. This was required since only radial strains were measured in the isotropic compression phase of the triaxial compression test.

5.3.3 Isotropic Compression Phase of Triaxial Shear Tests

A summary of the initial and final conditions of the isotropic compression testing phase of the 23 triaxial shear tests is listed in Table 5.3. Listed in the table are; test designation, material tested, temperature of the test, initial specific volume, density index, initial mean stress, final mean stress, final specific volume, final volume strain and final shear strain. Tests T1815, T1816 and T1825 were performed on Ballotini, all other tests from T1814 through T1836 were performed on 20 - 40 'Frac' sand. The tests have been similarly

grouped according to temperature, in Table 5.3 through Table 5.6. Tests performed at room temperature were T1817, T1818, T1821, T1822, T1828, T1829 and T1831. Tests performed at about 65°C were T1814, T1819, T1820, T1823, T1826, T1830 and T1835. Tests performed at about 100°C were T1824, T1827, T1832, T1833, T1834 and T1836.

The three tests on Ballotini were formed at an initial specific volume of 1.5370±0.0062, corresponding to an initial density index of 0.986±0.028. Results of the isotropic compression testing are plotted in Figure 5.5. A plot of the tests in mean stress, p *versus* volume strain, ε_v space, is shown in Figure 5.5a. The isotropic compression results are also plotted in mean stress, *ln* p *versus* specific volume, V space, as shown in Figure 5.3b. This plot indicates good consistency between the three tests, which all show broadly linear behaviour although specimen T1825 is noticeably less stiff than the others. The reason is unknown.

The specimens for the 20 isotropic compression tests were formed at average initial specific volumes of 1.4844±0.007, 1.4853±0.002 and 1.4844±0.012 for tests at 27°C, 65° and 100°C, respectively. The average initial specific volume for all of these tests is 1.4847.

Figure 5.6 plots results from isotropic compression of 'Frac' sand at room temperature. Results are plotted in both mean stress, p *versus* volume strain, ε_v space, shown in Figure 5.6a, and specific volume V *versus ln* p space, shown in Figure 5.6b. Similarly, Figure

5.7 plots results of the isotropic compression at 65°C, and Figure 5.8 plots results of isotropic compression at 100°C.

The testing results plotted in Figures 5.6b through 5.8b show that the results of the isotropic compression are broadly linear. The plotted deformation pattern at the different temperatures is broadly similar bearing in mind the technical difficulties of measuring lateral deformations inside cells under high pressures up to 7.5 MPa and temperatures up to 100°C. Comparisons of these data are presented in chapter 6.

5.4 Triaxial Shear Results

5.4.1 Introduction

Drained triaxial compression shear tests (TXC) were performed using the standard method of increasing axial stress, σ_a while maintaining a constant radial stress, σ_r. The tests were performed at much higher stress levels than are typical in such tests. The triaxial compression test data have been plotted as: deviator stress, q *versus* shear strain, ε_s and volume strain, ε_v *versus* shear strain, ε_s. Unload-reload cycles were performed during some of the tests.

5.4.2 Ballotini

Three triaxial compression tests were conducted on Ballotini at room temperature. The initial conditions for the tests are shown in Table 5.3. They are: test designation, temperature, final specific volume (initial for the shear phase), final mean stress (constant radial stress) and final specific volume (initial specific volume for shear phase). The initial specific volume, V at the start of shearing ranged from 1.5241 to 1.5348. The radial stresses at which the tests were performed were: 2.50 MPa, 5.00 MPa and 7.55 MPa.

Results of the three triaxial compression tests on Ballotini are plotted in Figure 5.9. Figure 5.9a plots the results in terms of deviator stress, q *versus* shear strain, ε_s. Figure 5.9b plots the results in terms of the volume strain, ε_v *versus* shear strain, ε_s. These three tests displayed responses to shearing typical of dense sand. The deviator stress increases to a peak value, and then decreases, finally approaching constant values of shear stress. The specimens compressed initially (positive values of volume strain) to a transition, and then expanded with further increases in shear strain.

A loss of strain control occurred in the triaxial compression test with a radial stress of 7.5 MPa. Values of the initial, transition, peak and end of test conditions are included in Tables 5.3 through Table 5.6. In these three tests the following trends were noted:

1. The peak deviator stress value increased with increased radial stress. The peak deviator stress was 3.76 MPa, 6.13 MPa and 11.99 MPa for radial stresses of 2.5 MPa, 5.0 MPa and 7.55 MPa, respectively.
2. The shear strain at transition increased with increasing radial stress. The shear strain at the transition was 0.96%, 2.7% and 2.9% for radial stresses of 2.5 MPa, 5.0 MPa and 7.55 MPa, respectively.
3. The shear strain at which the peak deviator stress occurred was increased by increasing radial stress. The shear strain at the peak deviator stress was 2.2%, 2.9% and 3.3% for radial stresses of 2.5 MPa, 5.0 MPa and 7.55 MPa, respectively.
4. Volume strains decreased with increasing radial stress.

In these three tests, no significant change in the grain size distribution following testing was noted. Further discussion is included in section 5.5.

5.4.3 Room Temperature Tests on 'Frac' Sand

Seven triaxial compression shear tests were conducted on 'Frac' sand at room temperature. The initial conditions for the tests are shown in Table 5.3. They are: test designation, temperature, final specific volume (initial for the shear phase), final mean stress (constant radial stress) and final specific volume (initial specific volume for shear phase). The initial specific volume, V at the start of shearing, ranged from 1.4710 to

1.4842. The radial stresses used in the tests were: 5.03 MPa, 2.45 MPa, 7.01 MPa, 2.05 MPa, 1.51 MPa, 3.80 MPa, and 5.12 MPa.

Results of the seven triaxial compression tests are plotted in Figure 5.10. Figure 5.10a plots the results in terms of deviator stress, q *versus* shear strain, ε_s. Figure 5.10b plots the results in terms of the volume strain, ε_v *versus* shear strain, ε_s. These tests displayed the typical response of dense sand response to shearing. The deviator stress increases to the peak value, and then decreases, approaching a constant value of shear stress at shear strains typically beyond those reached in these tests. The specimen compressed initially (positive value of volume strain), to a transition, then it expanded with further increases in shear strain.

Three of the seven tests included some unload-reload testing. These were: T1828 (radial stress of 1.51 MPa), T1829 (radial stress of 3.8 MPa) and T1831 (radial stress of 5.12 MPa). Values of the initial, transition, peak and end of test conditions are included in Tables 5.3 through Table 5.6. Similar to the tests on Ballotini, the following trends were noted in these seven tests on 'Frac' sand:

1. The peak deviator stress value increased with increased radial stress. The peak deviator stress was 4.44 MPa, 5.36 MPa, 6.47 MPa, 9.56 MPa, 11.84 MPa, 9.93 MPa, and 15.09 MPa for radial stresses of 1.51 MPa, 2.05 MPa, 2.45 MPa, 3.8 MPa, 5.03 MPa, 5.12 MPa and 7.01 MPa, respectively.

2. The shear strain at transition increased with increasing radial stress. The shear strain at the transition was 0.76%, 0.93%, 1.03%, 1.12%, 1.82%, 1.08% and 2.28% for radial stresses 1.51 MPa, 2.05 MPa, 2.45 MPa, 3.8 MPa, 5.03 MPa, 5.12 MPa and 7.01 MPa, respectively.
3. The shear strain at which the peak deviator stress occurs is increased by increasing radial stress. The shear strain at the peak deviator stress was 3.41%, 4.02%, 4.17%, 3.82%, 4.22%, 3.98% and 4.36% for radial stresses of 1.51 MPa, 2.05 MPa, 2.45 MPa, 3.8 MPa, 5.03 MPa, 5.12 MPa and 7.01 MPa, respectively.
4. Dilatacy (volume expansion during shear) decreased with increasing radial stress. Volume strain rates $\delta\varepsilon_v/\delta\varepsilon_s$ were approximately constant. Volume strains decreased with increasing radial stress.

In these tests, changes in the grain size distribution following testing were noted. Tests at higher stress levels appeared to have more changes to the grain size than tests at lower stress levels. Further discussion of these changes is included in section 5.5.

5.4.4 65°C Tests on 'Frac' Sand

Seven triaxial compression tests were conducted on 'Frac' sand at 65°C. The initial conditions for the tests are shown in Table 5.3. They are: test designation, temperature, final specific volume (initial for the shear phase), final mean stress (constant radial stress) and final specific volume (initial specific volume for shear phase). The initial specific

volume, V at the start of shearing, ranged from 1.4759 to 1.4849. The radial stresses used in the tests were: 1.51 MPa, 5.02 MPa, 2.48 MPa, 6.02 MPa, 3.75 MPa, 3.65 MPa, and 7.14 MPa.

Results of the seven triaxial compression tests are plotted in Figure 5.11. Figure 5.11a plots the results in terms of deviator stress, q *versus* shear strain, ε_s. Figure 5.11b plots the results in terms of the volume strain, ε_v *versus* shear strain, ε_s. These tests displayed typical response of dense sand to shearing. The deviator stress increases to the peak value, and then decreases, towards a constant value of shear stress at large strains. The specimen compressed initially (positive value of volume strain), to a transition, then it expanded with further increases in shear strain.

Two of the seven tests included some unload-reload testing. These were: T1814 (radial stress of 1.51 MPa) and T1830 (radial stress of 3.65 MPa). Values of the initial, transition, peak and end of test conditions are included in Tables 5.3 through Table 5.6. Similar to the tests on Ballotini, the following trends were noted in these seven tests:

1. The peak deviator stress value increased with increased radial stress. The peak deviator stress was 4.25 MPa, 6.53 MPa, 9.00 MPa, 9.23 MPa, 11.76 MPa, 12.52 MPa, and 15.57 MPa for radial stresses of 1.51 MPa, 2.49 MPa, 3.65 MPa, 3.28 MPa, 5.03 MPa, 6.02 MPa and 7.14 MPa, respectively.
2. The shear strain at transition increased with increasing radial stress. The shear strain at the transition was 0.86%, 1.47%, 1.12%, 1.33%, 2.11%, 3.07% and 1.96% for

radial stresses 1.51 MPa, 2.49 MPa, 3.65 MPa, 3.28 MPa, 5.03 MPa, 6.02 MPa and 7.14 MPa, respectively.

3. The shear strain at which the peak deviator stress occurs is increased by increasing radial stress. The shear strain at the peak deviator stress was 3.94%, 3.9%, 2.23%, 3.87%, 3.7%, 4.13% and 2.96% for radial stresses of 1.51 MPa, 2.49 MPa, 3.65 MPa, 3.28 MPa, 5.03 MPa, 6.02 MPa and 7.14 MPa, respectively.
4. Dilatacy (volume expansion during shear) decreased with increasing radial stress. Volume strain rates $\delta\varepsilon_v/\delta\varepsilon_s$ were approximately constant although some variation was noted, possibly representing difficulties with the instrumentation at elevated temperature of 65°C. Volume strains decreased with increasing radial stress.

In these tests, some changes in the grain size distribution following testing were noted. Tests at higher stress levels appeared to have more changes to the grain size than tests at lower stress levels. Further discussion of these changes is included in section 5.5.

5.4.5 100°C Tests on 'Frac' Sand

Six triaxial compression tests were conducted on 'Frac' sand at 100°C. The initial conditions for the tests are shown in Table 5.3. They are: test designation, temperature, final specific volume (initial for the shear phase), final mean stress (constant radial stress) and final specific volume (initial specific volume for shear phase). The initial specific

volume, V at the start of shearing, ranged from 1.4716 to 1.4936. The radial stresses used in the tests were: 2.57 MPa, 1.56 MPa, 3.91 MPa, 4.93 MPa, 2.62 MPa, and 7.04 MPa.

Results of the six triaxial compression tests are plotted in Figure 5.12. Figure 5.12a plots the results in terms of deviator stress, q *versus* shear strain, ε_s. Figure 5.12b plots the results in terms of the volume strain, ε_v *versus* shear strain, ε_s. These tests displayed typical response of dense sand to shearing. The deviator stress increases to the peak value, and then decreases, approaching a constant value of shear stress at large strain. The specimens compressed initially (positive values of volume strain), to a transition, then they expanded with further increases in shear strain.

Two of the seven tests included some unload-reload testing. These were: T1827 (radial stress of 1.56 MPa) and T1832 (radial stress of 3.91 MPa). Values of the initial, transition, peak and end of test conditions are included in Tables 5.3 through Table 5.6. Similar to the tests on Ballotini, the following trends were noted in these six tests:

1. The peak deviator stress value increased with increased radial stress. The peak deviator stress was 3.03 MPa, 4.88 MPa, 4.99 MPa, 7.05 MPa, 8.83 MPa, and 11.98 MPa for radial stresses of 1.58 MPa, 2.57 MPa, 2.62 MPa, 3.91 MPa, 4.93 MPa and 7.03 MPa, respectively.
2. The shear strain at transition increased with increasing radial stress. The shear strain at the transition was 1.57%, 1.24%, 0.98%, 1.75%, 1.74% and 2.00% for radial

stresses of 1.58 MPa, 2.57 MPa, 2.62 MPa, 3.91 MPa, 4.93 MPa and 7.03 MPa, respectively.

3. The shear strain at which the peak deviator stress occurs is increased by increasing radial stress. The shear strain at the peak deviator stress was 3.33%, 3.55%, 3.33%, 3.55%, 3.84% and 2.89% for radial stresses of 1.58 MPa, 2.57 MPa, 2.62 MPa, 3.91 MPa, 4.93 MPa and 7.03 MPa, respectively.
4. Dilatacy (volume expansion during shear) decreased with increasing radial stress. Volume strain rates $\delta\varepsilon_v/\delta\varepsilon_s$ were approximately constant although some variation was noted, possibly representing difficulties with the instrumentation at elevated temperature of 100°C. Volume strains decreased with increasing radial stress.

In these tests, some changes in the grain size distribution following testing were noted. Tests at higher stress levels appeared to have more changes to the grain size than tests at lower stress levels. Further discussion of these changes is included in section 5.5.

5.5 Sieve Analysis Results

5.5.1 Introduction

After completion of most isotropic compression and triaxial compression tests sieve analysis was performed on the tested specimen to determine if grain crushing occurred during the test.

5.5.2 Isotropic Compression

A summary of the maximum mean stress levels applied throughout the tests as well as the breakage potential, total breakage and relative breakage is given in Table 5.7. Sieve analysis results for Ballotini before and after test T1839 are plotted in Figure 5.13a. Sieve analysis results for 'Frac' sand before and after the five separate isotropic compression tests, are shown in Figure 5.13b. As can be seen in Figure 5.13, very little change to the grain size distribution took place in the isotropic compression tests; no grain crushing occurred.

5.5.3 Triaxial Compression

A summary of the maximum mean and deviator stress levels applied throughout the test, as well as the breakage potential, total breakage and relative breakage are given in Table 5.7. Sieve analysis results on Ballotini used in triaxial compression tests at room temperature, are shown in Figure 5.14a. Sieve analysis results on 'Frac' sand used in triaxial compression tests at room temperature are shown in Figure 5.14b. Sieve analysis results on 'Frac' sand used in triaxial compression tests at 65°C are shown in Figure 5.15a. Sieve analysis results on 'Frac' sand used in triaxial compression tests at 100°C, are shown in Figure 5.15b. As shown in Figures 5.14 and 5.15 some changes to the grain size distribution were recorded. In the tests performed at the highest values of radial

stress, changes of individual grain size up to 5% by weight were recorded with some of the smaller grain sizes. The amount of recorded grain crushing was larger values of confining pressure were higher.

Chapter 6 Triaxial Compression Testing: Interpretation

6.1 Introduction

This chapter presents an elastic-plastic interpretation of the testing results presented in Chapter 5. Some results from one dimensional compression testing presented in Chapter 4, are used in this chapter to define parameters for the elastic plastic model. The base elastic plastic model used in this chapter is Cam Clay, as described by Roscoe and Burland (Wood 1990).

As discussed in Chapter 2, the main deficiency of the Cam Clay model when applied to sand is the apparent lack of a normal compression line in the stress range of most geotechnical problems. In addition, determination of the critical state line from triaxial compression tests on dense sand, is more difficult than testing loose sand, due to the formation of shear bands. Despite the difficulty of determining the critical state line for dense sand, provided some modifications are incorporated, the Cam Clay model can be successfully used to model sand behaviour.

The Cam Clay model, like all elastic plastic models, makes the fundamental assumption that strain can be divided into elastic and plastic components. In the Cam Clay model a yield surface defines the transition from elastic behaviour from plastic behaviour. Dense sand or overconsolidated clay sheared beyond failure leads to plastic softening and

reduction of the elastic region, while loose sands and normally consolidated clays produce plastic hardening and increased regions of elastic behaviour.

Due to the research needs of AECL the two sands ('Frac' sand and Ballotini) tested in triaxial compression in this program, were prepared to be consistently dense and therefore dilative in shear. Although a dense sand can be contractive if the applied mean stress large enough, all tests in this program were dilative and shear bands developed throughout the testing.

6.2 Particle Breakage

Modification of the individual particles due to high stresses was not part of the original Cam Clay model formulation. Cam Clay was developed for soils tested in low to medium stress ranges, that is, prior to the development of grain crushing.

Changes to particle size distribution were measured in eight of the 18 triaxial compression tests on 20-40 'Frac' sand. Only two of the 20 triaxial compression tests on 'Frac' sand did not include, a post-test sieve analysis. A summary of particle breakage which occurred in the triaxial compression shear test was given in Table 5.7. The amount of grain crushing which occurred in each test, and whether or not grain crushing occurred, varied with the applied stress. No consistent variation of grain crushing with temperature was noted in this testing (Appendix A). Grain crushing was not measured in any of the

isotropic compression testing ('Frac' sand or Ballotini), nor any of the triaxial compression testing on Ballotini. For the triaxial compression testing on 'Frac' sand, particle breakage occurred in the tests with high applied stresses. A plot of the maximum mean and deviator stresses applied to the 'Frac' sand specimens is presented in Figure 6.1a. The figure indicates whether particle breakage occurred or not. With one exception, the combination of mean stress and deviator stress at failure at which particle breakage began in these tests, was approximately p = 8 MPa and q = 10 MPa (this corresponds to an initial radial stress of approximately 4.7 MPa). In contrast, isotropic compression testing up to a mean stress of 10.4 MPa did not result in any measurable particle breakage. Testing 'Frac' sand in one dimensional compression (Chapter 4) indicates that particle breakage starts to occur at an axial stress of 25 MPa, corresponding to a mean stress of 15 MPa based on a K_0 of 0.4.

The maximum mean stress which was applied in the tests on 'Frac' sand, has been plotted against the relative breakage in Figure 6.1b, defined in section 2.8. Although there is considerable scatter in the results this figure highlights the intuitive relationship that more grain crushing occurs when the applied stress is greater. Coop and Lee (1994) plotted a similar relationship for weaker grained carbonate sands. They developed two separate relationships, one for isotropic compression and another for maximum mean stress in shearing. The two lines were drawn parallel in the B_r versus p space used in Figure 6.1b. It is thought that this reflects the parallel behaviour of the NCL and CSL once grain crushing is initiated. Coop's research on carbonate sand showed that the NCL is only defined when the stresses are sufficiently high to produce grain crushing. Typically, prior

to Coop's research, sand was considered to have NCLs that extended over all values of mean stress. The Cam Clay model assumes that the NCL and CSL are parallel. Coop's research suggests this is only true after grain crushing has been initiated.

6.3 Cam Clay Interpretation

6.3.1 Isotropic Compression

In Cam Clay, isotropic compression testing is used to determine three of the six parameters used in the model. These three parameters are V_λ, λ and κ, the definitions of which were given in Chapter 2. The parameters V_λ and λ define the position of the NCL, and κ defines the behaviour of an overconsolidated soil.

Stress-strain behaviour of a soil on its NCL has both elastic and plastic components, with the plastic strains being dominant. In Cam Clay, isotropic compression at stresses lower than required to develop the NCL, is strictly 'elastic'. The slope of the initial loading curve for sand varies with the initial specific volume (Figure 2.7). Due to the narrow range of initial specific volumes tested in this program, 1.4818±0.0057, the specific volume effect was not seen in this testing. Isotropic compression testing of the 'Frac' sand and Ballotini showed that some plastic strains were developed at large stress levels (Figure 5.3b). It was concluded that the isotropic compression tests could not be used to define NCL as the applied stress levels did not induce grain crushing. The value of λ can

also be calculated from the slope of the CSL, as it is parallel to the NCL. Large volume strains during shear meant that end-of-test values could be used to evaluate the CSL and hence λ.

Results presented by Coop (1990) showed that there is a NCL in sands, but that it is defined from the particle crushing behaviour, as shown in Figure 2.9. Coop also showed that the slope of the NCL, λ, is approximately equal to the slope of the grain crushing region of the one dimensional compression test, plotted in the same space. The line defining crushing behaviour in one dimensional compression plots to the left of the NCL, as shown in Figure 2.9.

Typically in CSSM when plotting the natural logarithmic of mean stress *versus* specific volume, the stress data is given in kPa, this convention was followed in this thesis report. Prior to plotting the data the natural logarithm of the value of mean stress was calculated. These values were then plotted *versus* specific volume.

In order to obtain another estimate of the value of λ for the Cam Clay model, further examination of the 1-D compression testing was performed. Results from a 1-D compression test, as well as two of the isotropic compression tests are plotted in Figure 6.2a. From this figure, it is apparent that the sand tested in 1-D compression has gone through a change in material behaviour at about 36.3 MPa, the 1-D compression data was converted to mean stress based on $K_0 = 0.4$. The isotropic compression tests did not reach this level but are broadly similar in the pre-yield range. Coop and Lee did 1-D and

isotropic compression testing on a carbonate sand and found that the transition from non-crushing to crushing behaviour occurred on the weaker grained sand at a pressure of about 600 kPa in 1-D compression and about 800 kPa in isotropic compression. Therefore the stress level at which 'Frac' sand will begin to crush (which defines the NCL) can be expected to be greater than 36.3 MPa in isotropic compression. Based on the slope of the grain crushing region of the three 1-D compression tests, the value of λ for 'Frac' sand is 0.108.

Data from isotropic and 1-D compression tests on Ballotini are plotted in Figure 6.2b. They indicate that the transition to crushing behaviour was not reached in either of the test types at pressures up to 40 MPa. Based on grain size analysis, there was no measured particle crushing in these tests. Therefore, the slope of the NCL could not be defined from either test.

In order to define the isotropic elastic behaviour prior to reaching yield at the NCL, the Cam Clay model uses a 'κ' line with a slope of κ in specific volume versus mean stress space. In remolded clay soils, the initial slope of isotropic compression results can be used to define the κ line. Normally, the behaviour of the soil when unloaded and reloaded in used to define the κ line. Using the unload-reload portion of the isotropic compression tests in this program (Ferris and Graham 1996 e,f) , the slope of the κ line for 'Frac' sand is $\kappa = 0.0065$. The calculated κ value for Ballotini is 0.0092.

The end of consolidation for all the tests on 'Frac' sand are plotted in Figure 6.3a. The best fit line for these data has a slope of 0.0063, which compares well with the value calculated from the unload-reload behaviour of the isotropic compression tests. As previously discussed, the slope of the isotropic compression test results depends on the initial specific volume. The agreement between the values of 0.0065 obtained from the unload-reload plots and the 0.0063 obtained from the end-of-consolidation results is expected since all of the initial specific volumes were within a narrow band near the minimum specific volume of the dense sand that was tested.

The end of consolidation for the tests on Ballotini are plotted in Figure 6.3b. Due to the limited number of tests and the scatter of the results, a comparison of the best fit line to the calculated slope of the κ line was not performed.

6.3.2 Triaxial Shearing

The shearing phase of the triaxial compression test is used to define three additional parameters of the Cam Clay model, G, M and N. Definition of the parameters was given in Chapter 2. The term N locates the CSL (with slope λ) in specific volume *versus* lnp space, G defines the shear stiffness within the yield surface, and M defines the ratio of deviator to mean stress at the CSL. Since the slope of the NCL was not defined by the isotropic compression testing on Ballotini, determination of the slope of the CSL will be used to define the slope of the NCL since the two are parallel in the Cam Clay model.

Results from the end of test on 'Frac' sand, (ignoring any final unloading data) are shown in Figure 6.4a plotted as specific volume *versus ln* p space. The data were separated according to whether grain crushing occurred or not. While there is considerable scatter in the data in the figure, it should be remembered that the range of specific volume is small, close to the limit of where it can be successfully measured. Linear interpretation of each of the data sets plotted in Figure 6.4a, suggest that two distinct responses to stressing occurred, one stiff, and one more compressible. The two different types of behaviour were separated at a mean stress of 7.6 MPa. The slope of the end of test envelopes were 0.028 and 0.219 for non grain crushing and grain crushing behaviour, respectively. From the assumed parallel nature of the NCL and CSL the later number is believed to represent the slope λ.

The slopes of the NCL, CSL and results from a 1-D compression test that are plotted as specific volume versus ln p are approximately equal (Coop 1990, Atkinson 1993). However in this case, the value of λ from 1-D compression tests was 0.108, versus 0.219 calculated from the end of test results from triaxial shearing tests. These values are different by a factor of 2. Possible explanations for this difference include:

1. Yielding due to grain crushing began at about 7.6 MPa and the maximum p was only 12 MPa, meaning that the λ was estimated from only a short length of the specific volume versus ln p curve;
2. Difficulties associated with determining the CSL from dense sand, because of the development of shear bands; and,

3. In the 1-D compression results K_0 may change when grain crushing occurs, this will change the conversion from vertical stress to mean stress space.

Although these problems exist, it is considered that the end of test values are the best available estimate of the slope of the CSL.

In order to define the CSL in specific volume versus mean stress space, the value of Γ, (the specific volume at a mean stress of 1 kPa) needs to be defined. The calculated value of Gamma was 1.8701 and 2.9551 for 'Frac' sand and Ballotini respectively. For 'Frac' sand, the gamma value is defined for the non grain crushing region of the CSL.

No consistent effects from temperature on either the grain crushing or the slope of the end of test values were observed (Appendix A).

The end of shearing results from the tests on Ballotini, plotted in terms of specific volume versus ln p space, are shown in Figure 6.4b. As noted previously, no grain crushing was noted in the tests on Ballotini, therefore the slope of the CSL could only be defined in the non-grain crushing region. The slope of the CSL in Figure 6.4b corresponds to λ of 0.148.

Figures 6.5a and Figure 6.5b plot values of initial specific volume and mean stress at the end of consolidation for 'Frac' sand and Ballotini respectively. The figures also show the calculated CSL's that were inferred from Figures 6.4a and 6.4b, respectively. These plots show that the state of the sand prior to triaxial compression is 'dry', that is, on the dense

side of the critical state line. Based on the data in Figure 6.5a, isotropic compression of the specimens along a kappa line to a mean stress of approximately 14.0 MPa would be required to produce loose (contractive) behaviour.

Unlike some previous researchers Coop and Lee did not find any curvature of the CSL in q-p space, in their tests on carbonate sand. They postulated that any curvature in the q-p plot is likely due to incomplete testing of the soil. In their triaxial compression tests on carbonate sands the initial mean stress varied up to 9 MPa, and grain crushing became the dominant mechanism at a mean stress as low as 0.6 MPa. In the tests reported here crushing began at a mean stress of 5.7 MPa and the maximum initial mean stress was approximately 7 MPa. Therefore, behaviour before grain crushing and after grain crushing were examined separately.

The end-of-test strength results for 'Frac' sand, separated according to grain crushing, are plotted as mean stress *versus* deviator stress in Figure 6.6a. The slope (M) of the linear fit (through the origin) of the data prior to grain crushing is 1.15, and after grain crushing is 0.97. The transition stress between the two linearly interpreted lines to define the end of test envelope is, 4.8 MPa. This value is significantly lower than the transition in the specific volume *versus* mean stress space, 7.6 MPa calculated previously.

In the three tests performed on Ballotini, the stress levels were not high enough to induce grain crushing Therefore, the end of test envelope plotted in Figure 6.6b which defines the CSL, is only defined prior to grain crushing. As in other plots of Ballotini data there

is some statter in the results. It is expected that if the stress levels were high enough, a bilinear line could also be defined for Ballotini. The slope of the linear interpolation line (M) for these limited results, is 0.83.

Triaxial tests on dense sand produce shear bands. As a result, there are always questions about the validity of the CSL determined from this type of test. A check on the CSL values in mean stress *versus* deviator stress space can be obtained from the transition point where the change in volume strain is instantaneously zero. This occurs relatively early in the test and has been correlated with CSL behaviour by Atkinson 1993. The transition point data are plotted along with end-of-test data for 'Frac' sand in Figure 6.7a. The transition point data plot slightly above the end-of-test data in this figure, indicating that the transition points suggest a higher ratio of q/p in this case. In the same way as the end-of-test data, the transition points were separated in terms of crushing and noncrushing, and linear interpolation was performed. The envelope of transition point data produces η (q/p) = 1.26 in the pre-crushing range, and a η = 1.17 in the post-crushing range. The pressure at which behaviour changes to post-crushing behaviour is 6.4 MPa. Compared to the value of 4.8 MPa from the corresponding end of test data, this value of 6.4 MPa is closer to the value calculated from the specific volume *versus* mean stress plot of 7.6 MPa.

The transition data from the tests on Ballotini are plotted in q-p space, along with the end-of-test data in Figure 6.7b. The calculated ratio of q/p from the transition point data is essentially the same as the ratio calculated from the end-of-test data. This re-confirms

that in the pre-crushing region of stress, the CSL for Ballotini can be characterized by an M value of 0.83.

As noted previously, a sand which shows dilative behaviour at low stress levels gradually changes to having compressive behaviour at high stress levels. Although the stress levels applied in this testing program were not high enough to produce compressive behaviour, there was a trend to less dilative behaviour at high confining stress. If in fact the behaviour had become compressive, the transition, peak and critical state conditions would have been coincident. Measured values for these three separate conditions are plotted in terms of stress ratio, η versus confining pressure in Figure 6.8a. As expected the trend of the data for all three conditions is for the stress ratio η to decrease with increasing values of initial radial stress. The data for the end-of-test condition are considerably more scattered and do not converge like the other two conditions, probably due to the formation of shear bands. The linear fits to the data from the transition and peak conditions meet at a confining stress of about 9.6 MPa.

In general, more compressible sands require more strain to reach peak stress than dilative sands. Therefore, the strain required to reach the peak stress should increase as the confining stress increases (and modifies the behaviour from dilative to compressive). Figure 6.8b plots shear strain versus confining stress for 'Frac' sand at both peak stress ratio and the zero volume change rate transition point. The shear strain at which the peak stress ratio occurs varies only slightly in the tested range of stress. However, the shear strain at which the transition point is reached, increases with increasing confining

pressure. This indicates reduced brittleness. It is expected that once the strain at which the transition condition occurs is equal to the strain at the peak stress the sand can be considered compressive. The interpreted "transition" confining stress was calculated to be 14.0 MPa and 13.0 MPa from Figure 6.5a and Figure 6.8b, respectively.

The data plotted in Figures 6.8a and 6.8b confirm that increases in confining pressure were changing the response of the sand from dilative to compressive. The consistency of the transition condition data as compared to the end of test data, makes them a better indicator of the CSL than end of test data, and were therefore used to define the CSL.

Figure 6.9a and 6.9b summarize the strength envelope results for 'Frac' sand and Ballotini, respectively. The data show that the peak stress envelopes are greater than the critical state stress envelopes, but not by large amounts as measured in terms of stress ratio, $\eta=q/p$. At the lower end of the stresses shown in Figure 6.9a for 'Frac' sand, there is a larger difference between the peak stress and critical state stress than at the upper end of the stress range. The difference is due to dilatancy which is inhibited at larger values of confining pressure. The data plotted in Figure 6.9b for Ballotini, should be considered incomplete. It is expected that with more tests, the results would show a similar trend to that for 'Frac' sand.

Dilatancy is the term used to describe volume expansion of dense granular soils, including sands, when sheared. Dense sand expands when sheared because the current specific volume is smaller than the specific volume on the CSL at the current value of

mean stress. Expansion during shearing beyond the peak stress increases the specific volume towards the value it would have on the CSL at the current value of stress.

Bolton (1986) discussed the effects of dilatancy, and showed that the peak stress ratio was greater than critical stress ratio. He showed that at a given pressure, the initial density (relative density) controls the amount of dilatancy which will occur when the sand is sheared. The lower the specific volume the more dilatancy that will occur at a given mean stress. A measure of the dilatancy angle for 'Frac' sand can be calculated from the difference between the slope M of the CSL and the q/p ratio at peak stress. This value is plotted Figure 6.10a *versus* the confining pressure. The data plotted in the figure indicate that the level of dilatancy decreased as the confining pressure increased. As discussed previously, this reflects the transition from dilative to compressive behaviour. The same effect is shown in a different manner in Figure 6.10b, which plots of the peak q/p ratio *versus* the confining pressure. Also included on this figure is the critical state stress ratio. The difference between the critical state stress ratio and the plotted data is the dilatancy effect.

The final parameter needed to complete the Cam Clay model, is the value of elastic shear modulus. It will be remembered that the Cam Clay model assumes that elastic volumetric strains due to changes of the mean stress are defined by the value of κ, the current value of specific volume and the mean stress. For shear, it assumes that elastic shear strains are caused by changes to the deviator stress, and that these are related through a constant

shear modulus G within the yield surface. That is, the volumetric and shear strains are uncoupled, and the material is isotropic.

The shear modulus can be determined from the shearing phase of the triaxial test. Three different approaches were used to calculate the shear modulus for the 'Frac' sand;

1. based on the peak deviator stress, taken as the secant modulus, q/ε_s at peak q;
2. based on the strain at 50% of the peak deviator stress, calculated as the secant modulus between the start of shearing and the 50% pf peak deviator stress; and,
3. based on the slope of unload-reload segments of the stress strain curve.

Values of shear modulus calculated for each of these conditions are summarized in Table 6.1. The column of shear modulus calculated from unload-reload segments has multiple entries when multiple unload-reload cycles were performed.

Regression shows the the shear modulus calculated based on the peak deviator stress, is approximately related to the initial mean stress by the equation $3G = 64.2\ \sigma_r$, where σ_r is the confining pressure. This relationship is shown in Figure 6.11a. Similarly, the relationship was calculated to be $3G_{50} = 214.9\ \sigma_r$ for data from the secant modulus at 50% of maximum deviator stress. The data are shown in Figure 6.11b. These two figures are evidence that the shear modulus depends on the confining pressure during the test, to which deviator stresses are added. In contrast with the Cam Clay model, the shear modulus does not appear to be constant. Shear strain and pressure level both affect the value of the shear modulus.

Calculated values of the shear modulus at both peak stress and 50% of the peak are shown in Figure 6.12a and Figure 6.12b, respectively stress for Ballotini. Similar to the data from 'Frac' sand testing shown in Figure 6.11, the shear modulus depends on the initial mean stress. The limited data suggest the relationships between confining pressure and shear modulus are $3G = 49.3\ \sigma_r$ for peak deviator stress data and $3G = 146.5\ \sigma_r$ for secant modulus at 50% of the peak value of deviator stress.

Values of shear modulus calculated from unload reload cycles on 'Frac' sand (listed in Table 6.1) are plotted versus the confining pressure in Figure 6.13. The calculated linear relationship for this data is $3G = 208.2\ \sigma_r$ which is very similar to the data from the 50% of the peak, although there is large scatter in the data. As shown in Figure 6.13 the linear relationship between the initial radial stress and shear modulus is not strong. A numeric average of the data 3G = 761.0 MPa has a similar correlation factor to the linear correlation with confining pressure.

The unload-reload testing performed on the 'Frac' sand avoids the effects of initial fabric due to the specimen formation. It should therefore be a better estimate of the shear modulus. Based on the results for 'Frac' sand shown in Table 6.1, the unload-reload data are similar to the modulus calculated from the 50% peak deviator stress. For Ballotini, the average of the 50% peak deviator stress was used to define the shear modulus. This produced a value of 3G = 762.6 MPa.

Results presented in Figures 6.11, 6.12 and 6.13 show that a relationship exists between the behaviour in shear and confining pressure. Although the initial specific volumes for all the tests were within a narrow range for 'Frac' sand, the differences in shear modulus with confining pressure indicates behaviour inconsistent with the Cam Clay model. As stated earlier, the Cam Clay model uses only one value for the shear modulus. From the calculated values of shear modulus, the best interpretation of shear modulus for use in a generalized Cam Clay model would be the average value at 50% peak strength and the unload-reload value. This produces 3G = 761 MPa.

The test data on 'Frac' sand indicate that as the confining pressure is increased the stiffness increases, as shown in Figure 6.11 and Figure 6.12, but the peak strength ratio decreases, as shown in Figure 6.10b.

The bilinear CSL curve shown in Figure 6.4a involves a necessary modification to the Cam Clay model. Similar non-linear CSLs have been noted by Vesic and Clough (1968) and Lee and Seed (1967). The non-linear CSL was attributed by those researchers to variations in the components making up the shear resistance, namely sliding friction, dilatancy and grain crushing. In this thesis report, the CSL has been treated as bilinear, with a change in slope at the mean stress defining the onset of grain crushing. Grain crushing in the 'Frac' sand began at a mean stress of approximately 7 MPa. Prior to grain crushing, the CSL can be described by the equation V=1.8701-0.028 *ln*p. The parameter Γ_c = 1.6217 combined with the transition stress of 7 MPa define the change in slope of

the CSL. At stresses larger than 7 MPa the CSL is defined by the equation V = 1.6217 - 0.108 *ln*p. Similarly in q-p space, the CSL is defined by the slope M = 1.26 prior to grain crushing and M = 1.17 after grain crushing. Table 6.2 summarizes of the Cam Clay parameters used to describe the 'Frac' sand and the Ballotini tested in this program. Parameters missing from this table could not be determined from the test program that was performed.

6.4 Cam Clay Modifications

6.4.1 Shear Modulus

Previous sections of this chapter have proposed modifications to the basic Cam Clay model to reflect changes in the CSL in both q-p plots and V-*ln*p plots due to grain crushing. Although a single-value was given in Table 6.2 for the shear modulus $3G \approx 760$ MPa, comparison of the data in figures 6.11 and 6.12 shows the shear modulus depends on strain levels. The single value shear modulus used in the Cam Clay model should clearly be modified in order to model the observed behaviour more effectively. Section 6.4.1 outlines an approach which expresses the shear modulus as a function of shear strain and uses this relationship to define 'pre-failure' behaviour of 'Frac' sand and Ballotini.

Many laboratory and field programs have shown that small-strain behaviour during pre-failure deformation can not be described by a constant shear modulus, but that the shear modulus varies with the amount of strain. This produces 'G-γ' relationships such as those shown by Iwasaki et al (1978) and Jardine et al. (1986).

Variations in the shear modulus with strain levels was first reported in literature in 1979 by Simpson et al.(1979). Description of the pre-failure deformation of soils has received increasing attention over the last decade, and the consensus regarding the small strain behaviour is that there are different phases of behaviour. The first at very small strains is truly elastic behaviour. The behaviour was modeled by Al-Tabbaa and Wood (1989) using an inner Cam Clay ellipse to define the truly elastic behaviour.

The shear stiffness can be calculated incrementally in successive segments in plots of q *versus* shear strain. When this is done for Ballotini throughout the initial parts of the shear tests, the results reveal that the shear modulus is approximately constant initially, and then gradually decreases to zero, as shown in Figure 6.14a. In the three tests on Ballotini, values of the initial incrementally calculated shear modulus are approximately 190 MPa, 260 MPa and 400 MPa for confining pressures of 2.50 MPa, 5.0 MPa and 7.55 MPa, respectively.

The results of the initial loading on 'Frac' sand were similarily calculated and plotted in Figure 6.14b, Figure 6.15a and Figure 6.15b for the low, medium and high stress ranges of the tests. The calculated shear modulus is approximately constant, then reduces to

approximately zero. From these three figures, the initial value of the incrementally calculated shear modulus is approximately 200 MPa, 300 MPa, 400 MPa, 450 MPa and 600 MPa for confining pressure values of 1.5 MPa, 2.5 MPa, 3.75 MPa, 5.00 MPa and 7.00 MPa, respectively. As is common with the instrumentation and plotting that were used, there is considerable statter in the data.

As previously discussed, unload-reload cycles were performed during some of the triaxial compression tests. Plots of the incrementally calculated shear modulus *versus* shear strain for the reloading portion of the tests are shown in Figure 6.16. Based on reloading, the initial incrementally calculated shear modulus is approximately 300 MPa, 500 MPa and 800 MPa for confining pressure values of 1.51 MPa, 3.7 MPa and 5.00 MPa, respectively. These values are slightly higher than those calculated from the initial loading segments of the test. Particle rearrangement and particle crushing during the initial loading are likely causes of the observed increase in stiffness at low strain levels.

As mentioned earlier, the single shear modulus used by Cam Clay to describe pre yield stiffness is inappropriate. An 'S' shapes curve should be incorporated into the model, such as described by Jardine et al. (1986). Further analysis was therefore undertaken on the data shown in Figures 6.14 through 6.16 to reduce the scatter introduced by insensitivity of the instrumentation when successive data points are used to calculate the shear modulus 3G. For example, Figure 6.17a shows moving average (six adjacent values) of shear modulus plotted versus the shear strain for the Ballotini tests. This plot shows, as with the raw data, that the general shape of the three test curves is similar. The

starting values are different corresponding to three different confining pressures. When the data shown in Figure 6.17a are normalized by dividing the 3G values by the initial shear modulus in each of the tests, the curves are closely similar as shown in Figure 6.17b. This figure shows that in a drained triaxial compression test on Ballotini, the limit of truly linear elastic shear behaviour is bounded by a shear strain of about 0.2%. At shear strain levels beyond 0.2% the shear modulus reduces to a value of zero at a strain of 3%, corresponding approximately to the peak deviator stress. Figure 6.18 plots the linear relationship $3G_{max} = 93.269 + 36.56\ \sigma_r$ between the initial shear modulus and the confining pressure.

A similar approach was taken to evaluating the initial loading behaviour of 'Frac' sand. The moving average (six data points) of the calculated shear modulus for the 'Frac' sand tests are plotted in Figure 6.19a. The data are then replotted in Figure 6.19b as the moving average normalized by the maximum shear modulus experienced at the beginning of each of the tests. While the data may at first sight appear highly scattered, it is possible in Figure 6.19b to identify a fairly constant initial range up to a shear strain of about 0.2% and thereafter a S-shaped curve decreasing to zero at 3.0%. Figure 6.20 plots the relationship between the maximum shear modulus and the radial stress. A linear relationship $3G_{max} = 191.41 + 34.94\ \sigma_r$ was calculated from this data.

6.4.2 Isotropic Compression

Other researchers have shown that the behaviour of sand in isotropic compression appears to be controlled by the initial specific volume and to a lesser extent by the stress range through which the specimen is loaded. Although the triaxial testing described in this thesis report did not reach pressure levels where grain crushing occurred, other researchers have reached such levels. Based on the literature review and some testing results in Section 6.4.2 a set of equations is proposed to describe the isotopic compression behaviour of sand prior to grain crushing.

The testing program for this research project was performed on dense 'Frac' sand prepared with an average initial specific volume of 1.4818. Isotropic compression behaviour from other publications in the literature, Figure 2.7 and 2.8, show that for large ranges of stresses and initial specific volumes:

1. at low stresses the responses to stress increases were similar for all values of initial specific volume.
2. dense specimens showed only a minor change in the response to stressing until large values of stress were reached.
3. loose specimens showed significant change in the response to stress increments, larger changes in specific volume for the same increment of stress change when stress levels were higher.

4. results for all isotropic compression tests converge at an NCL at high stress levels, at the onset of behaviour dominated by grain crushing.

Although this test program examined only a narrow range of the possible specific volumes, corresponding to the very dense specimens required by the research needs of AECL, it was clear that the Cam Clay model did not effectively describe the observed behaviour in isotropic compression. From previous research, the NCL in sands is defined only in the grain crushing region (Coop and Lee, 1993). The basic Cam Clay model treats behaviour prior to the NCL as elastic, defined by a κ-line. The data presented in Figure 5.4b for tests performed on 'Frac' sand clearly show that this is not the case.

Most geotechnical projects are in non-calcareous sands and operate at stresses below those required for grain crushing. The following section presents equations that describe the isotropic behaviour observed in this test program. The equation uses: (1) the slope of the κ line; (2) the slope, λ of the NCL/CSL; (3) the mean stress, p_c that defines grain crushing on the NCL; and, (4) the minimum and maximum specific volumes that describe the behaviour of sand prior to the initiation of crushing. The specific volume and mean stress at the onset of crushing defines the initiation of the NCL.

Using this framework the equations defining the isotropic compression behaviour become;

1. $V = V_\lambda - \lambda \ln p$, for stresses beyond the crushing mean stress, p_c, and

2. $V = V_0 - \kappa \ln((p_c-p)/p_c))((V_{max} - V)/(V_{max} - V_{min})) - \lambda \ln((p)/p_c)((V-V_{min})/(V_{max} - V_{min}))$, for stresses less than the crushing mean stress.

In equations 1 and 2:

p_c is the value of mean pressure at which grain crushing begins in isotropic compression.

V_o is the initial specific volume

V is the current specific volume

p is the current mean stress (kPa)

V_{min} is the minimum specific volume

V_{max} is the maximum specific volume

V_{crush} is the specific volume which with the crushing mean stress defines the start of the NCL.

Values for these parameters as determined from this testing program are shown in Table 6.3. The mean stress that would define the start of the NCL, p_c was estimated as 45 MPa for these calculations. Two values are given in Table 6.3 for λ, one value determined one dimensional compression and the other from the grain-crushing region of the CSL.

Using the above equation (2) and the parameters calculated for 'Frac' sand, predictions of the isotropic compression behaviour can be made for the entire specific volume range. Results of the use of equation and the constant parameters listed in Table 6.3 (with λ = 0.108) are plotted in Figure 6.21. The results of using this equation match well

experimental results of sand tested over the full range of initial specific volume in the tests. That is, initially loose sands experience more significant volume reductions with increased confining pressure than dense sand. Also in the low confining pressure region, all the specimens are quite stiff. Results of the use of the equation, shown in Figure 6.21a compare well with measured results, as shown in Figure 2.8. The equation was then used to compare to the measured initial loading from the isotropic compression tests. The test data are plotted alongside the equation predictions in Figure 6.21b. The equation predictions plotted in Figure 6.21b are for both $\lambda = 0.108$ and $\lambda = 0.219$. From a careful examination of the data it appears that the use of $\lambda = 0.108$ better captures the overall slope of the measured data, but neither captures the initial loading.

Chapter 7 Conclusions and Recommendations for Further Research

7.1 Conclusions from the Testing Program

Drained triaxial compression tests were performed on two quartz sands; 'Frac' sand and Ballotini. These two sands are candidate fillers for stiffening thin walled canisters which may be used to contain spent nuclear fuel. The testing program was performed to determine strength and deformation properties of the sands under high stress and high temperature conditions. All tests were performed on air dry, dense specimens. The major conclusions made during this experimental research can be summarized as follows:

1. No temperature effects, were encountered for the tested temperature range of 27°C to 100°C.
2. Cam Clay can be used as a basis for modeling sand behaviour. However the basic model needs some modifications as it does not capture all the different affects of behaviour. This is especially true for high stress levels and low strain levels.
3. From triaxial tests, the critical state line is bilinear in V versus *ln*p space. The transition between the two lines corresponds with the onset of grain crushing at high stresses.
4. The CSL is bilinear in q versus p space. Again the transition between the two linear portions is due to grain crushing at high stresses.

5. The behaviour of the sand tested at high stresses in the 1-D compression tests is dominated by the onset of grain crushing which produces a yield point. At stresses greater than the start of grain crushing, relatively large plastic deformations result from increases in the applied stress. Grain crushing began, for the 'Frac' sand, at an applied axial stress of 36.6 MPa in 1-D compression. In triaxial tests it began under a combined stress state of approximately 8 MPa mean stress and a deviator stress of approximately 10 MPa.
6. The behaviour of sand prior to the onset of grain crushing can be described using an equation which relates the current 'state' of the sand to the potential 'state' of the sand (prior to grain crushing). The equation provides a reasonable prediction of the response to stress increases based on the slopes of the NCL, slope of the κ line and the onset of grain crushing.

7.2 Recommendations for further research

Recommendations for further research include some recommendations which will help define the specific soil properties used to define 'Frac' sand for modeling purposes. They also include further research which will examine the behaviour of the sand at high stresses. The recommendations can be summarized as follows:

1. Testing loose specimens of 'Frac' sand and Ballotini should be performed to aid in the definition of their CSL and the NCL.
2. Effects of initial specific volume should be explored to confirm the 'S' shaped curves developed to describe the stiffness of 'Frac' sand and Ballotini at small strains in the

pre-failure region. The initial stiffness (G_{max}) should be defined for the range of possible initial specific volumes.

3. Testing should be performed to define the shape of the yield surface defined by the onset of grain crushing. This should consist of testing along various stress paths in addition to isotropic compression.
4. The effects of the initial specific volume on the grain crushing behaviour of the sand should be evaluated.
5. Testing of sands in the regions of behaviour where crushing is dominant should be performed in a load controlled manner. Clay strength and deformation is rate dependent. Strength and deformation properties of sand in the grain crushing region may also be rate dependent, as yet no evidence is available.
6. The effects of water on the crushing behaviour of sand should be examined. It is expected that the addition of water into the sand matrix will lower the stress levels required to begin particle crushing.

References

Agar, J.G., Morgenstern, N.R. and Scott, J.D. 1986. "Thermal expansion and pore pressure generation in oil sands" Canadian Geotechnical Journal 23, 327-333

AL-Tabbaa, A. and Wood, D.M. 1989. "An experimentally based "bubble" model for clay, in Pietruszczak, S. and Pandne, G.N. eds," Numerical models in geomechanics, NUMOG III, 91-99, London:Elsevier

American Society for Testing and Materials, 1993. "Standard test methods for Maximum Index Density and Unit weight of Soils using a Vibratory Table (D4253-93)"

American Society for Testing and Materials, 1993. "Standard test methods for Minimum Index Density and unit weight of soils and Calculation of Relative Density (D4254-91)"

American Society for Testing and Materials, 1993. "Standard test methods for Specific Gravity of soils (D854-92)"

Atkinson, J.H. and Bransby, P.L. 1978, "The Mechanics of soils. An introduction to critical state soil mechanics" McGraw-Hill, Maidenhead

Atkinson, J.H., Richardson, D. and Stallebrass, S.E. 1990. "Effect of recent stress history on the stiffness of overconsolidated soil" Geotechnique 40(4), 531-540

Atkinson, J.H. 1993. "The mechanics of soils and foundations" McGraw-Hill, London

Been, K. and Jefferies, M.G. 1985. "A state parameter for Sands" Geotechnique 35(2), 99-112

Been, K., Jefferies, M.G. and Hachey, J. 1991. "The critical states of sands" Geotechnique 41, No. 3, 365-381

Been, K., Jefferies, M.G. and Hachey, J. 1992. "Discussion: The critical states of sands" Geotechnique 42(4), 655-663

Bishop, A.W. and Henkle, D.J., 1957. "The measurement of soil properties in the triaxial test" William Arnold, London

Bolton, M.D. 1986. "The strength and dilatancy of sands" Geotechnique, 36, No. 1, 65-78

Burland, J.B. 1989. "Ninth Laurits Bjerrum Memorial Lecture: "Small is beautiful"- the stiffness of soils at small strains" Canadian Geotechnical Journal, 26, 499-516

Casagrande, A., 1936. "Characteristics of cohesionless soils affecting the stability of slopes and earth fills" J. Boston Society of Civil Engineers 23(1), 13-32

Chu, J., 1995. "An experimental examination of the critical state and other similar concepts for granular soils" Canadian Geotechnical Journal 32, 1065-1075

Chu, J., Lo, S.-C.R. and Lee, I.K. 1996. "Strain softening and shear band formation of sand in multi-axial testing" Geotechnique 46(1), 62-82

Coop, M.R. 1990 " The mechanics of uncemented carbonate sands" Geotechnique 40(4), 607-626

Coop, M.R. and Lee, I.K. 1993 "The behaviour of granular soils at elevated stresses" Predictive soil mechanics. Thomas Telford, London

Crilly, T., 1995. "Unload-reload tests on saturated illite specimens at elevated temperature" M.Sc. Thesis, University of Manitoba, Department of Civil and Geological Engineering

Crosthwaite, J.L., 1994. "The performance, Assessment and Ranking of Container Design Options for the Canadian Nuclear Fuel Waste Management Program", Atomic Energy of Canada Limited Technical Record, TR-500

Dafalias, Y. F. and Herrmann, L. R. 1980 "A bounding surface soil plasticity model" International symposium on Soils under Cyclic and Transient Loading, Swansea, 1, 355-345

Davies and Newson 1993. "A critical state constitutive model for anisotopic soil" in Predictive Soil Mechanics, Thomas Telford, London

Duncan, J.M. and Chang, C.-Y. 1970 "Nonlinear analysis of stress and strain in soils" ASCE Soil Mechnanics and Foundation Division, 96(SM5), 1629-1653

Ferris, G.W. and Graham, J., 1996a. "One dimensional confined compression of 1mm diameter ballotini", unpublished research report number 3 to AECL

Ferris, G.W. and Graham, J., 1996b. "One dimensional confined compression of 1mm diameter ballotini", unpublished research report number 4 to AECL

Ferris, G.W. and Graham, J., 1996c. "One dimensional confined compression of 16-25 sieve Fractionated Sand", unpublished research report number 5 to AECL

Ferris, G.W. and Graham, J., 1996d. "One dimensional confined compression of 20-40 sieve Fractionated Sand", unpublished research report number 6 to AECL

Ferris, G.W. and Graham, J., 1996e. "Isotropic compression testing of 1 mm diameter Ballotini", unpublished research report number 11 to AECL

Ferris, G.W. and Graham, J., 1996f. "Isotropic compression testing of 20-40 FRAC sand with temperature control", unpublished research report number 13 to AECL

Ferris, G.W. and Graham, J., 1996g. "Triaxial compression testing of 1 mm diameter Ballotini at room temperature", unpublished research report number 12 to AECL

Ferris, G.W. and Graham, J., 1996h. "Triaxial compression testing of 20 - 40 Frac. Sand at room temperature", unpublished research report number 14 to AECL

Ferris, G.W. and Graham, J., 1996i. "Triaxial compression testing of 20 - 40 Frac. Sand at 65°C", unpublished research report number 15 to AECL

Ferris, G.W. and Graham, J., 1996j. "Triaxial compression testing of 20 - 40 Frac. Sand at 100°C", unpublished research report number 16 to AECL

Hagerty, M.M., Hite, D.R., Ullrich, C.R. and Hagerty, D.J. 1993. 'One-dimensional high-pressure compression of granular media" J. Geotech. Engrg., ASCE, 119(1), 1-18

Hardin, B.O. 1985. "Crushing of soil particles" J. Geotech. Engrg., ASCE, 111(10), 1177-1192

Hardin, B.O. 1987. "1-D strain in normally consolidated cohesionless soils" J. Geotech. Engrg., ASCE, 113(12), 1449-1467

Head, K.H. 1991 "Manual of Soil Laboratory Testing, Volume 3: Effective Stress Tests" Pentech Press, London

Iwasaki, T., Tatsuoka, F. and Takagi, Y. 1978. "Shear moduli of sands under cyclic torsional shear loading" Soils and Foundations 18(1), 39-56

Jardine, R.J., Potts, D.M., Fourie, A.B. and Burland, J.B. 1986. "Studies of the influence of non-linear stress-strain characteristics in soil-structure interaction" Geotechnique 36(3), 377-396

Jefferies, M.G. and Been, K. 1992 "Undrained Response of Nor-Sand" 45th Canadian Geotechnical Conference, Toronto

Jefferies, M.G. 1993. "Nor-Sand: a simple critical state model for sand" Geotechnique 43(1), 91-103

Konrad, J.-M. 1996. "Factors affecting the CPT response in Sands" 49th Canadian Geotechnical Conference, St. John's, 841- 848

Konrad, J.-M. and Pouliot N. 1997. " Ultimate state of reconstituted and intact samples of deltaic sand" Canadian Geotechnical Journal, 34, 737-748

Lambe, T.W. and Whitman, R.V. 1979. "Soil Mechanics" John Wiley, New York

Lee, K.L. and Seed, H.B. 1967. "Drained strength characteristics of sands" ASCE Soil Mechcanics and Foundations, 93(SM 6), 117-141

Lingnau, B.E., 1993. "Consolidated Undrained-Triaxial Behavior of a Sand-Bentonite Mixture at elevated Temperature" Ph.D. Thesis, University of Manitoba, Department of Civil and Geological Engineering

Lo, K.Y. and Roy, M. 1973 "Response of particulate materials at high pressures" Soils and Foundations, 13(1), 61-76

Porovic, E. and Jardine, R.J. 1994. "Some observations on the static and dynamic shear stiffness of Ham River sand" in Pre-failure Deformation of Geomaterials. Shibuya, Mitachi and Miura (eds), Rotterdam:Balkema

Roscoe, K.H., Schofield, A.N. and Wroth, C.P. 1958. "On the yielding of soils" Geotechnique 8(1), 22-52

Schofield, A.N. and Wroth, C.P. 1968. "Critical State Soil Mechanics" London:McGraw-Hill

Simpson, B., O'Roirdan, N.J. and Croft, D.D. 1979. "A computer model for the analysis of ground movements in London Clay" Geotechnique 29(2), 149-175

Simpson, B. 1992. "32nd Rankine Lecture: Retaining structures: displacement and design" Geotechnique 42(4), 541-576

Sladen, J.A. and Oswell, J.M., 1989. "The behaviour of very loose sand in the triaxial compression test" Canadian Geotechnical Journal, 26, 103-113

Stallebrass, S.E., Jovičić, V. and Taylor, R.N. 1994. "The influence of recent stress history on ground movements around tunnels" in Pre-failure Deformations of Geomaterials, Shibuya, Mitachi and Miura (eds), Rotterdam: Balkema

Tanaka, N., 1995. "Thermal Elastic Plastic Behavior and Modelling of Saturated Clays" Ph.D. Thesis, University of Manitoba, Department of Civil and Geological Engineering

Teper, B., 1980. "Particulate Compaction tests for a particulate-packed thin-wall container for irradiated-fuel disposal", Atomic Energy of Canada Limited Technical Record, TR-131

Vesic, A.S. and Clough, G.W. 1968. "Behaviour of granular materials under high stresses" ASCE Soils and Foundations, 94(SM3), 661-688

Wood, D.M. 1984. "On stress Parameters", Geotechnique, 34(2), 282-287

Wood, D.M., 1990. "Soil Behaviour and Critical State Soil Mechanics" Cambridge University Press.

Wood, D.M., Belkheir, K. and Liu, D.F. 1994. "Strain softening and state parameter for sand modelling" Geotechnique, 44(2), 335-339

Yudhbir and Wood, D.M. 1989. "Recent developments in laboratory strength and deformation testing" Proc. 12th International Conference of Soil Mechanics and Foundation Engineering, 4:2303-2337

[size limits (mm)] Material	G_s	D_i (MPa)	p_c (MPa)	D_f (MPa)
[0.6-0.425] wedron sand[2]	--	358	54.6	--
[0.85-0.425] Ottawa sand[1]	2.65	379	22.8	11 450
[0.85-0.425] Black Beauty[1]	2.78	74	3.6	13 030
[0.85-0.425] angular glass beads[1]	2.5	23	2.6	14 550
[1.2-0.8] glass beads[2]	--	640	27.3	--
[0.85-0.6] glass beads[1]	2.5	583	33.8	12 690
[0.725-0.363] glass beads[1]	2.5	827	48.3	13 790
[0.425-.25] glass beads[1]	2.5	484	48.3	11 860
[0.3-0.02] glass beads[2]	--	795	32.8	--

D_i - confined modulus initial segment p_c - yield stress

D_f - final confined modulus at extreme high stress G_s - specific gravity

[1] Hagerty et al. 1993

[2] Teper 1980

Table 2.1 Results from one dimensional compression testing of various materials

	e_{min}	e_{max}	G_s	B_p	ρ_{max} (Mg/m^3)	ρ_{min} (Mg/m^3)
1 mm Diameter Ballotini	0.538	0.661	2.491	92.8	1.62	1.50
16-25 Frac Sand	0.416	0.707	2.644	70.1	1.867	1.549
20 -40 Frac Sand	0.432	0.712	2.654	48.2	1.853	1.550

e_{min} - minimum void ratio

e_{max} - maximum void ratio

G_s - specific gravity

ρ_{max} - maximum density

ρ_{min} - minimum density

B_p - breakage potential

Table 3.1 Physical properties of materials tested

Test	Material	e_0	I_d	B_p	Max. σ_a (MPa)
T1804	Ballotini	0.5382	0.998	92.8	40.3
T1805	Ballotini	0.5440	0.951	92.8	38.9
T1806	Ballotini	0.5390	0.992	92.8	40.3
T1807	Ballotini	0.5567	0.848	92.8	47.2
T1808	Ballotini	0.5416	0.971	92.8	52.8
T1809	16-25 sand	0.4711	0.811	70.1	80.5
T1810	16-25 sand	0.4685	0.820	70.1	80.5
T1811	20-40 sand	0.4730	0.854	48.2	80.5
T1812	20-40 sand	0.5124	0.713	48.2	80.5
T1813	20-40 sand	0.5221	0.678	48.2	80.5

e_0 - initial void ratio

I_d - density index $(e_{max}-e_0)/(e_{max}-e_{min})$

B_p - breakage potential

Max. σ_a - maximum axial stress

Table 4.1 Summary of initial conditions for one-dimensional confined compression tests

Test	Material	B_t	B_r	noise (MPa)	Max. σ_a (MPa)
T1804	Ballotini	3.3	0.036	--	40.3
T1805	Ballotini	12.2	0.131	--	38.9
T1806	Ballotini	11.0	0.119	33	40.3
T1807	Ballotini	2.7	0.029	36	47.2
T1808	Ballotini	0.1	0.001	39	52.8
T1809	16-25 sand	15.9	0.226	44	80.5
T1810	16-25 sand	13.3	0.189	28	80.5
T1811	20-40 sand	15.7	0.327	50	80.5
T1812	20-40 sand	15.9	0.330	39	80.5
T1813	20-40 sand	16.3	0.339	25	80.5

B_t - total breakage

B_r - relative breakage

noise - stress level at which sounds of particle breakage begin

Max. σ_a - maximum axial stress

Table 4.2 Summary of particle breakage in one-dimensional compression tests

Test	Material	C_r initial	Yield Stress (MPa)	C_c	C_r Unload-reload
T1804	Ballotini	0.0154	--	--	--
T1805	Ballotini	0.0158	--	--	--
T1806	Ballotini	0.0179	--	--	--
T1807	Ballotini	0.0274	--	--	--
T1808	Ballotini	0.0187	--	--	--
T1809	16-25 sand	0.0288	55.6	0.3682	0.0153
T1810	16-25 sand	0.0162	52.7	0.3183	0.0053
T1811	20-40 sand	0.0193	50	0.2751	0.0084
T1812	20-40 sand	0.0184	44.4	0.2737	0.0041
T1813	20-40 sand	0.0251	44.4	0.2743	0.0024

C_c - compression index

C_r - unload-reload index

yield stress - transition from C_c to C_r

Max. σ_a - maximum axial stress

Table 4.3 Summary of Indices describing one-dimensional compression in *log* axial stress, σ_a versus void ratio, e space

Test	Material	D_i (MPa)	Yield Stress (MPa)	D_c (MPa)	D_r (MPa)
T1804	Ballotini	2040	--	--	--
T1805	Ballotini	2645	--	--	--
T1806	Ballotini	2317	--	--	--
T1807	Ballotini	2416	--	--	--
T1808	Ballotini	2980	--	--	--
T1809	16-25 sand	2349	52.4	651	12240
T1810	16-25 sand	1982	53.3	780	8937
T1811	20-40 sand	1988	51.3	838	9893
T1812	20-40 sand	2018	45.8	785	9181
T1813	20-40 sand	1547	40.0	899	10699

D_i - initial confined modulus

yield stress - onset of grain crushing

D_c - crushing confined modulus

D_r - unload reload confined modulus

Table 4.4 Summary of confined modulus describing one-dimensional compression in axial stress, σ_a versus axial strain, ε_a space

Test	Material	Temperature	V_0	I_d	B_p	Max. σ_r (MPa)
T1837	20-40 sand	27	1.4818	0.822	48.2	10.4
T1838	20-40 sand	27	1.4837	0.815	48.2	10.4
T1839	Ballotini	27	1.5408	0.977	92.8	10.2
T1840	20-40 sand	65	1.4761	0.842	48.2	10.35
T1841	20-40 sand	65	1.4877	0.801	48.2	10.4
T1842	20-40 sand	100	1.4798	0.829	48.2	8.8

V_0 - initial specific volume

I_d - density index $(V_{max}-V_0)/(V_{max}-V_{min})$

B_p - breakage potential

Max. σ_r - maximum radial stress

Table 5.1 Summary of initial conditions for isotropic compression tests

Test	Material	Temp	V_0	I_D	p_0	p_{max}	V	ε_v	ε_s
		(°C)			(MPa)	(MPa)	(at p_{max})	(%)	(%)
T1837	sand	27.2	1.4818	0.822	0.1	10.4	1.4568	1.689	-0.148
T1838	sand	27.1	1.4837	0.815	0.1	10.4	1.4588	1.678	0.312
T1839	Ballotini	29	1.5408	0.977	0.1	10.2	1.5042	2.378	-0.202
T1840	sand	65	1.4761	0.842	0.1	10.35	1.4415	2.341	-0.288
T1841	sand	65	1.4877	0.801	0.1	10.4	1.4552	2.189	-0.240
T1842	sand	100	1.4798	0.829	0.1	8.8	1.4592	1.391	0.111

Table 5.2 Summary of isotropic compression tests

Test	Material	Temp	V_0	I_D	p_0	p_f	V_f	ε_v	ε_s
		(°C)			(MPa)	(MPa)		(%)	(%)
T1815	Ballotini	27.2	1.5311	1.000	0.1	5.00	1.5241	0.456	-0.066
T1816	Ballotini	27.1	1.5432	0.958	0.1	2.50	1.5276	1.014	-0.182
T1825	Ballotini	29	1.5369	1.000	0.1	7.55	1.5348	0.456	-0.066
T1817	sand	27.4	1.4887	0.798	0.1	5.03	1.4780	0.723	-0.017
T1818	sand	27.3	1.4895	0.795	0.1	2.45	1.4842	0.358	-0.015
T1821	sand	29.1	1.4787	0.833	0.1	7.01	1.4745	0.288	-0.003
T1822	sand	30.6	1.4835	0.816	0.1	2.05	1.4806	0.186	-0.009
T1828	sand	27.8	1.4775	0.838	0.1	1.51	1.4752	0.151	-0.007
T1829	sand	26.2	1.4842	0.814	0.1	3.80	1.4710	0.892	-0.029
T1831	sand	27	1.4891	0.796	0.1	5.12	1.4751	0.938	-0.022
T1814	sand	65	1.4850	0.811	0.1	1.51	1.4849	0.004	-0.000
T1819	sand	65.4	1.4851	0.811	0.1	5.02	1.4759	0.616	-0.016
T1820	sand	64.8	1.4830	0.818	0.1	2.48	1.4770	0.408	-0.018
T1823	sand	65.6	1.4870	0.804	0.1	6.02	1.4837	0.225	-0.004
T1826	sand	65	1.4871	0.803	0.1	3.75	1.4821	0.342	-0.011
T1830	sand	65	1.4835	0.816	0.1	3.65	1.4774	0.414	-0.014
T1835	sand	65	1.4868	0.804	0.1	7.14	1.4798	0.473	-0.005
T1824	sand	98.6	1.5092	0.795	0.1	2.57	1.5084	0.048	-0.002
T1827	sand	100.2	1.4935	0.790	0.1	1.56	1.4936	-0.002	0.000
T1832	sand	100	1.4820	0.828	0.1	3.91	1.4806	0.098	-0.003
T1833	sand	100	1.4920	0.785	0.1	4.93	1.4868	0.350	-0.009
T1834	sand	100	1.4790	0.832	0.1	2.62	1.4766	0.163	-0.006
T1836	sand	100	1.4717	0.858	0.1	7.04	1.4716	0.004	-0.000

Table 5.3 Summary of triaxial compression tests, isotropic compression phase

Test	Material	Temp (°C)	V	p (MPa)	q (MPa)	ε_v (%)	ε_s (%)	tanβ *	ε_a (%)
T1815	Ballotini	27.2	1.5110	6.876	5.613	0.857	1.695	-	1.981
T1816	Ballotini	27.1	1.5176	3.487	2.896	0.657	0.955	-	0.736
T1825	Ballotini	29	1.4951	11.516	11.983	2.588	2.596	-	3.459
T1817	sand	27.4	1.4566	8.448	10.273	1.448	1.825	-	2.308
T1818	sand	27.3	1.4685	4.253	5.428	1.054	1.031	-	1.382
T1821	sand	29.1	1.4395	11.479	13.354	2.369	2.284	-	3.074
T1822	sand	30.6	1.4664	3.487	4.355	0.960	0.928	-	1.248
T1828	sand	27.8	1.4599	2.747	3.666	1.034	0.755	-	1.100
T1829	sand	26.2	1.4553	6.424	7.843	1.069	1.120	-	1.476
T1831	sand	27	1.4569	8.624	10.446	1.235	1.080	-	1.491
T1814	sand	65	1.4675	2.715	3.634	1.175	0.863	-	1.255
T1819	sand	65.4	1.4521	8.681	10.967	1.611	2.114	-	2.651
T1820	sand	64.8	1.4678	4.361	5.599	0.621	1.472	-	1.679
T1823	sand	65.6	1.4433	10.155	12.417	2.722	3.067	-	3.964
T1826	sand	65	1.4673	6.408	7.877	0.996	1.331	-	1.663
T1830	sand	65	1.4579	6.307	7.936	1.322	1.116	-	1.557
T1835	sand	65	1.4426	12.177	15.094	2.514	1.956	-	2.794
T1824	sand	98.6	1.4918	4.593	6.139	1.103	1.241	-	1.609
T1827	sand	100.2	1.4807	2.954	4.042	0.860	1.573	-	1.859
T1832	sand	100	1.4616	6.771	8.545	1.285	1.750	-	2.178
T1833	sand	100	1.4630	8.586	10.813	1.579	1.748	-	2.274
T1834	sand	100	1.4598	4.671	6.107	1.138	0.975	-	1.354
T1836	sand	100	1.4406	11.896	14.655	2.108	1.997	-	2.700

* - by definition

Table 5.4 Summary of triaxial compression tests, transition point

Test	Material	Temp	V	p	q	ε_v	ε_s	tanβ	η
		(°C)		(MPa)	(MPa)	(%)	(%)		
T1815	Ballotini	27.2	1.5271	7.039	6.129	-0.196	3.339	-0.850	0.871
T1816	Ballotini	27.1	1.5325	3.754	3.757	-0.322	2.172	-0.907	1.001
T1825	Ballotini	29	1.4966	11.991	11.521	2.486	2.895	-0.899	1.041
T1817	sand	27.4	1.4732	8.970	11.838	0.321	4.224	-0.824	1.320
T1818	sand	27.3	1.5080	4.616	6.468	-1.608	4.168	-1.016	1.401
T1821	sand	29.1	1.4623	12.049	15.088	0.825	4.361	-1.075	1.252
T1822	sand	30.6	1.5000	3.835	5.364	-1.283	4.015	-0.979	1.399
T1828	sand	27.8	1.4923	3.001	4.437	-1.159	3.409	-0.976	1.479
T1829	sand	26.2	1.4797	7.002	9.560	-0.595	3.819	-1.000	1.365
T1831	sand	27	1.4924	9.199	12.255	-0.489	3.984	-0.745	1.314
T1814	sand	65	1.5058	2.924	4.250	-1.404	3.935	-1.041	1.454
T1819	sand	65.4	1.4645	8.951	11.758	0.777	3.700	-1.329	1.314
T1820	sand	64.8	1.4858	4.666	6.526	-0.599	3.900	-1.046	1.398
T1823	sand	65.6	1.4464	10.206	12.524	2.515	4.132	-0.091	1.227
T1826	sand	65	1.4914	6.867	9.238	-0.625	3.869	-1.019	1.345
T1830	sand	65	1.4646	6.653	9.004	0.864	2.234	-0.303	1.354
T1835	sand	65	1.4461	12.336	15.573	2.277	2.955	-0.480	1.262
T1824	sand	98.6	1.5133	4.885	6.985	-0.322	3.554	-0.457	1.430
T1827	sand	100.2	1.4980	3.028	4.342	-0.295	3.333	-0.776	1.434
T1832	sand	100	1.4760	7.049	9.414	0.286	3.553	-0.986	1.335
T1833	sand	100	1.4776	8.833	11.519	0.621	3.839	-0.593	1.304
T1834	sand	100	1.4870	4.990	6.997	-0.704	3.330	-0.904	1.402
T1836	sand	100	1.4477	11.978	14.915	1.627	2.895	-0.824	1.245

Table 5.5 Summary of triaxial compression tests, at peak stress

Test	Material	Temp (°C)	V	p (MPa)	q (MPa)	ε_v (%)	ε_s (%)	tanβ	ε_a (%)
T1815	Ballotini	27.2	1.7033	6.463	4.417	-11.754	13.407	-1.121	9.489
T1816	Ballotini	27.1	1.7395	3.313	2.444	-13.867	14.481	-0.751	9.858
T1825	Ballotini	29	1.5952	10.176	7.803	-3.939	11.640	-1.206	10.327
T1817	sand	27.4	1.5858	7.978	8.907	-7.297	13.828	-0.959	11.396
T1818	sand	27.3	1.7923	3.867	4.320	-19.210	18.118	-1.186	11.715
T1821	sand	29.1	1.6163	10.684	11.151	-9.618	15.877	-0.859	12.671
T1822	sand	30.6	1.5840	3.668	4.796	-6.988	9.272	-1.078	6.943
T1828	sand	27.8	1.6184	2.555	3.121	-9.710	12.662	0.667	9.426
T1829	sand	26.2	1.7309	5.686	5.695	-17.669	17.919	-2.584	12.029
T1831	sand	27	1.5693	8.074	8.880	-6.385	12.493	-0.417	10.365
T1814	sand	65	1.6219	2.694	3.560	-9.227	11.568	-0.836	8.492
T1819	sand	65.4	1.6158	7.879	8.576	-9.477	15.460	-0.860	12.300
T1820	sand	64.8	1.6186	4.227	5.258	-9.589	11.458	-1.505	8.261
T1823	sand	65.6	1.4495	9.631	10.884	2.306	8.416	0.320	9.184
T1826	sand	65	1.6641	6.201	7.244	-12.279	13.568	-1.226	9.474
T1830	sand	65	1.5646	6.366	8.177	-5.904	9.944	-1.007	7.976
T1835	sand	65	1.5400	11.061	11.744	-4.071	13.018	-0.191	11.661
T1824	sand	98.6	1.6674	4.421	5.412	-10.535	13.261	-1.091	9.749
T1827	sand	100.2	1.6850	2.549	2.936	-12.815	14.614	-1.518	10.342
T1832	sand	100	1.7057	6.050	6.384	-14.206	15.765	1.302	11.697
T1833	sand	100	1.5507	7.976	9.015	-4.300	13.976	1.261	12.543
T1834	sand	100	1.6981	4.071	4.406	-14.999	14.755	-1.163	9.755
T1836	sand	100	1.6538	10.503	10.039	-12.375	16.231	0.762	12.106

Table 5.6 Summary of triaxial compression tests, end of test values

Test	Material	Temp		Max. p	Max.q			Grain
		(°C)	B_p	(MPa)	(MPa)	B_t	B_p	Crushing
T1837	sand	27	48.2	10.4	-	0	0	No
T1838	sand	27	48.2	10.4	-	0	0	No
T1840	sand	65	48.2	10.35	-	0	0	No
T1841	sand	65	48.2	10.4	-	0	0	No
T1842	sand	100	48.2	8.8	-	0	0	No
T1839	Ballotini	27	92.8	10.2	-	0	0	No
T1815	Ballotini	27.2	92.8	7.039	6.129	0	0	No
T1816	Ballotini	27.1	92.8	3.754	3.757	0	0	No
T1825	Ballotini	29	92.8	11.521	11.991	0	0	No
T1817	sand	27.4	48.2	8.970	11.838	0	0	No
T1818	sand	27.3	48.2	4.616	6.468	0.286	0.006	Yes
T1821	sand	29.1	48.2	12.049	15.088	0.874	0.018	Yes
T1822	sand	30.6	48.2	3.835	5.364	0	0	No
T1828	sand	27.8	48.2	3.001	4.437	0	0	No
T1829	sand	26.2	48.2	7.002	9.560	0	0	No
T1831	sand	27	48.2	9.129	9.933	0.208	0.004	Yes
T1814	sand	65	48.2	2.924	4.250	0	0	No
T1819	sand	65.4	48.2	8.951	11.758	0	0	No
T1820	sand	64.8	48.2	4.666	6.526	NA	NA	Not tested
T1823	sand	65.6	48.2	10.206	12.524	1.198	0.025	Yes
T1826	sand	65	48.2	6.867	9.238	NA	NA	Not tested
T1830	sand	65	48.2	6.653	9.004	0	0	No
T1835	sand	65	48.2	12.336	15.573	1.483	0.031	Yes
T1824	sand	98.6	48.2	4.885	6.985	0	0	No
T1827	sand	100.2	48.2	3.028	4.342	0	0	No
T1832	sand	100	48.2	7.049	9.414	0.288	0.006	Yes
T1833	sand	100	48.2	8.833	11.519	1.823	0.038	Yes
T1834	sand	100	48.2	4.990	6.997	0	0	No
T1836	sand	100	48.2	11.978	14.915	1.723	0.036	Yes

Table 5.7 Summary of maximum stresses applied and change to particle size distribution as measured by total breakage.

Test	Material	Temp	σ_r	q	ε_s	$3G_{peak}$	$3G_{50}$	$3G_{url}$
		(°C)	(MPa)	(MPa)	(%)	(MPa)	(MPa)	(MPa)
T1815	Ballotini	27.2	5.00	6.129	3.339	183.6	699.5	--
T1816	Ballotini	27.1	2.50	3.757	2.172	173.0	507.1	--
T1825	Ballotini	29	7.55	11.521	2.895	398.0	1081.1	--
T1817	sand	27.4	5.03	11.838	4.224	280.3	921.2	--
T1818	sand	27.3	2.45	6.468	4.168	155.2	830.8	--
T1821	sand	29.1	7.01	15.088	4.361	346.0	740.1	--
T1822	sand	30.6	2.05	5.364	4.015	133.6	721.3	--
T1828	sand	27.8	1.51	4.437	3.409	130.2	498.4	1006.1, 397.2
T1829	sand	26.2	3.80	9.560	3.819	250.3	975.7	518.5, 549.0
T1831	sand	27	5.12	12.255	3.984	249.3	1723.0	934.3, 943.6
T1814	sand	65	1.51	4.250	3.935	108.0	639.1	884.3
T1819	sand	65.4	5.03	11.758	3.700	317.8	1029.3	--
T1820	sand	64.8	2.49	6.526	3.900	176.4	524.2	--
T1823	sand	65.6	6.02	12.524	4.132	303.1	1144.9	--
T1826	sand	65	3.78	9.238	3.869	238.8	949.1	--
T1830	sand	65	3.65	9.004	2.234	403.0	988.4	1171.4, 764.2
T1835	sand	65	7.14	15.573	2.955	527.0	1417.5	--
T1824	sand	98.6	2.57	6.985	3.554	196.5	810.0	--
T1827	sand	100.2	1.58	4.342	3.333	130.3	329.1	1046.5, 562.2
T1832	sand	100	3.91	9.414	3.553	265.0	890.5	354.8
T1833	sand	100	4.93	11.519	3.839	300.1	1121.9	--
T1834	sand	100	2.62	6.997	3.330	210.1	970.7	--
T1836	sand	100	7.03	14.915	2.895	515.2	1247.5	--

Table 6.1 Summary of Calculated Shear Modulus

Parameter	'Frac' Sand Before Crushing	After Crushing	Ballotini
κ	0.0065	0.0065	0.0092
λ	0.028	0.108, 0.219	0.1478
V_λ	--	--	--
Γ	1.8701	--	2.9551
Transition (kPa)	7,636	--	--
Γ_c	--	1.6217	--
M	1.256	1.172	0.827
3G (MPa)	761	--	763

Table 6.2 Summary of Cam Clay parameters

Parameter	Figure 2.21b	Plotted in Figure 6.21b
V_{max}	1.712	1.712
V_{min}	1.43	1.43
P_c	45,000 kPa	45,000 kPa
κ	0.0065	0.0065
λ	0.108	0.219

Table 6.3 Summary of parameters used in equation predictions

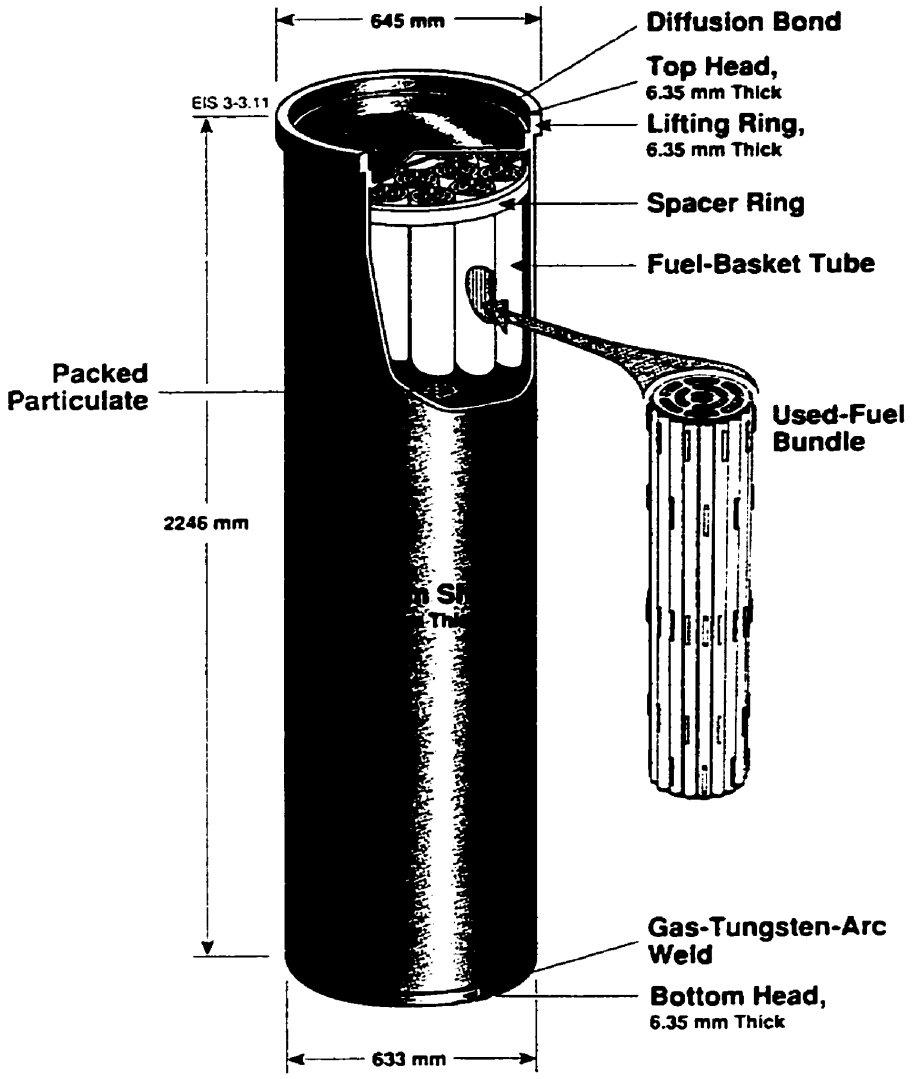

Figure 1.1 Packed-Particulate Fuel Disposal Container (from Crosthwaite 1994)

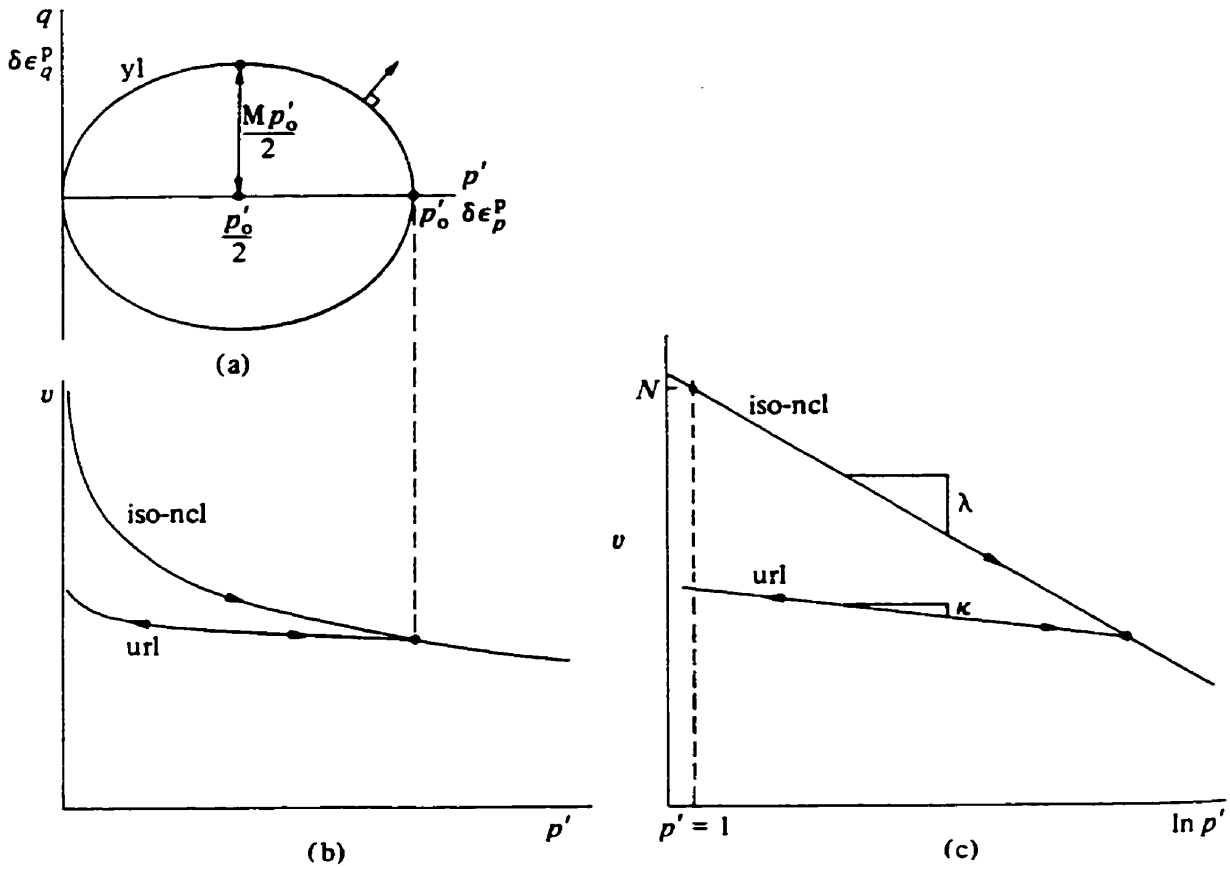

Figure 2.1 (a) Elliptical yield locus for Cam clay model in p:q plane; (b), (c) normal compression line and unloading-reloading line in compression plane (from Wood 1990)

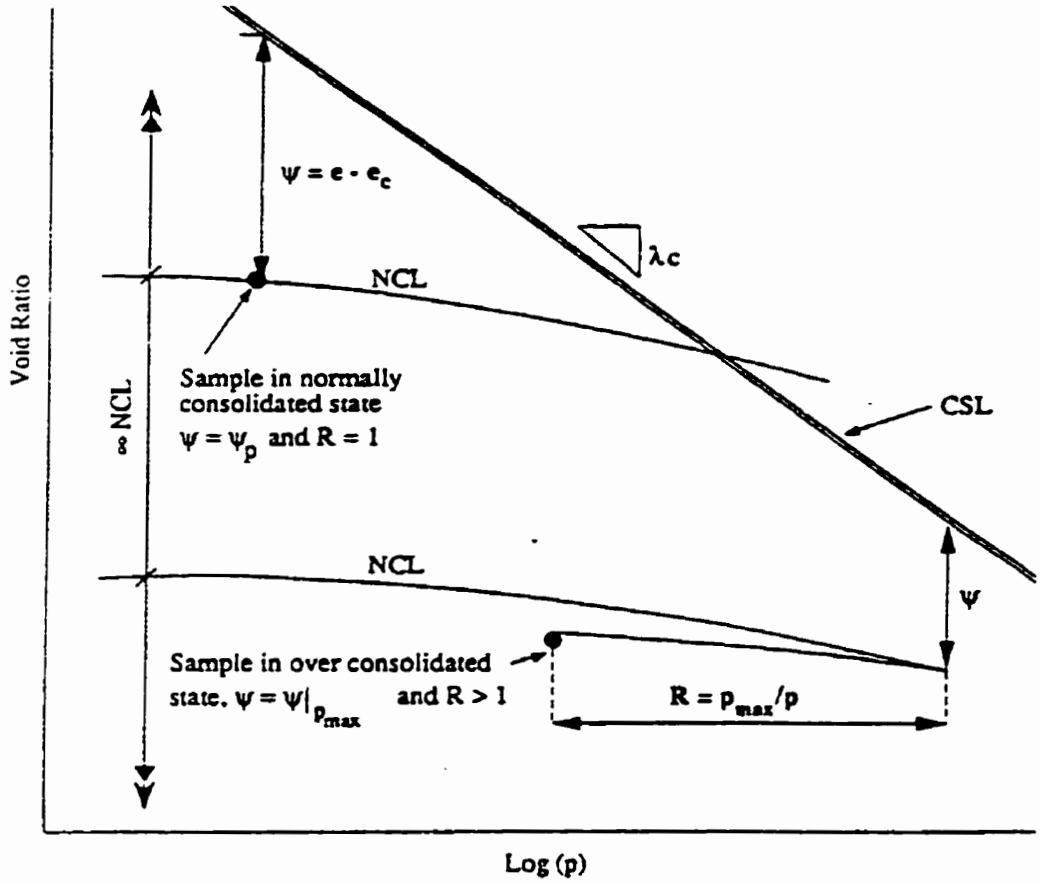

Figure 2.2 Definition of State Parameter, and R (from Jefferies and Been 1992)

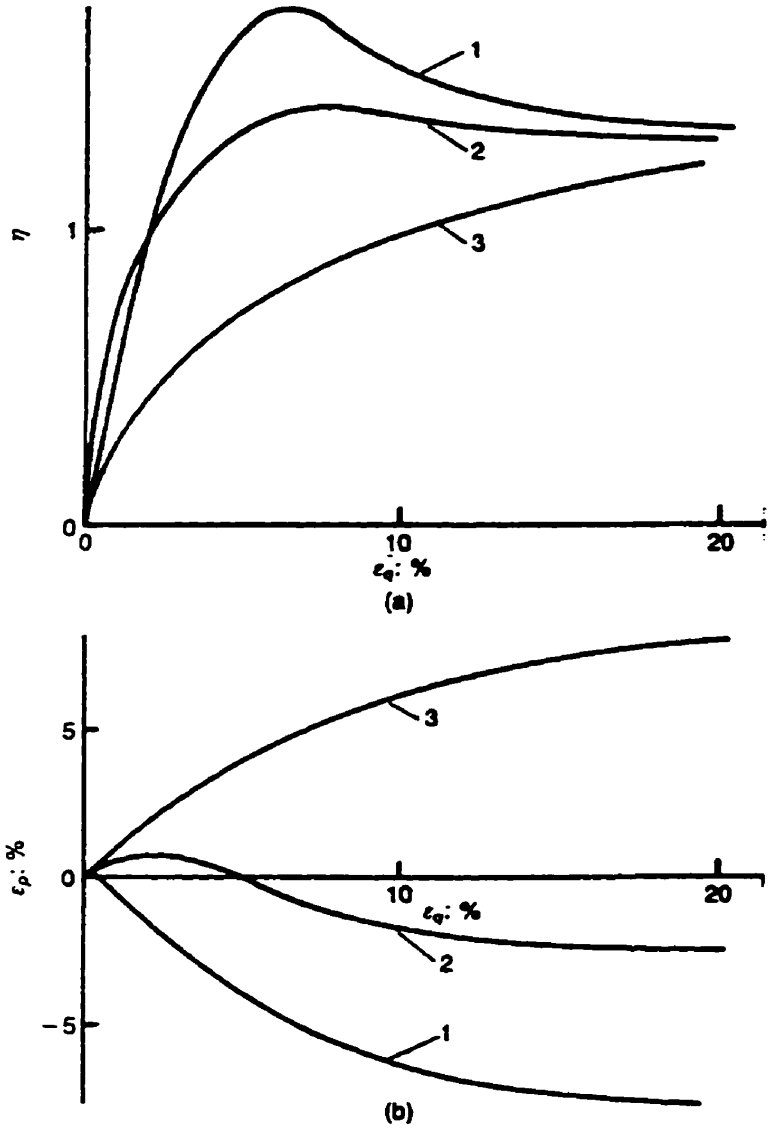

Figure 2.3 Typical results of drained triaxial compression tests on sand; curve 1: dense sand at low stress level; curve 2: dense sand at medium stress level; curve 3; loose sand at low stress level (from Muir Wood et al. 1994)

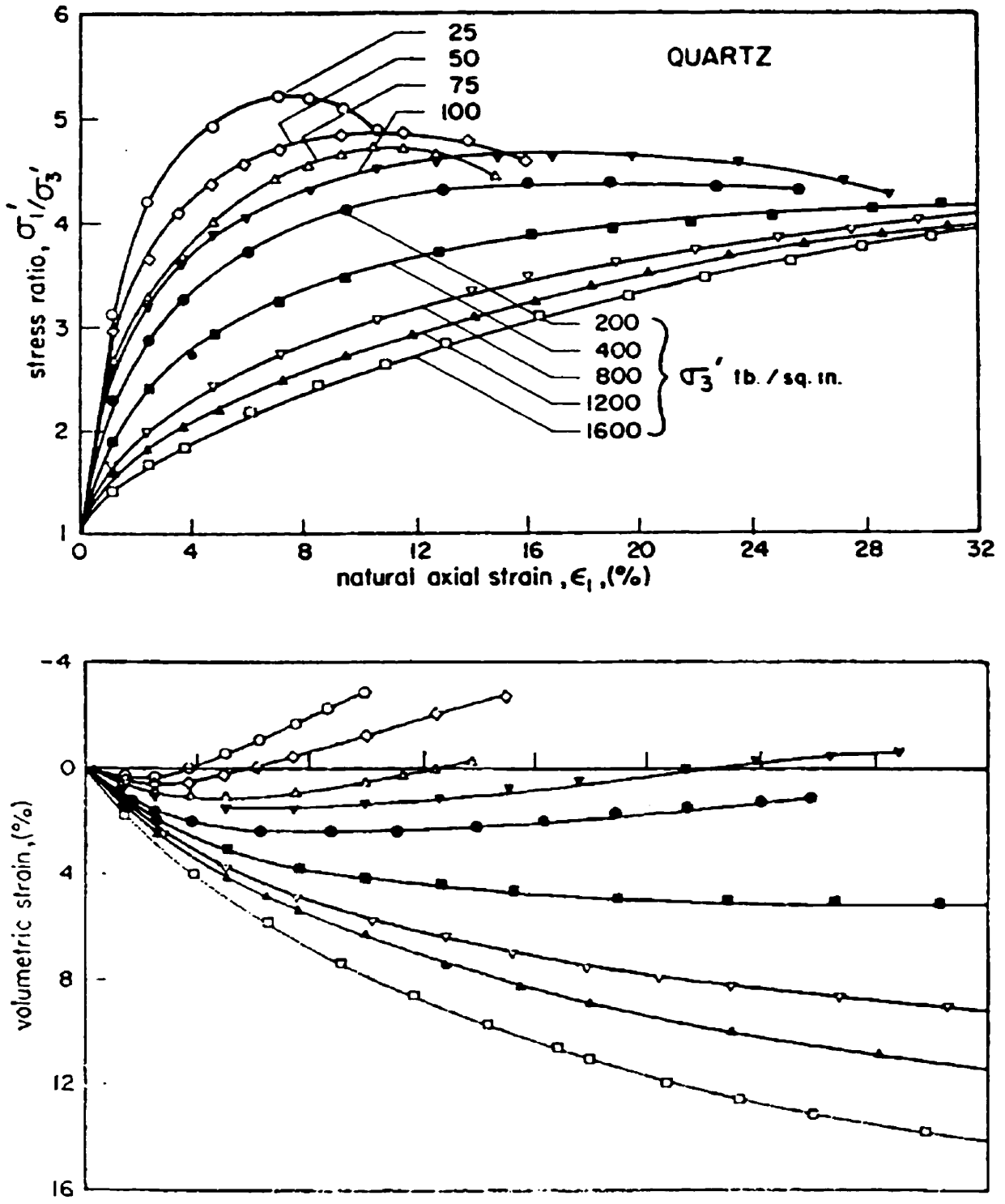

Fig. 3. Results of drained triaxial tests on quartz sand

Figure 2.4 Results of drained triaxial compression tests on quartz sand for a large range of confining pressures (from Lo and Roy 1973)

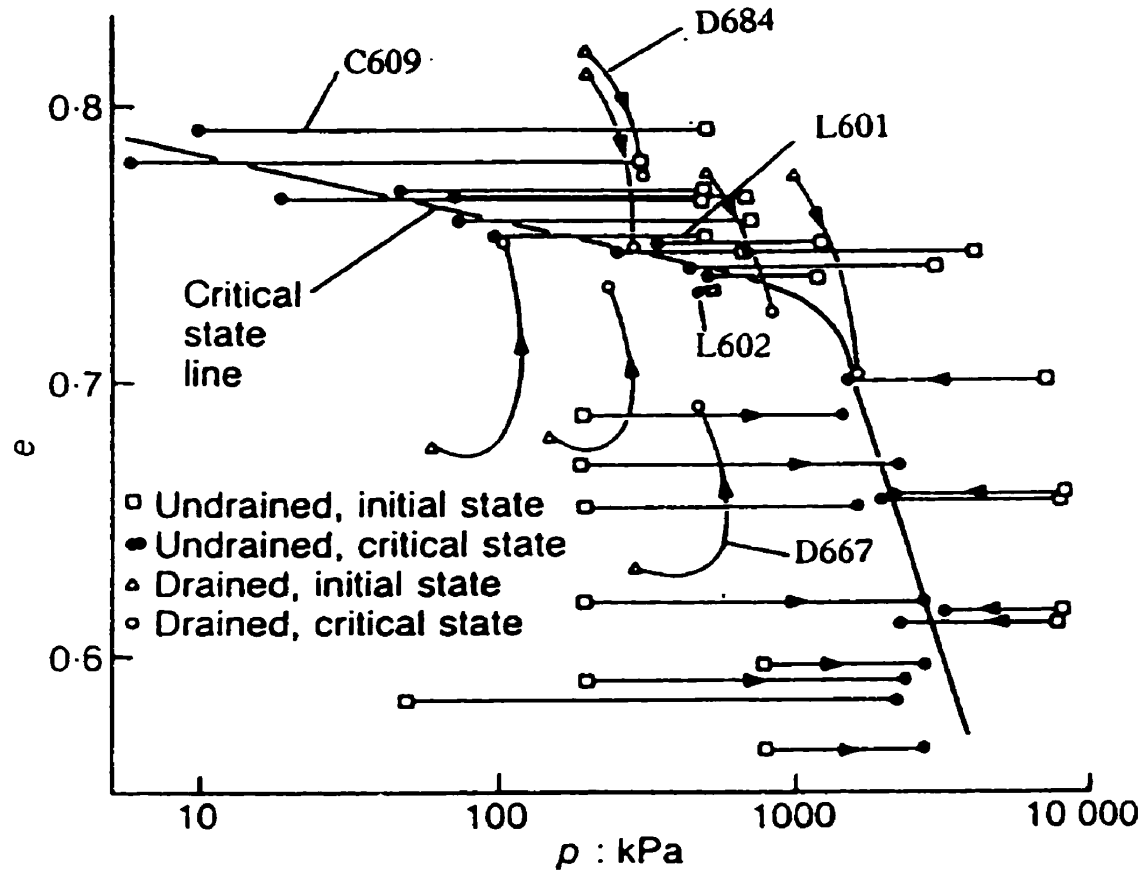

Figure 2.5 State diagram for drained and undrained triaxial compression tests (from Jefferies and Been, 1992)

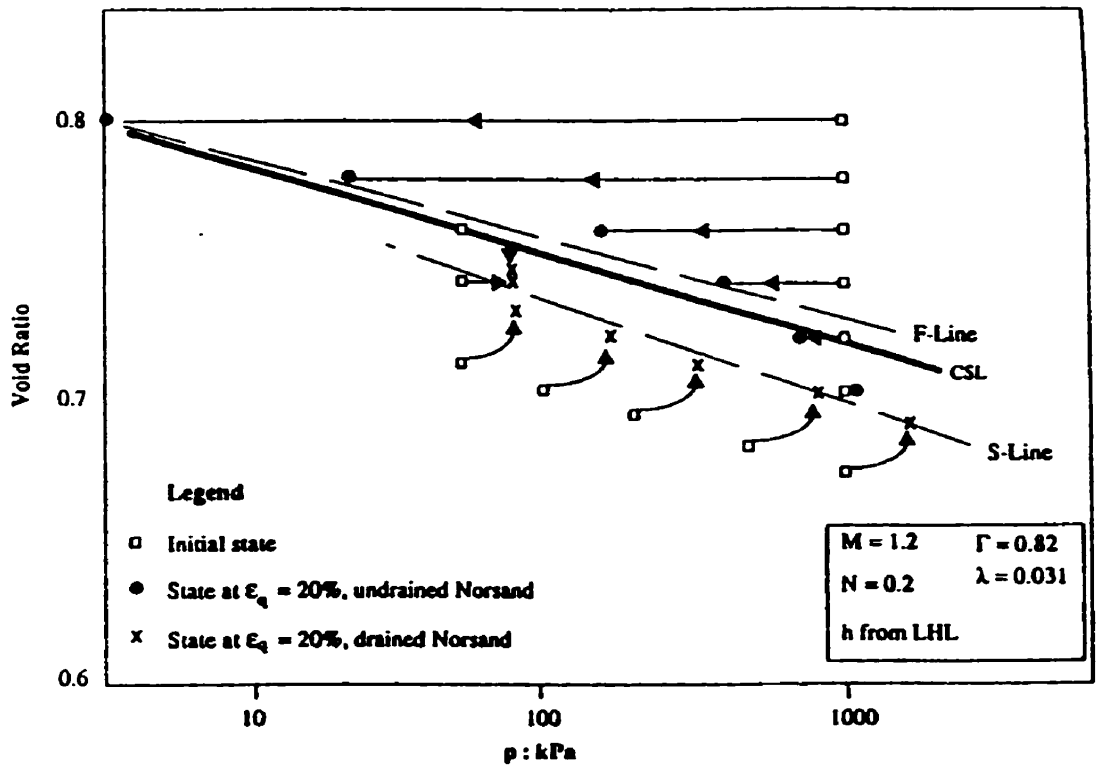

Figure 2.6 State diagram showing results of Nor-sand simulations for drained and undrained tests with "S" and "F" line criteria Epslon q = 20% (from Jefferies and Been 1992)

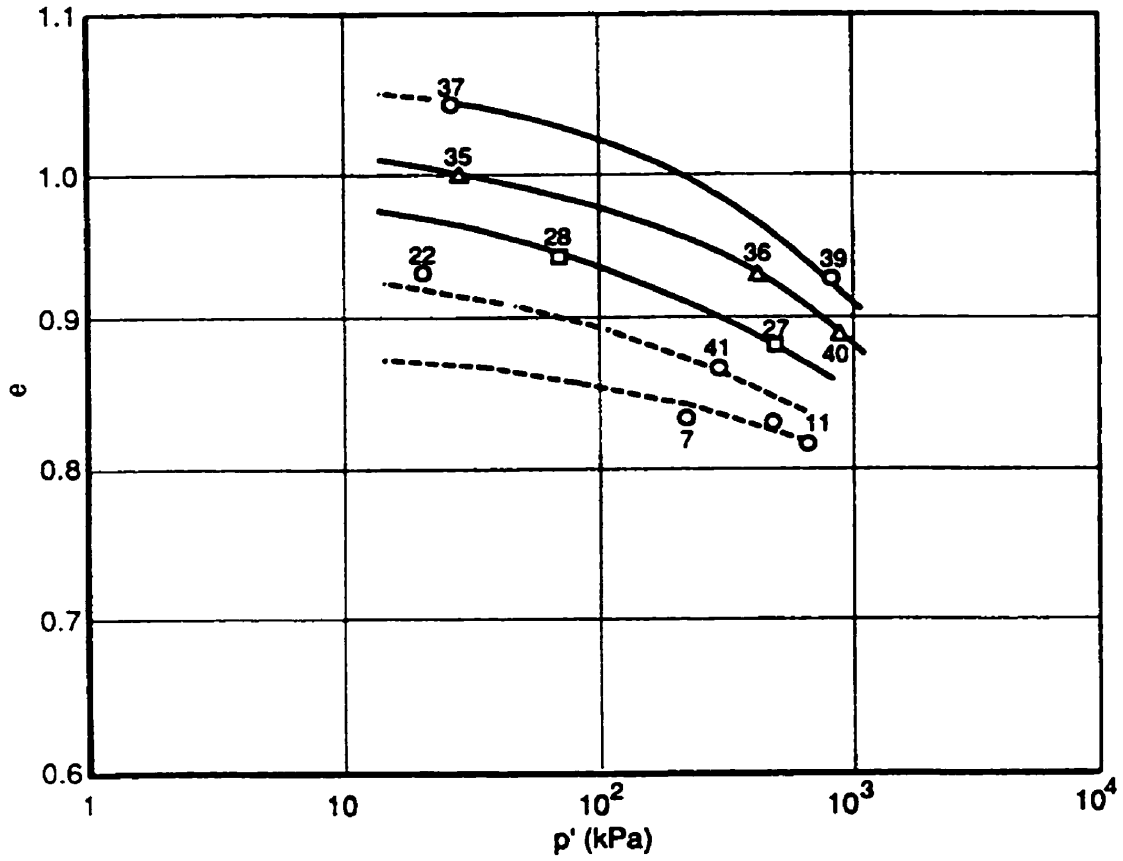

Figure 2.7 Relationship between void ratio and mean effective stress (from Konrad and Pouliot 1997)

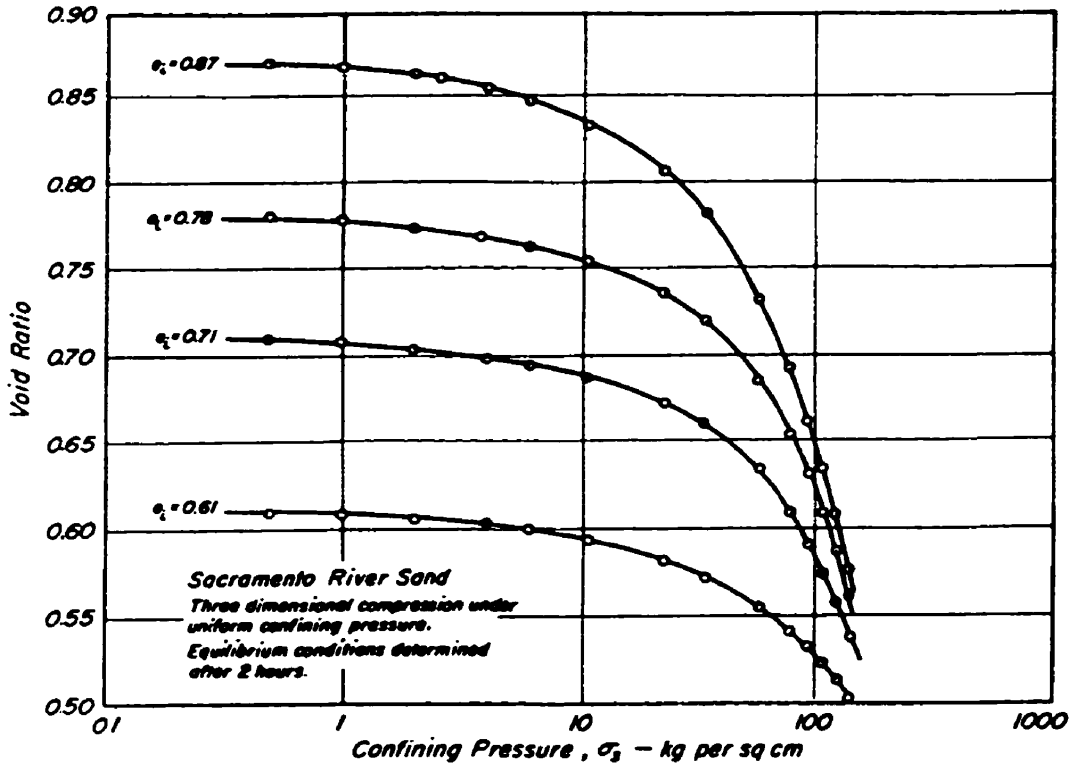

Figure 2.8 Pressure-void ratio curves for sand at four initial densities (from Lee and Seed 1967)

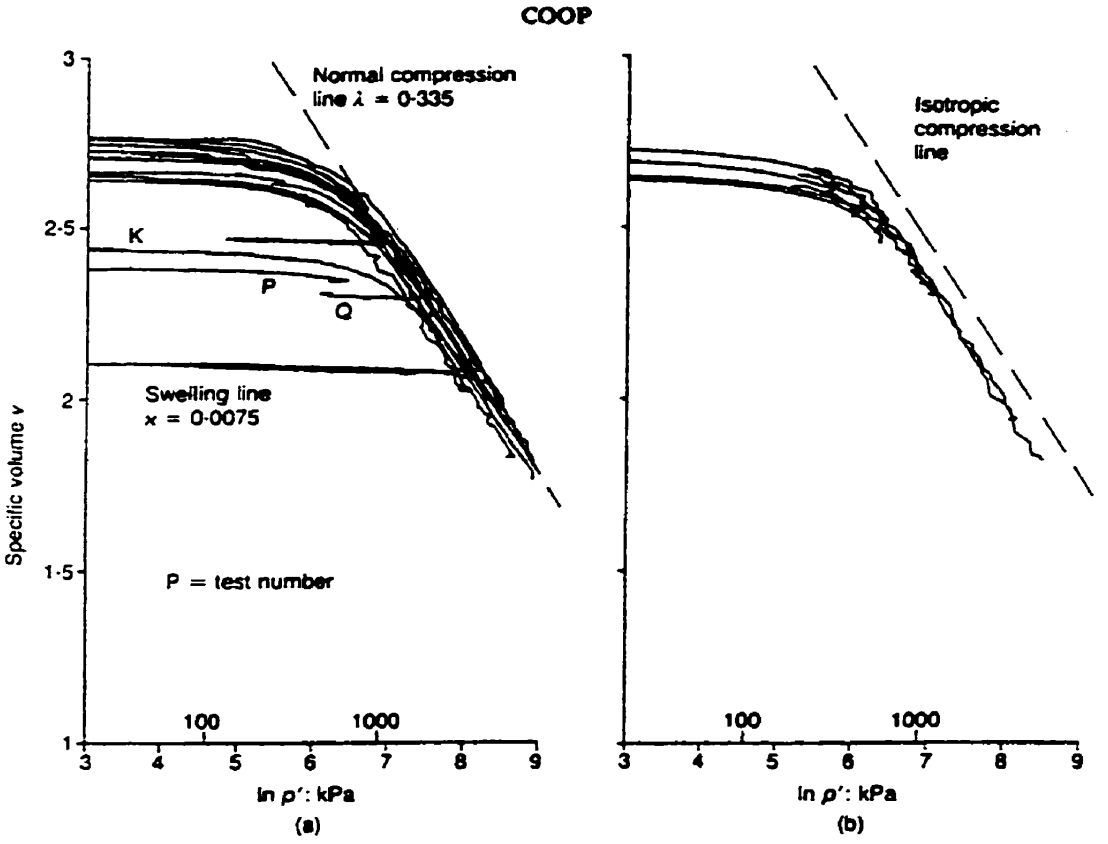

Figure 2.9 (a) Isotropic and (b) one-dimensional compression data (from Coop 1990)

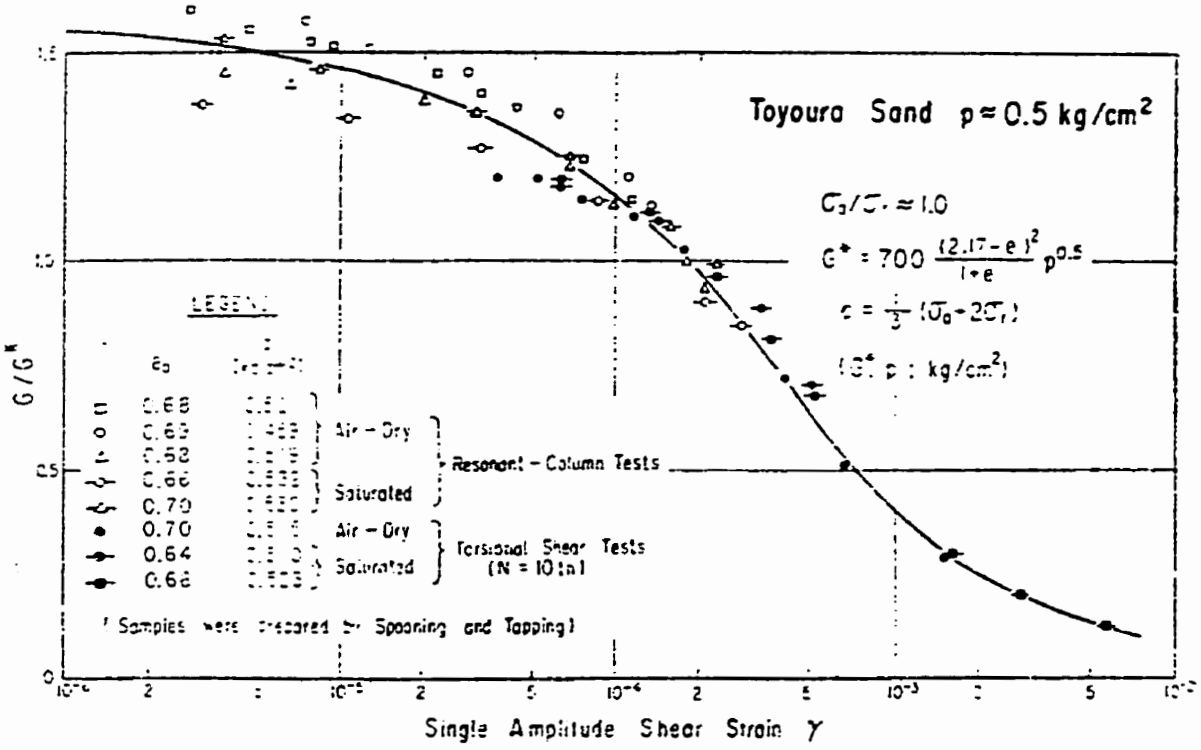

Figure 2.10 Normalized shear modulus versus natural shear strain (from Iwasaki et al. 1978)

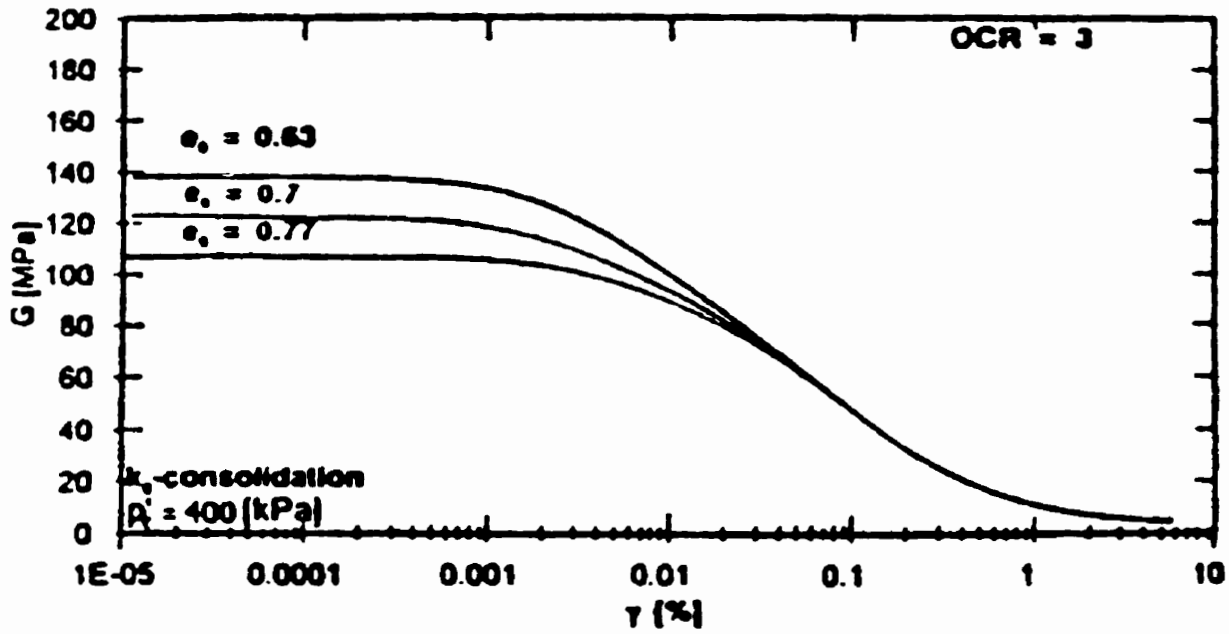

Figure 2.11 Effect of initial void ratio on shear modulus versus shear strain curves (from Porovic and Jardine 1994)

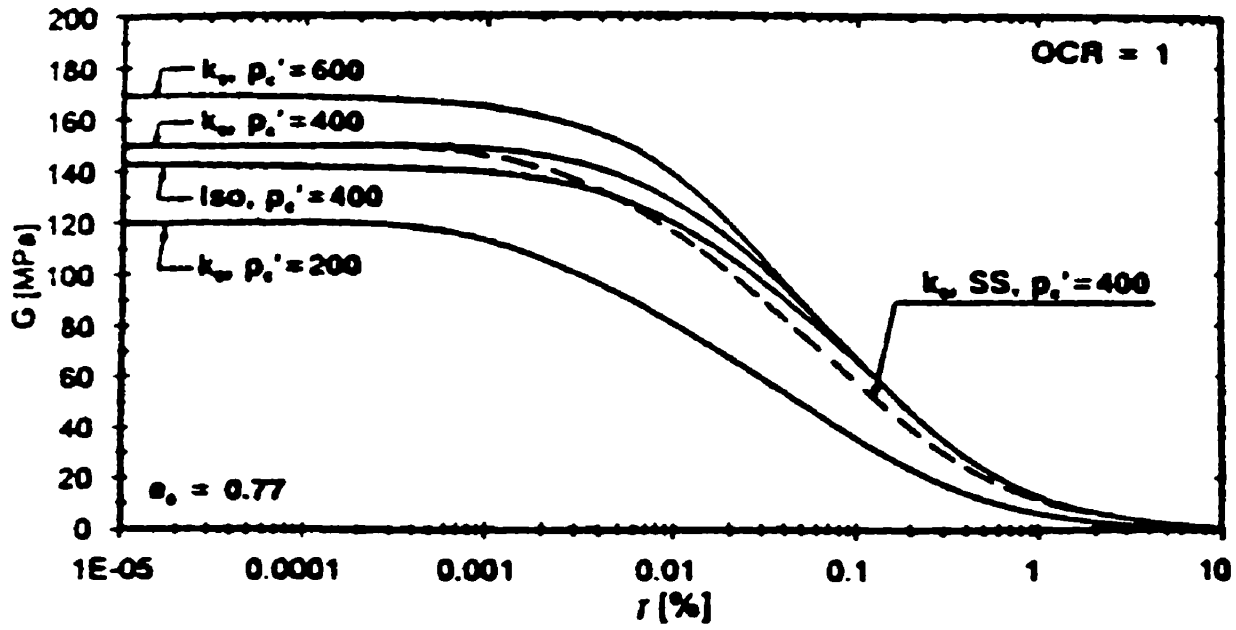

Figure 2.12 Effect of confining stress on shear modulus versus shear strain curves (from Porovic and Jardine 1994)

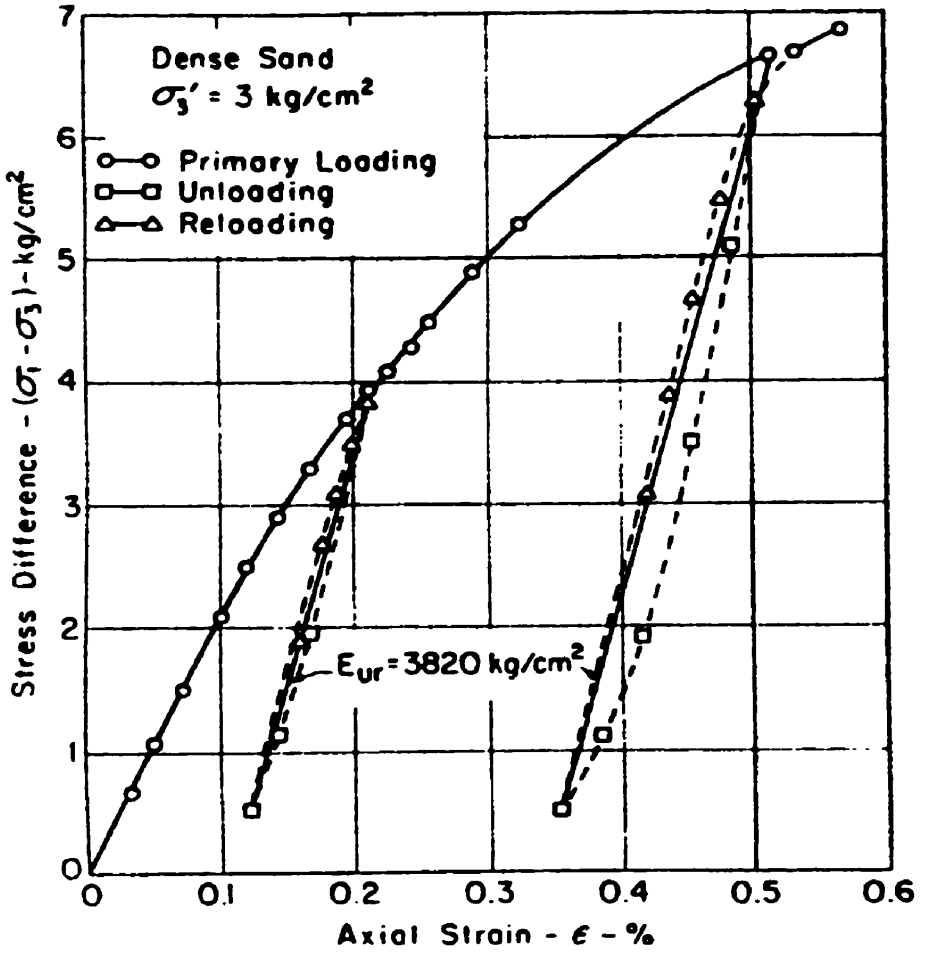

Figure 2.13 Unloading and reloading of a silica sand under drained loading triaxial compression test conditions (from Duncan and Chang 1970)

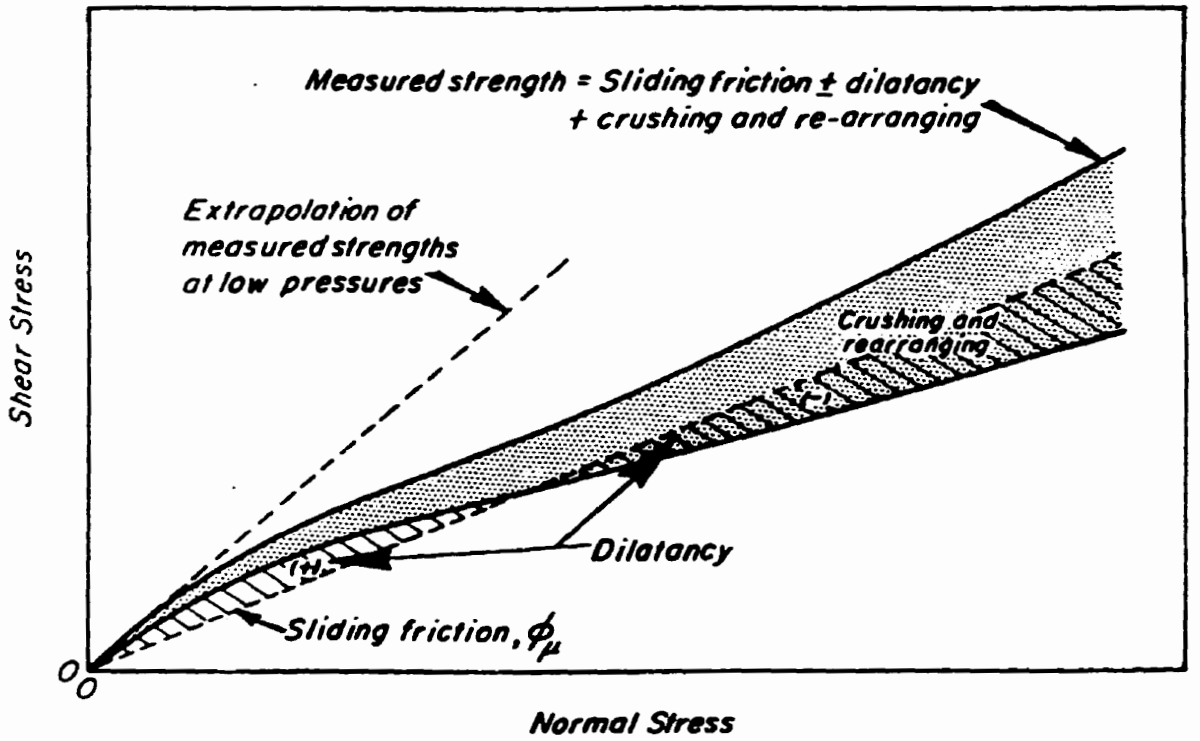

Figure 2.14 Schematic illustration of contribution of sliding friction, dilatancy and crushing to the measured mohr envelope for drained tests on sand (from Lee and Seed 1967)

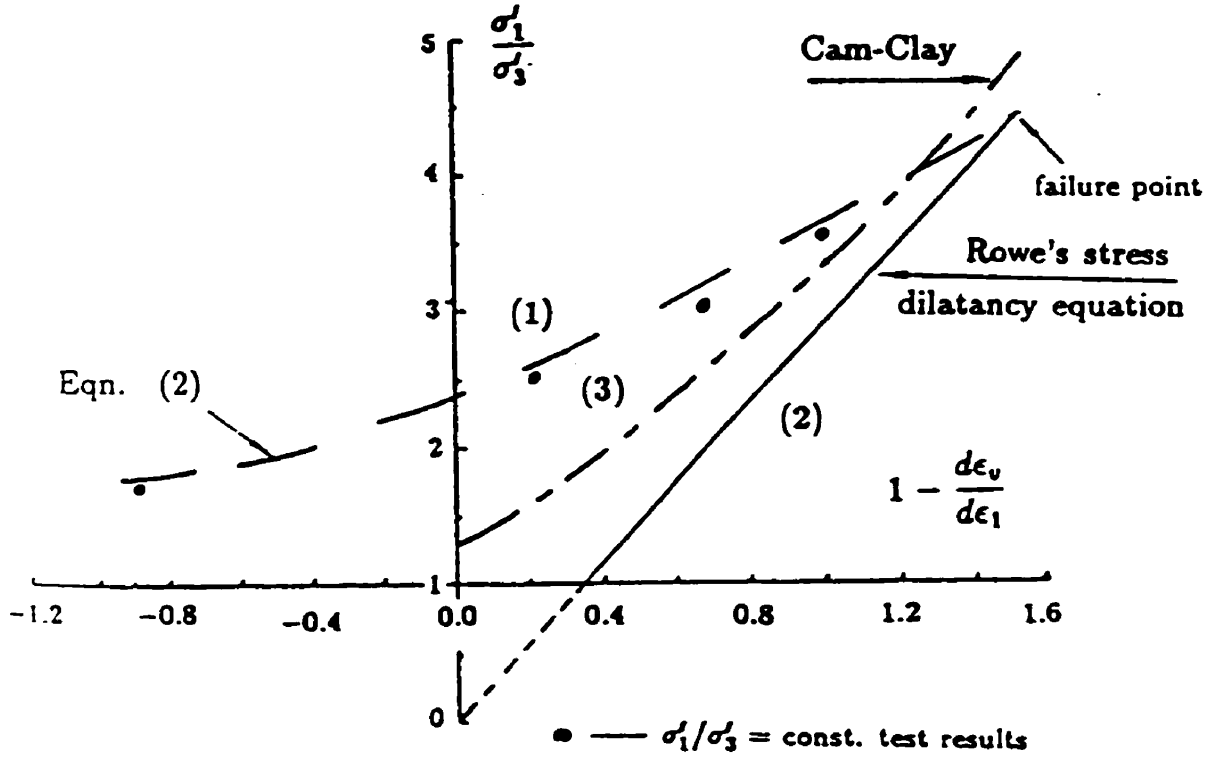

Figure 2.15 Stress-dilatancy plot (from Chu 1994)

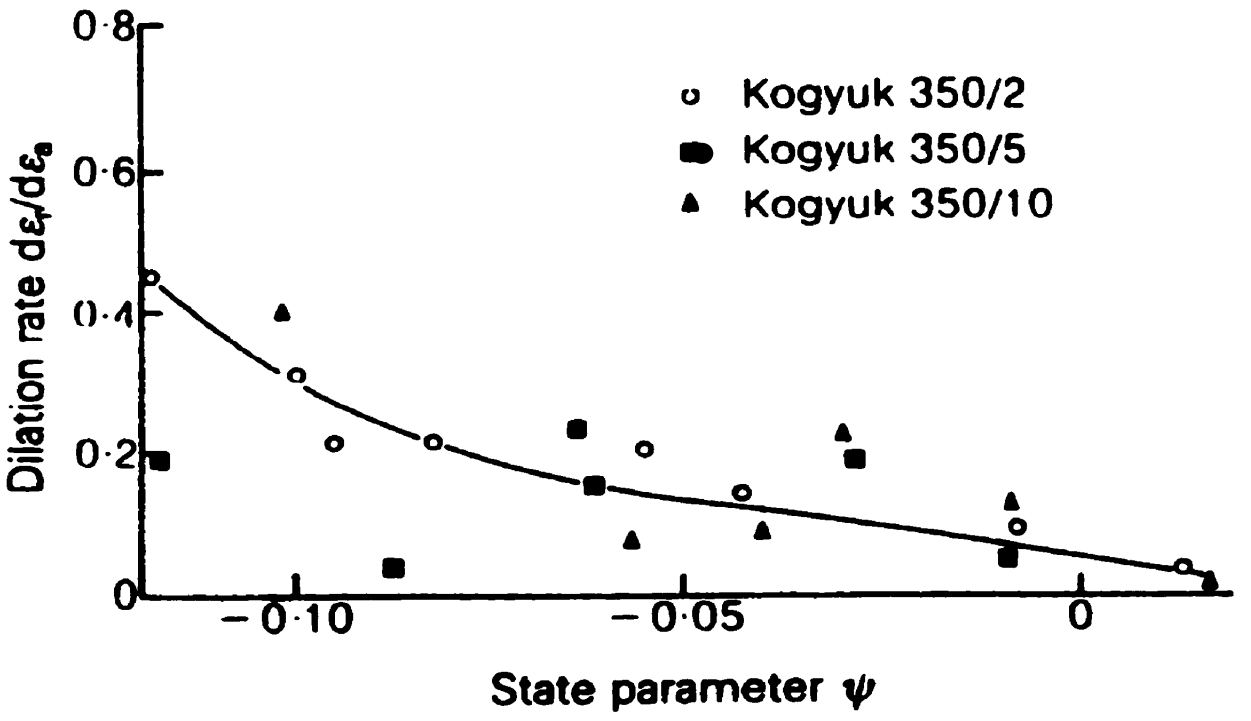

Figure 2.16 Peak angle of shearing resistance as a function of state parameter (from Been and Jefferies 1985)

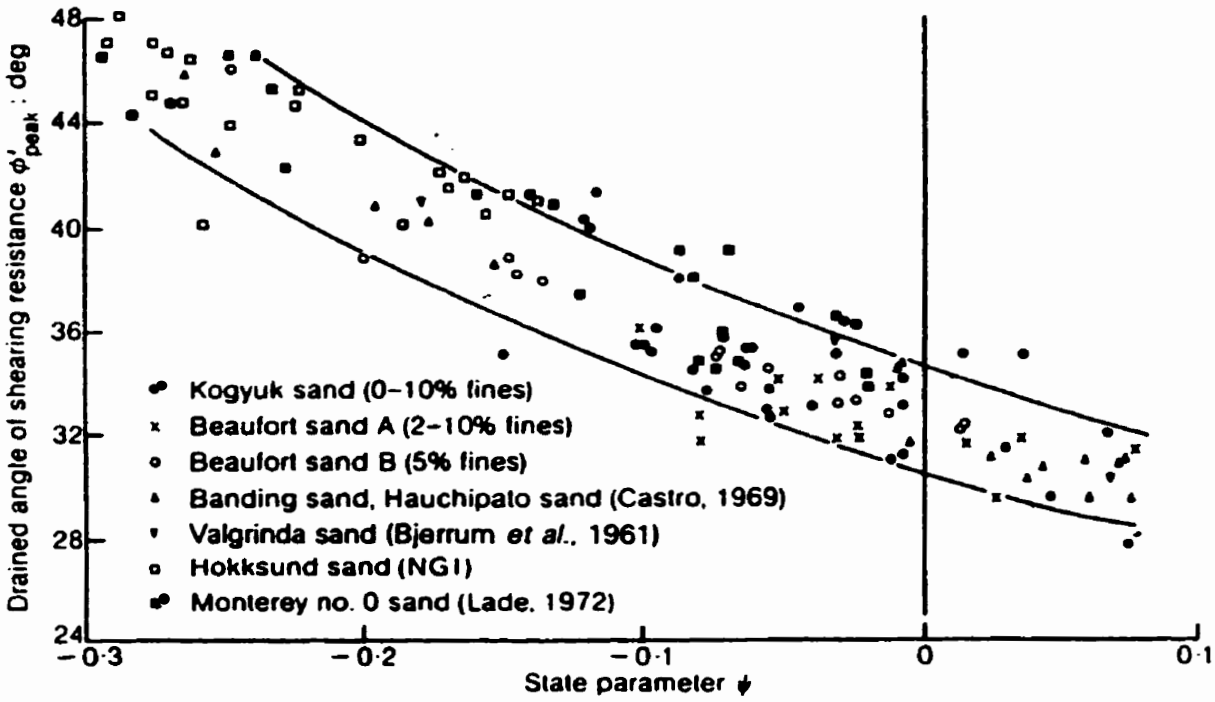

Figure 2.17 Ratio of the difference between the peak interpreted phi angle and critical state phi angle versus state parameter (from Been and Jefferies 1985)

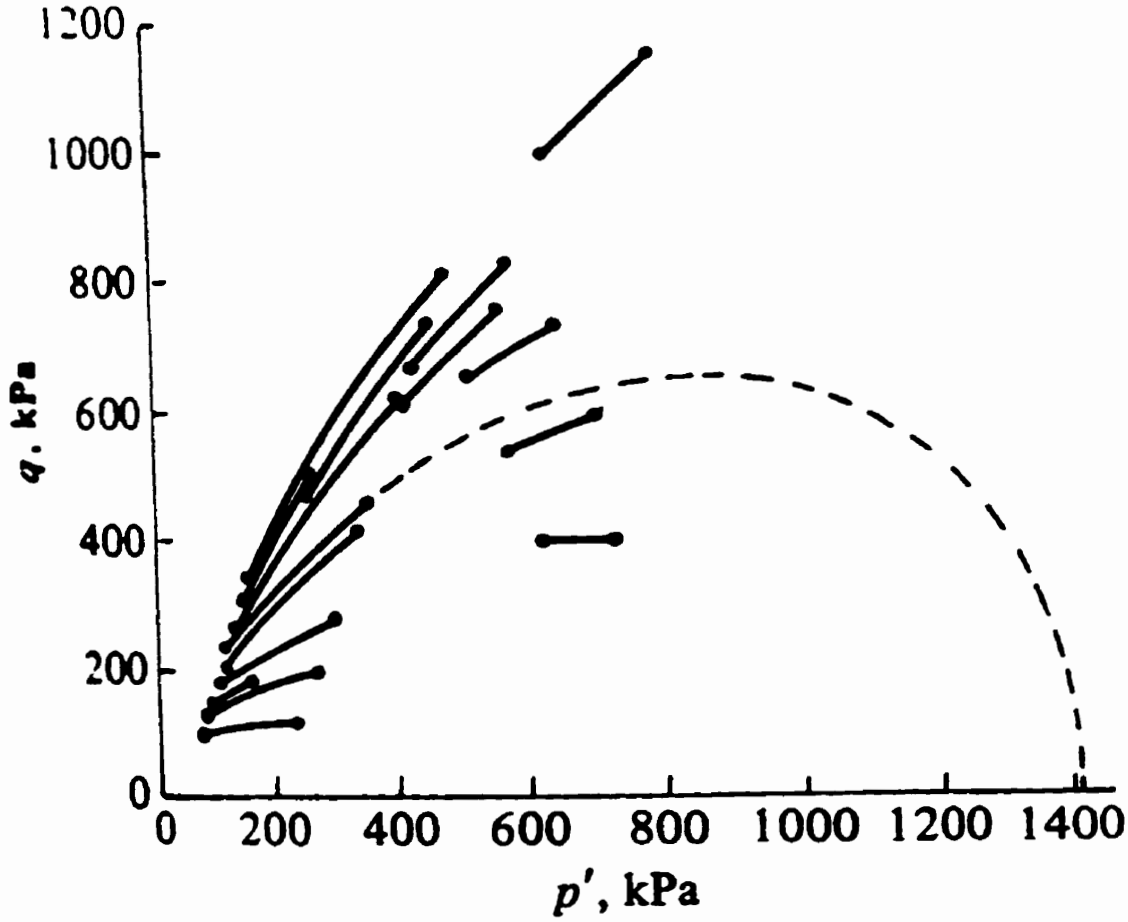

Figure 2.18 Interpreted yield surface shapes for sand (from Wood 1990)

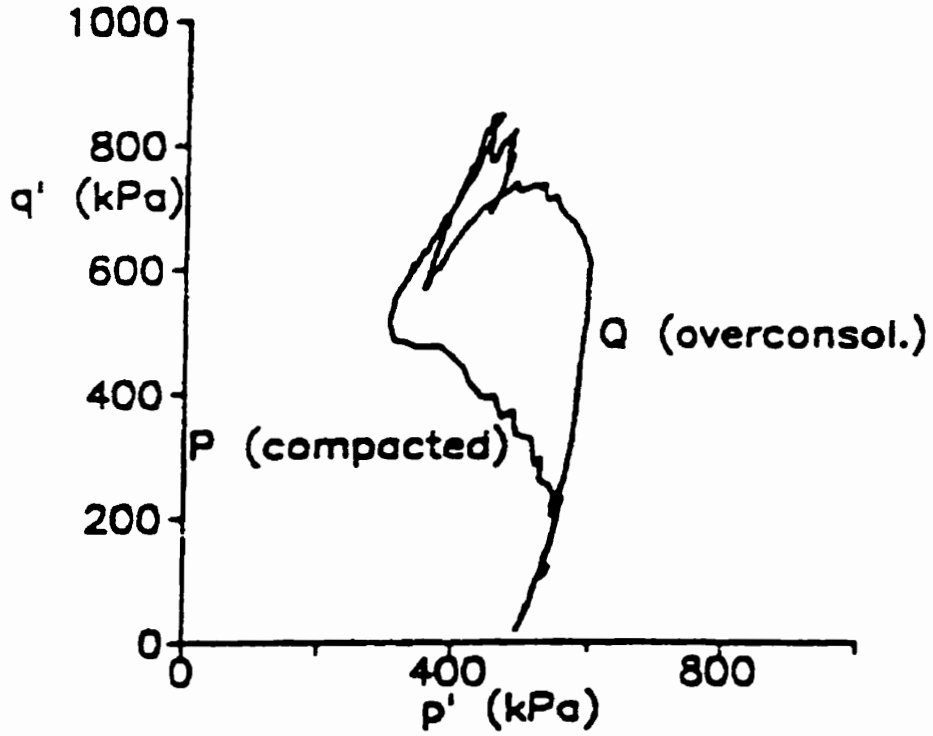

Figure 2.19 Undrained triaxial compression tests on compacted sand and overconsolidated sand (from Coop and Lee 1993)

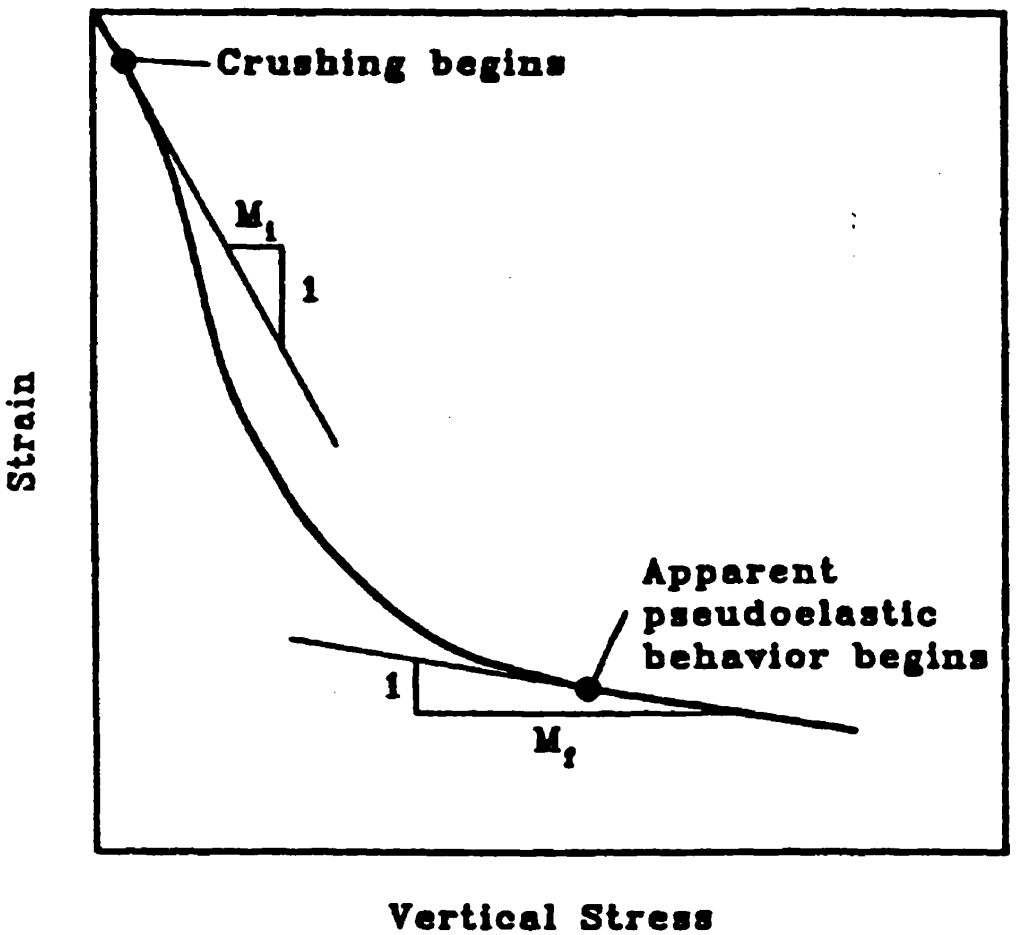

Figure 2.20 Strain versus Applied vertical stress – three phase of one dimenisonal compression (from Hagerty et al. 1993)

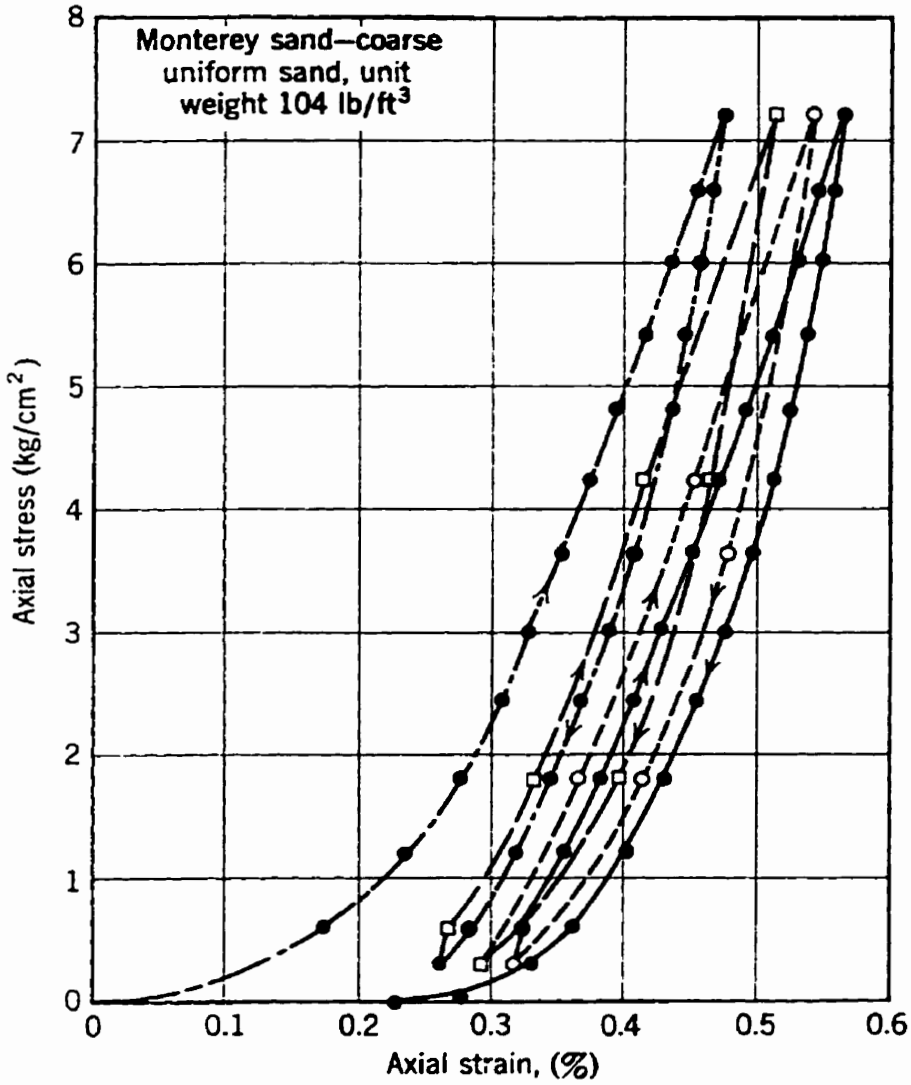

Figure 2.21 Stress-strain curves during several cycles of loading in oedometer test (from Lambe and Whitman 1969)

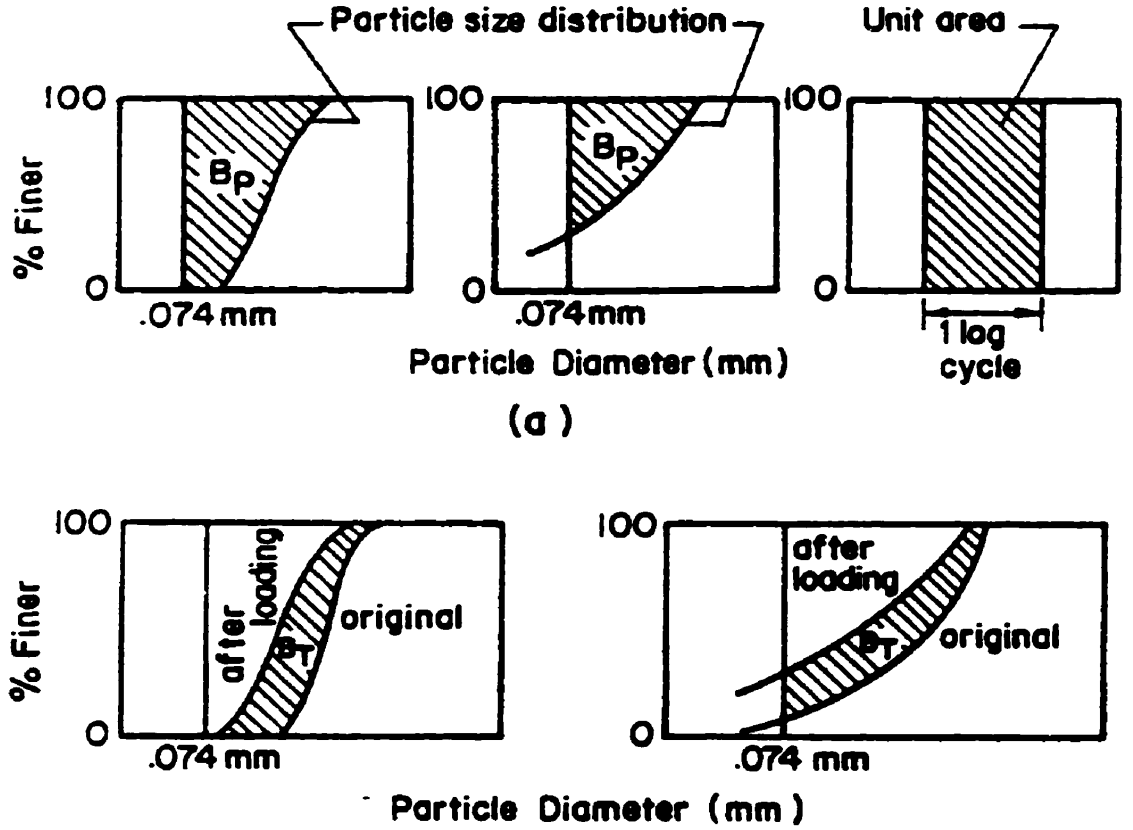

Figure 2.22 Definition of breakage potential (a) and total breakage (b) (from Yudhbir and Wood 1989)

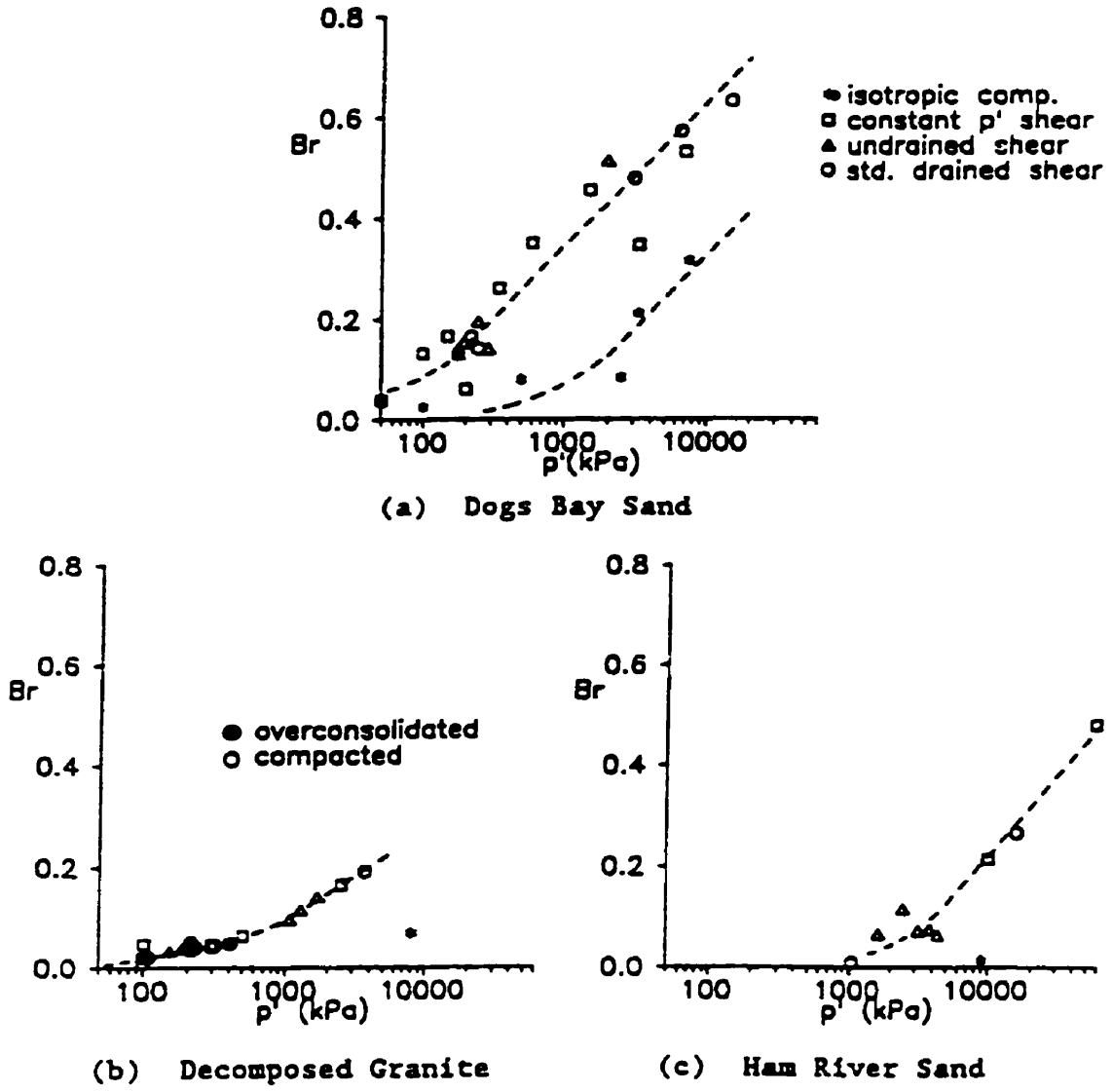

Figure 2.23 Relationship between relative breakage and mean stress for three different sands (from Coop and Lee 1993)

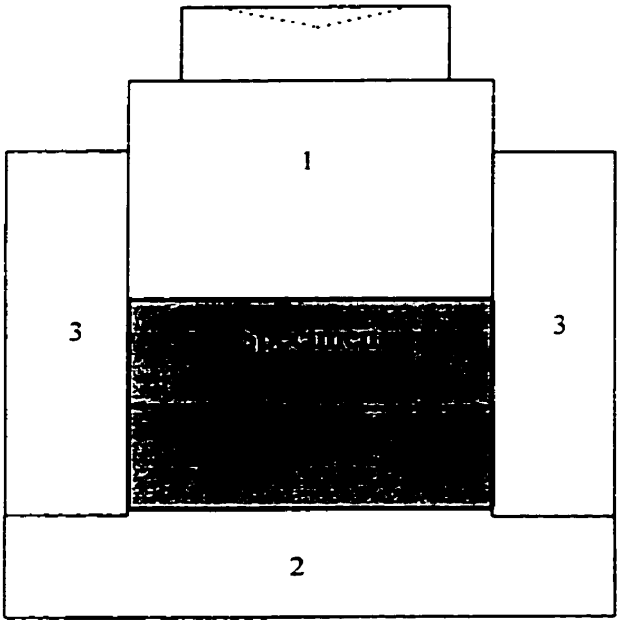

1 - Top cap

2 - Base

3 - Confining ring

Figure 3.1 One dimensional compression cell

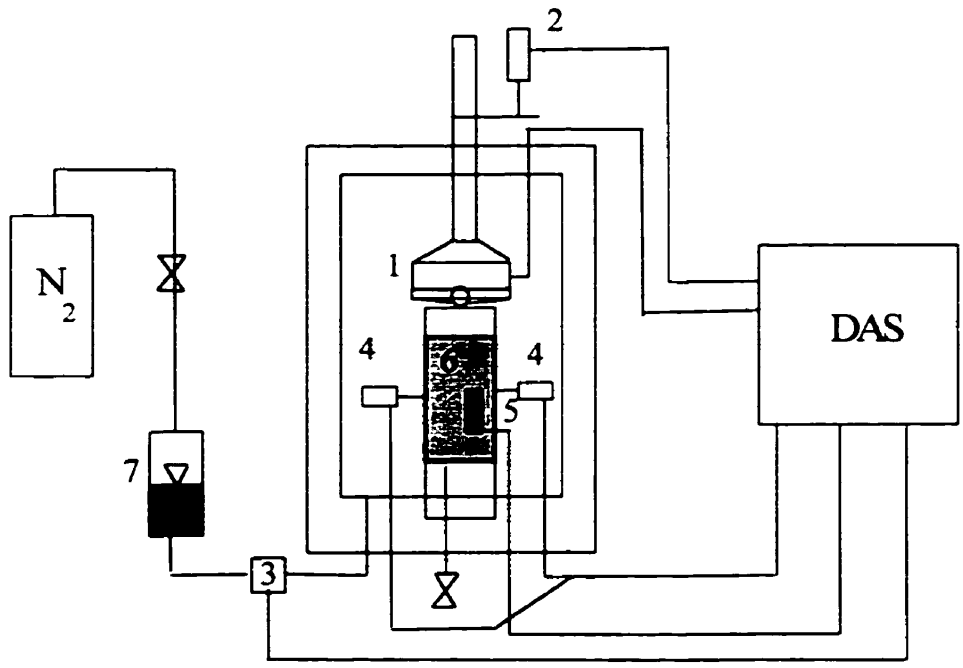

1 - Load cell

2 - External axial LVDT

3 - Cell pressure transducer

7 - Accumulator

DAS - Data acquisition system

4 - Internal radial LVDT

5 - RTD

6 - Specimen

N_2 - Nitrogen supply

Figure 3.2 HITEP Triaxial cell

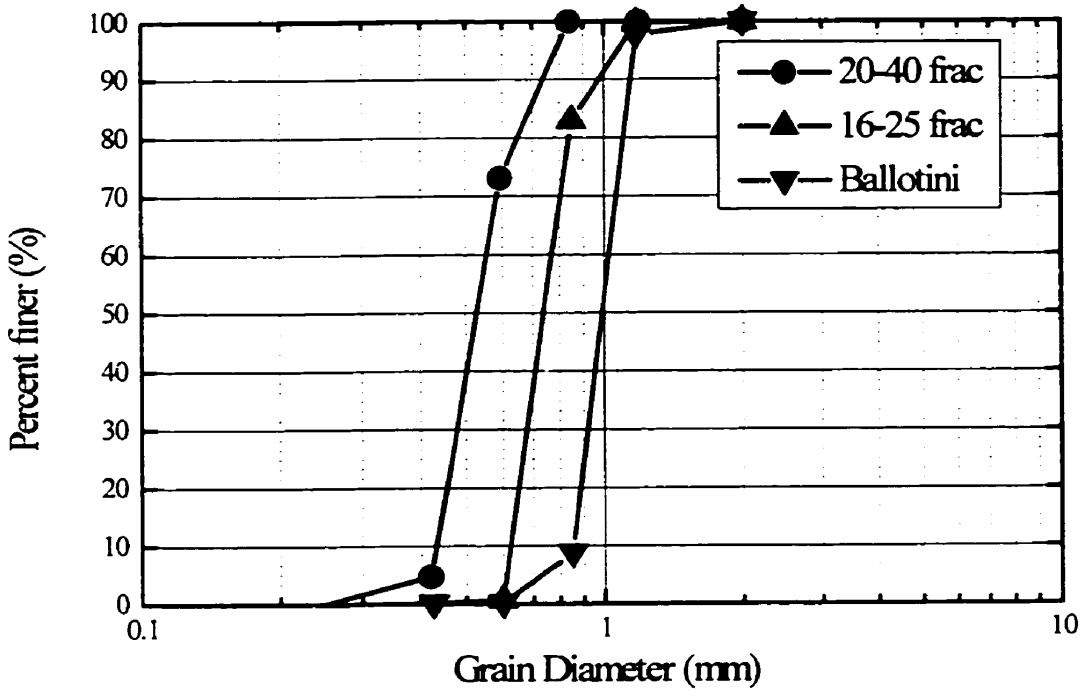

Figure 3.3 Grain size analysis prior to testing

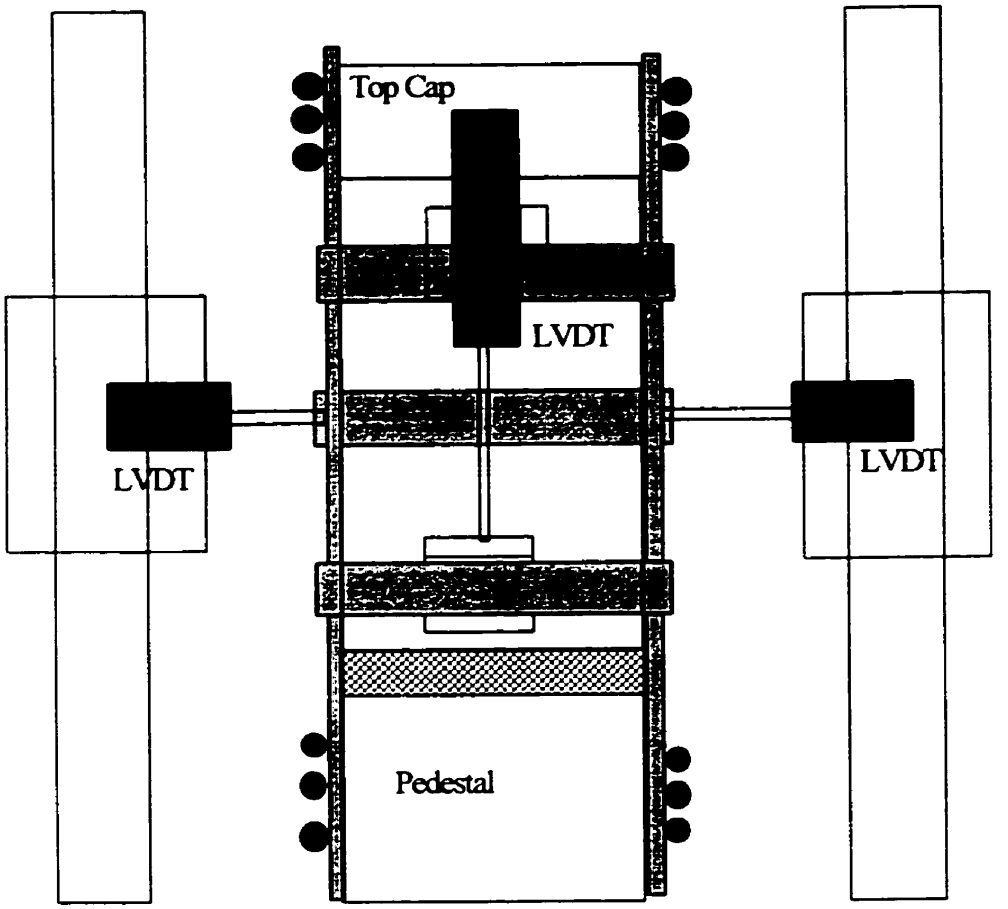

Figure 3.4 Internal instrumentation used for isotropic compression testing

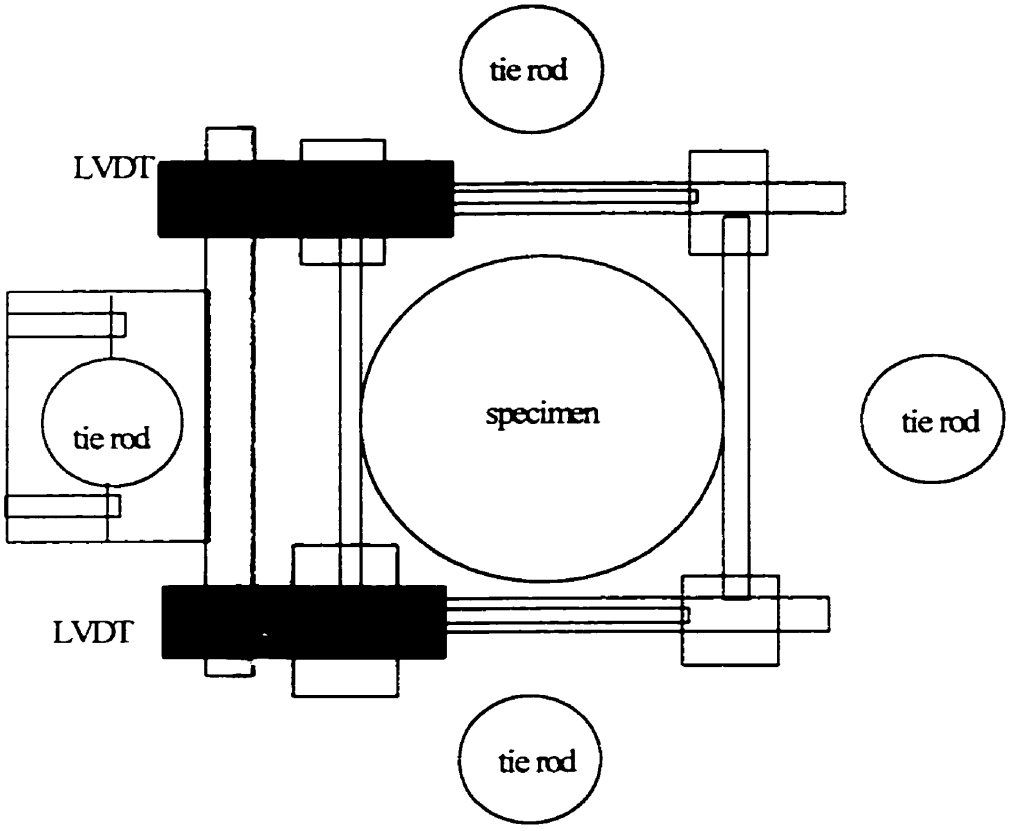

Figure 3.5 Internal instrumentation used to measure radial deformation in triaxial compression

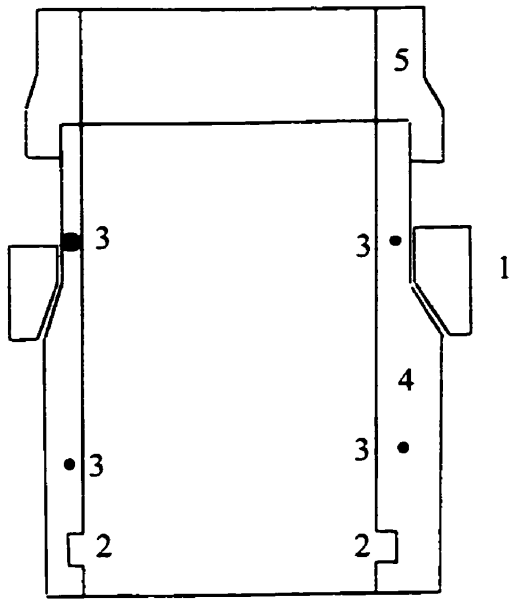

1 - clamping ring

2 - gap for o-ring

3 - alignment pins

4 - split mold

5 - top spacer

Figure 3.6 Split mold specimen former

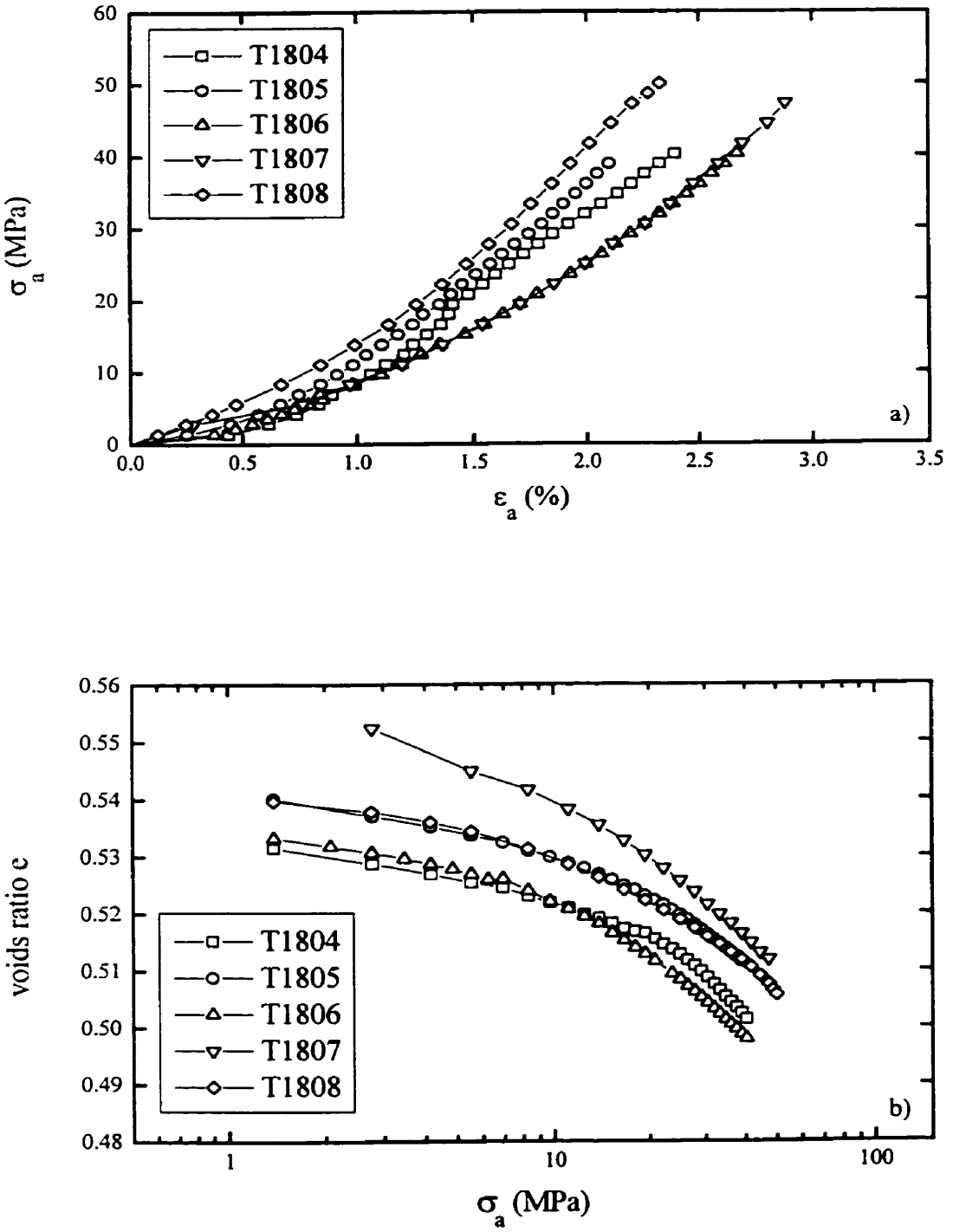

Figure 4.1 One-dimension confined compression of Ballotini plotted in a) applied axial stress *versus* axial strain space and b) *log* applied axial stress *versus* voids ratio space

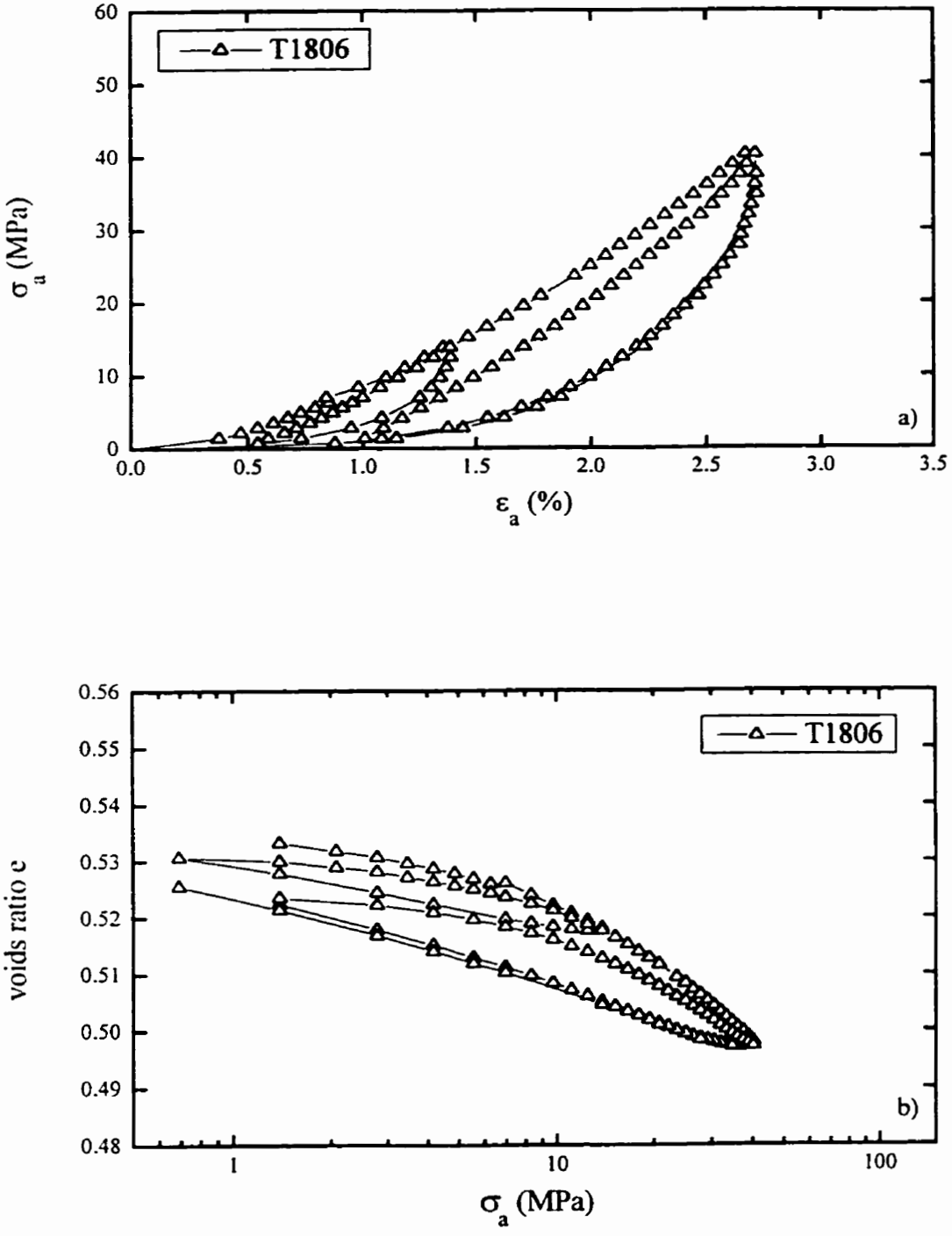

Figure 4.2 One-dimensional compression with unload-reloading cycles for test T1806 on Ballotini plotted in a) applied axial stress *versus* axial strain space and b) *log* applied axial stress *versus* voids ratio space

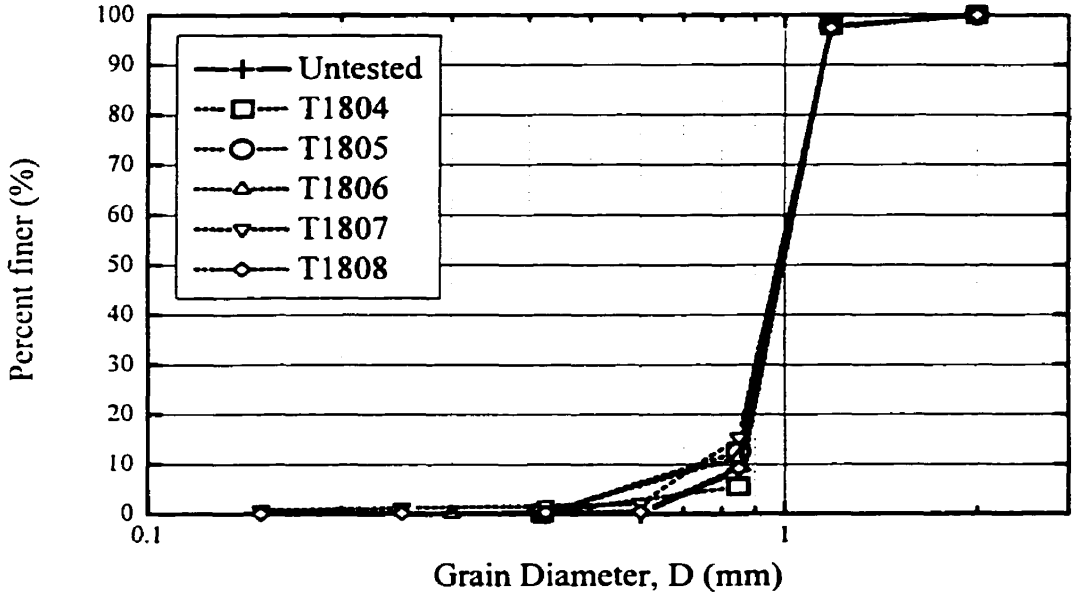

Figure 4.3 Sieve analysis results from tests on Ballotini

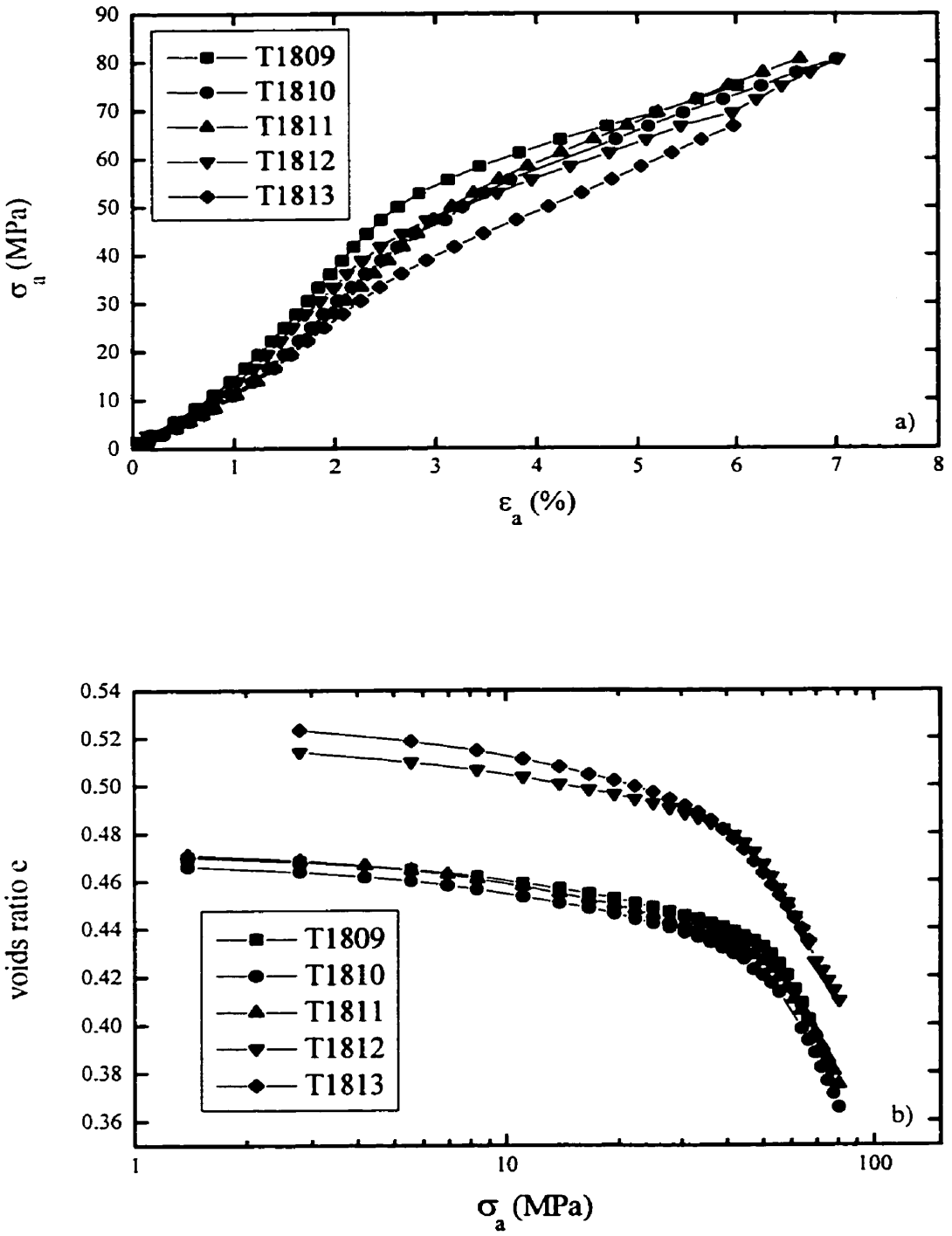

Figure 4.4 One-dimensional compression of 'Frac' sand plotted in a) applied axial stress *versus* axial strain space and b) *log* applied axial stress *versus* voids ratio space

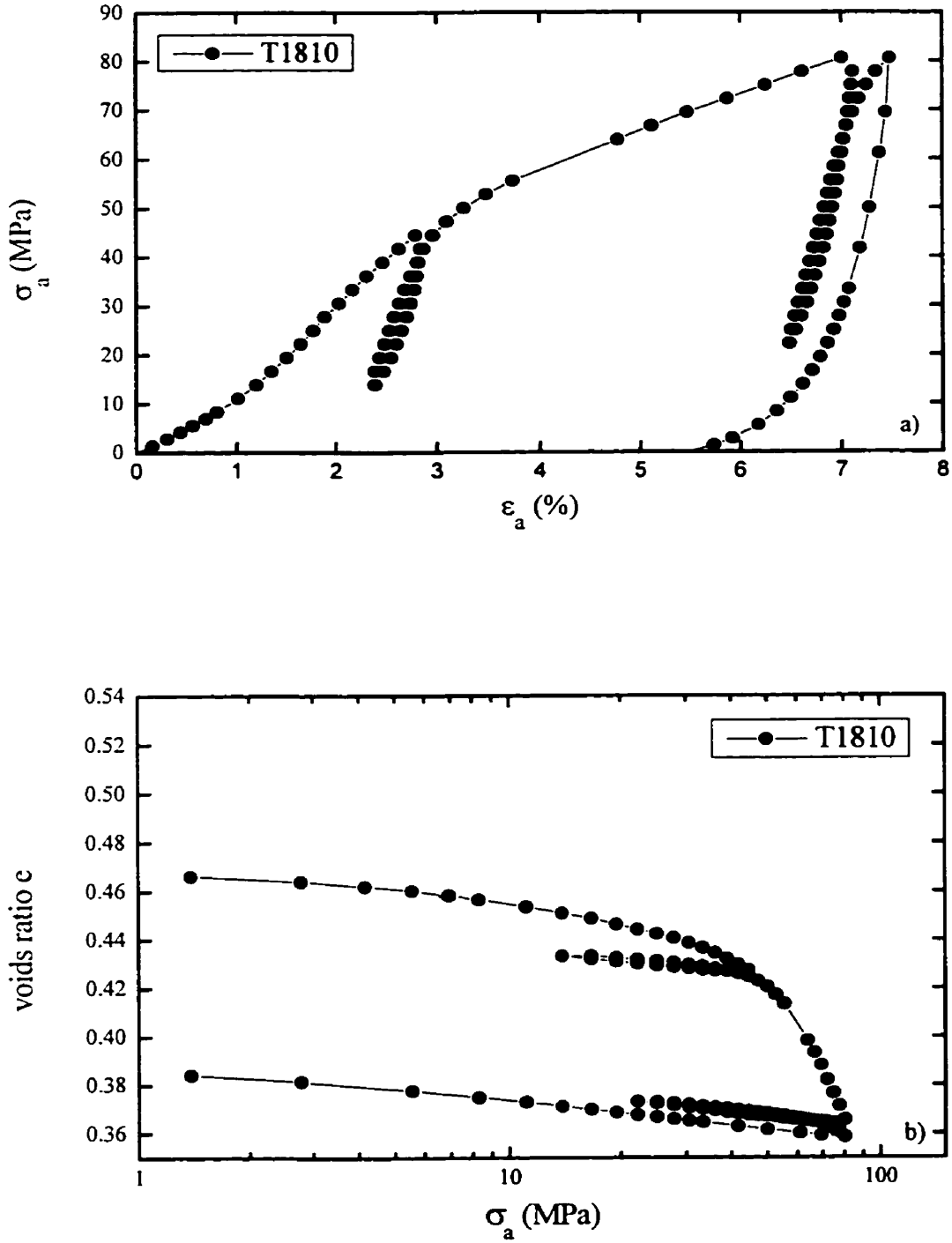

Figure 4.5 One-dimensional compression including unload-reload cycles for T1810 on 16-25 'Frac' sand plotted in a) applied axial stress *versus* axial strain space and b) *log* applied axial stress *versus* voids ratio space

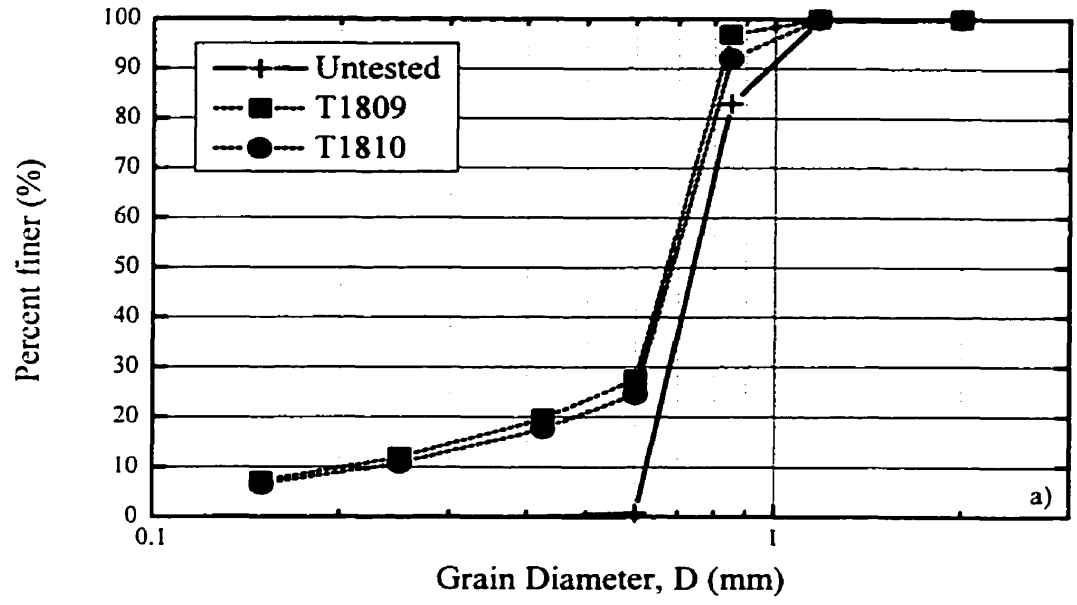

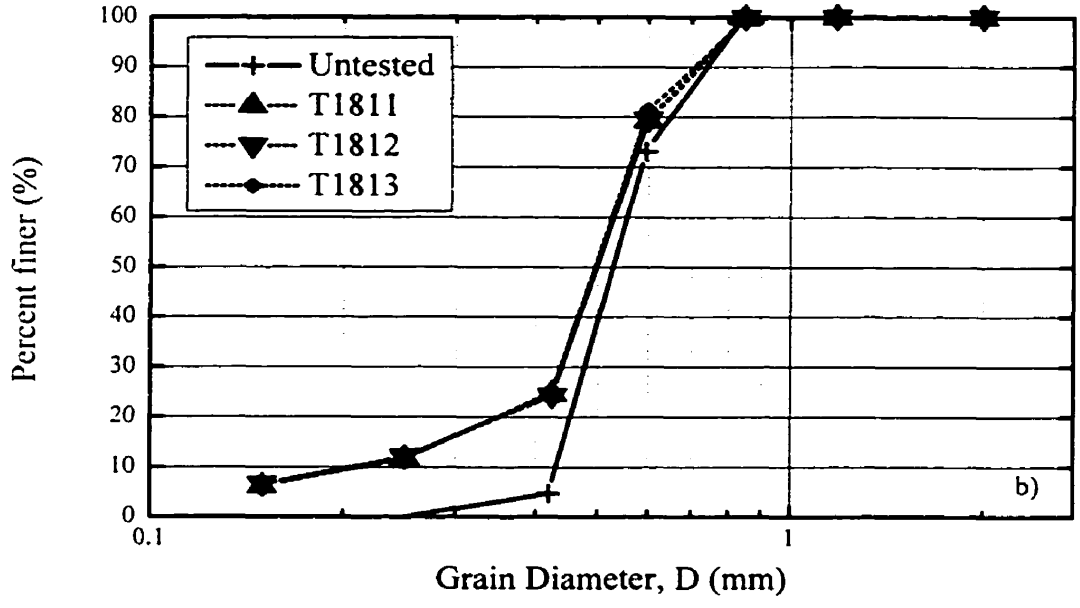

Figure 4.6 Sieve analysis results before and after tests on a) 16-25 'Frac' sand and b) 20-40 'Frac' sand

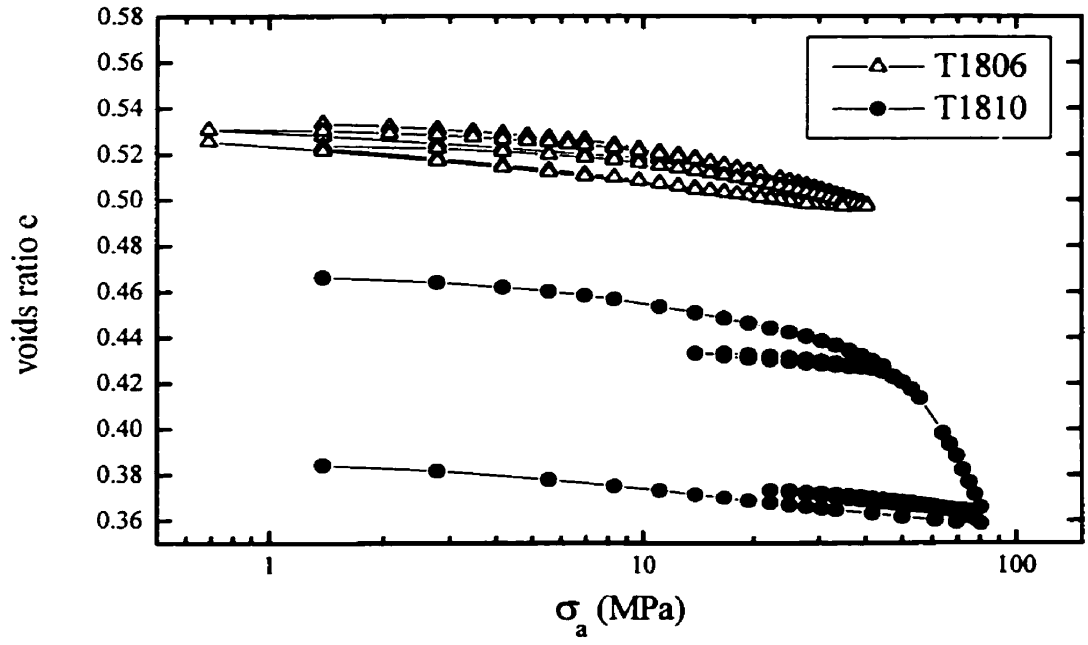

Figure 4.7 One-dimensional compression results including unload-reload cycles plotted in *log* axial stress *versus* voids ratio space for T1806, Ballotini and T1810, 16-25 'Frac' sand

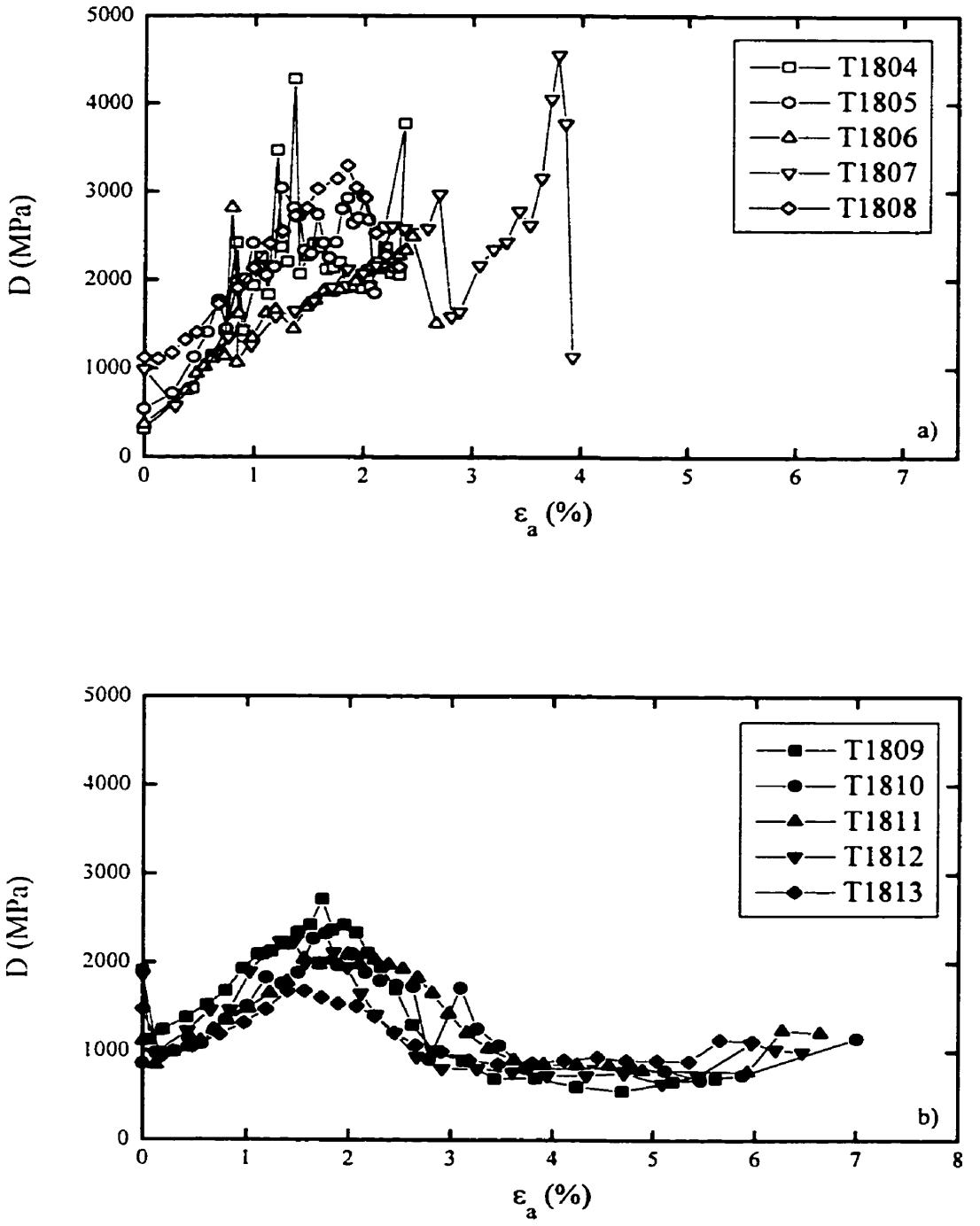

Figure 4.8 Confined modulus, calculated incrementally plotted *versus* axial stress for tests on a) Ballotini and b) 'frac' sand

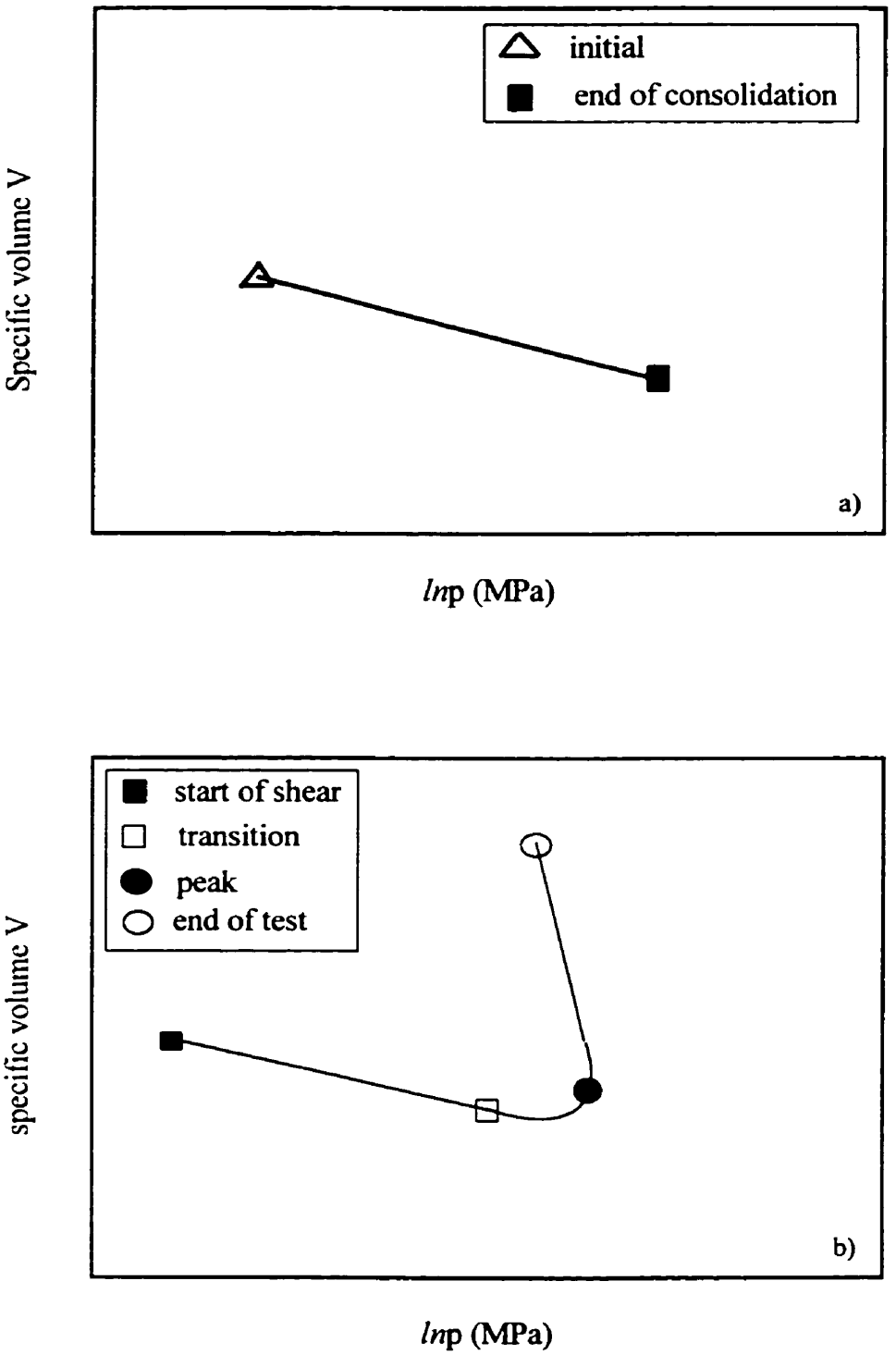

Figure 5.1 Key "state" points in a triaxial compression test in specific volume V *versus* mean stress, p space a) isotopic compression b) shearing

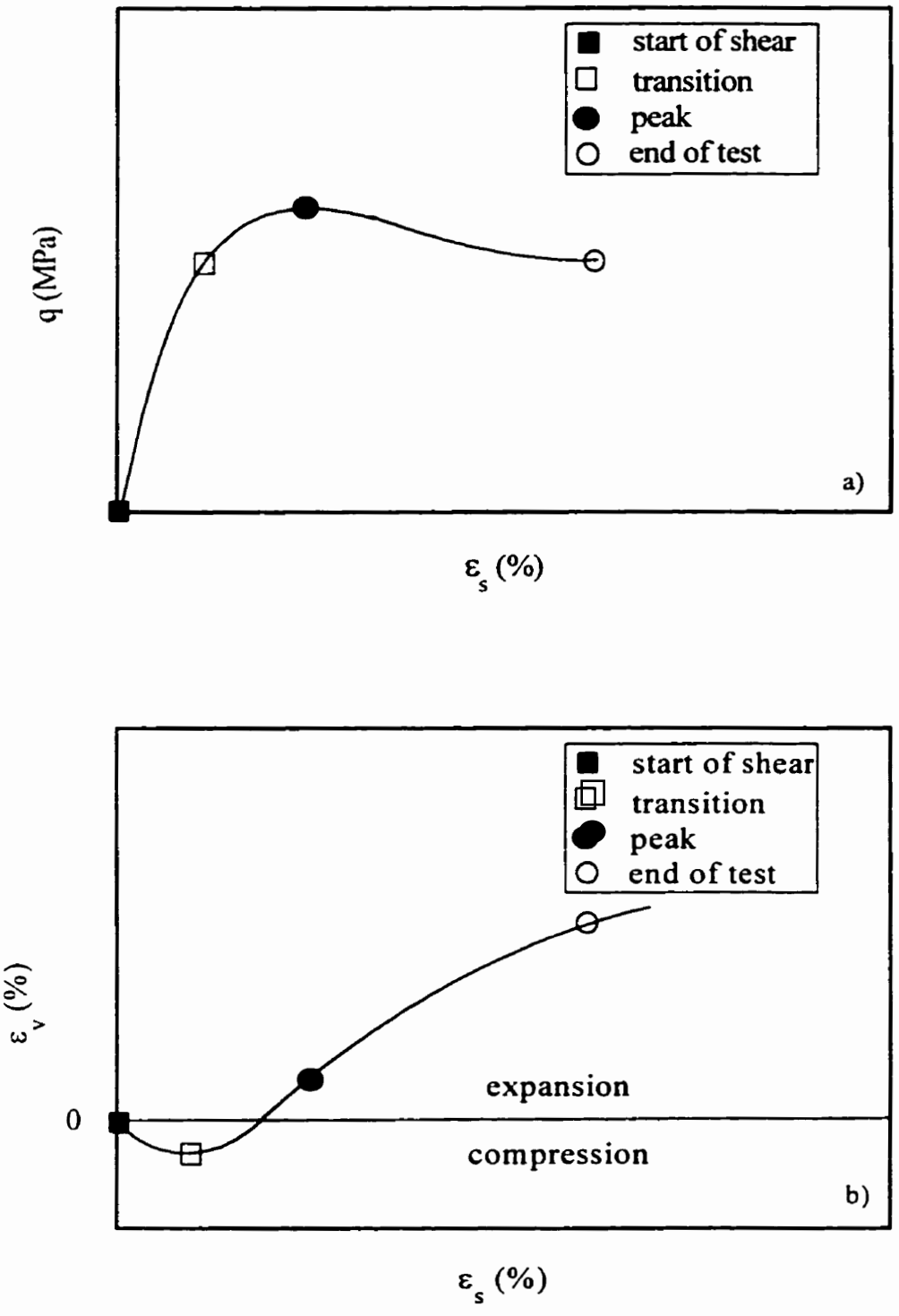

Figure 5.2 Key "state" points in a triaxial compression test a) plotted in shear stress, q *versus* shear strain, ε_s, space and b) plotted in shear strain, ε_s, *versus* volume strain, ε_v, space

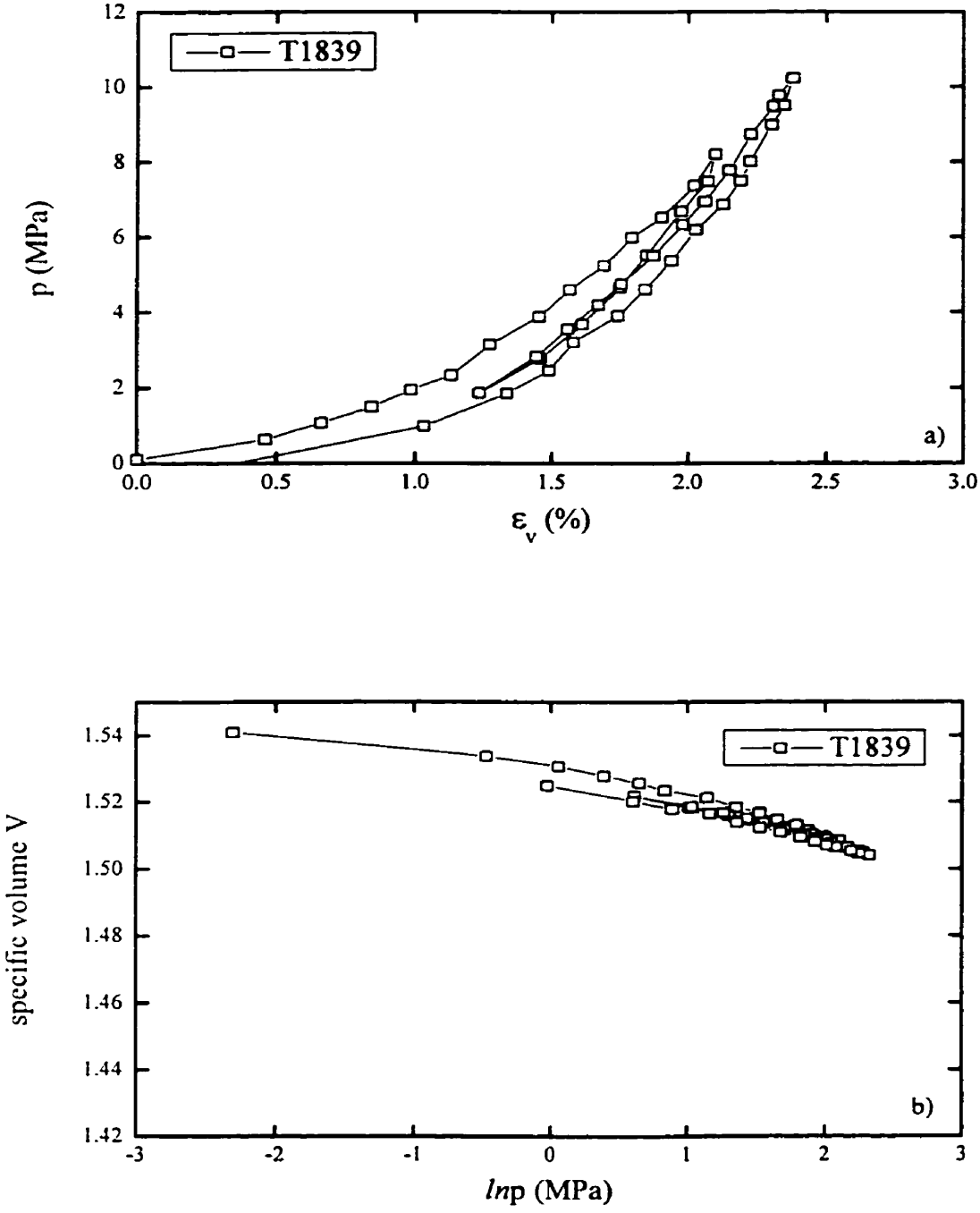

Figure 5.3 Isotropic compression of Ballotini at room temperature plotted as; a) mean stress, p *versus* volume strain, ε_v and b) natural logathirm of mean stress *ln* p *versus* specific volume, V

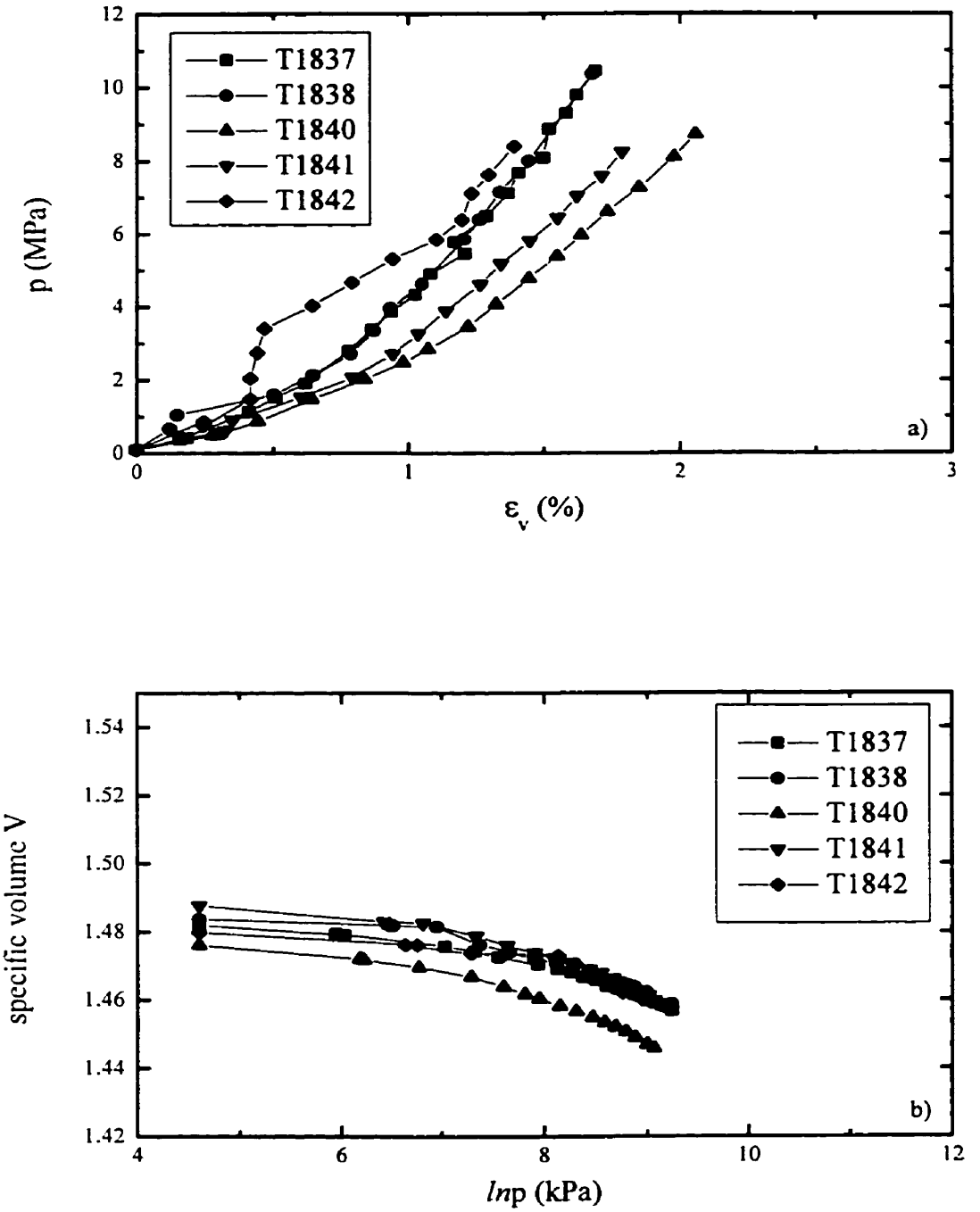

Figure 5.4 Isotropic compression of 20-40 'frac' sand at room temperature plotted as; a) mean stress, p *versus* volume strain, ε_v and b) natural logathirm of mean stress *ln* p *versus* specific volume, V

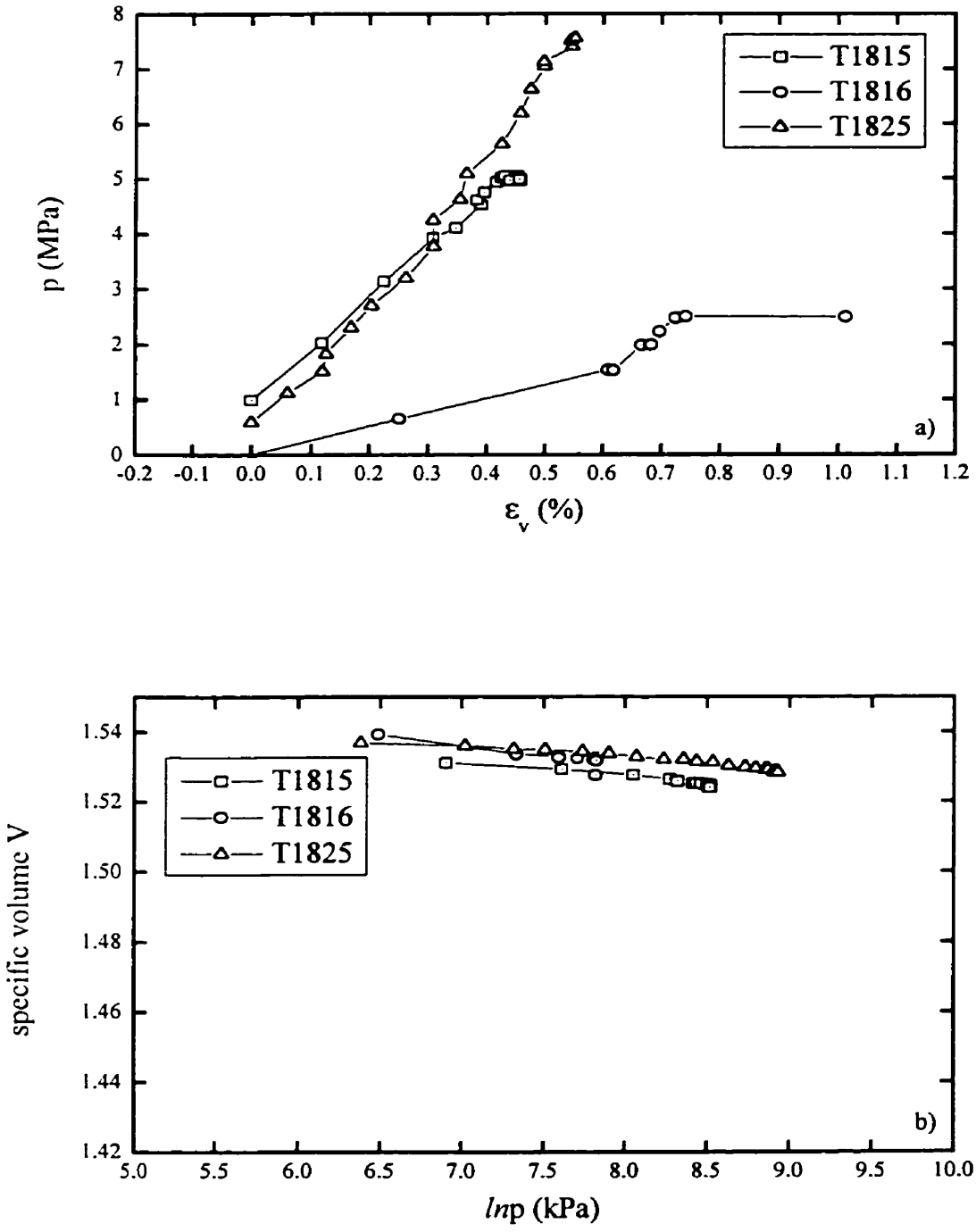

Figure 5.5 Isotropic compression prior to shearing for tests on Ballotini at room temperature plotted as: a) mean stress, p *versus* volume strain, ε_v and b) natural logathirm of mean stress *ln* p *versus* specific volume, V

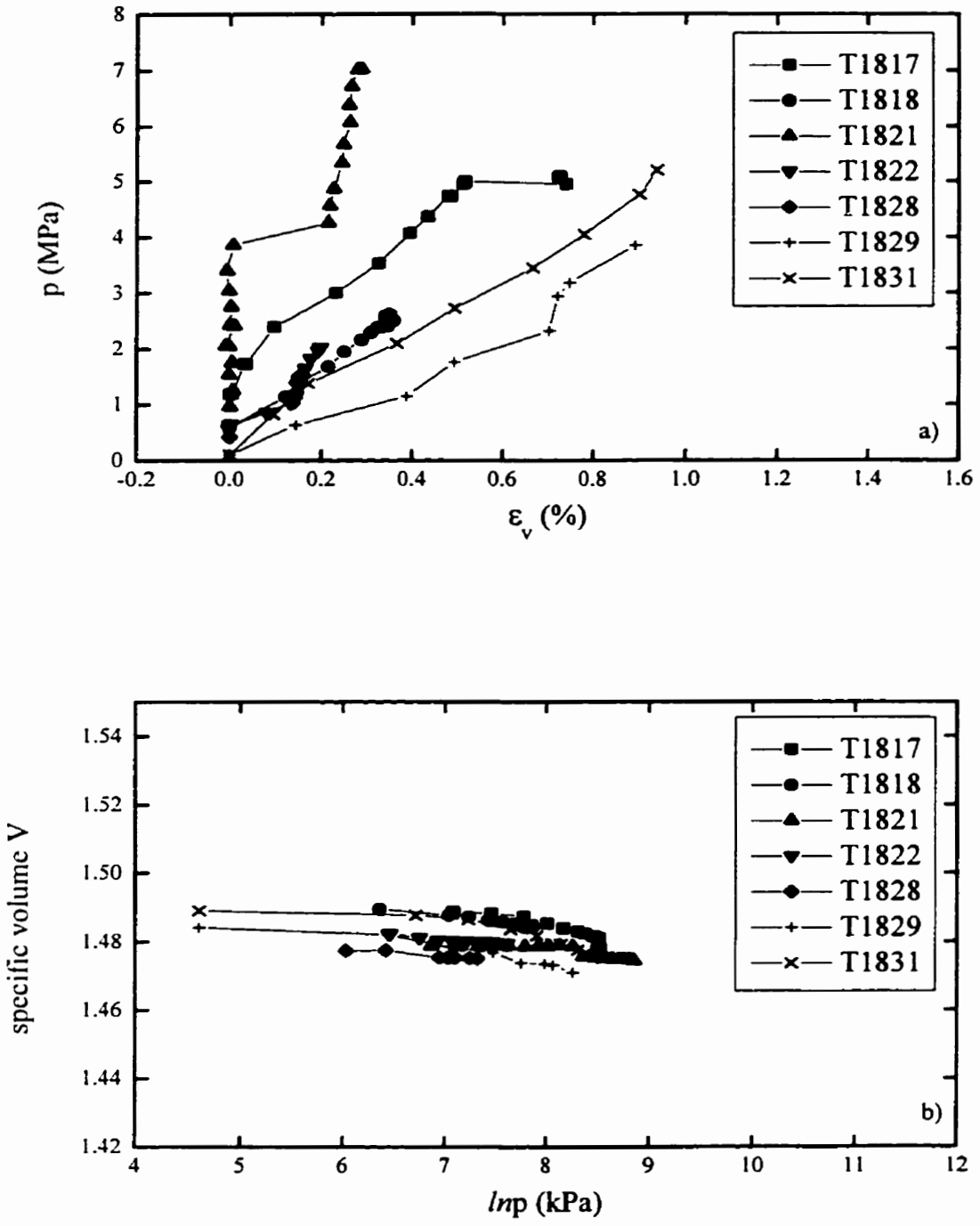

Figure 5.6 Isotropic compression prior to shearing for tests on 20-40 'frac' sand at room temperature plotted as: a) mean stress, p *versus* volume strain, ε_v and b) natural logathirm of mean stress *ln* p *versus* specific volume, V

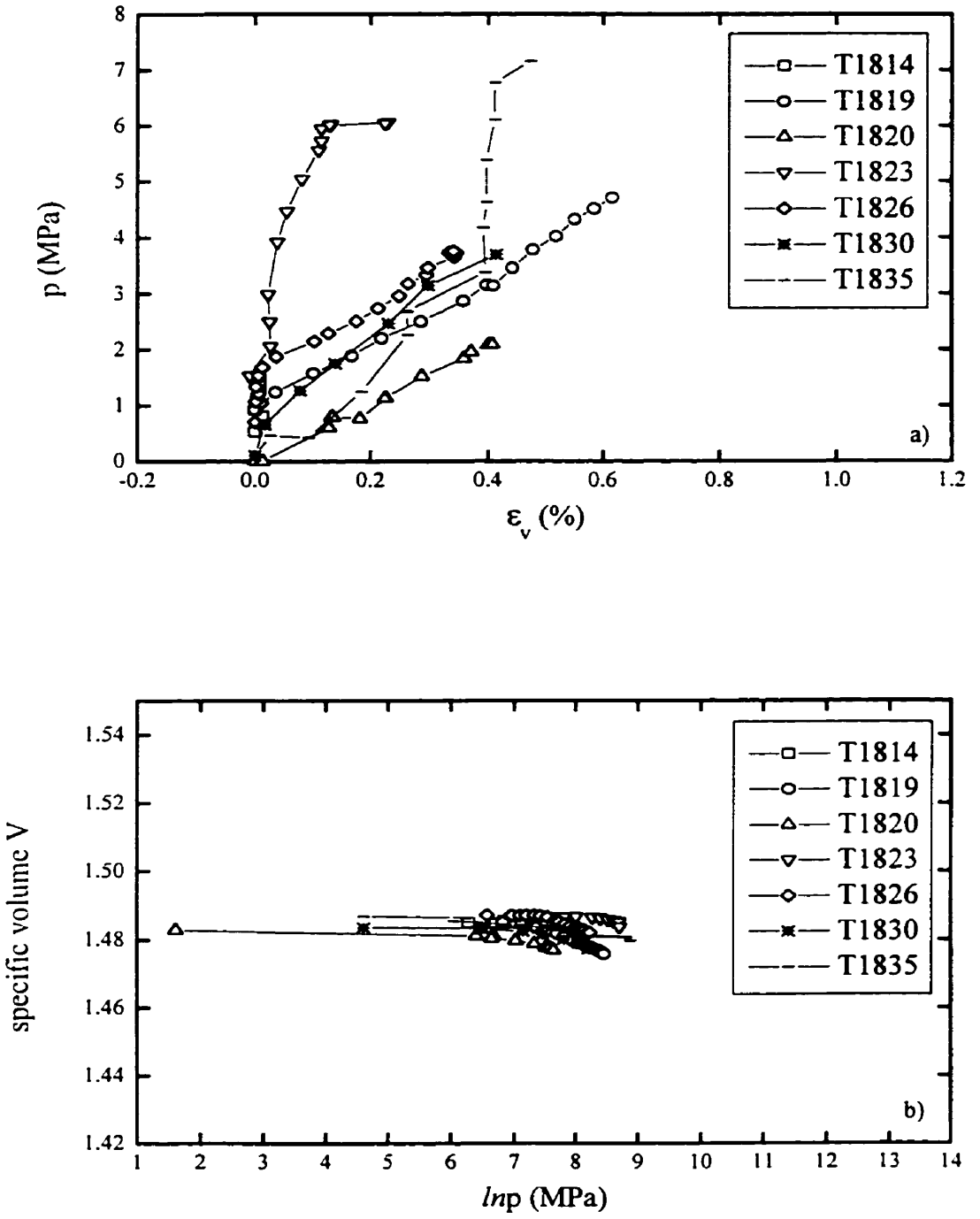

Figure 5.7 Isotropic compression prior to shearing for tests on 20-40 'frac' sand at 65°C plotted as: a) mean stress, p *versus* volume strain, ε_v and b) natural logathirm of mean stress *ln* p *versus* specific volume, V

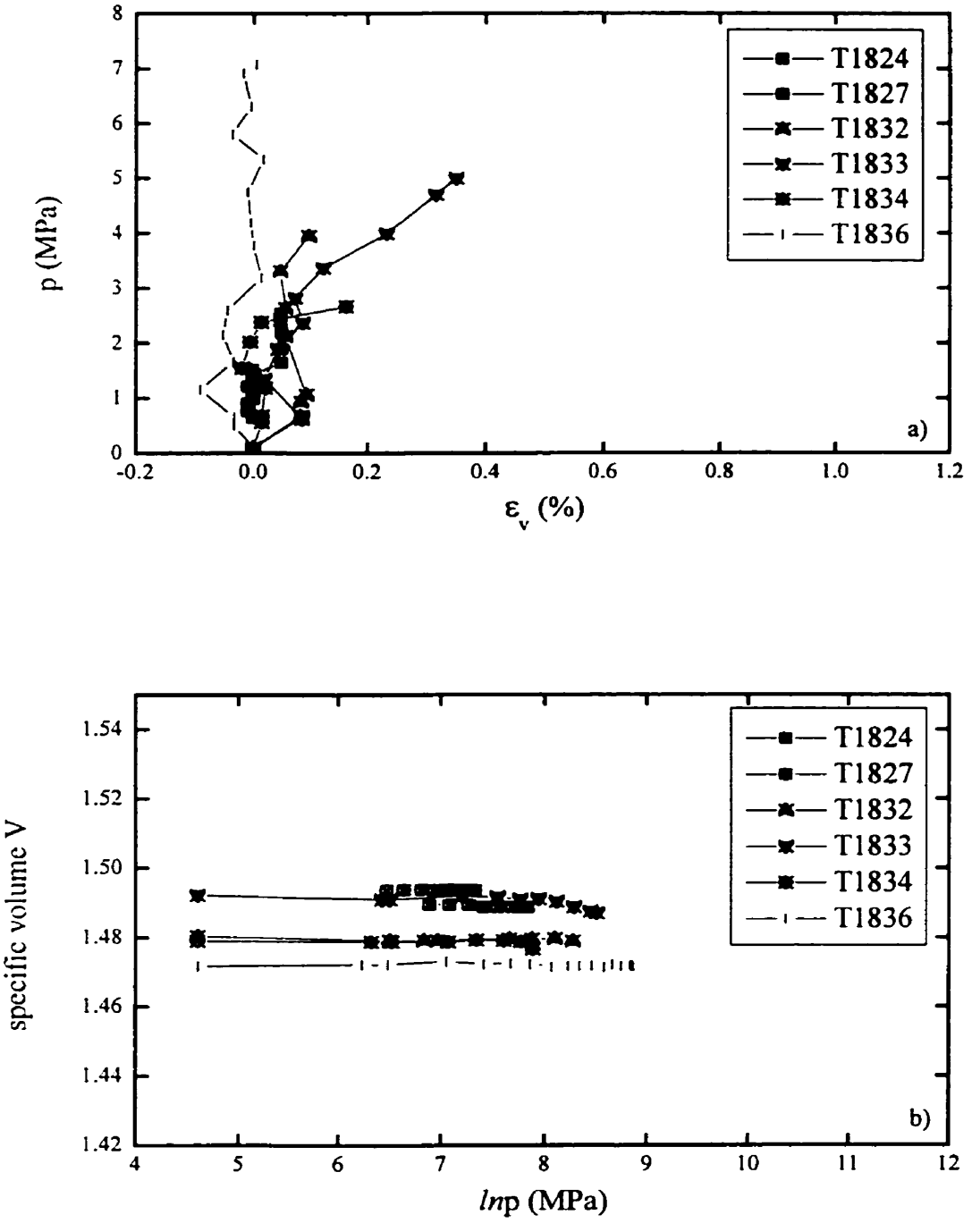

Figure 5.8 Isotropic compression prior to shearing for tests on 20-40 'frac' sand at 100°C plotted as: a) mean stress, p *versus* volume strain, ε_v and b) natural logathirm of mean stress *ln* p *versus* specific volume, V

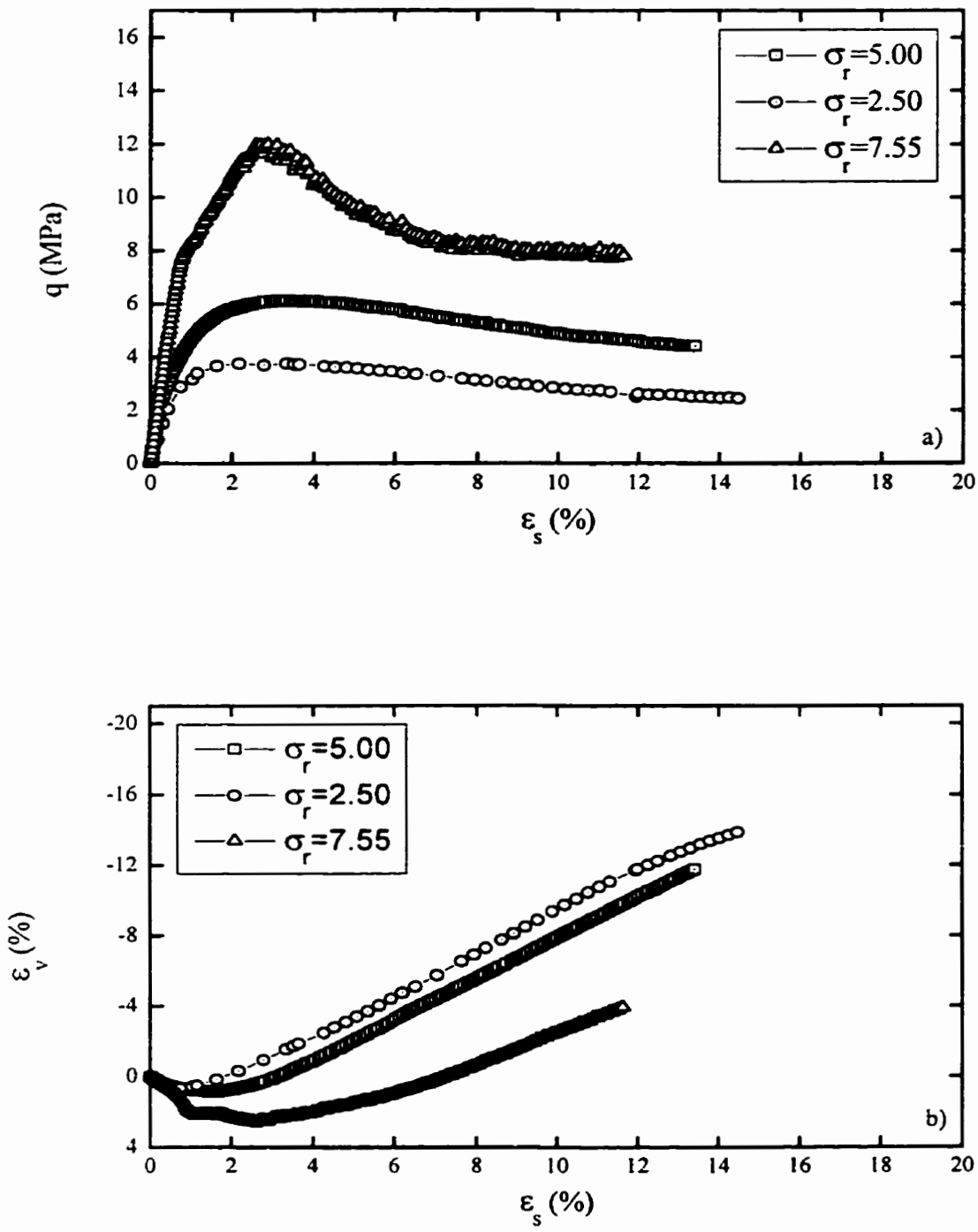

Figure 5.9 Triaxial shearing of Ballotini for different radial stress, σ_r at room temperature plotted as; a) deviator stress, q *versus* shear strain, ε_s and b) volume strain, ε_v *versus* shear strain, ε_s

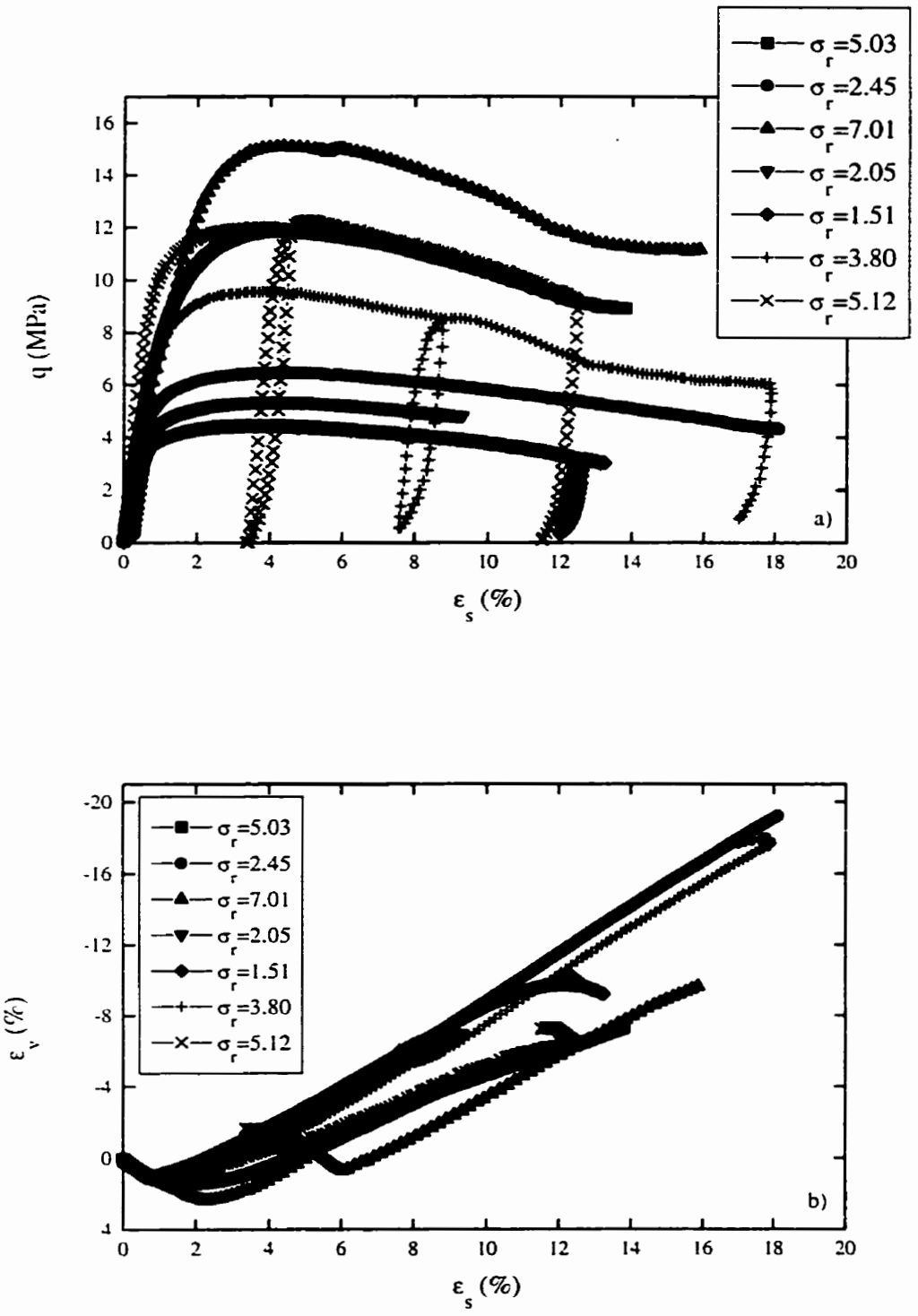

Figure 5.10 Triaxial shearing of 20-40 'frac' sand for different radial stress, σ_r at room temperature plotted as; a) deviator stress, q *versus* shear strain, ε_s and b) volume strain, ε_v *versus* shear strain, ε_s

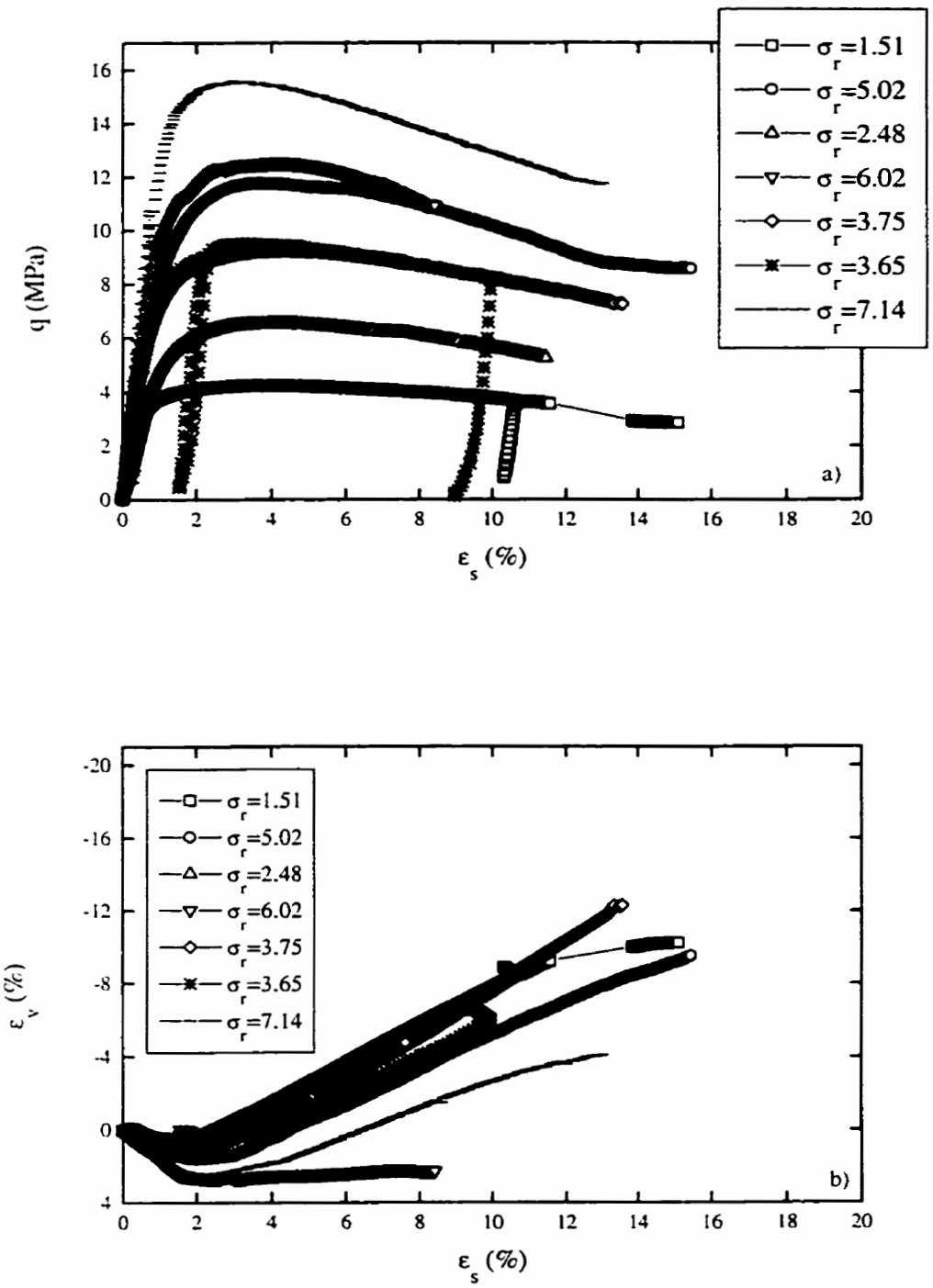

Figure 5.11 Triaxial shearing of 20-40 'frac' sand for different radial stress, σ_r at 65°C plotted as; a) deviator stress, q *versus* shear strain, ε_s and b) volume strain, ε_v *versus* shear strain, ε_s

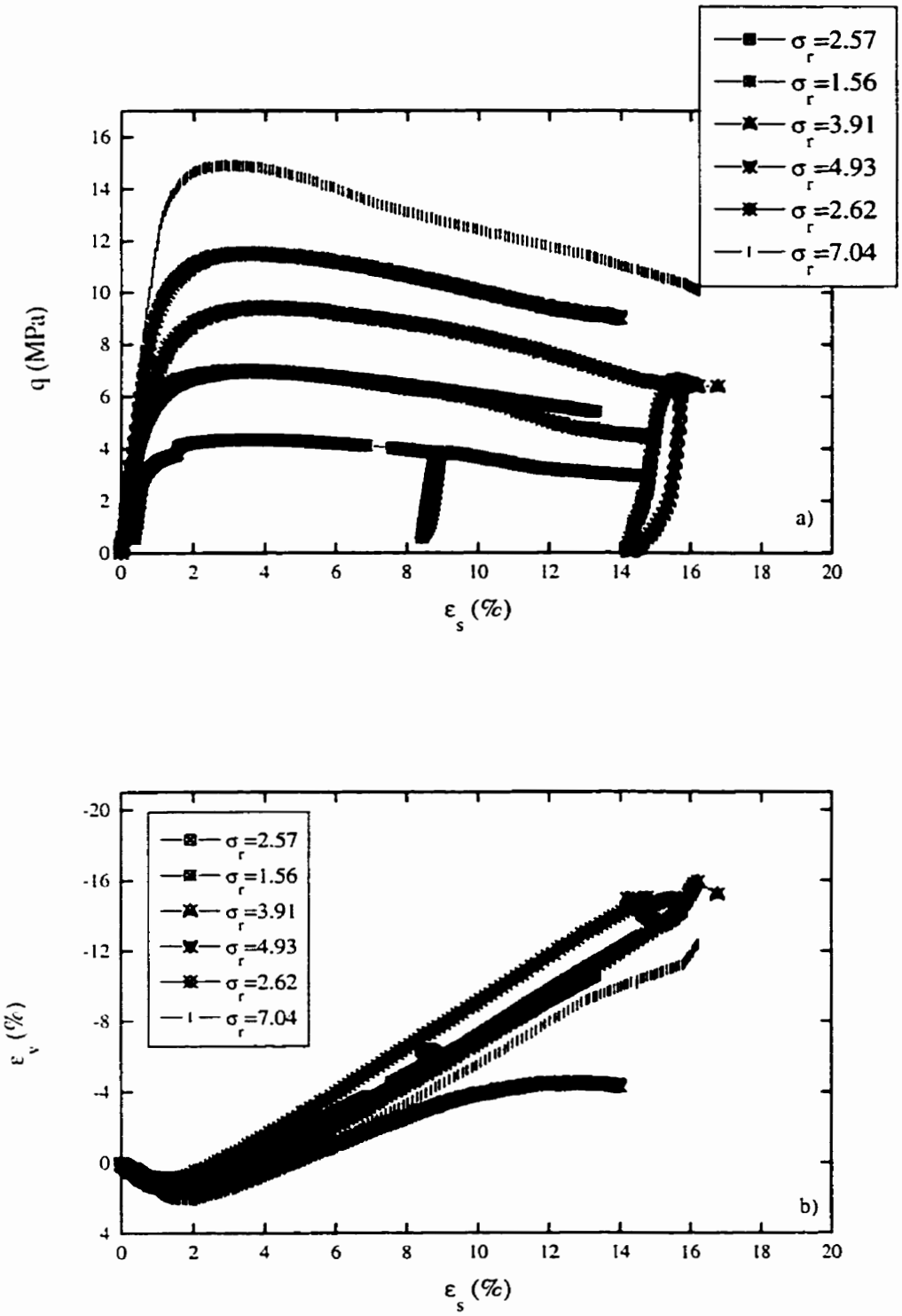

Figure 5.12 Triaxial shearing of 20-40 'frac' sand for different radial stress, σ_r at 100°C plotted as; a) deviator stress, q *versus* shear strain, ε_s and b) volume strain, ε_v *versus* shear strain, ε_s

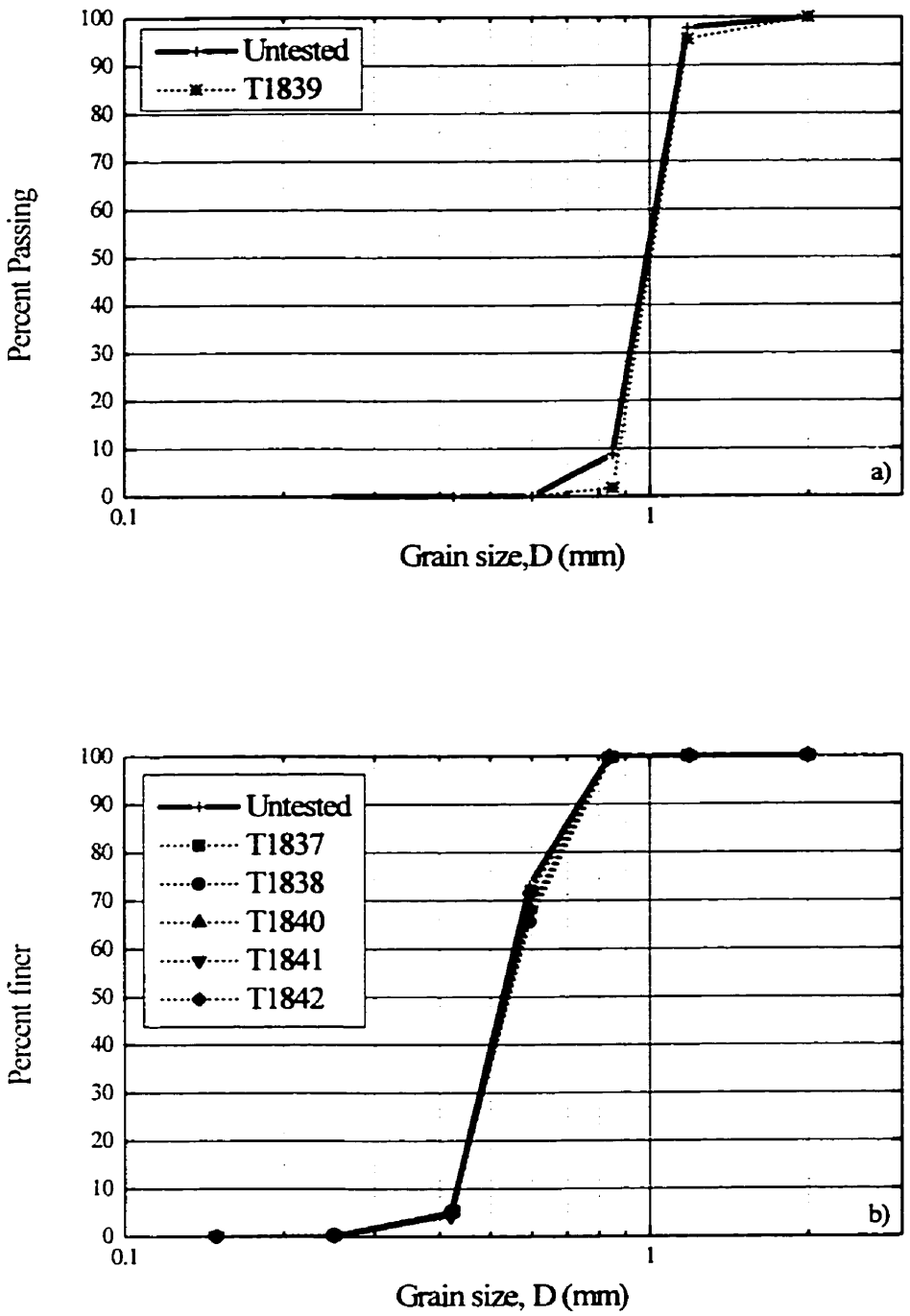

Figure 5.13 Grain size distribution results after isotropic compression for a) Ballotini and b) 20-40 'frac' sand

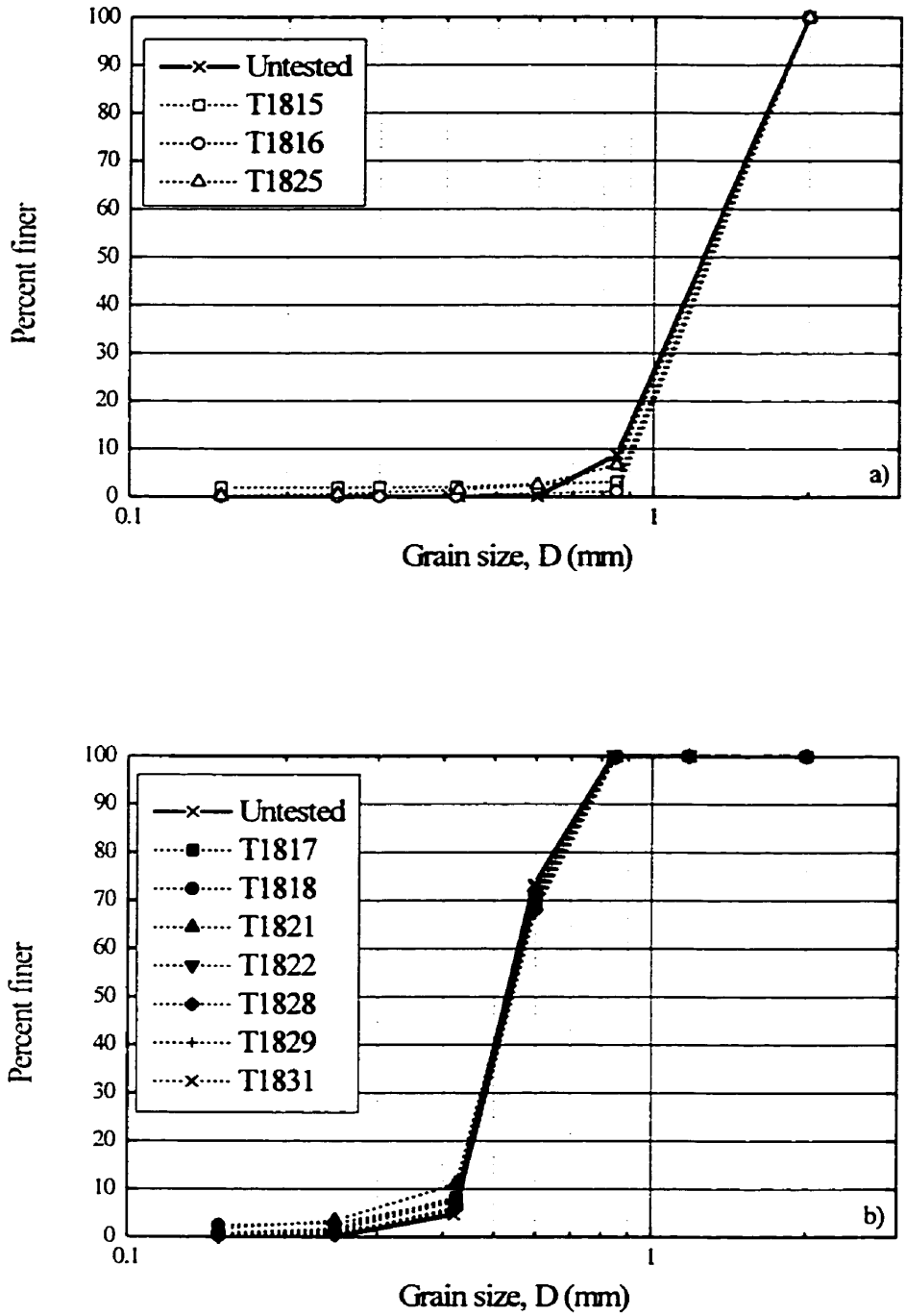

Figure 5.14 Grain size distributions after shear testing at room temperature for a) Ballotini and b) 20-40 'frac' sand

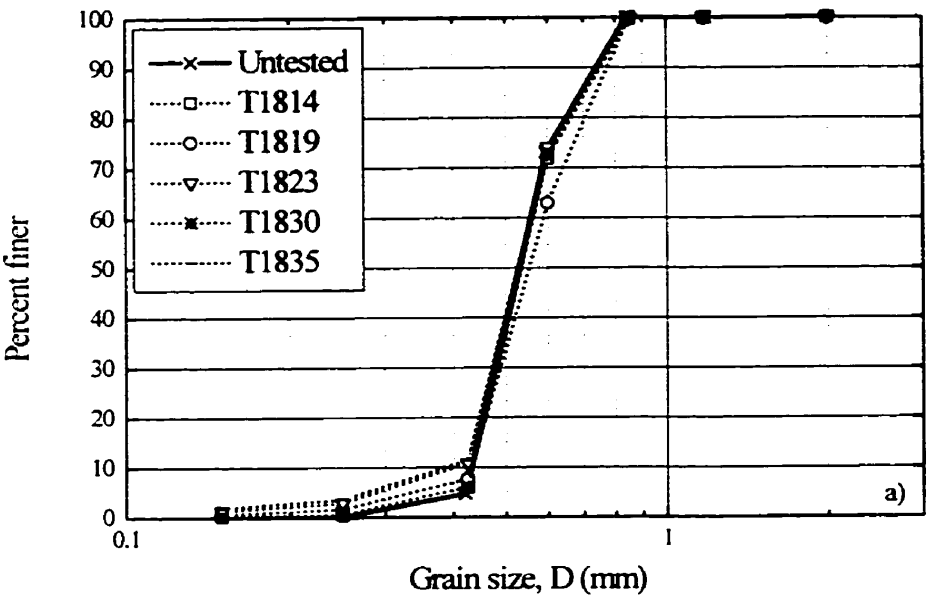

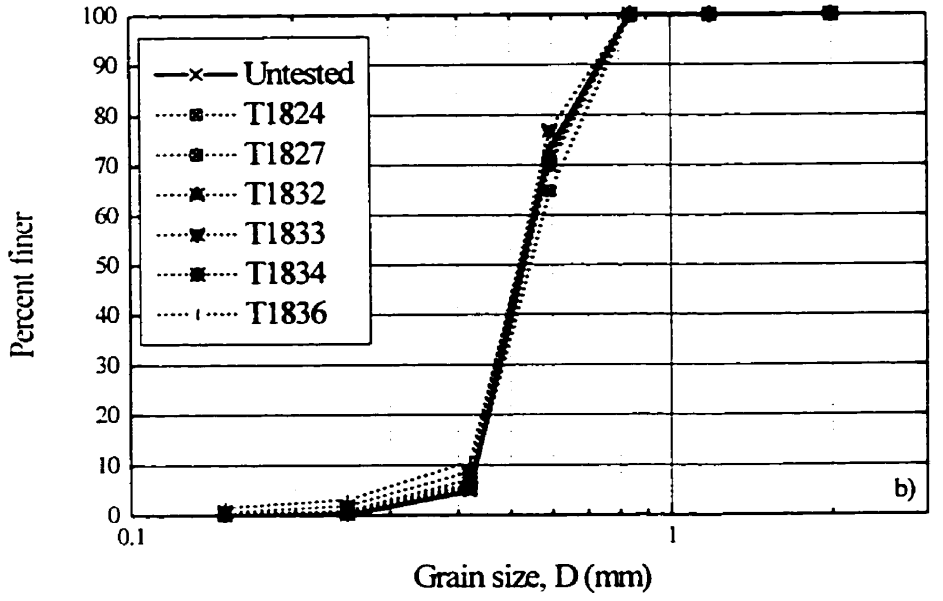

Figure 5.15 Grain size distribution after shearing of 20-40 'frac' sand where the test was at a temperature of a) 65°C and b) 100°C

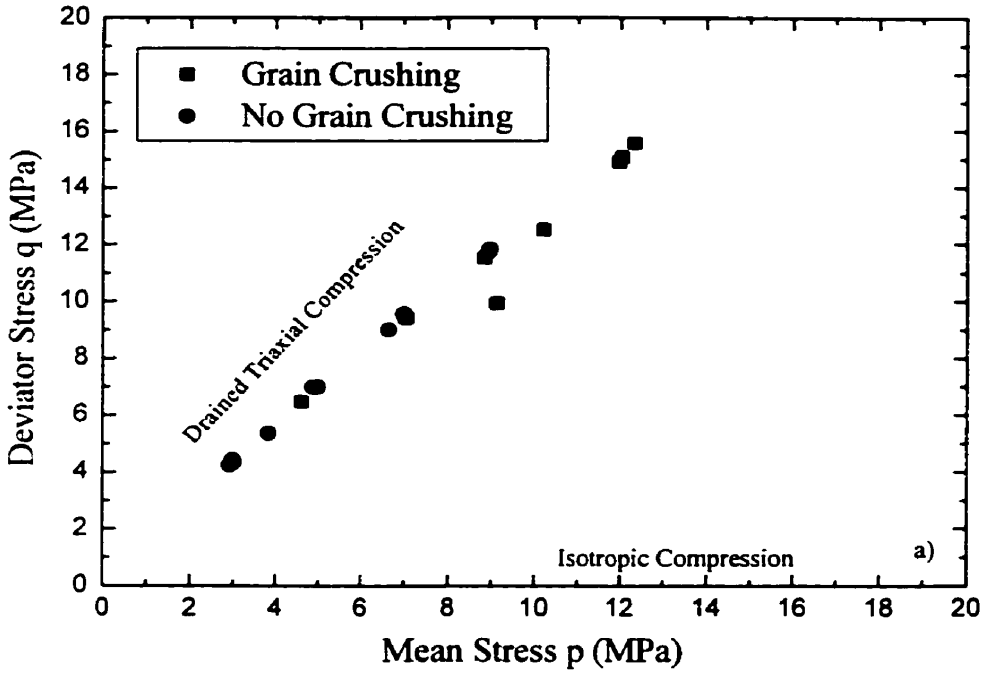

Figure 6.1a Peak stress condition for 'Frac' sand, separated according to grain crushing

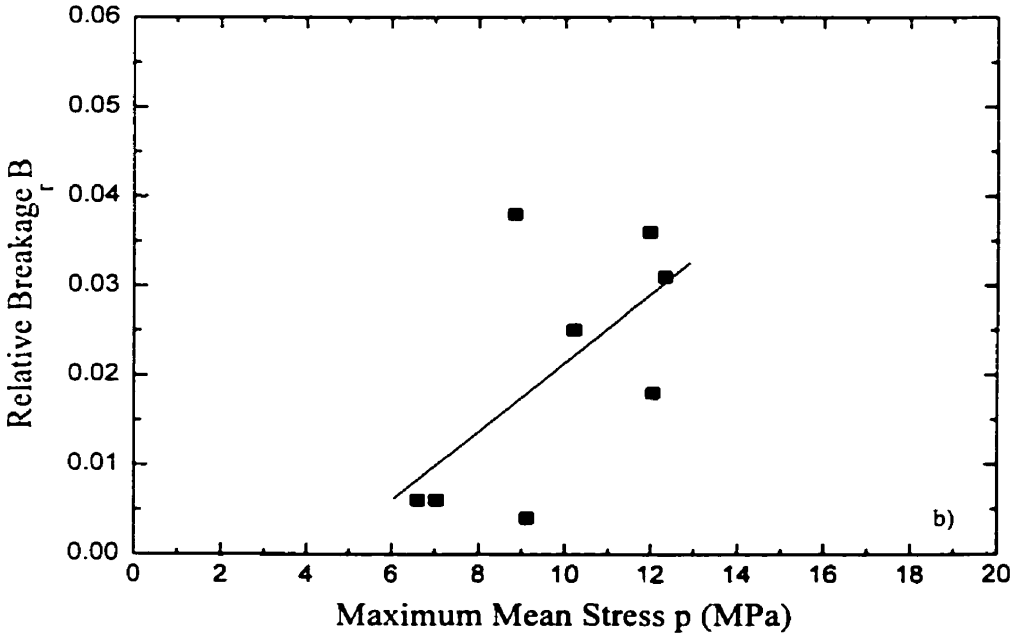

Figure 6.1b The relative breakage of 'Frac' sand versus the maximum mean stress applied during triaxial compression

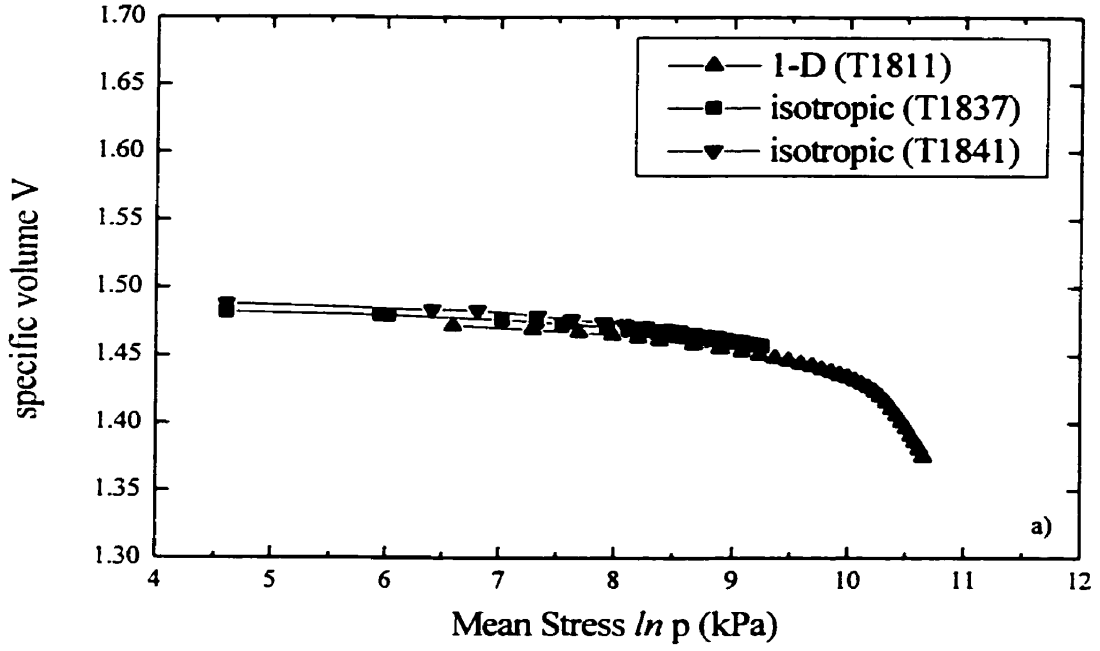

Figure 6.2a Behaviour of 'Frac' sand in isotropic compression and in 1-D compression

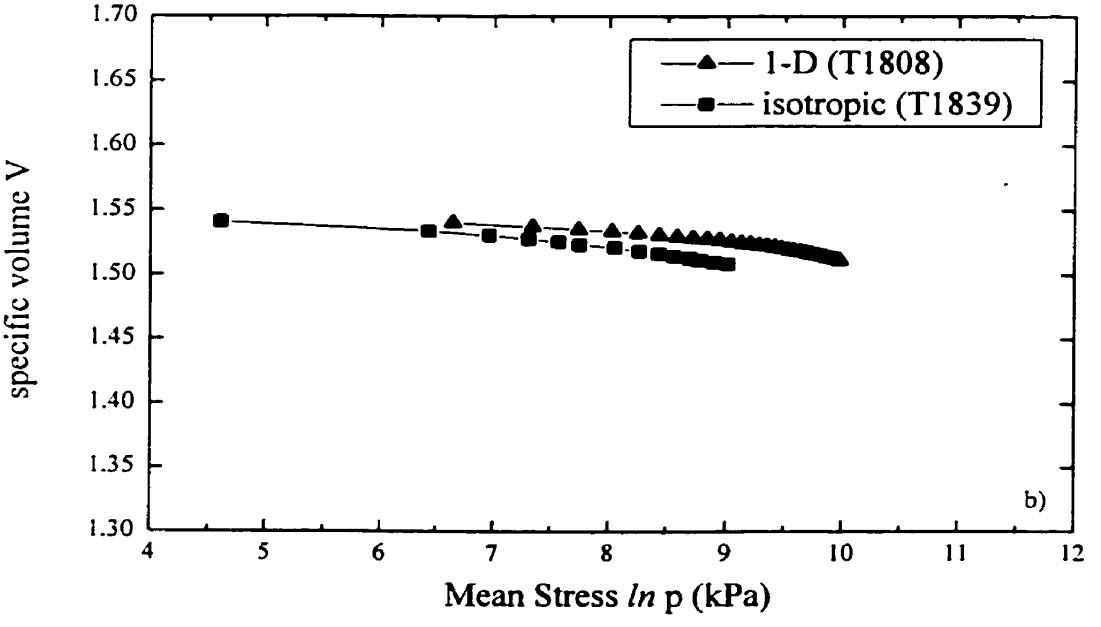

Figure 6.2b Behaviour of Ballotini in isotropic compression and 1-D compression

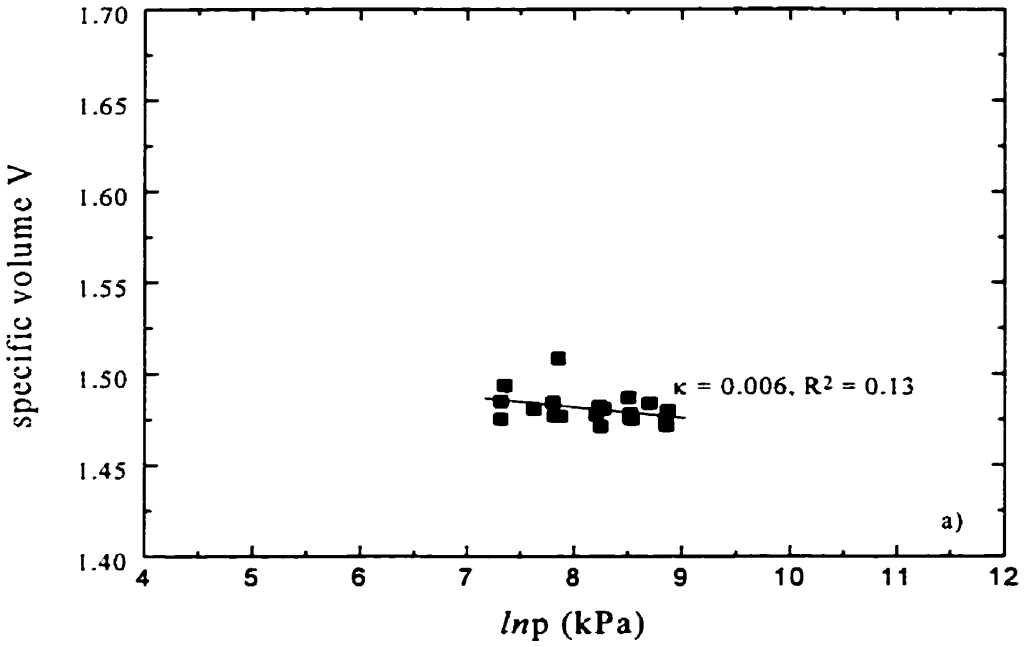

Figure 6.3a End of consolidation phase for 'Frac' sand

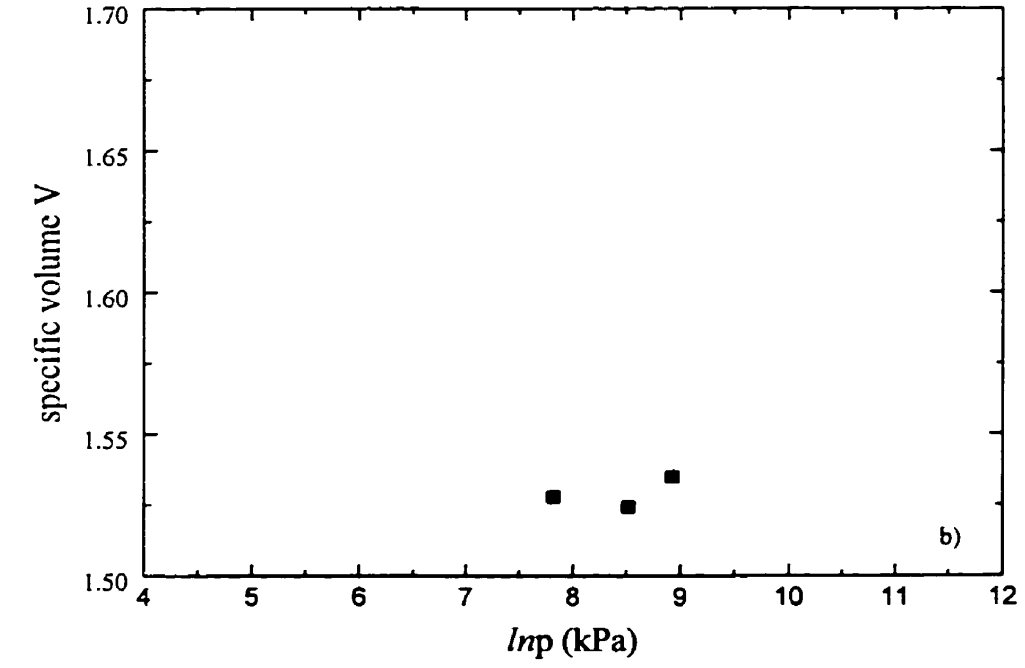

Figure 6.3b End of consolidation phase for Ballotini

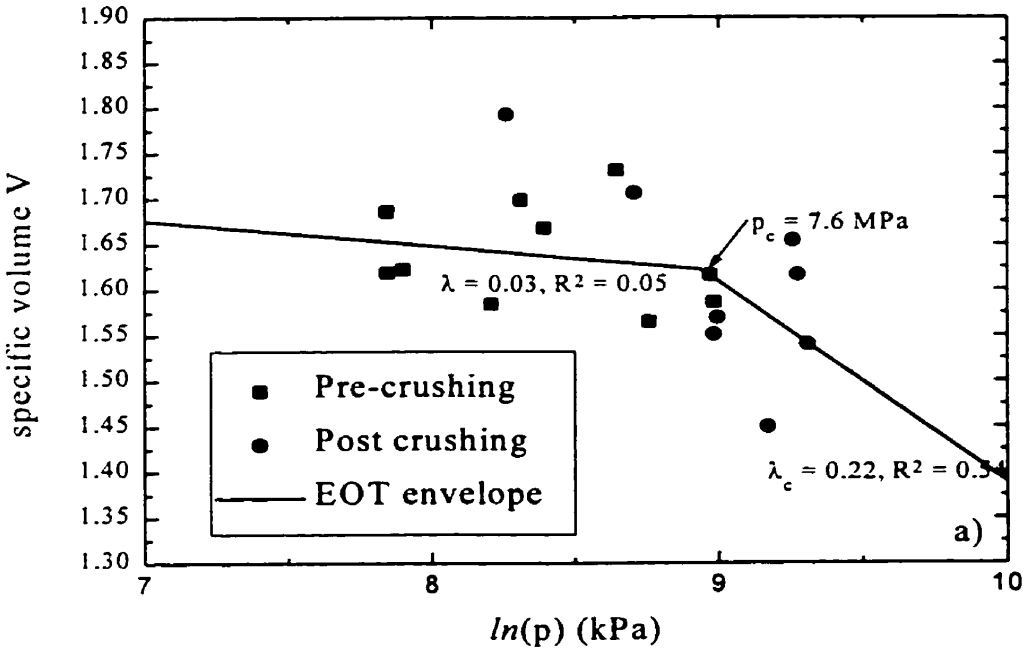

Figure 6.4a End of test (CSL) plotted for 'Frac' sand

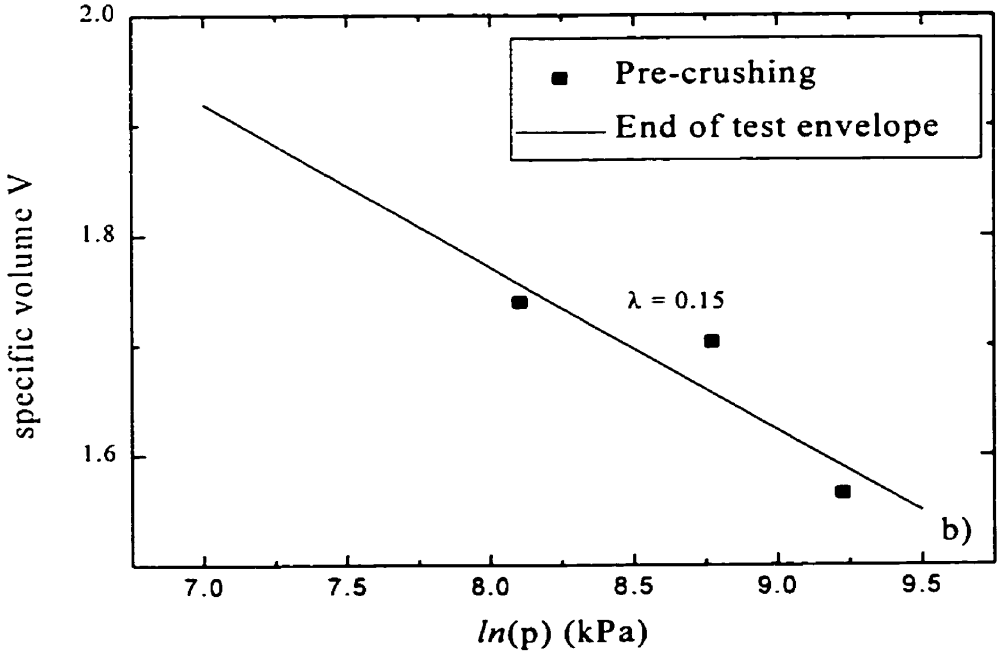

Figure 6.4b End of test (CSL) results for Ballotini

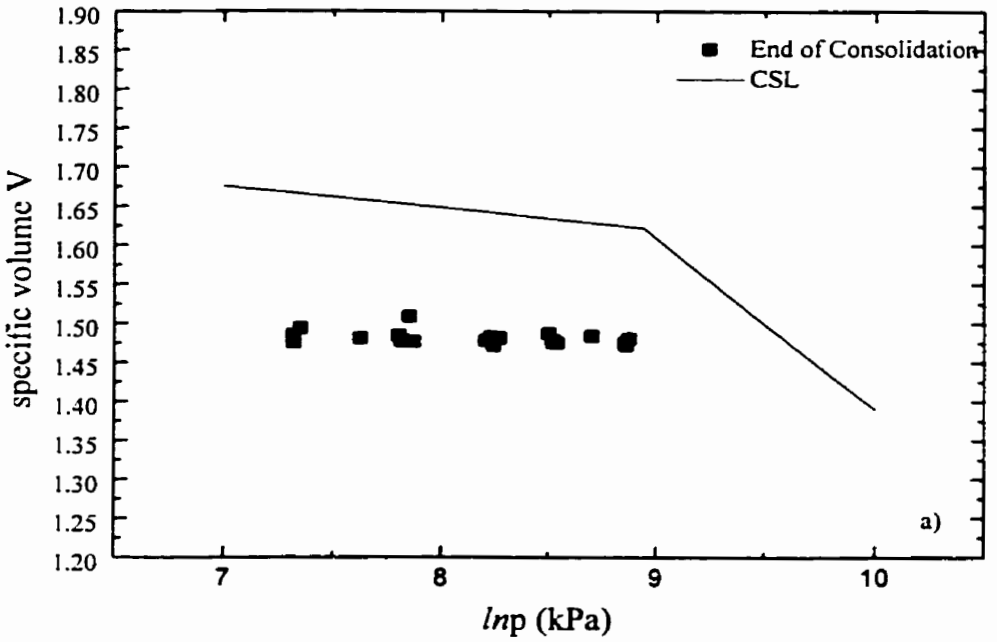

Figure 6.5a End of consolidation results plotted *versus* the CSL for 'Frac' sand

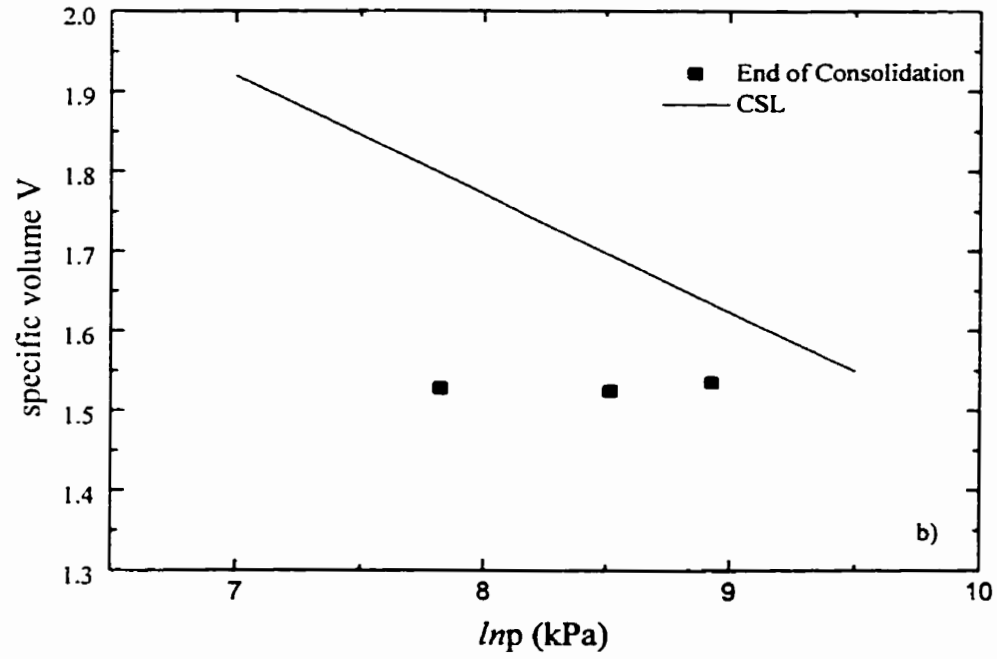

Figure 6.5b End of consolidation results plotted *versus* the CSL for Ballotini

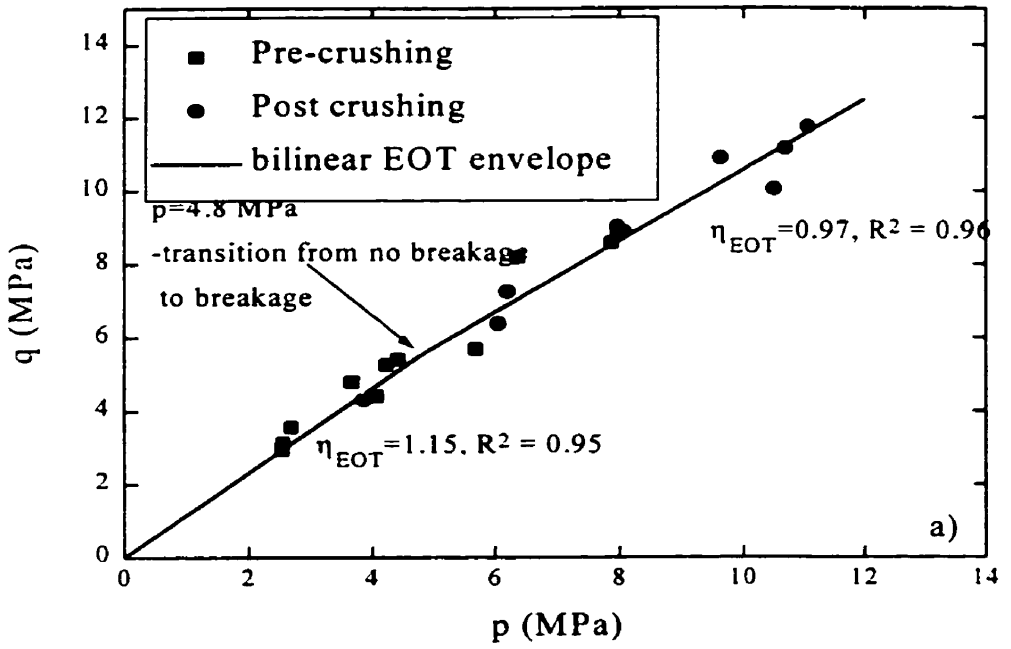

Figure 6.6a End of test conditions for 'Frac' sand, data was divided according to grain crushing

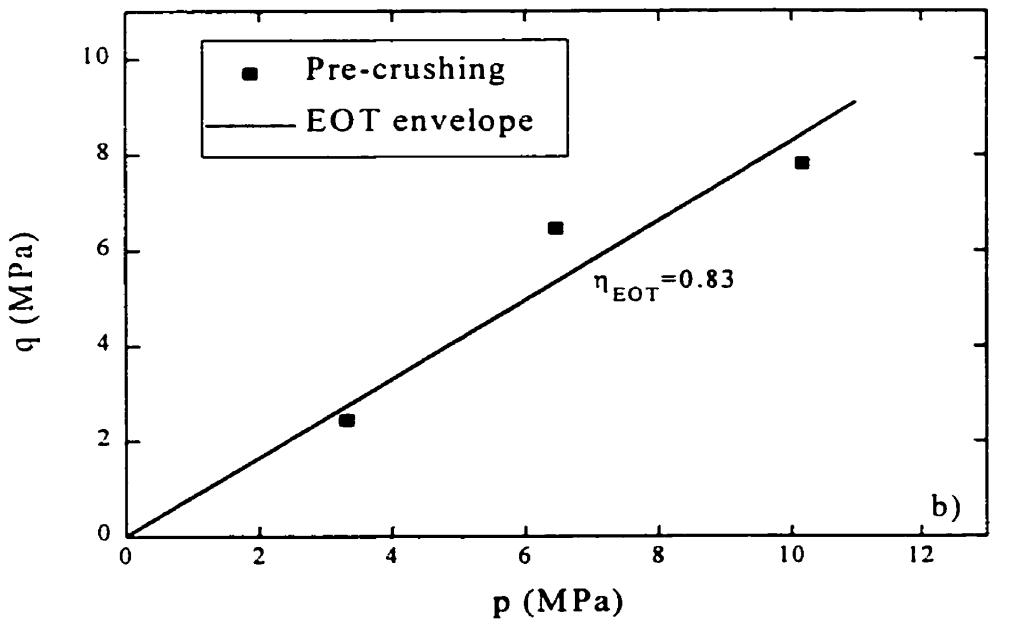

Figure 6.6b End of test data for Ballotini, no grain crushing was measured in these specimens

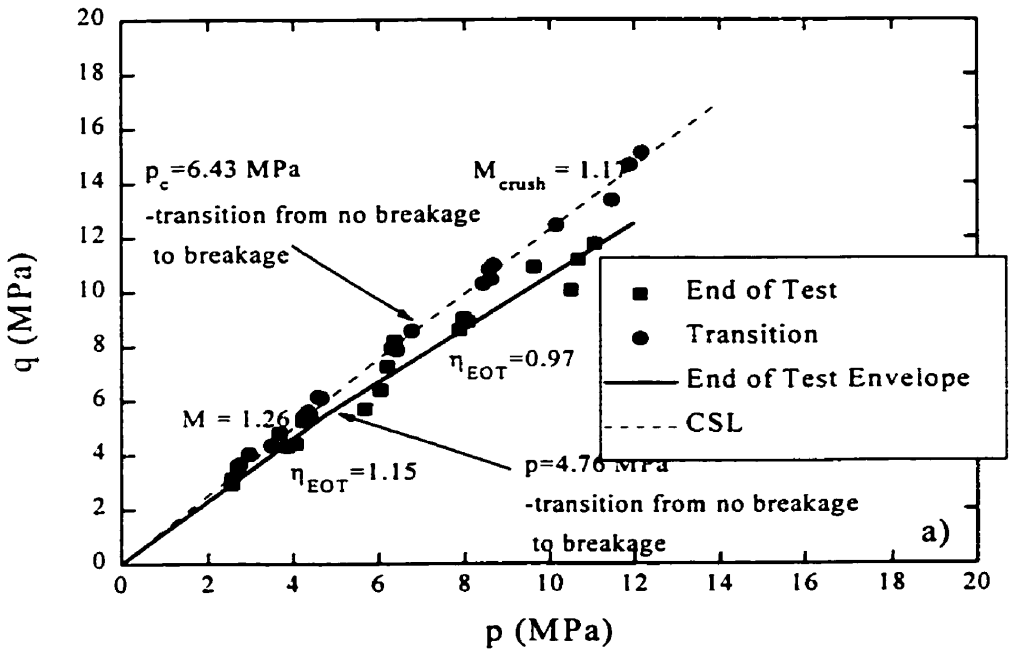

Figure 6.7a End of test data plotted with transition data, the transition data were used to define the CSL

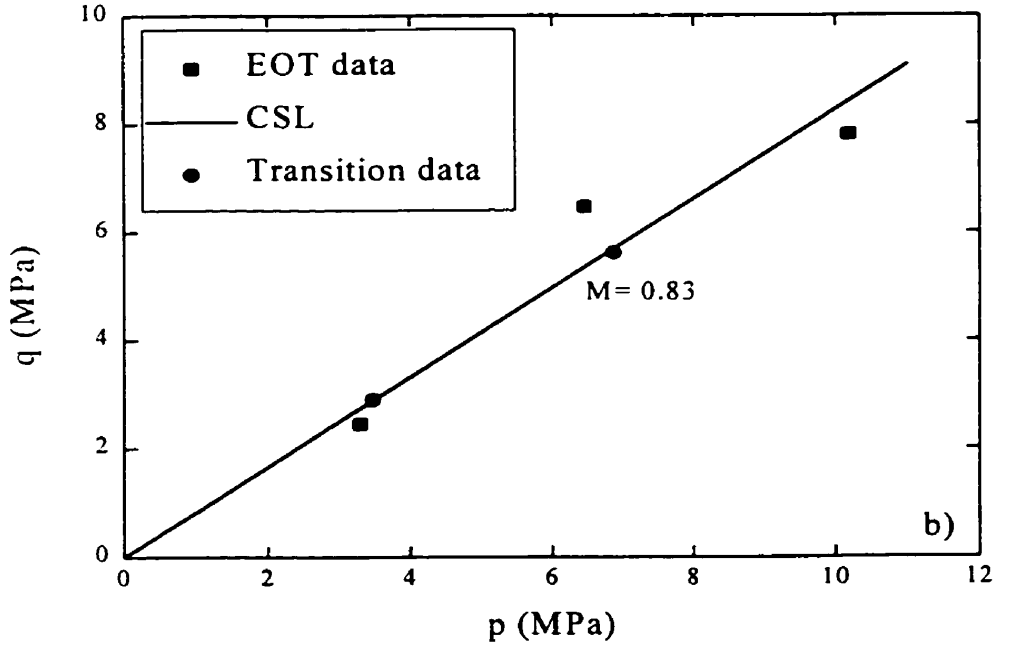

Figure 6.7b End of test data plotted with transition data, both sets of data were used to define the CSL

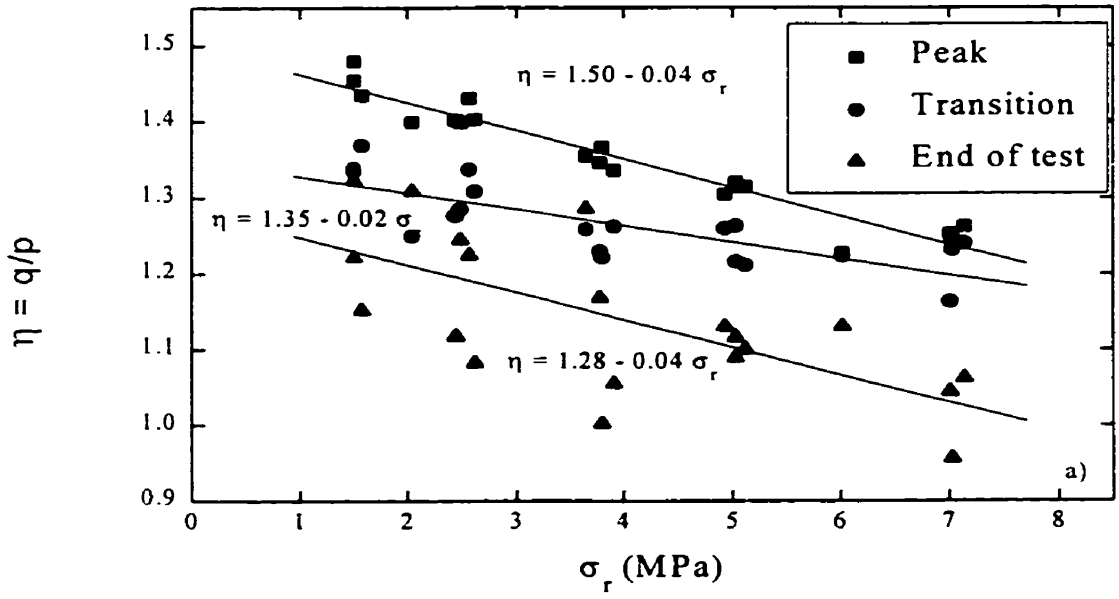

Figure 6.8a Stress ratio at the end of test, transition condition and the peak stress plotted versus the radial stress for 'Frac' sand

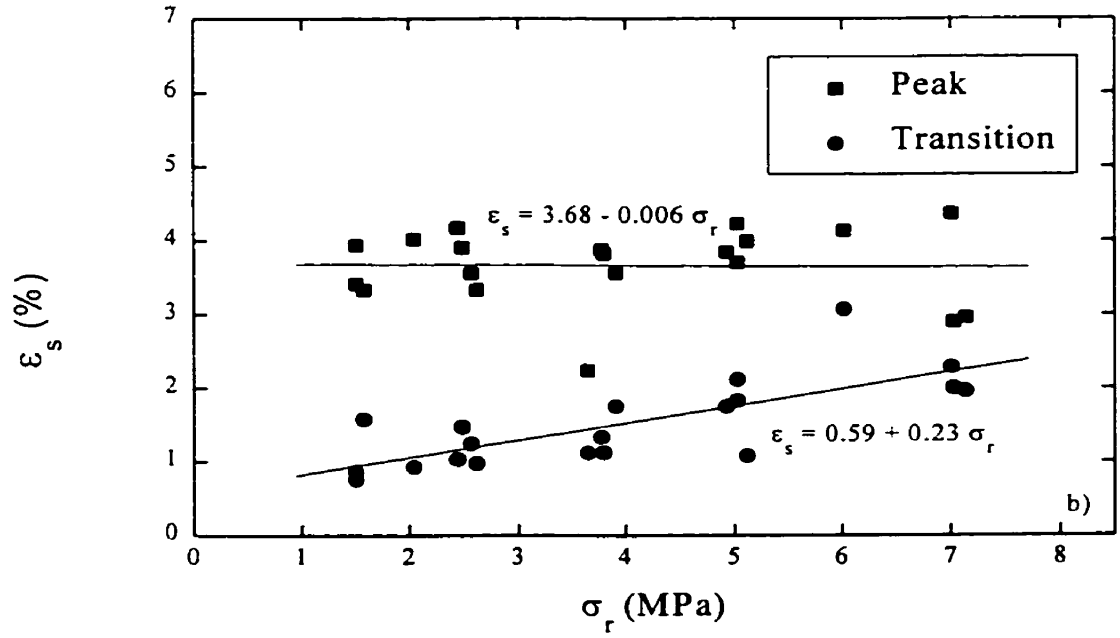

Figure 6.8b Shear stress versus the radial stress at the peak stress and transition stress conditions for 'Frac' sand

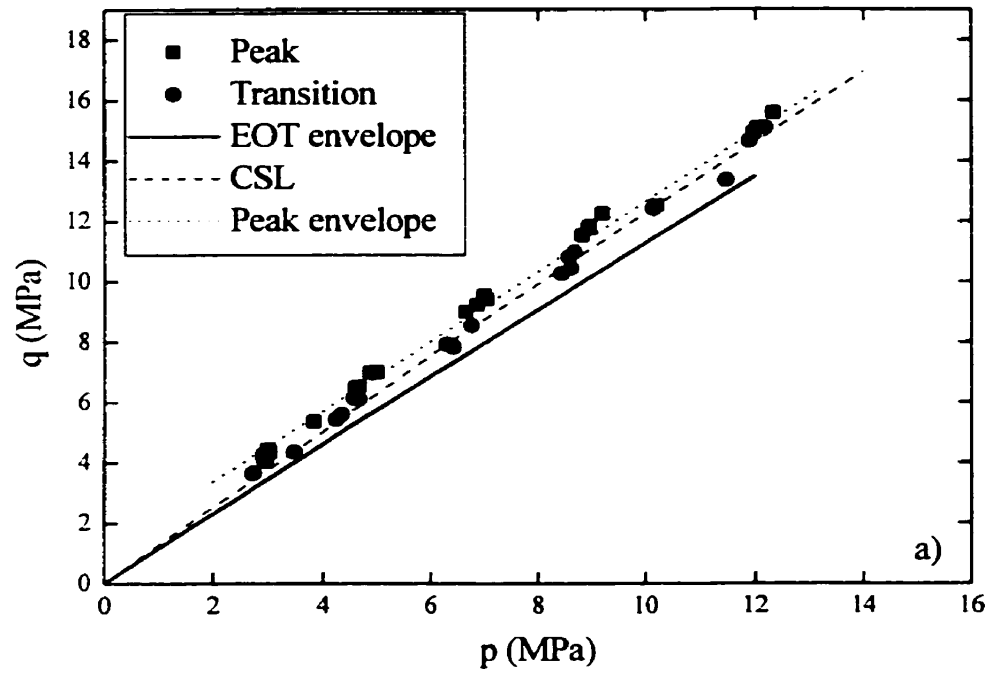

Figure 6.9a Peak stress envelope plotted alongside the CSL for 'Frac' sand

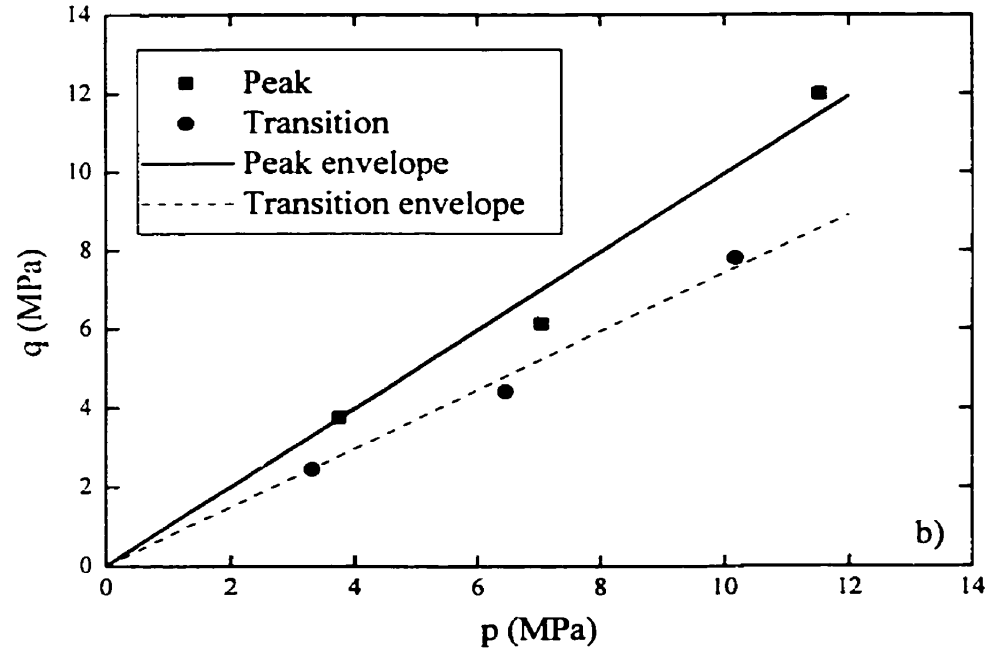

Figure 6.9b Peak stress envelope plotted along with the CSL for Ballotini

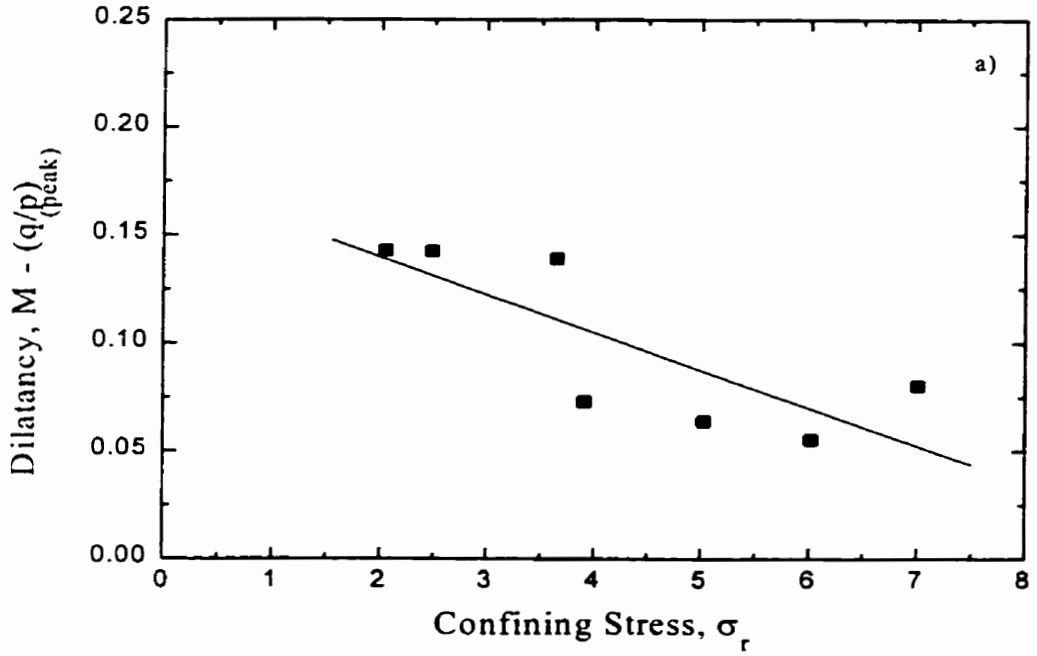

Figure 6.10a Dilatancy angle versus the confining stress, 'Frac' sand

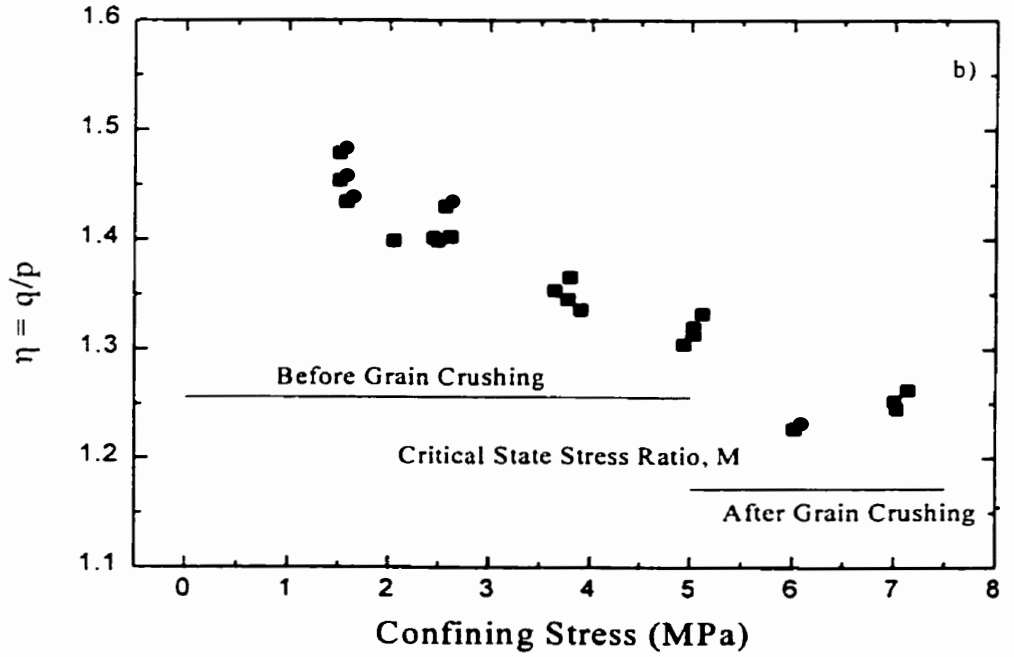

Figure 6.10b Peak stress ratio *versus* the confining stress for 'Frac' sand, the critical state stress ratio, M is plotted for comparison, defined for both no grain crushing and grain crushing

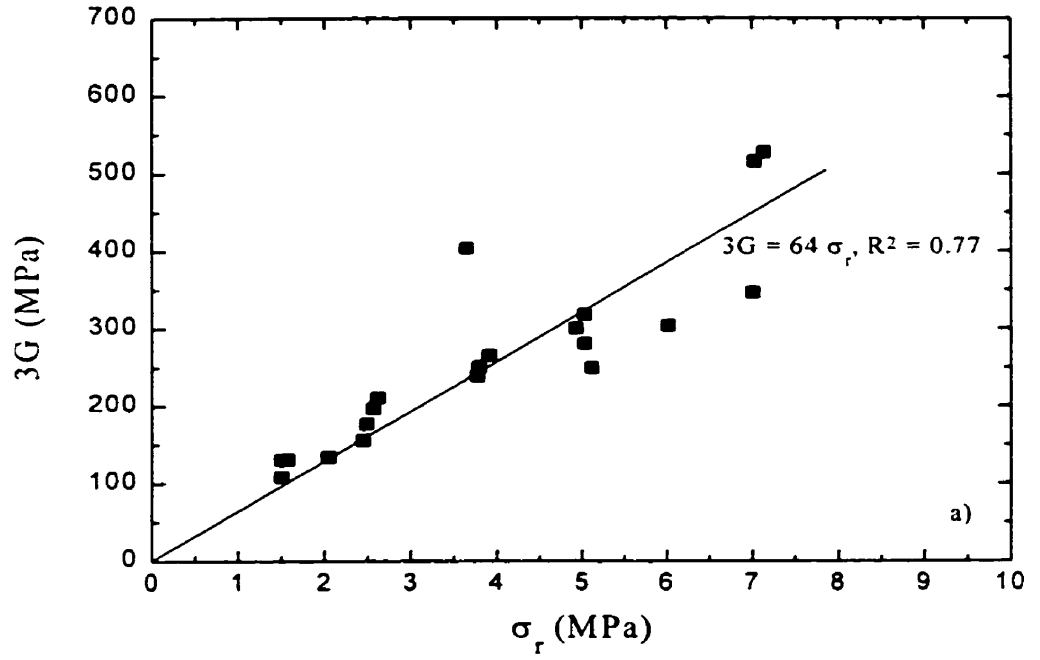

Figure 6.11a Secant Shear modulus calculated at the peak stress plotted versus the confining stress for 'Frac' sand

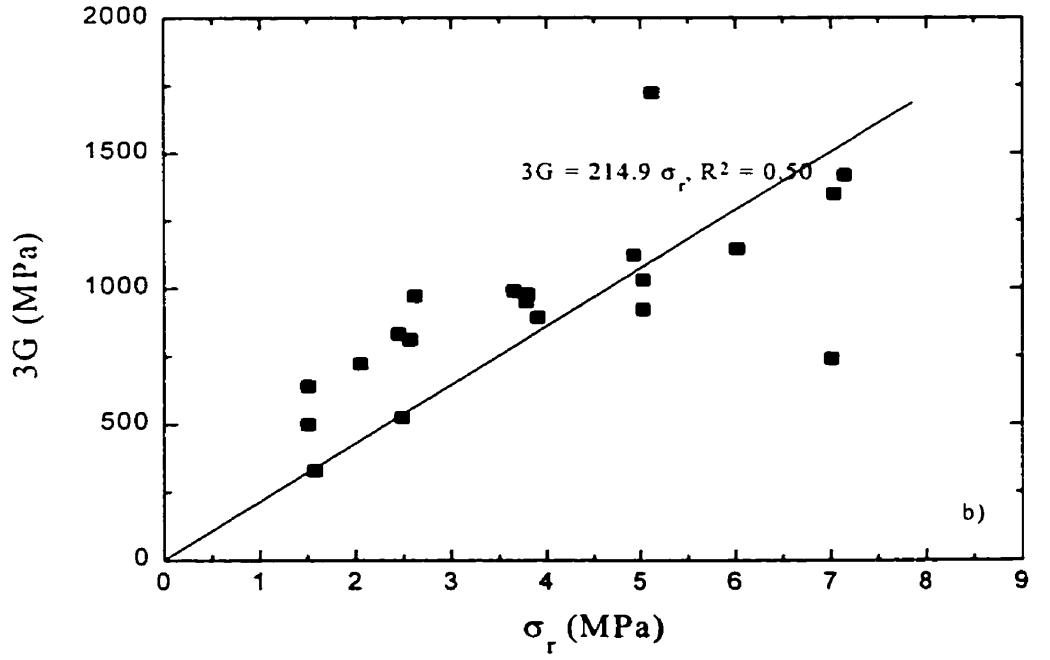

Figure 6.11b Secant shear modulus calculated at 50% of the peak stress versus the confining stress for 'Frac' sand

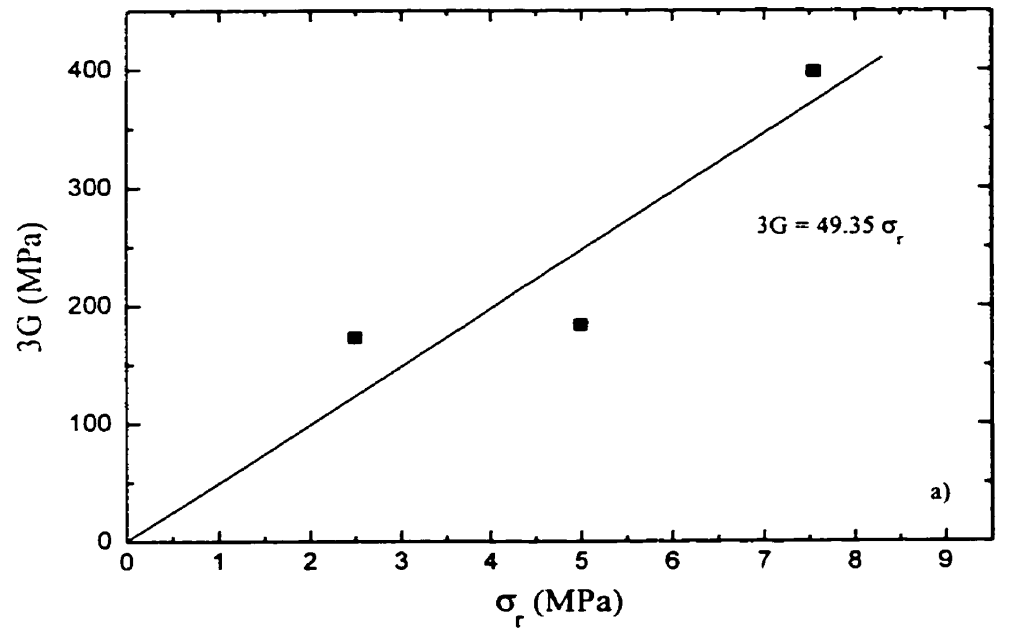

Figure 6.12a Secant shear modulus calculated at the peak stress versus the confining stress for Ballotini

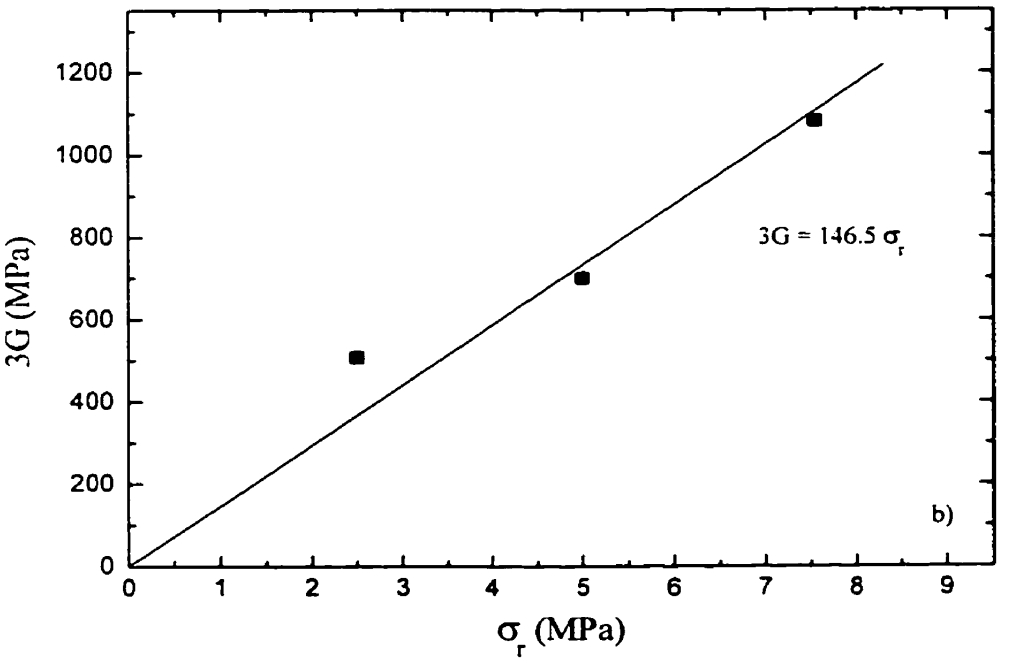

Figure 6.12b Secant shear modulus calculated at 50% of the peak stress versus the confining stress for Ballotini

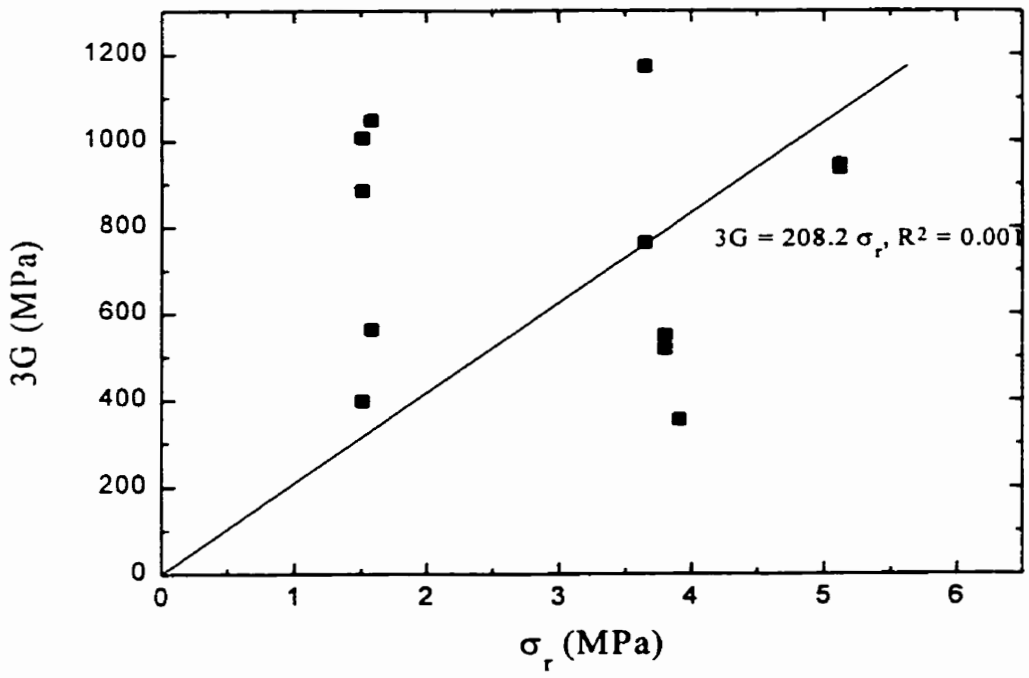

Figure 6.13 Shear modulus calculated from unload reload cycles versus the confining stress for 'Frac' sand

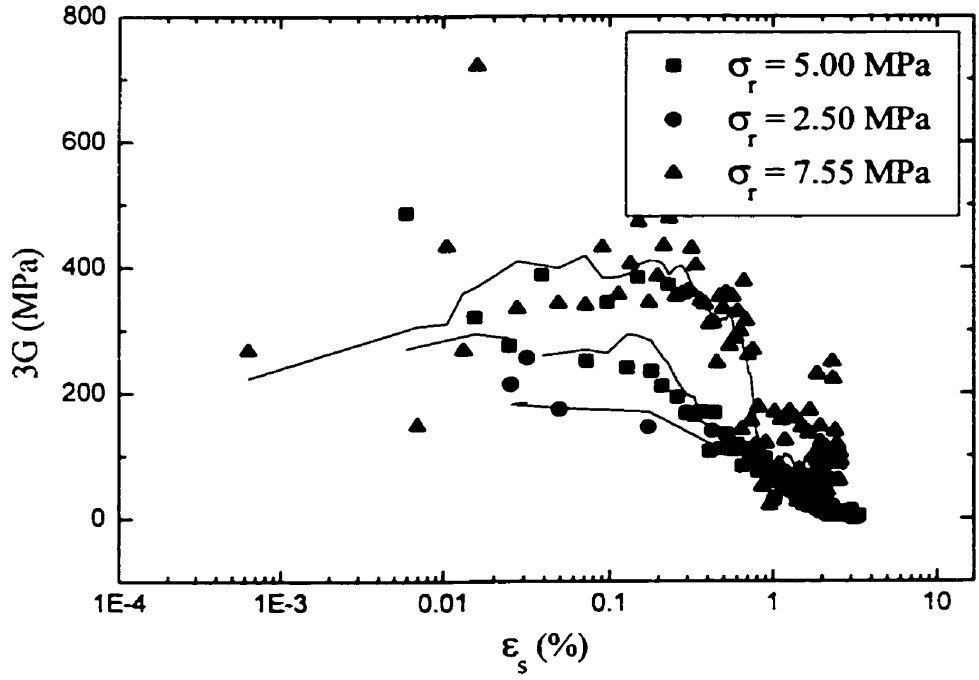

Figure 6.14a Incrementally calculated shear modulus, 3G versus logarithm of shear strain (%) for Ballotini

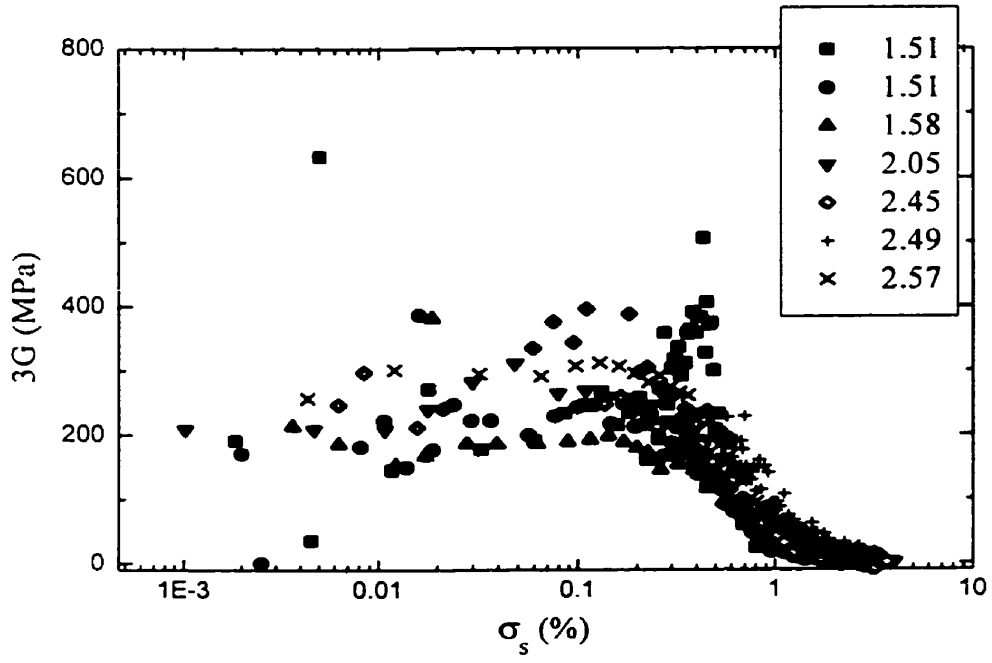

Figure 6.14b Incrementally calculated shear modulus, 3G versus logarithm of shear strain (%) for 'Frac' sand, the low stress region

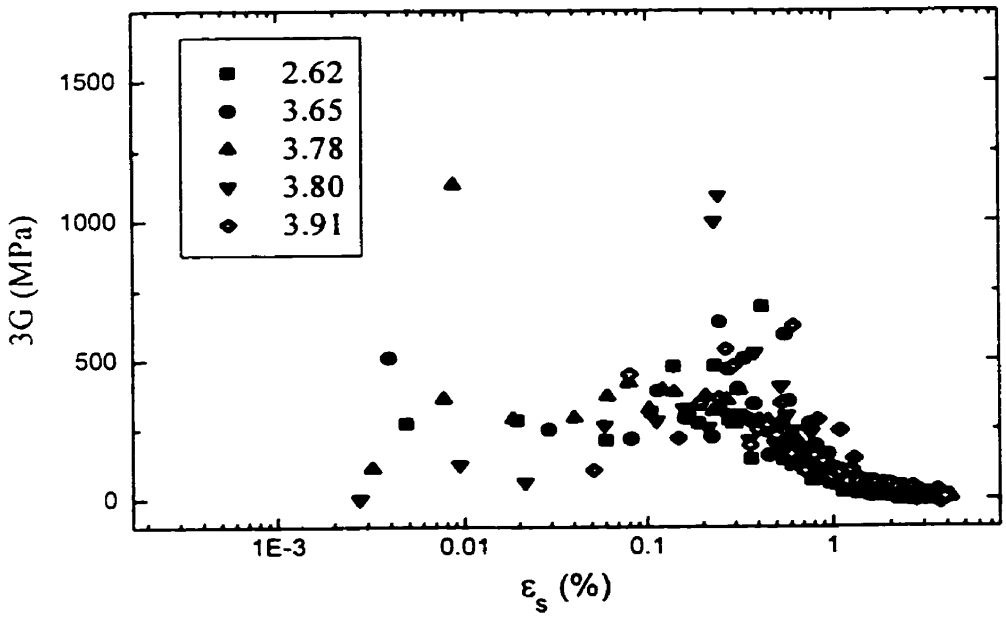

Figure 6.15a Incrementally calculated shear modulus, 3G versus logarithm of shear strain (%) for 'Frac' sand, medium stress region

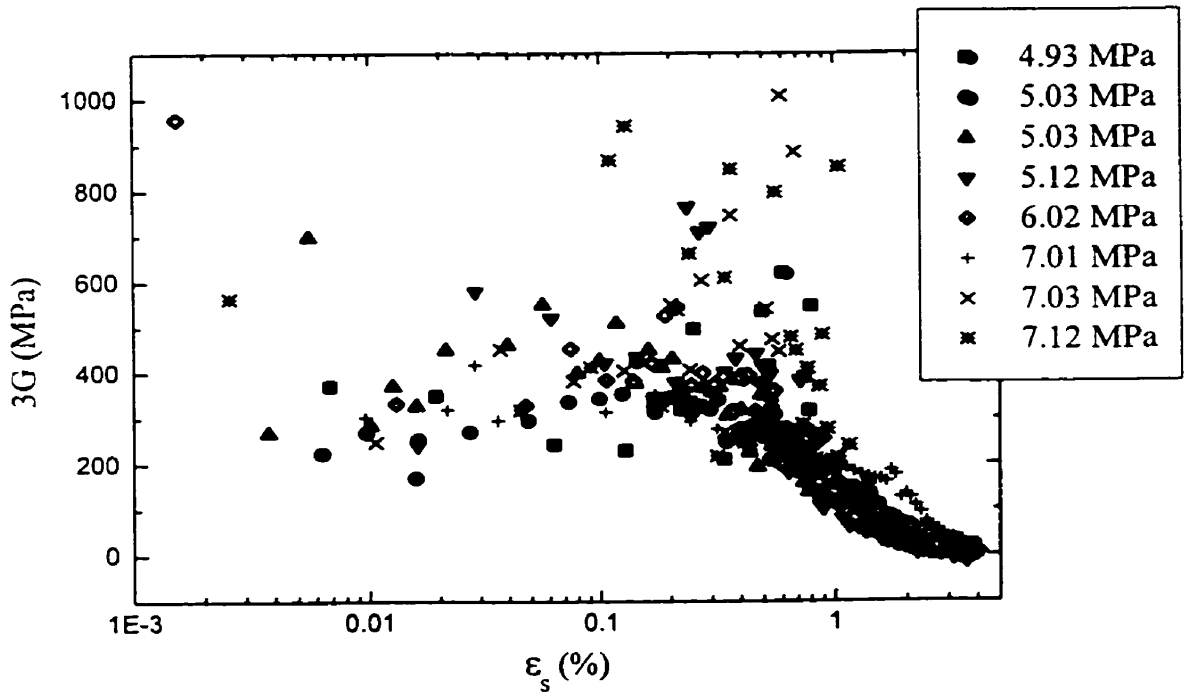

Figure 6.15b Incrementally calculated shear modulus, 3G versus logarithm of shear strain (%) for 'Frac' sand, high stress tests

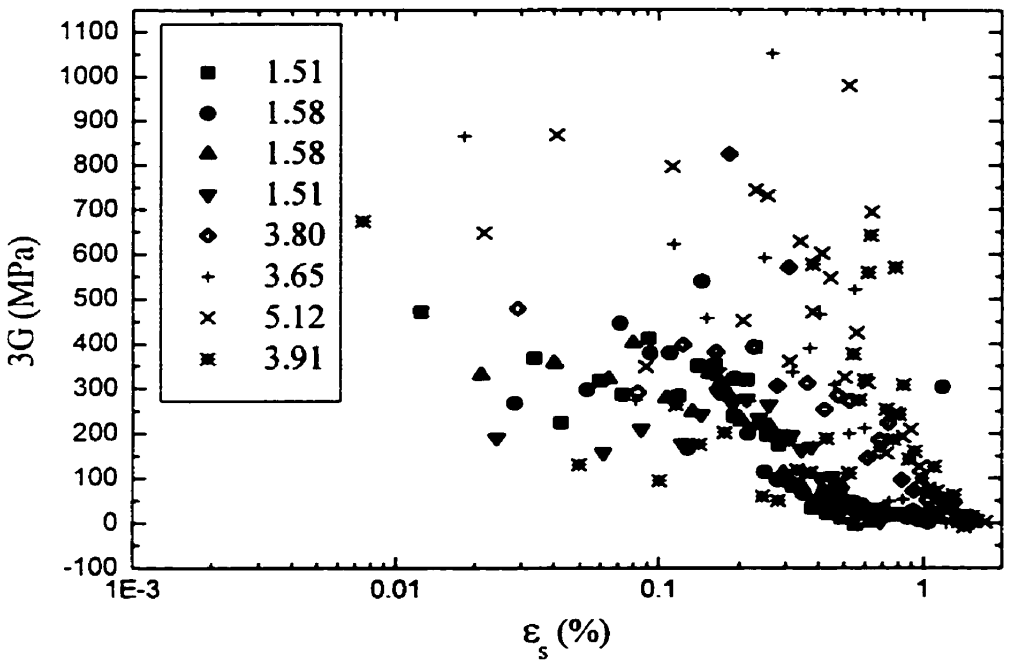

Figure 6.16 Incrementally calculated shear modulus, 3G versus logarithm of shear strain, % for the reload portion of the tests on 'Frac' sand

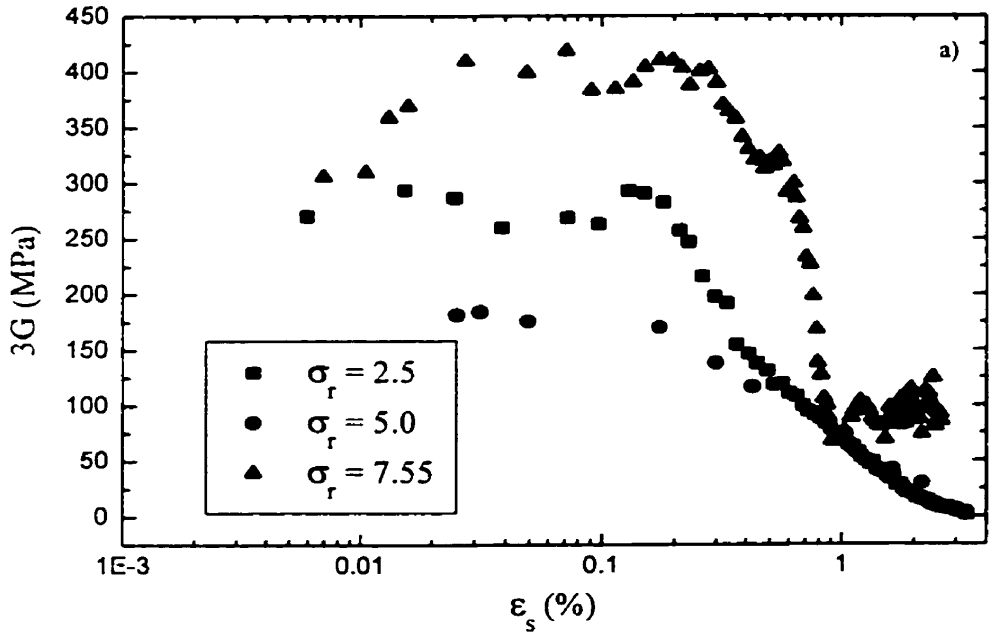

Figure 6.17a Incrementally calculated shear modulus, 3G versus logarithm of shear strain (%) for all tests on Ballotini

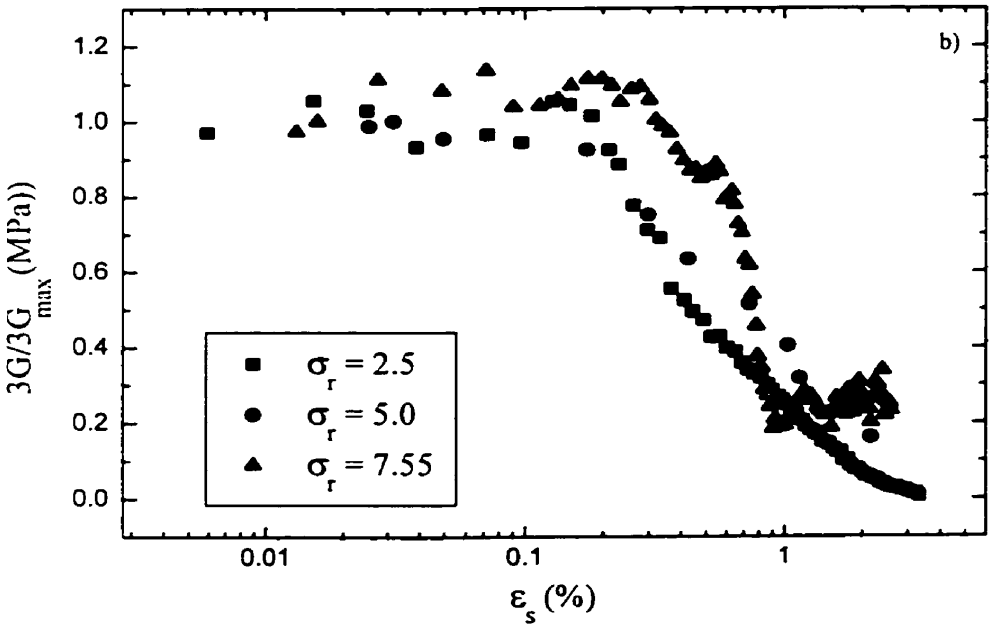

Figure 6.17b Incrementally calculated shear modulus normalized by the initial shear modulus $3G_{max}$ versus the shear strain (%) for all tests on Ballotini

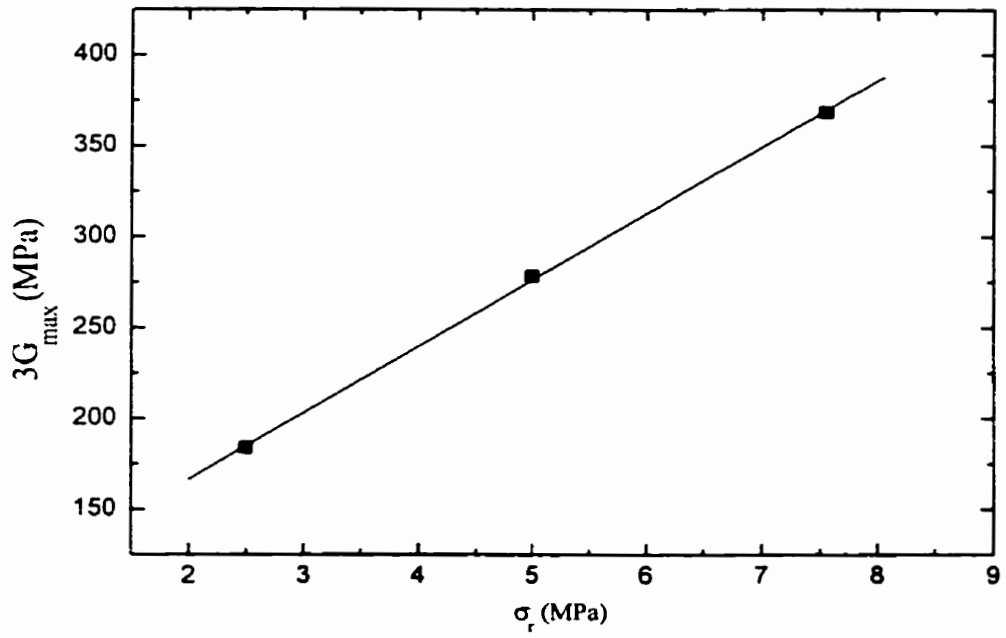

Figure 6.18 Linear relationship between the initial radial stress and the initial shear modulus $3G_{max}$

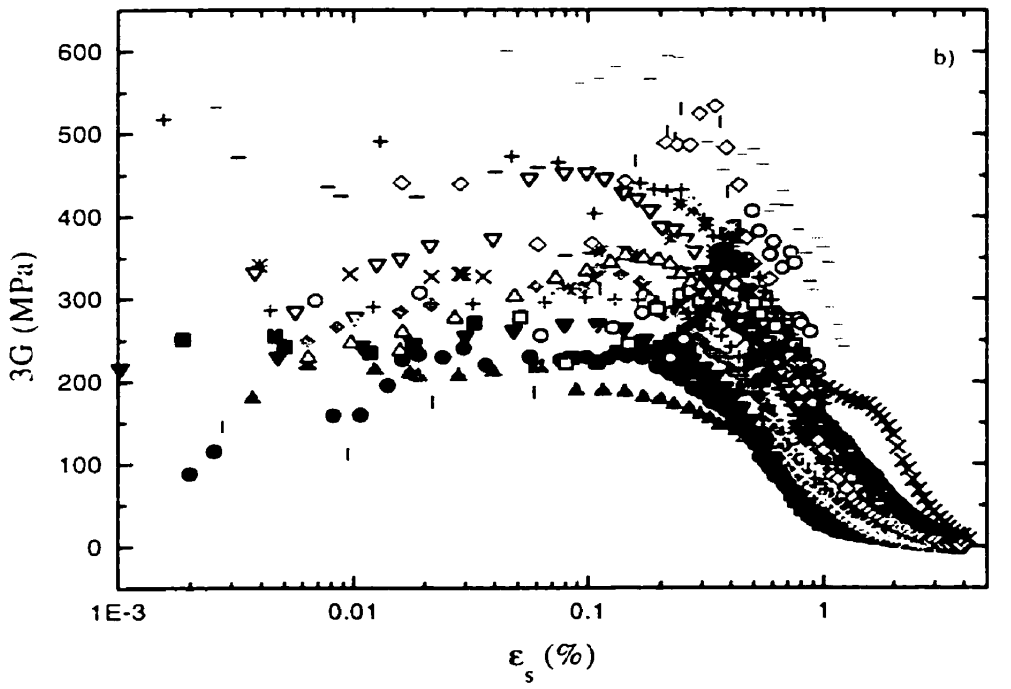

Figure 6.19a Incrementally averaged values of shear modulus versus the logarthim of shear strain for 'Frac' sand

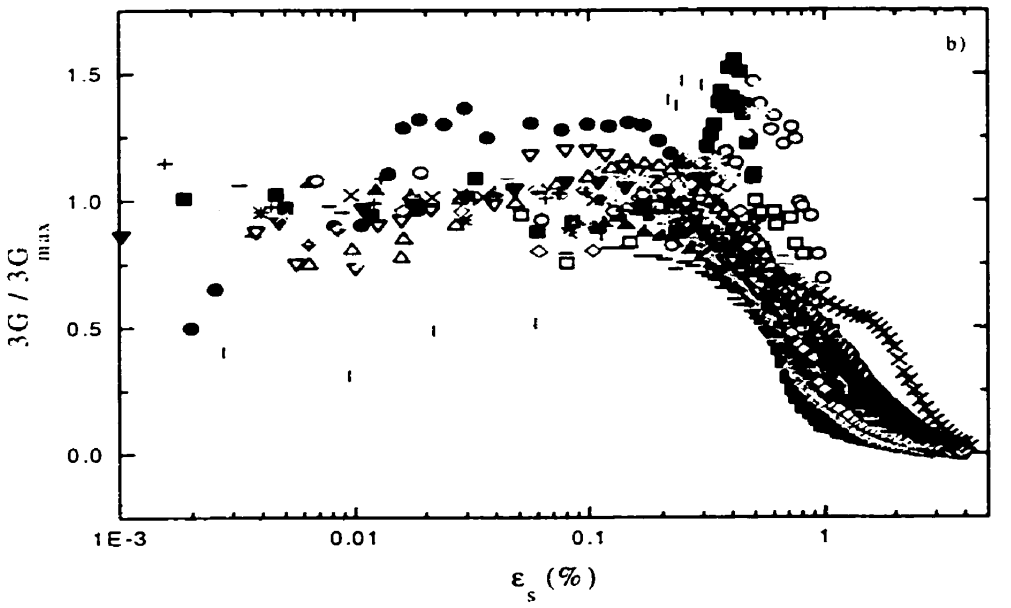

Figure 6.19b Incrementally averaged values of shear modulus normalized with the peak shear modulus versus the logarthim of shear strain for 'Frac' sand

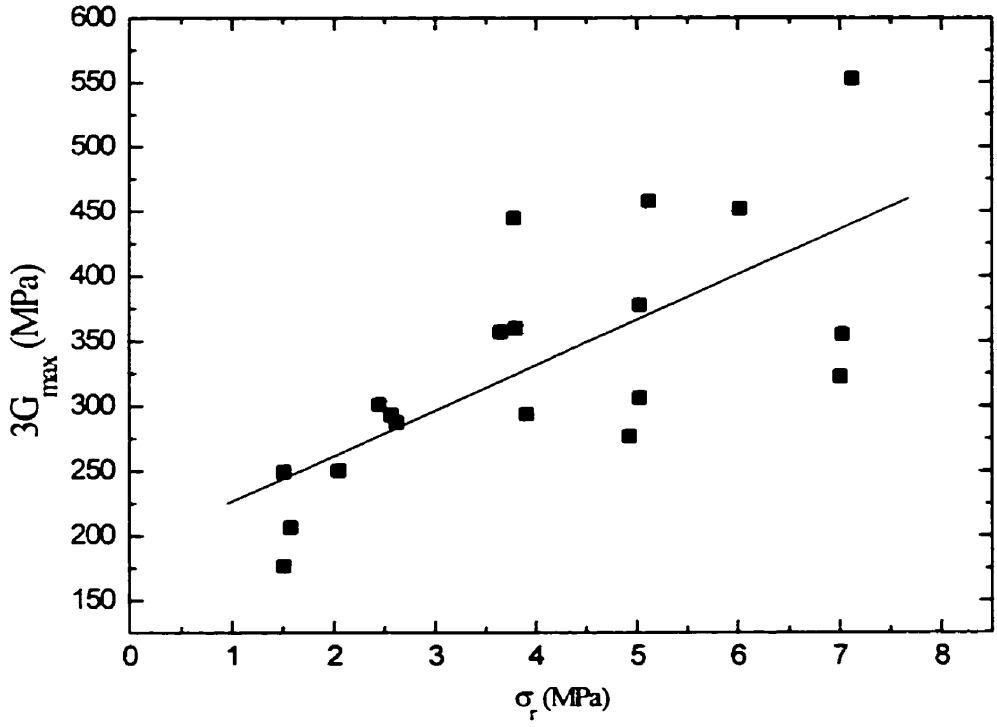

Figure 6.20 Linear relationship between the confining pressure and the initial shear modulus $3G_{max}$ for 'Frac' sand

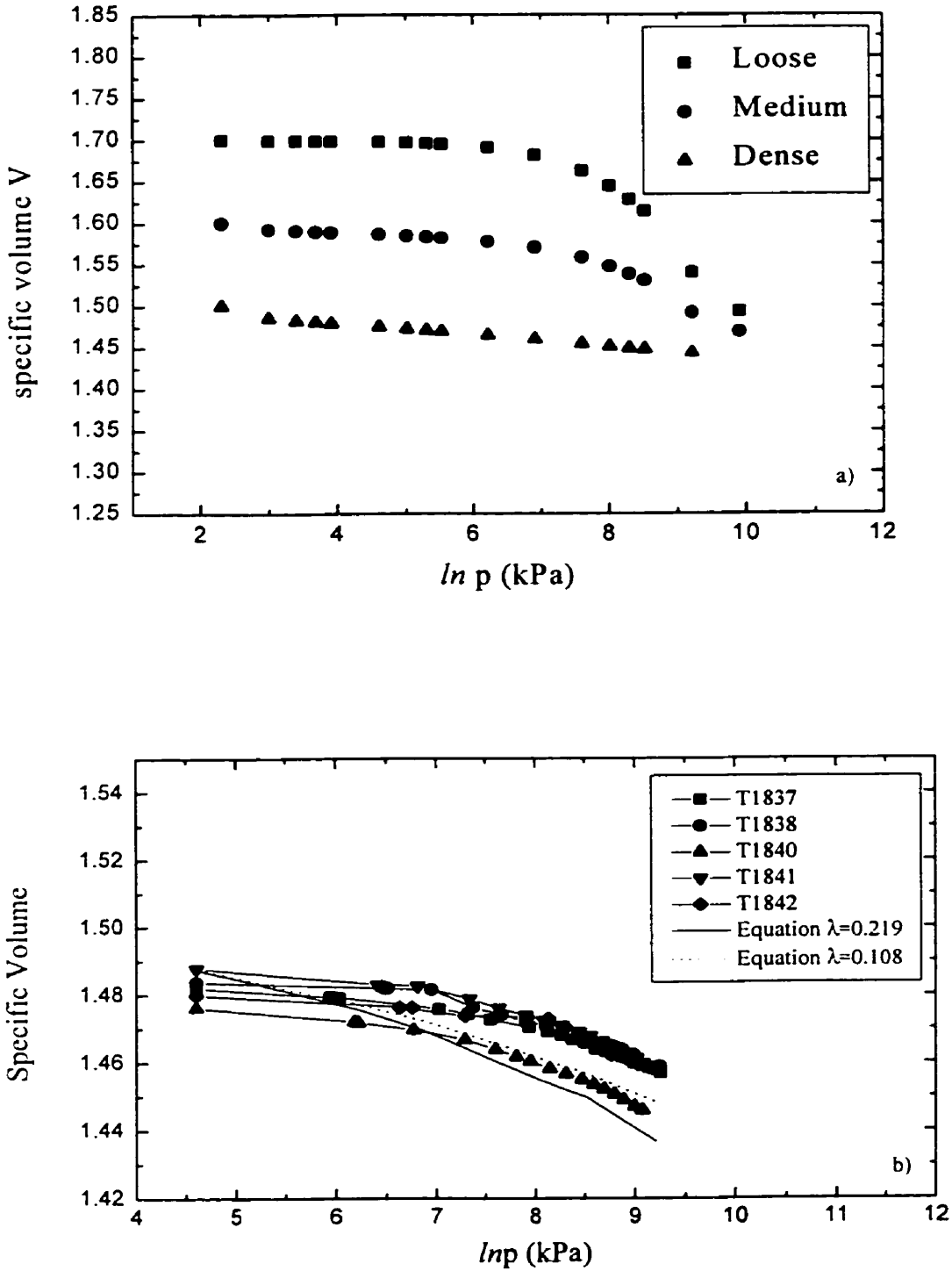

Figure 6.21 Specific volume versus *ln* p (a) predicted response for loose and dense 'Frac' sand and (b) predicted response and measured data

Appendix A - Temperature Effects

As discussed in chapter 3 of this thesis report triaxial compression testing was performed with temperature control. The purpose of temperature control was to determine the effect of temperature on sand behaviour, if any. The triaxial tests on 20-40 'Frac' sand were performed at three different temperatures; room temperature (25°C), 65°C and 100°C.

The instruments used in the testing program were designed to withstand the applied temperatures and were separately calibrated at each temperature. Throughout the testing some small differences in test results were encountered at different temperatures, but the observed effects were not consistent.

Isotropic Compression

As discussed in Chapters 5 and 6 two different types of isotropic compression tests were performed, one where both the radial and axial strain were measured and another series of tests where only the radial strain was measured. Results from both series of isotropic compression tests are shown in Figure A1 and A2 respectively. The volume strain for a confining pressure of 10.4 MPa increased from 1.7% to 2.2% for a temperature of 27°C to 65°C respectively, as shown in Figure A1a. For the test performed at 100°C the trend was reversed, a strain of 1.3% at a confining pressure of 8.8 MPa. The test performed at 100°C did not reach the same vertical stress levels but as shown in Figure 5.4a it was

experiencing less strain than the test performed at a temperature of 27°C. Although the test performed at 100°C experienced a small "jump" it appears that the measured strain was not less than those measured in the room temperature test.

The end of consolidation data for the isotropic compression tests where only the radial strain was measured are plotted in Figure A2. The final volume strain experienced in the consolidation phase of each test, grouped according to temperature of the test, represent confining pressures ranging from 1.5 MPa to 7.2 MPa. Based on the data plotted in Figure A2a it would appear that volume strain is decreased with increasing temperature, that is, increasing temperature increases the stiffness.

End of consolidation results of the isotropic compression tests were plotted in specific volume versus temperature in Figure A1b and Figure A2b. These data are a reflection of both the amount of strain experienced due to the increase in confining pressure and the initial specific volume. The effect of the initial specific volume especially evidenced for the tests at 100°C in Figure A2b where, although the volume strain was consistent, the specific volume at the end of consolidation showed the widest variability. The opposite was true of the tests performed at 27°C where the widest range of volume strain resulted in the narrowest range of final specific volumes.

As discussed in Chapter 6 the isotropic compression testing did not reach stress levels high enough to begin normal compression behaviour. The Cam Clay model considers that the behaviour in isotropic compression prior to reaching the NCL as being described

able to be described by a κ line. The κ values were calculated for the isotropic compression tests where both the axial and radial deformation were measured and are listed in Table A1. Two different values were calculated, that from the initial loading sequence and also from unload-reload cycles. The κ calculated from initial loading increased with increasing temperature, from 0.009 at 27°C to 0.015 at 100°C. The κ calculated for the unload-reload increased when the temperature increased from 27°C to 65°C but at 100°C the value is approximately the same as at 27°C.

The increasing value of κ with temperature in the initial loading of the isotropic compression (radial and axial deformation measured) can be thought of as decreasing stiffness with increasing temperature. The data plotted in Figure A2a show that smaller amounts of strain are occurring with increases in temperature (tests with radial deformation measured). This results in increasing stiffness with increasing temperature. Based on these contradictory results, from independent data sets, temperature seems not to affect the isotropic compression of dilative 'Frac' sand.

Triaxial Shearing

The triaxial compression test results were presented in Chapter 5. A discussion of the results in terms of the Cam Clay model was presented in Chapter 6. The results of the testing in Chapter 5 were grouped according to the temperature at which the test was performed, but treated as one data set in Chapter 6.

The stress ratio, η was plotted versus temperature at two of the 'key' points of the triaxial test in Figure A3, the transition condition and the peak deviator stress. The transition condition was considered the best estimate of critical state (Chapter 6) and although considerable statter is evidenced in the data, shown in Figure A3a the overall trend is for the stress ratio to increase slightly with increasing temperature. The opposite occurred for the stress ratio at the peak stress, shown in Figure A3b, where increases in temperature decreased the peak stress ratio slightly.

The stress ratio is a measure of the strength of the sand. The effects of temperature on the stress ratio at critical state and peak deviator stress were opposite. Based on the scatter in the data, Figure A3 it is unlikely that temperature had any systematic effect on the strength of the sand.

In order to determine if temperature had an effect on the stiffness of the sand, the shear stiffness was plotted versus temperature in Figures A4 and A5. Figure A4a is a plot of the secant shear modulus calculated at 50% of the maximum deviator stress. The overall trend of this data shows a small decrease in the stiffness with increasing temperature. The plotted data series at each temperature is for a confining pressure range between 1.5 MPa to 7.2 MPa.

As discussed in Chapter 6 the stiffness of the sand is dependent on the shear strain levels, with the shear modulus being approximately constant until 0.2% strain and reducing to

zero at 3% strain. The confining pressure was related to the maximum shear modulus, as shown in Figure 6.20. The maximum shear modulus was plotted versus temperature in Figure A4b, the data shows a slight trend towards decreasing stiffness with increasing temperature.

Although there appears to be an overall trend towards decreasing stiffness in both Figure A4a and Figure A4b there is considerable statter in the data. The secant modulus calculated from unload-reload cycles was plotted versus temperature in Figure A5. There does not appear to be any trend of these data with temperature. The data also shows considerable scatter in the calculated shear modulus.

The data plotted in Figure A4 indicates that while shear stiffness of the 'Frac' sand tends to be decreased with increasing temperature, the trend is not strong. The shear stiffness in the unload reload testing did not follow this trend, as shown in Figure A5. Based on this, and the data which indicates that temperature did not affect the strength of the sand, temperature was considered to affect the stiffness of the sand only a small extent.

Test	Initial Specific Volume	Temperature	κ (initial loading)	κ (unload-reload)
T1837	1.4818	27°C	0.0086	0.00576
T1838	1.4837	27°C	0.0092	0.00541
T1840	1.4761	65°C	0.0106	0.00860
T1841	1.4877	65°C	0.0103	0.00722
T1842	1.4798	100°C	0.0155	0.00554

Table A1 Calculated kappa values from isotropic compression testing, from tests measuring both axial and radial strain

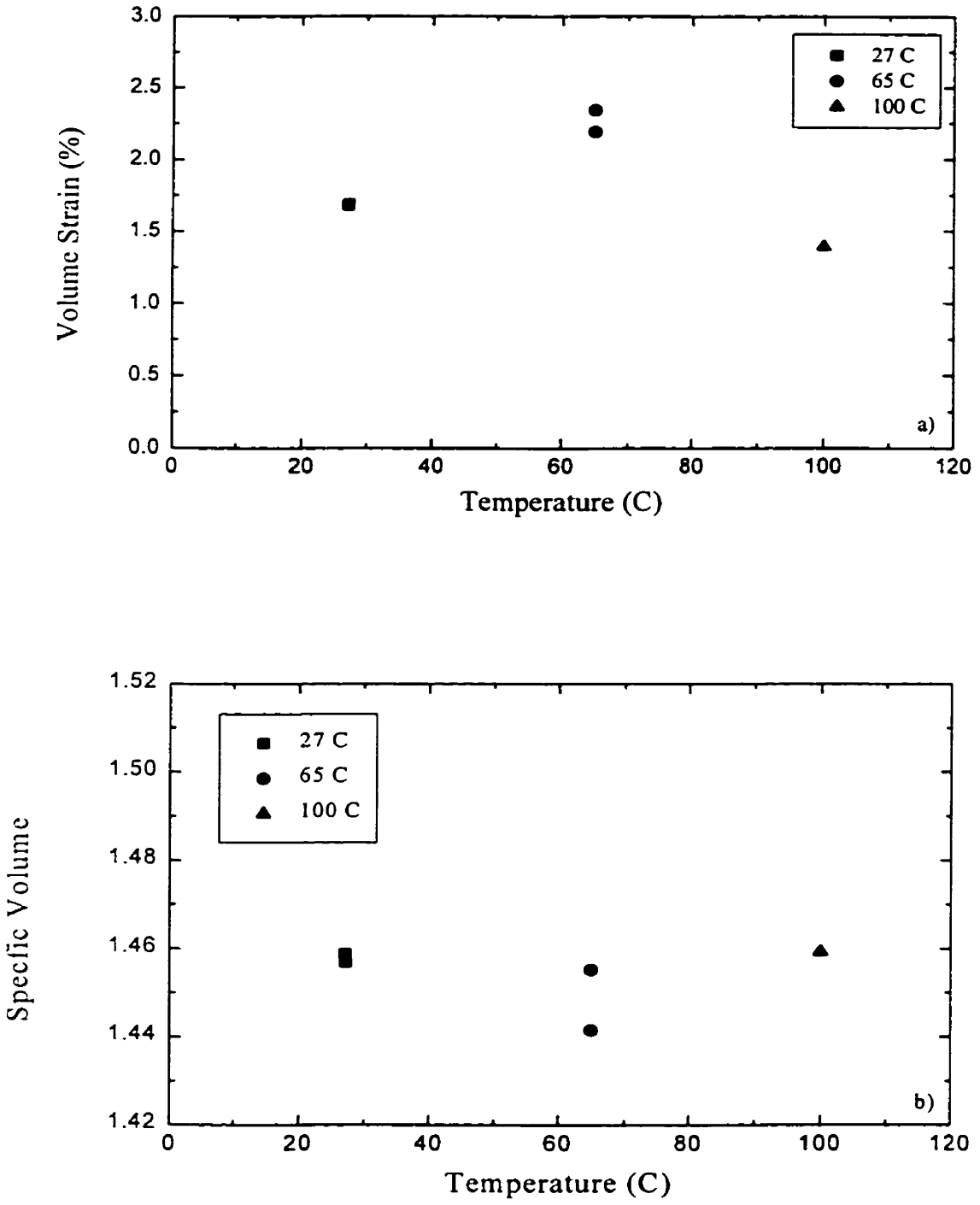

Figure A1 Isotropic compression of 20-40 'Frac' sand plotted as: a) volume strain versus temperature and b) specific volume versus temperature

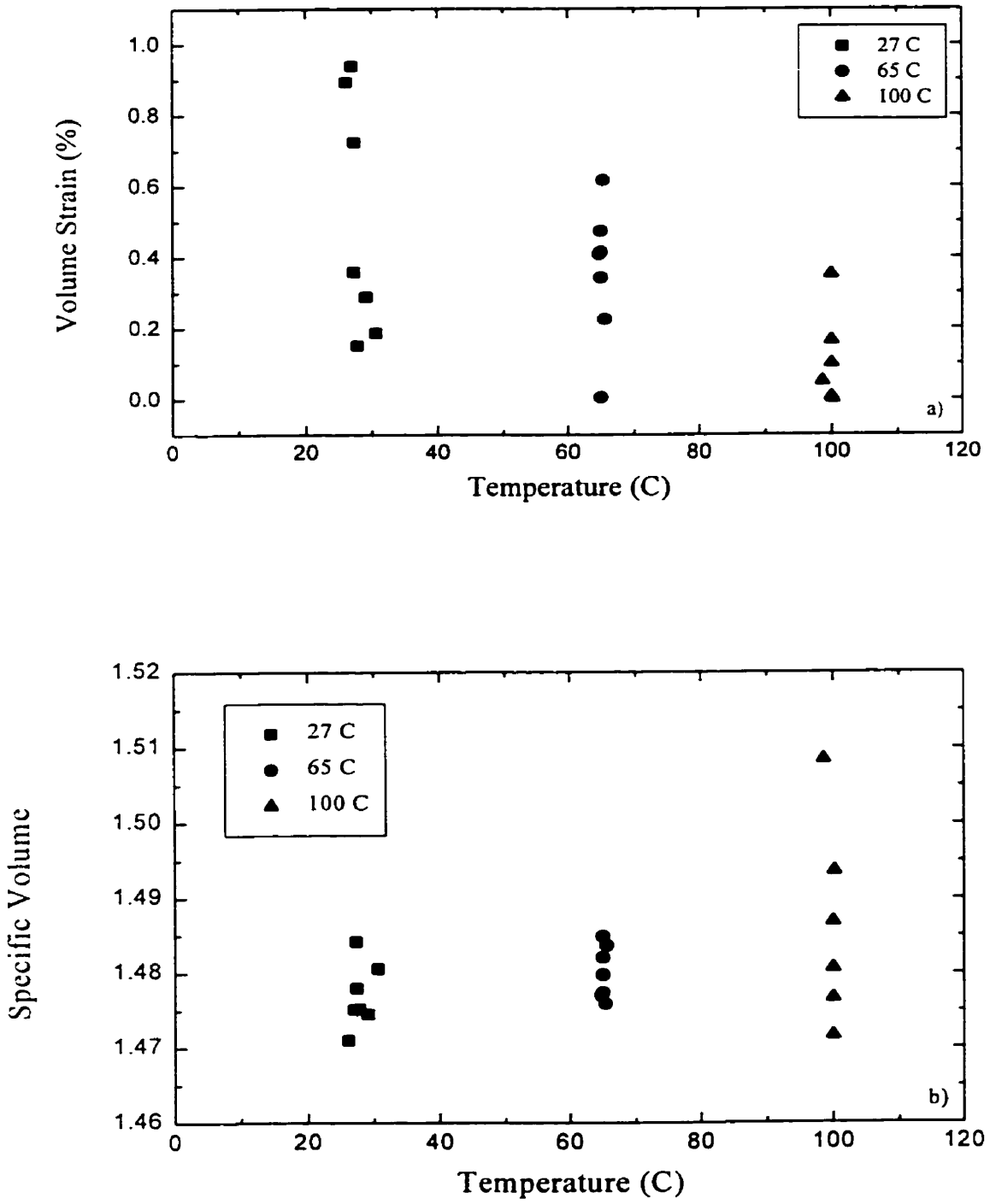

Figure A2 Isotropic compression prior to shearing for tests on 'Frac' sand plotted as: a) volume strain versus temperature and b) specific volume versus temperature

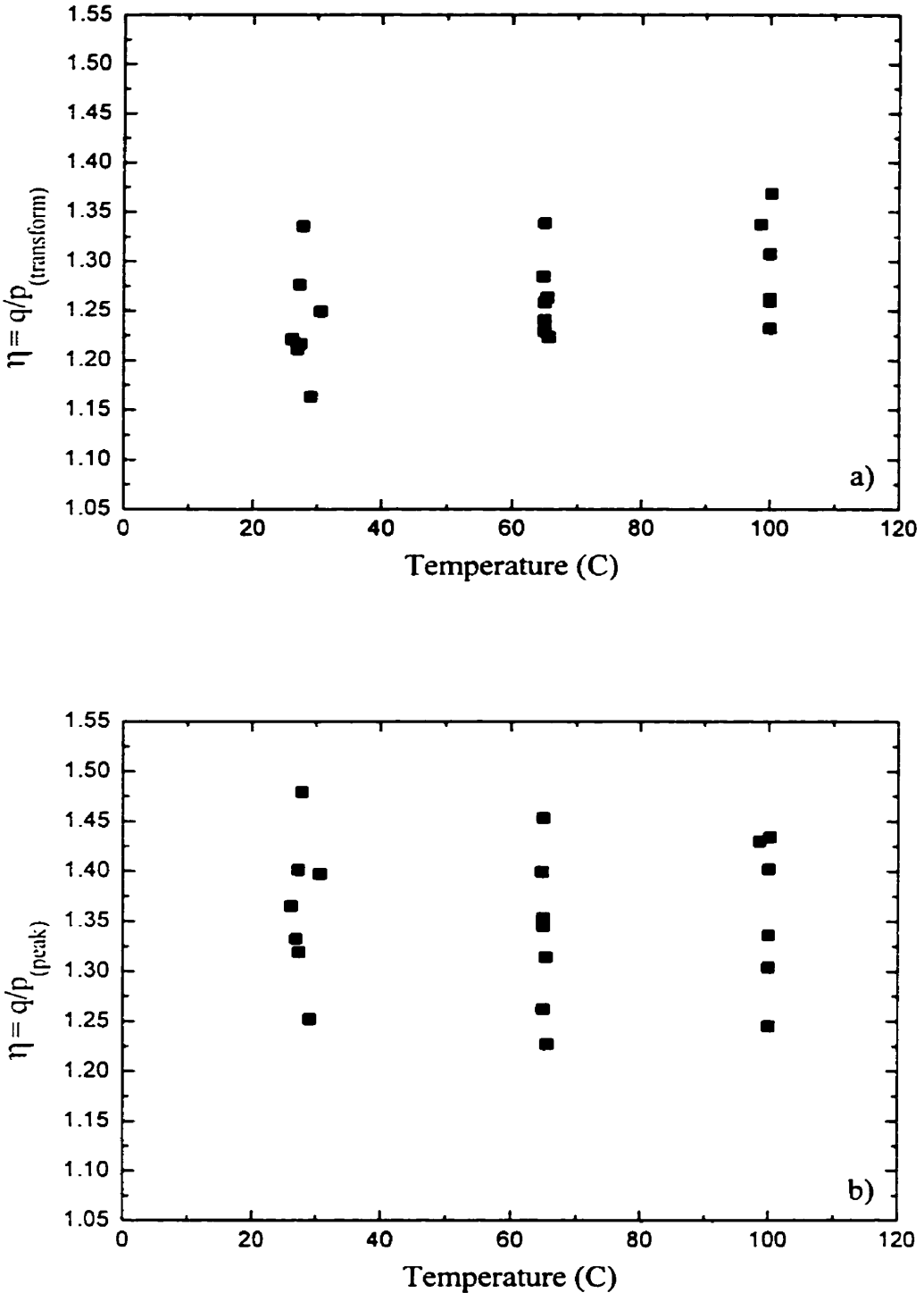

Figure A3 Stress ratio versus temperature at a) transformation condition and b) peak deviator stress

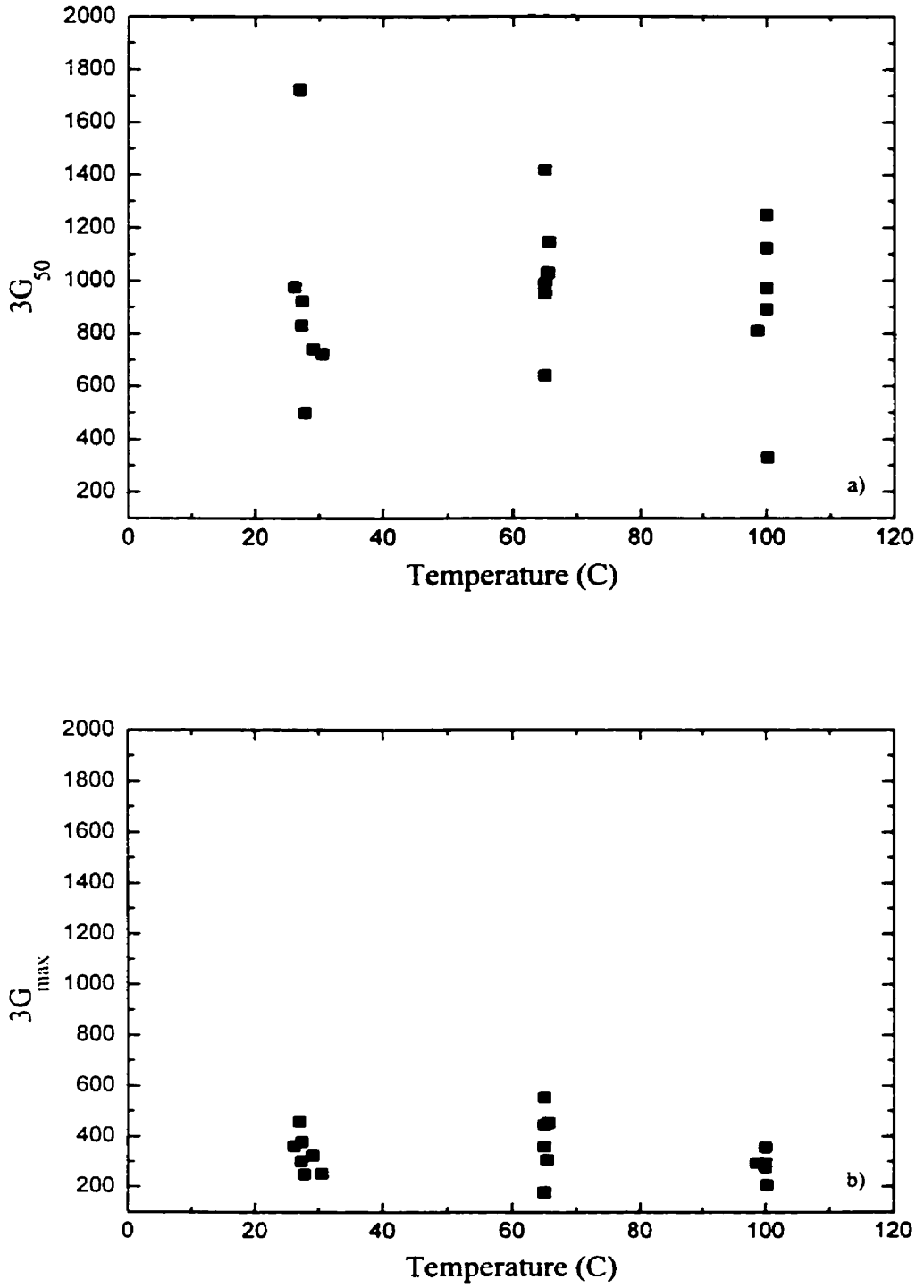

Figure A4 Shear modulus versus temperature plotted for a) secant shear modulus calculated at 50% of the maximum deviator stress and b) maximum tangent shear modulus

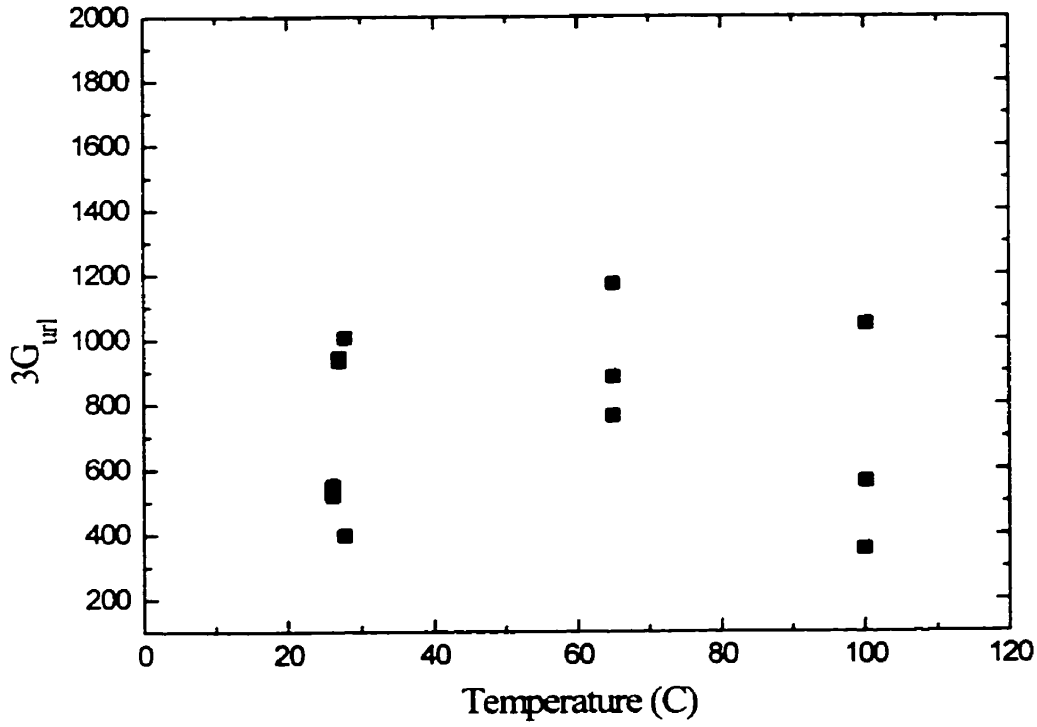

Figure A5 Shear modulus versus temperature, secant shear modulus calculated from unload reload testing